Digging up the past:

Postcranial perspectives on mammals across the Cretaceous-Paleogene boundary

Lauren Berg DeBey

A dissertation

submitted in partial fulfillment of the

requirements for the degree of

Doctor of Philosophy

University of Washington

2015

Reading Committee:

Gregory P. Wilson, Chair

Christian A. Sidor

Caroline A. E. Strömberg

Program Authorized to Offer Degree:

Biology

University of Washington

Abstract

Digging up the past:

Postcranial perspectives on mammals across the Cretaceous-Paleogene boundary

Lauren Berg DeBey

Chair of the Supervisory Committee:
Professor Gregory P. Wilson, Chair
Biology Department

The extinction of non-avian dinosaurs at the Cretaceous-Paleogene (K-Pg, 66.04 Ma, million years ago) boundary is arguably the most seminal event in mammalian history. The K-Pg mass extinction and subsequent recovery marked the onset of rapid morphological, ecological, and phylogenetic diversification in mammals into the wide range of body sizes and ecological niches occupied throughout the Cenozoic. Most mammalian patterns across the K-Pg boundary are based on dental data; however, postcrania are uniquely suited to inform the locomotor ecologies and substrate preferences of mammals. As such, K-Pg mammalian postcrania can be used to test (1) locomotor-based patterns of extinction selectivity that are predicted in certain mass extinction scenarios, and (2) increases in early

Paleogene locomotor diversity predicted by ecological release from dinosaur-imposed selection during the Cretaceous.

This study represents the first comprehensive description and assessment of mammal postcrania across the K-Pg boundary. Femora, humeri, and astragali from the well-sampled and well-studied K-Pg deposits of eastern Montana were studied qualitatively and quantitatively to infer taxonomic affinities and locomotor modes, and to investigate changes in body size. This study encompasses three faunas: the latest Cretaceous pre-extinction fauna, earliest Paleocene "survival" fauna, and later Paleocene more "recovered" fauna. Results show significant changes in body size throughout these three faunas that are consistent with patterns derived from dental data. Among mammals in the "survival" fauna, the average body size of latest Cretaceous mammals that survived the K-Pg mass extinction was smaller than during the latest Cretaceous, which is consistent with the 'Lilliput Effect'; however, early Paleocene immigrants actually had significantly increased body sizes. Mammals in the later "recovered" fauna have the largest body size of all mammals in this study. Results from analyses of locomotor mode show latest Cretaceous mammals had semifossorial and arboreal locomotor modes, and there was an expansion of scansorial and arboreal locomotor modes among the early Paleocene mammals. These ecomorphological findings are consistent with hypotheses concerning the transition from open Cretaceous landscapes to more closed, forested Paleocene habitats. Postcrania represent a valuable, independent dataset for examination of extinction and recovery dynamics that can deepen our ecological understanding of the Cretaceous-Paleogene mass extinction.

TABLE OF CONTENTS

LIST OF FIGURES

CHAPTER 4: LOCOMOTOR FUNCTION IN MAMMAL ASTRAGALI FROM THE CRETACEOUS-PALEOGENE BOUNDARY IN EASTERN MONTANA

LIST OF TABLES

Acknowledgements

My graduate school experience has been an incredible journey personally and professionally, and I have many people to thank for their support and encouragement along the way.

First and foremost I thank my advisor, Greg Wilson. He has at various times been an advisor, a co-founder, a boss, and a friend. He has many times gone above and beyond the expectations of an advisor (e.g., helping me move!), and I have always known I can count on him. In six years of fieldwork in eastern Montana, we have driven together enough miles to circle the planet, and I am appreciative of every mile of our journey together.

My committee members, Caroline Strömberg, Christian Sidor, and Elizabeth Nesbitt allowed me to explore many options for my dissertation project and supported me every step of the way. They have been an honest sounding board during my time at UW, and I am especially appreciative of their understanding as I took the time to develop new skill sets and test the waters of life beyond academia.

The UW Department of Biology has been a wonderful place to mature as a scientist and educator. The community of faculty, staff, and students has been supportive and generous, and I cannot thank them enough. The special people in UW Biology are numerous, but I would like to thank the following people in particular. Scott Freeman and Karen Petersen are among the best educators I have ever had the pleasure of working with, and both have been incredible mentors for my own development as an educator. The fourth floor of Kincaid, occupied by the faculty, students, and staff of the Wilson, Sidor, Hille

Ris Lambers, Kerr, and Bergstrom labs, (and at various times the Daniel and Buckley labs) has been a wonderful source of camaraderie and inspiration. Dave Hurley has shown me kindness and understanding time and time again as I navigated technological hurdles or needed to hear words of encouragement. And I am ever so grateful to the Biology Graduate Program Coordinator, Marissa Herringer, for her tireless efforts to help graduate students succeed and thrive.

The UW, UCMP, UC Berkeley, and SVP paleontology communities have been instrumental in facilitating and encouraging my research. In particular, the UW paleontology community, composed of faculty, staff, and students from the UW Biology Department, Earth and Space Science Department, Anthropology Department, and the Burke Museum, has grown tremendously since I started as a graduate student; it has been fun to help develop the traditions of this blossoming group. Additionally, the faculty and staff of the UCMP and UC Berkeley vertebrate paleontology and paleoanthropology research groups have been wonderful mentors for the last 10 years, and it has been my pleasure to work with and learn from Tim White, F. Clark Howell, Bill Clemens, Nick Pyenson, Kevin Padian, and Pat Holroyd.

For financial support during my time as a graduate student, I sincerely thank the National Science Foundation, UW Department of Biology, UW Graduate School, UW Graduate and Professional Student Senate, Evolving Earth Foundation, University of California Museum of Paleontology, Bureau of Land Management, Society of Vertebrate Paleontology, North American Paleontology Convention, and Discoveries in Geosciences (DIG) Field School. I am especially honored and appreciative to have received the Charlotte

Cornell Crary and Henry and Frances Decker Distinguished Teaching Fellowship, which critically supported the completion of this work.

Also a source of financial support, the Dimensions of Biodiversity Distributed Graduate Seminar (DBDGS for "short") provided the unique opportunity to step outside of the world of paleontology and into those of citizen science, science outreach, and metadata collection and analyses. Working with this group has been one of the most challenging, rewarding, and fun experiences of my graduate career; it has also been the source of many valuable friendships. For this I thank the faculty advisors Julia Parrish, Janneke Hille Ris Lambers, and Josh Tewksbury, and especially my graduate colleagues: Hillary Burgess, Halley Froehlich, Elli Theobald, Ailene Ettinger, Natalie Schmidt, and Cherie Wagner.

My Wilson labmates have kept me sane, positive, and motivated and I cannot thank them enough. We are a motley crew of students from around the country and world and I do not think it is possible to assemble a more diverse lab in terms of experiences, world views, hobbies, and personalities; however, our little, sometimes dysfunctional, family takes incredible care of one another. I cherish my friendships with each of them and will dearly miss seeing them daily. Meng Chen and I started together as Greg's first students, and as academic "twins" our bond (and love of "Space Jam") is forever. Dave DeMar is one of the most kind, gentle people I have ever met; however, we will never like the same music. Jonathan Calede needs everyone to know he is French, but he is also an old soul and would do anything for a friend. Stephanie Smith is a tenacious, intelligent, and compassionate ally, and she is the best seamstress I know. Alex Brannick is considerate and thoughtful, and has brought a quiet strength to the lab that has been refreshing.

My research assistants transformed the way I do science. Their excitement for contributing to my research invariably left me invigorated and motivated to persevere; seeing my research through their eyes is an experience I will treasure. Despite not knowing me, Sean Wang trusted me to keep him alive and well in rural Montana, and we had a lot of fun that summer. My friend, Michael "Mikey" Washington also served as my field assistant, and among many fun times, the image of him working the grill is forever burned into my brain. Another dear friend, Ali Kriedberg, volunteered many hours after work and on weekends, and I am so appreciative of her friendship. As my research assistant, Neha Kunwar was more generous with her time than I could have imagined, and she was an incredible help as I undertook the research for my final chapter. Nandita Gilroy is one of the most reliable undergraduates I have ever met and she never failed to surpass my expectations. Leeyah Heilicher is a former student, was my right hand as I finished my research, and is now a dear friend. She is one of the most competent people I have had the pleasure of working with. She will do incredible things in her future, and she has a job with me any time she wants.

The DIG Field School has been a source of pride and inspiration during my graduate career. I cannot thank Greg enough for the opportunity to build something so special. To the teachers of the DIG Field Schools from 2010–2014, thank you for your enthusiasm, confidence, and support as we made mistakes, learned, and grew. I trust the DIG will continue to develop into something wonderful in the years to come.

Since I began down the path of paleontology research, my family, friends, and family-friends have been my cheerleaders. My friends kept my life balanced and fun.

My family and family-friends always reminded me how far I had come, and to celebrate my accomplishments. My mom LouAnn and brother Michael push me to be and do better, and they keep my head from getting too big. My dad Craig passed away shortly before I applied to graduate school, and my graduate school journey has been longer and harder without him. He shared his love of science with me from the time I was very young, taught me to do whatever makes me happy, and reminded me to try things even if I might not be the best at them. I promised him I would finish my PhD and I am so proud of myself for keeping that promise, difficult as it was. I miss him every minute of every day, and I dedicate this dissertation to him.

Without the love, support, generosity, and encouragement of my husband David, I would not be where I am today. He is the strongest (and funniest!) person I know, and he has shown me the meaning of courage. I am so proud of who he is and what he has accomplished, and I am a better person because he is my partner. Thank you for these last three and a half years. They have been the best of my life, and I am so excited to see where we go next on our journey together.

CHAPTER 1:

INTRODUCTION AND OVERVIEW

> *"During the Cretaceous terrestrial field, both forest and such open country as may have existed, appears to have been pretty closely held by the dinosaurs, and the opportunities for mammals to expand were thereby limited… Their disappearance at the end of the Cretaceous, to whatever cause it be assigned, left the field of terrestrial adaptation open for mammalian occupation, and the mammals proceeded to expand first into terrestrial forest dwellers and then more slowly into terrestrial open county, plains and desert adaptations."*
> — W.D. Matthew (1937, pp. 325)

The extinction of non-avian dinosaurs at the Cretaceous-Paleogene (K-Pg, 66.04 Ma, million years ago) boundary is arguably the most seminal event in mammalian history. The K-Pg mass extinction and subsequent recovery marked the onset of rapid morphological, ecological, and phylogenetic diversification in terrestrial mammals into the wide range of body sizes and ecological niches occupied throughout the Cenozoic (Alroy 1998, 1999; Stucky 1990; Hunter 1999; Wible et al. 2007; Smith et al. 2010; O'Leary et al. 2013; Wilson 2013; but see e.g., Springer et al. 2003; Bininda-Emonds et al. 2007). Most mammalian patterns across the K-Pg boundary are based on dental data, but recent research suggests postcranial data can capture more diversity than dental data alone (e.g., Luo and Wible 2005; Chester et al. 2012). Postcrania are uniquely suited to inform the locomotor ecologies and substrate preferences of mammals (Szalay and Decker 1974; Szalay 1984, 1994; Van Valkenburgh 1987; Damuth 1992; Iwaniuk et al. 1999; Szalay and Sargis 2001; Bloch and Boyer 2002; Weisbecker and Warton 2006; Fabre et al. 2014).

Though taxonomically numerous, Mesozoic mammals have historically been hypothesized to be largely confined to marginal roles as small-bodied, ecological generalists in terrestrial ecosystems due to competition and selection pressures imposed

by non-avian dinosaurs (e.g., Romer 1959; Van Valen 1978; Lillegraven et al. 1987; Archibald 1983; Alroy 1998, 1999; Kielan-Jaworowska et al. 2004). However, newly discovered Mesozoic skeletons show far greater locomotor diversity among early mammals than previously recognized (e.g., Kielan-Jaworowska and Gambaryan 1994; Luo et al. 2003; Luo and Wible 2005; Luo 2007; Ji et al. 2006; Meng et al. 2006; Hurum and Kielan-Jaworowska 2008; Chen and Wilson 2015). This increase in mammalian ecomorphological diversity in the Mesozoic (e.g, Jurassic and Early Cretaceous) conceivably suggests an increase in mammalian ecomorphological diversity among latest Cretaceous faunas; however, this hypothesis has yet to be tested robustly and in the context of the extinction and survival at the K-Pg boundary.

The K-Pg postcranial record allows for testing hypotheses at the intersection of ecological and evolutionary processes, and allows for a comparison with patterns derived from dental data (e.g., Archibald 1982; Lofgren 1995; Hunter 1999; Lillegraven and Eberle 1999; Clemens 2002; Hunter and Archibald 2002; Wilson 2013, 2014). Extinction and survival patterns of many vertebrate lineages across the K-Pg boundary appear to suggest a complex set of causal factors, with both long-term and short-term environmental influences (e.g., Archibald 1983; Archibald and Bryant 1990; Clemens 2002; Wilson 2005, 2013; Wilson et al. 2014). K-Pg mammalian postcrania can thus be used to test (1) for locomotor-based patterns of extinction selectivity that are predicted in certain mass extinction scenarios (e.g., Robertson et al. 2004), and (2) for increases in locomotor diversity predicted by ecological release from dinosaur-imposed selection across the K-Pg boundary (e.g., Romer 1959; Lillegraven et al. 1987; Alroy 1998, 1999).

The Hell Creek and Tullock formations in eastern Montana represent some of the best-sampled, temporally constrained K-Pg outcrops of terrestrial deposits in the world (Archibald 1982; Swisher et al. 1993; Lofgren 1995; Clemens 2002; Renne et al. 2013; Wilson 2005, 2014; LeCain et al. 2014; Moore et al. 2014; Sprain et al. 2015). With a few exceptions, all fossils in this study come from these Cretaceous-Paleogene deposits in Garfield and McCone counties in northeastern Montana (e.g., Archibald 1982; Lofgren 1995; Clemens 2002; Wilson 2005). In total, this study samples 64 femora, 50 humeri, and 24 astragali from 48 localities.

Research on stratigraphically well-constrained latest Cretaceous and earliest Paleogene mammal postcranial specimens has been limited to taxon- or element-specific analyses on a small number of specimens (e.g., Deischl 1964; Szalay and Decker 1974; Borths and Hunter 2008; Chester et al. 2015), rather than comprehensive assemblage analyses (e.g., early Paleocene faunas from the San Juan Basin of New Mexico; Matthew 1937). Many of the previous morphological studies on Hell Creek and Tullock postcrania have included material from the Bug Creek Anthills (e.g., Deischl 1964; Sloan and Van Valen 1965), which though yielding large sample sizes, have poor stratigraphic resolution (interpreted as a mix of lowermost Paleocene and reworked upper Maastrichtian fossils; Lofgren 1995). As such, these materials cannot be used to interpret change across the mass extinction boundary.

Research on mammal postcrania from the study area has been hindered by a lack of articulated or associated skeletons, relatively small sample sizes, and high rates of breakage among functionally informative limb elements (e.g., Deischl 1964; Krause and Jenkins 1983; Borths and Hunter 2008). Perhaps the most difficult barrier to the study of

these isolated elements is determining which dentally-based taxa are the most likely candidates for attribution of postcranial material. As a result, all analyses herein take a parataxonomic approach and group specimens that are similar in morphology and size into morphotypes (e.g., Deischl 1964; Chester et al. 2010; 2012; Szalay and Sargis 2001). Subsequently, specimens in each morphotype were compared to previously published descriptions of Cretaceous- and Paleogene-aged postcrania to constrain taxonomic assignments (e.g., Gidley 1909; Simpson and Elftman 1928; Granger and Simpson 1929; Simpson 1935; Matthew 1937; Deischl 1964; Szalay and Decker 1975; Szalay and Dagosto 1980; Krause and Jenkins 1983; Kielan-Jaworowska and Gambaryan 1994; Szalay and Sargis 2001; Chester et al. 2010, 2012, 2015; Argot 2001, 2002, 2010, 2013). These taxonomic assignments were refined using sizes of dental taxa known from the study area (Wilson et al. 2012; Wilson 2013, 2014). All taxonomic attributions thus represent working hypotheses that should be further tested as additional material is discovered and described.

Together, these chapters represent the first comprehensive description and assessment of mammal postcrania across the K-Pg boundary. *Chapters Two*, *Three*, and *Four* focus on the femur, humerus, and astragalus, respectively. Analyses within each chapter are descriptive, diagnostic, qualitative, and quantitative and the results represent a significant contribution to the continually growing body of research on the K-Pg mass extinction. Below, I summarize the objectives, methods, and results of each chapter.

Chapter Two qualitatively and quantitatively examines femora to investigate patterns of taxonomic and ecomorphological diversity dynamics among K-Pg mammals. The femur is the proximal hind limb element and it articulates proximally with elements of

the pelvic girdle and distally with the tibia. This study focuses on proximal fragments of femora, which are much more abundant in museum collections than distal fragments of femora; this pattern is likely due to how recognizable proximal femora are in general. Functionally, the shapes and sizes of the articular surfaces and areas for muscle attachment on the proximal humerus are indicative of e.g., flexibility, rotation, and power. Femur specimens were grouped into morphotypes within higher-level taxa (Multituberculata, Eutheria) and each morphotype was whenever possible attributed, on the basis of morphology and size, to a lower-level taxon known from dental specimens from the study area (Wilson et al. 2012; Wilson 2013, 2014). Morphotype richness was computed for each biozone within and among higher-level taxa (i.e., multituberculates and eutherians) and according to "immigrant" and "resident" taxon status (e.g., Clemens 2002; Wilson 2013, 2014). Changes in body size through time were investigated using linear measurements on femora and univariate analyses. Locomotor modes were tentatively assigned qualitatively by comparing the functional morphology of K-Pg femora with published material.

The results of *Chapter Two* indicate significant body size changes and more morphological diversity among K-Pg femora than previously recognized. Cretaceous femora showed a greater diversity of multituberculate femur morphotypes present in North America than previously recognized (e.g., Gidley 1909; Deischl 1964; Krause and Jenkins 1983); however, femora of metatherians and eutherians were conspicuously absent. Femur morphotype richness decreased slightly across the K-Pg boundary, but was replenished by the appearance of immigrant taxa. These taxa include two early Puercan archaic ungulates, and a very large eutherian (a taeniodont, pantodont, or triisodontid) a possible "plesiadapiform" primate in the later Puercan. Body size increased across the K-Pg

boundary, specifically among early Paleocene immigrant taxa. In contrast, specimens of Puercan resident or "survivor" taxa were significantly smaller than both Puercan immigrant taxa and Lancian taxa present before the K-Pg mass extinction. Although preliminary and largely qualitative, my ecomorphological results suggest locomotor diversity expanded from mainly arboreal and/or terrestrial/saltatorial multituberculates in the Lancian to include a fossorial multituberculate and potentially an arboreal eutherian in the middle/late Puercan.

Chapter Three qualitatively and quantitatively analyzes humeri size and shape to infer locomotor modes among K-Pg mammals. The humerus is the proximal forelimb element and it articulates proximally with elements of the shoulder girdle and distally with the radius and ulna. This study focuses on distal fragments of humeri, which are much more abundant in museum collections than proximal fragments of humeri; this pattern is likely a consequence of how recognizable distal humeri are in general. The shapes and sizes of the articular surfaces and areas for muscle attachment on the distal humerus are indicative of function (e.g., flexibility, rotation, grasping abilities). I use a combined qualitative and quantitative analytical approach in this chapter. First, using a method similar to that in *Chapter Two*, I assigned all humeri material to a morphotype, compared these morphotypes to published Cretaceous and Paleogene material, and used size and relative abundances to attribute these humerus morphotypes to lower-level taxa known from dental specimens in my study area. Second, I analyzed humeri quantitatively in two ways: (1) with linear measurements and univariate and multivariate analyses across morphotypes and across biozones, and (2) using landmark- and semilandmark-based two-dimensional geometric morphometrics and multivariate analyses to compare select, well-

preserved K-Pg distal humeri to a large, comparative dataset of extant mammals of known locomotion. This extant sample included 109 distal humeri from 71 species in 13 marsupial and placental orders.

The results of the humeri analyses in *Chapter Three* show humeri morphotype richness and size patterns that largely mirror results from *Chapter Two*. Humeri morphotype richness is greatest in the Lancian, which included humeri from mostly multituberculates and at least one metatherian and one eutherian. Humeri richness was lowest during the early Puercan. Though small sample size may be driving this pattern, a relatively depauperate "survival" fauna is also documented from dental fossils from the study area (e.g., Lofgren 1995; Wilson 2014). Humeri richness increased again in the Pu3, and included larger eutherians than previously seen in the Lancian and Pu1 record from the study area. With respect to body size, multituberculates are larger in the Lancian than in the younger biozones; conversely, eutherian size increased across the K-Pg boundary and then greatly and significantly increased in the Pu3. Results from two-dimensional geometric morphometrics indicate that Lancian and Puercan humeri all had strong hand flexor muscles, useful for grasping activities associated with climbing or digging. I interpret the locomotor mode of one Lancian morphotype as possibly arboreal and semifossorial, and the Puercan morphotypes as semifossorial, fossorial, scansorial, and generalized terrestrial.

Chapter Four uses an even more quantitative approach to examine complete astragali and infer locomotor modes of early Paleogene eutherians. The astragalus, the second largest tarsal bone, articulates proximally with the distal elements of the leg, inferiorly with the heel bone, and distally with the proximal elements of the foot. As such,

morphology of the astragalus and the shapes of its articular surfaces are correlated with both locomotor mode and substrate preference (e.g., Szalay and Decker 1974; Carrano 1997; Polly 2008; Fabre et al. 2014). As with *Chapter Three*, this study uses landmark- and semilandmark-based geometric morphometrics and an extant comparative dataset of mammals of known locomotion. Unlike *Chapter Three*, this chapter takes a three-dimensional (3D) geometric morphometrics approach to analysis of postcranial shape and uses micro-CT scanned and reconstructed 3D models of astragali (e.g., Polly 2008; Fabre et al. 2014).

The quantitative results of *Chapter Four* suggest that the sampled early Paleocene (Pu1 and Pu3) specimens had largely semifossorial locomotor habits. When these results are interpreted using additional qualitative characters and a perspective informed by functional morphology, specimens attributed to ?*Protungulatum* appear the most semifossorial, whereas those attributed to ?*Procerberus* had slightly more scansorial tendencies. A specimen attributed to ?*Purgatorius* that was previously hypothesized to be arboreal (i.e., Chester et al. 2015), exhibits semifossorial affinities; however, this specimen was located nearer to arboreal and scansorial specimens in our ecomorphospace than other fossil specimens and had qualitative characteristics suggestive of scansoriality. The final fossil specimen in this study was a larger specimen that I attributed to an ?archaic ungulate, and which had a shape that was quantitatively similar to semifossorial specimens but additionally had qualitative morphologies suggestive of scansorial capabilities. The Pu1 sample thus included taxa with semifossorial and/or scansorial locomotor modes (?*Protungulatum* and ?*Procerberus*). The Pu3 included these taxa and additionally included two taxa with additional scansorial affinities (?*Purgatorius* and ?archaic ungulate).

Chapter Five provides concluding remarks that synthesize and interpret results of this dissertation in light of our understanding of the latest Cretaceous ecosystems, the K-Pg mass extinction, and the subsequent early Paleogene recovery.

Together, these chapters represent the most comprehensive study on mammal postcrania from a series of latest Cretaceous and early Paleocene faunas. This study is unique in its use of traditional qualitative (i.e., functional morphology) methods to study K-Pg specimens while additionally applying a quantitative framework from two- and three-dimensional analyses of extant taxa. The ecomorphological findings herein are largely consistent with hypotheses concerning the transition from open Cretaceous landscapes to more closed and forested Paleocene habitats (e.g., Fastovsky 1987; Wing and Boucher 1998; Clemens 2002; Wilf et al. 2003; Nichols and Johnson 2008). These findings are also consistent with patterns derived from dental material that show an initial decrease in body size across the K-Pg boundary, and a subsequent large increase in body size in early Paleocene mammals (e.g., Archibald 1983; Maas and Krause 1994; Alroy 1999; Clemens 2002; Wilson 2004, 2013; Smith et al. 2010; Wilson et al. 2012). Thus, postcrania represent a valuable, independent dataset for examination of extinction and recovery dynamics that can deepen our ecological understanding of the Cretaceous-Paleogene mass extinction.

References Cited

Alroy, J. 1998. Cope's rule and the dynamics of body mass evolution in North American fossil mammals. Science 280: 731–734.

Alroy, J. 1999. The fossil record of North American mammals: evidence for a Paleocene evolutionary radiation. Systematic Biology 48: 107–118.

Archibald, J.D. 1982. A study of Mammalia and geology across the Cretaceous-Tertiary boundary in Garfield County, Montana. University of California Publications in Geological Sciences 122: 1–286.

Archibald, J.D. 1983. Structure of the K-T mammal radiation in North America: speculations on turnover rates and trophic structure. Acta Palaeontologica Polonica 28: 7–17.

Archibald, J.D. and L.J. Bryant. 1990. Differential Cretaceous-Tertiary extinctions of non-marine vertebrates: evidence from northeastern Montana, in: V.L. Sharpton and P.D. Ward (Eds.), Global Catastrophes in Earth History: An Interdisciplinary Conference on Impacts, Volcanism, and Mass Mortality. Geological Society of America Special Paper 247, pp. 549-562.

Argot, C. 2001. Functional-adaptive anatomy of the forelimb in the Didelphidae, and the paleobiology of the Paleocene marsupials *Mayulestes ferox* and *Pucadelphys andinus*. Journal of Morphology 247: 51–79.

Argot, C. 2002. Functional-Adaptive Analysis of the Hindlimb Anatomy of Extant Marsupials and the Paleobiology of the Paleocene Marsupials *Mayulestes ferox* and *Pucadelphys andinus*. Journal of Morphology 253: 76–108.

Argot, C. 2013. Postcranial analysis of a Carnivoran-like archaic ungulate: the case of *Arctocyon primaevus* (Arctocyonidae, Mammalia) from the Late Paleocene of France. Journal of Mammalian Evolution 20: 83–114.

Argot, C. 2013. Postcranial analysis of a Carnivoran-like archaic ungulate: the case of *Arctocyon primaevus* (Arctocyonidae, Mammalia) from the Late Paleocene of France. Journal of Mammalian Evolution 20: 83–114.

Bininda-Emonds, O.R., M. Cardillo, K.E. Jones, R.D.E. MacPhee, R.M.D. Beck, R. Grenyer, S.A. Price, R.A. Vos, J.L. Gittleman, and A. Purvis. 2007. The delayed rise of present-day mammals. Nature 446: 507–512.

Bloch, J.I. and D.M. Boyer. 2002. Grasping primate origins. Science 298: 1606–1610.

Borths, M. and J. Hunter. 2008. Gimme shelter? Locomotor trends and mammalian survivorship at the K-Pg boundary. Journal of Vertebrate Paleontology 28: 3A.

Carrano, M.T. 1997. Morphological indicators of foot posture in mammals: a statistical and biomechanical analysis. Zoological Journal of the Linnean Society 121: 77–104.

Chen, M. and G.P. Wilson. 2015. A multivariate approach to infer locomotor modes in Mesozoic mammals. Paleobiology 41: 280–312.

Chester, S.G.B., E.J. Sargis, F.S. Szalay, J.D. Archibald, and A.O. Averianov. 2010. Mammalian distal humeri from the Late Cretaceous of Uzbekistan. Acta Palaeontologica Polonica 55: 199–211.

Chester, S.G.B., E.J. Sargis, F.S. Szalay, J.D. Archibald, and A.O. Averianov. 2012. Therian femora from the Late Cretaceous of Uzbekistan. Acta Palaeontologica Polonica 57: 53–64.

Chester, S.G.B., J.I. Bloch, D.M. Boyer, and W.A. Clemens. 2015. Oldest known euarchontan tarsals and affinities of Paleocene *Purgatorius* to primates. Proceedings of the National Academy of Sciences 112: 1487–1492.

Clemens, W.A. 2002. Evolution of the mammalian fauna across the Cretaceous-Tertiary boundary in northeastern Montana and other areas of the Western Interior, in: J.H. Hartman, K.R. Johnson, and D.J. Nichols (Eds.), The Hell Creek Formation and the Cretaceous-Tertiary Boundary in the Northern Great Plains: An Integrated Continental Record of the End of the Cretaceous. Geological Society of America Special Paper 361, Boulder, pp. 217–245.

Damuth, J.D. 1992. Taxon-free characterization of animal communities, in: AK Behrensmeyer, J.D. Damuth, W.A. Di Michele, R. Potts, H.-D. Sues, and S.L. Wing (Eds.) Terrestrial Ecosystems Through Time. The University of Chicago Press, Chicago, pp 183–203.

Deischl, D.G. 1964. The postcranial anatomy of Cretaceous multituberculate mammals, unpublished M.Sc. thesis, University of Minnesota, Minneapolis.

Fabre, A.-C., R. Cornette, A. Perrard, D.M. Boyer, G.V.R. Prasad, J.J. Hooker, and A. Goswami. 2014. A three-dimensional morphometric analysis of the locomotory ecology of *Deccanolestes*, a eutherian mammal from the Late Cretaceous of India. Journal of Vertebrate Paleontology 34: 146–156.

Fastovsky, D.E. 1987. Paleoenvironments of vertebrate-bearing strata during the Cretaceous-Paleogene transition, eastern Montana and western North Dakota. PALAIOS 2: 282–295.

Gidley, J.W. 1909. Notes on the fossil mammalian genus *Ptilodus*, with descriptions of new species. Proceedings of the United States National Museum 36: 611–627.

Granger, W. and G.G. Simpson. 1929. A revision of the Tertiary Multituberculata. Bulletin of the American Museum of Natural History 56: 601–676.

Hunter, J.P. 1999. The radiation of Paleocene mammals with the demise of the dinosaurs: evidence from southwestern North Dakota. Proceedings of the North Dakota Academy of Science 53: 141–144.

Hunter, J.P. and J.D. Archibald. 2002, Mammals from the end of the age of dinosaurs in North Dakota and southeastern Montana, with a reappraisal of geographic differentiation among Lancian mammals, in: J.H. Hartman, K.R. Johnson, and D.J. Nichols (Eds.), The Hell Creek Formation and the Cretaceous-Tertiary Boundary in the Northern Great Plains: An Integrated Continental Record of the End of the Cretaceous. Geological Society of America Special Paper 361, Boulder, pp. 191–216.

Hurum, J.H. and Z. Kielan-Jaworowska. 2008. Postcranial skeleton of a Cretaceous multituberculate mammal *Catopsbaatar*. Acta Palaeontologica Polonica 53: 545–566.

Iwaniuk, A.N., S.M. Pellis, and I.Q. Whishaw. 1999. The relationship between forelimb morphology and behavior in North American carnivores (Carnivora). Canadian Journal of Zoology 77: 1064–1074.

Ji, Q., Z.-X. Luo, C.–X. Yuan, and A.R. Tabrum. 2006. A swimming mammaliaform from the Middle Jurassic and ecomorphological diversification of early mammals. Science 311: 1123–1127.

Kielan-Jaworowska, Z. and P.P. Gambaryan. 1994. Postcranial anatomy and habits of Asian multituberculate mammals. Fossils and Strata 36: 1–92.

Kielan-Jaworowska, Z., R. Cifelli, and Z.-X. Luo. 2004. Mammals from the Age of Dinosaurs: Origins, Evolution, and Structure. Columbia University Press, New York.

Krause, D.W. and F.A. Jenkins, Jr. 1983. The postcranial skeleton of North American multituberculates. Bulletin of the Museum of Comparative Zoology 150: 199–246.

LeCain, R., W.C. Clyde, G.P. Wilson, and J. Riedel. 2014. Magnetostratigraphy of the Hell Creek and lower Fort Union Formations in northeastern Montana, in: G.P. Wilson, W.A. Clemens, J.R. Horner, and J.H. Hartman (Eds.), Through the End of the Cretaceous in the Type Locality of the Hell Creek Formation in Montana and Adjacent Areas. Geological Society of America Special Paper 503, Boulder. pp. 137–147.

Lillegraven, J.A. and J.J. Eberle. 1999. Vertebrate faunal changes through Lancian and Puercan time in southern Wyoming. Journal of Paleontology 73: 691–710.

Lillegraven, J.A., S.D. Thompson, B.K. McNab, and J.L. Patton. 1987. The origin of eutherian mammals. Biological Journal of the Linnean Society 32: 281–336.

Lofgren, D.L. 1995. The Bug Creek Problem and the Cretaceous-Tertiary transition at McGuire Creek, Montana. University of California Publications in Geological Sciences 140: 1–185.

Luo, Z.-X. 2007. Transformation and diversification in early mammal evolution. Nature 450: 1011–1019.

Luo, Z.-X. and J.R. Wible 2005. A Late Jurassic digging mammal and Early mammalian diversification. Science 308: 103–107.

Luo, Z.-X., Q. Ji, J.R. Wible, and C.-X. Yuan. 2003. An Early Cretaceous tribosphenic mammal and metatherian evolution. Science 302: 1934–1940.

Matthew, W.D. 1937. Paleocene faunas of the San Juan Basin, New Mexico. Transactions of the American Philosophical Society 30: 1–523.

Maas, M.C., and D.W. Krause. 1994. Mammalian turnover and community structure of the Paleocene of North America. Historical Biology 8: 91–128.

Meng, J., Y.-M. Hu, Y.-Q. Wang, X.-L. Wang, and C.-K. Li. 2006. A Mesozoic gliding mammal from northeastern China. Nature 444: 889–893.

Moore, J.R., G.P. Wilson, M. Sharma, H.R. Hallock, D.R. Braman, and P. Renne. 2014. Assessing the relationships of the Hell Creek–Fort Union contact, Cretaceous-Paleogene boundary, and Chicxulub impact ejecta horizon at the Hell Creek Formation lectostratotype, Montana, USA, in: G.P. Wilson, W.A. Clemens, J.R. Horner, and J.H. Hartman (Eds.), Through the End of the Cretaceous in the Type Locality of the Hell Creek Formation in Montana and Adjacent Areas. Geological Society of America Special Paper 503, Boulder, pp. 123–136.

Nichols, D.J. and K.R. Johnson. 2008. Plants and the K–T Boundary. Cambridge University Press, Cambridge.

O'Leary, M.A., J.I. Bloch, J.J. Flynn, T.J. Gaudin, A. Giallombardo, N.P. Giannini, S.L. Goldberg, B.P. Kraatz, Z.-X. Luo, J. Meng, X. Ni, M.J. Novacek, F.A. Perini, Z.S. Randall, G.W. Rougier, E.J. Sargis, M.T. Silcox, N.B. Simmons, M. Spaulding, P.M. Velazco, M. Weksler, J.R. Wible, and A.L. Cirranello. 2013. The placental mammal ancestor and the post-K-Pg radiation of placentals. Science 339: 662–67.

Polly, P.D. 2008. Adaptive zones and the pinniped ankle: a 3D quantitative analysis of carnivoran tarsal evolution, in: E. Sargis and M. Dagosto (Eds.), Mammalian Evolutionary Morphology: a Tribute to Frederick S. Szalay. Springer, Dordrecht, pp. 167–196.

Renne, P.R., A.L. Deino, F.J. Hilgen, K.F. Kuiper, D.F. Mark, W.S. Mitchell III, L.E. Morgan, R. Mundil, and J. Smit. 2013. Time scales of critical events around the Cretaceous-Paleogene boundary. Science 339: 684–687.

Robertson, D.S., M.C. McKenna, O.B. Toon, S. Hope, and J.A. Lillegraven 2004. Survival in the first hours of the Cenozoic. Geological Society of America Bulletin 116: 760–768.

Romer, A.S. 1959. *The Vertebrate Story*. University of Chicago Press, Chicago, IL. pp. 1–437.

Simpson, G.G. 1935. The Tiffany Fauna, Upper Paleocene II.–Structure and relationships of *Plesiadapis*. American Museum Novitates 816: 1–30.

Simpson, G.G., and H.O. Elftman. 1928. Hind limb musculature and habits of a Paleocene Multituberculate. American Museum Novitates 333: 1–19.

Sloan, R.E. and L. Van Valen. 1965. Cretaceous mammals from Montana. Science 148: 220–227.

Smith, F.A., A.G. Boyer, J.H. Brown, D.P. Costa, T. Dayan, S.K.M. Ernest, A.R. Evans, M. Fortelius, J.L. Gittleman, M.J. Hamilton, L.E. Harding, K. Lintulaakso, S.K. Lyons, C. McCain, J.G. Okie, J.J. Saarinen, R.M. Sibly, P.R. Stephens, J. Theodor, and M.D. Uhen. 2010. The evolution of maximum body size of terrestrial mammals. Science 330: 1216–1219.

Sprain, C.J., P.R. Renne, G.P. Wilson, and W.A. Clemens. 2015. High-resolution chronostratigraphy of the terrestrial Cretaceous-Paleogene transition and recovery

interval in the Hell Creek region, Montana. Geological Society of America Bulletin. 127: 393–409.

Springer, M.S., W.J. Murphy, E. Eizirik, and S.J. O'Brien. 2003. Placental mammal diversification and the Cretaceous-Tertiary boundary. Proceedings of the National Academy of Sciences 100: 1056–1061.

Stucky, R.K. 1990. Evolution of land mammal diversity in North America during the Cenozoic. Current Mammalogy 2: 375–432.

Swisher, C.C., III, L. Dingus, and R.F. Butler. 1993. 40Ar/39Ar dating and magnetostratigraphic correlation of the terrestrial Cretaceous-Paleogene boundary and Puercan mammal age, Hell Creek–Tullock formations, eastern Montana. Canadian Journal of Earth Sciences 30: 1981–1996.

Szalay, F.S. 1984. Arboreality: is it homologous in metatherian and eutherian mammals?, in M.K. Hecht, B. Wallace, and G.T. Prance (Eds.), Evolutionary Biology Vol. 18. Plenum Press, New York, pp. 215–258.

Szalay, F.S. 1994. Evolutionary history of the marsupials and an analysis of osteological characters. Cambridge University Press, New York.

Szalay, F.S. and M. Dagosto. 1980. Locomotor adaptations as reflected on the humerus of Paleogene primates. Folia Primatologica 34: 1–45.

Szalay, F.S. and R.L. Decker. 1974. Origins, evolution, and function of the tarsus in Late Cretaceous Eutheria and Paleocene primates, in: F. A. Jenkins Jr. (Ed.), Primate Locomotion. Academic Press, Inc., New York, pp. 223–259.

Szalay, F.S. and E.J. Sargis, 2001. Model-based analysis of postcranial osteology of marsupials from the Palaeocene of Itaborai (Brazil) and the phylogenetics and biogeography of Metatheria. Geodiversitas 23: 139–302.

Van Valen, L.M. 1978. The beginning of the Age of Mammals. Evolutionary Theory 4: 45–80.

Van Valkenburgh, B. 1987. Skeletal indicators of locomotor behavior in living and extinct carnivores. Journal of Vertebrate Paleontology 7: 162–82.

Weisbecker, V. and D.I. Warton. 2006. Evidence at hand: diversity, functional implications, and locomotor prediction in intrinsic hand proportions of diprotodontian marsupials. Journal of Morphology 267: 1469–1485.

Wible, J.R., G.W. Rougier, M.J. Novacek, and R.J. Asher. 2007. Cretaceous eutherians and Laurasian origin for placental mammals near the K/T boundary. Nature 447: 1003–1006.

Wilf, P., K.R. Johnson, and B.T. Huber. 2003. Correlated terrestrial and marine evidence for global climate changes before mass extinction at the Cretaceous–Paleogene boundary. Proceedings of the National Academy of Sciences: 599–604.

Wilson, G.P. 2004. A quantitative assessment of evolutionary and ecological change in mammalian faunas leading up to and across the Cretaceous-Tertiary boundary in northeastern Montana. Unpublished Ph.D. dissertation, University of California Berkeley, Berkeley.

Wilson, G.P. 2005. Mammalian faunal dynamics during the last 1.8 million years of the Cretaceous in Garfield County, Montana. Journal of Mammalian Evolution 12: 53–75.

Wilson, G.P. 2013. Mammals across the K/Pg boundary in northeastern Montana, U.S.A.: dental morphology and body-size patterns reveal extinction selectivity and immigrant fueled ecospace filling. Paleobiology 39: 429–469.

Wilson, G.P. 2014. Mammalian extinction, survival, and recovery dynamics across the Cretaceous-Paleogene boundary in northeastern Montana, in: G.P. Wilson, W.A. Clemens, J.R. Horner, and J.H. Hartman (Eds.), Through the End of the Cretaceous in the Type Locality of the Hell Creek Formation in Montana and Adjacent Areas. Geological Society of America Special Paper 503, Boulder, pp. 365–392.

Wilson, G.P., A.R. Evans, I.J. Corfe, P.D. Smits, M. Fortelius, and J. Jernvall. 2012. Adaptive radiation of multituberculate mammals before the extinction of dinosaurs. Nature 483: 457–460.

Wilson, G.P., D.G. DeMar Jr., and G. Carter. 2014. Extinction and survival of salamander and salamander-like amphibians across the Cretaceous-Paleogene boundary in northeastern Montana, in: G.P. Wilson, W.A. Clemens, J.R. Horner, and J.H. Hartman (Eds.), Through the End of the Cretaceous in the Type Locality of the Hell Creek Formation in Montana and Adjacent Areas. Geological Society of America Special Paper 503, Boulder, pp. 271–297.

Wing, S.L. and L.D. Boucher. 1998. Ecological aspects of the Cretaceous flowering plant radiation. Annual Review of Earth and Planetary Science 26: 379–421.

CHAPTER 2:

MAMMALIAN FEMORA ACROSS THE CRETACEOUS-PALEOGENE BOUNDARY IN EASTERN MONTANA

Abstract

Our understanding of latest Cretaceous and earliest Paleogene mammalian evolution is based almost entirely on the dental fossil record. Mammalian postcranial fossils are rare and mostly found as isolated elements in latest Cretaceous and earliest Paleogene vertebrate microfossil assemblages of North America. Although placing these fossils in a tooth-based taxonomic framework is difficult, they can provide insight into locomotor diversity and habitat preference to complement diet reconstructions and diversity estimates from dental fossils. Here, we describe 64 femora of mammals recovered from latest Cretaceous (Lancian) and earliest Paleogene (Puercan) localities in eastern Montana. We sorted these based on morphology and size (morphotypes). In some cases, morphotypes were tentatively assigned to dentally based taxa that are known from these strata.

Although our resulting femoral dataset is small relative to the study area's dental dataset, we show several key findings. First, there is a greater morphological diversity of multituberculate femora than previously recognized, especially in the latest Cretaceous sample. In contrast, metatherians, which have a high relative abundance in Lancian Hell Creek Formation dental assemblages, are absent from our postcranial samples; eutherian femora are only present in the Puercan assemblages. Second, we record a minor decrease in morphotype richness across the KePg boundary that is associated with an increase in mean specimen size, due to the appearance of a few significantly larger-bodied, immigrant taxa. Among the eutherians, there are two specimens of larger-bodied early Puercan

archaic ungulates, a very large specimen of a middle/late Puercan taeniodont, pantodont, or triisodontid, as well as a specimen possibly attributed to a “plesiadapiform” archaic primate. Third, preliminary functional morphologic analyses of the more complete specimens suggest that locomotor diversity increased from mainly arboreal or terrestrial/saltatorial multituberculates in the latest Cretaceous to include a fossorial multituberculate and potentially an arboreal eutherian in the early Paleocene. These patterns parallel those previously reported from a dental dataset and indicate that postcranial data are valuable as an independent means to test hypotheses of taxonomic and ecomorphological diversity across the K-Pg boundary.

1. Introduction

The Cretaceous-Paleogene (K-Pg) boundary marks a critical turning point in mammalian evolution. The fossil record of Cretaceous and early Paleocene mammals consists predominantly of isolated teeth and fragmentary jaws. From this fossil material, researchers have tracked temporal patterns of taxonomic diversity and dental morphological disparity, reconstructed diets and body sizes, and interpreted these relative to K-Pg events (e.g., Alroy 1999; Smith et al. 2010; Wilson et al. 2012; Wilson 2013, 2014). Relatively complete latest Cretaceous and earliest Paleogene mammal skeletons are rare, particularly in North America (e.g., Kielan-Jaworowska 1977, 1979; Jenkins and Krause 1983; Krause and Jenkins 1983; Novacek et al. 1997; Muizon 1998; Ji et al. 2002; Luo et al. 2003, 2011); however, older, relatively complete Mesozoic mammal skeletons suggest greater ecological diversification among early mammals than previously inferred from the dental record, and highlight the importance of postcranial data in more fully assessing K-Pg taxonomic, morphological, and ecological diversity (e.g., Luo 2007).

Our study area in eastern Montana has an extensive fossil record of mammals that is tied into a high-resolution chronostratigraphic framework across the K-Pg boundary (Archibald 1982; Lofgren 1995; Clemens 2002; Wilson 2005, 2014). The chronostratigraphic framework spans ca. 3.2 Ma and integrates data from the K-Pg boundary clay layer, radiometric ages, as well as litho-, bio-, and magnetostratigraphy from multiple local sections (see Swisher et al. 1993; Renne et al. 2013; Wilson 2005, 2014; LeCain et al. 2014; Moore et al. 2014). A long history of paleontology field work in the study area (Clemens 2002; Clemens and Hartman 2014) has led to the recovery of thousands of

latest Cretaceous and earliest Paleocene mammalian fossils. The resultant collections of isolated teeth and fragmentary jaws have been intensively studied (e.g., Archibald 1982; Lofgren 1995; Wilson 2005); however, the hundreds of isolated postcranial elements have been largely neglected (Sloan and Van Valen 1965; Clemens 2002). There are a few exceptions, including analyses of the postcranial remains from the highly productive but temporally-mixed (latest Cretaceous–earliest Paleogene) Bug Creek Channel localities in western McCone County, Montana (e.g., Deischl 1964; Sloan and Van Valen 1965; Szalay and Decker 1974) and analyses of the postcranial remains of a few select taxa and/or elements (e.g., Deischl 1964; Szalay 1994; Borths and Hunter 2008; Chester et al. 2012a).

Here, we describe 64 partial mammalian femora from 27 localities in the Hell Creek and Tullock formations of eastern Montana with the aim of improving our understanding of K-Pg mammalian evolution and ecology, as well as the magnitude and selectivity of the mass extinction and subsequent recovery. We assign these partial femora to 16 morphotypes and attribute many of these to genus, and in rare cases species, resulting in taxonomic working hypotheses. We also assess body-size patterns and analyze functional morphology of select specimens to assess temporal patterns of mammalian ecological diversity in our study area. These results complement ongoing analyses of other postcranial elements (e.g., humerus, astragalus, calcaneum), and provide an independent means of testing hypotheses of mammalian extinction and recovery that have previously only been evaluated on the basis of the dental fossil record from this study area.

Institutional abbreviations.—**AMNH**, American Museum of Natural History, New York, New York, U.S.A.; **CCMGE**, Czernyshev's Central Museum of Geological Exploration, St.

Petersburg, Russia; **CR**, indicates specimens in the Cernay-lès-Reims collection, collected from the Mont du Berru locality, that are curated at the Musée National d'Histoire Naturelle, Paris, France; **DMNH**, Denver Museum of Nature and Science, Denver, Colorado, U.S.A.; **LSUMG**, Louisiana State University Museum of Geoscience (now the LSU Museum of Natural History), Baton Rouge, Louisiana, U.S.A.; **MOR**, Museum of the Rockies, Montana State University, Bozeman, Montana, U.S.A.; **MNHN**, Musée National d'Histoire Naturelle, Paris, France; **PM**, Paleontological Center of the Mongolian Academy of Sciences, Ulaanbaatar, Mongolia; **TMM**, Texas Memorial Museum, Austin, Texas, U.S.A.; **UALVP**, University of Alberta, Edmonton, Alberta, Canada; **UCM**, University of Colorado Museum, Boulder, Colorado, U.S.A.; **UCMP**, University of California Museum of Paleontology, Berkeley, California, U.S.A.; **UM**, University of Michigan Museum of Paleontology, Ann Arbor, Michigan, U.S.A.; **UMVP**, University of Minnesota, Minneapolis, Minnesota, U.S.A.; **UNM**, Department of Geology, University of New Mexico, Albuquerque, New Mexico, U.S.A.; **USGS**, U.S. Geological Survey, Denver, Colorado, U.S.A.; **USNM**, United States National Museum, Washington, D.C., U.S.A.; **UWBM**, University of Washington Burke Museum of Natural History and Culture, Seattle, Washington, U.S.A.; **ZPAL**, Institute of Paleobiology, Polish Academy of Sciences, Warsaw, Poland.

Other abbreviations.—**Eu**, Eutherian; **Mu**, Multituberculate; **m1**, first lower molar; **NALMA**, North American Land Mammal "age"; **Pu1**, early Puercan NALMA; **Pu2/3**, middle-late Puercan NALMA.

2. Materials

2.1. Study Area and Specimens

Our collection of partial femora across the Cretaceous-Paleogene boundary derive from channel-lag and overbank vertebrate microfossil sites in the Hell Creek and Tullock formations of the Williston Basin in eastern Montana (Garfield and McCone counties, with additional material from Carter and Dawson counties; Clemens 2002; Fig. 2.1). The fine-grained sediments characteristic of the Hell Creek Formation are fluvial in origin, largely flood-plain and crevasse-splay deposits representative of a broad, alluvial plain with meandering rivers of moderate size (Fastovsky 1987). Water table increases coincident with the deposition of the overlying Tullock Formation resulted in a landscape with more standing water and large ponds, and a formation that is characterized by larger and more laterally continuous coals and much larger channels than in the Hell Creek Formation (Fastovsky 1987). As in many other fluvial deposits, the microvertebrate localities in both the Hell Creek and Tullock Formations are spatially and temporally averaged to varying degrees, such that deposits in some cases likely broadly sample the landscape rather than specific microhabitats (Fastovsky 1987; Lofgren 1995; Clemens 2002).

In the Western Interior of North America, the K-Pg boundary approximates the boundary between the Lancian and Puercan North American Land Mammal "ages" (NALMAs; Cifelli et al. 2004; Lofgren et al. 2004). The fossil assemblages from the Hell Creek Formation are for the most part Lancian in age (ca. 68–66.04 Ma; Swisher et al. 1993; Renne et al. 2011, 2013; Wilson 2014). Those from the lowermost Tullock Formation are typically early Puercan in age (Pu1 interval zone, 66.04–65.99 Ma; Swisher et al. 1993;

Renne et al. 2011, 2013; Wilson 2014), although in eastern Garfield and western McCone counties a few Pu1 assemblages are from the uppermost Hell Creek Formation and a few assemblages from the lowermost Tullock Formation are reworked across the K-Pg boundary (Lancian/Pu1 mixed, e.g., Bug Creek Anthills; Lofgren 1995). The fossil assemblages from the middle of the Tullock Formation are here interpreted as middle/late Puercan or Pu2/3 undifferentiated (65.99–65.15 Ma; Swisher et al. 1993; Renne et al. 2011, 2013; Wilson 2014), following Clemens (2002).

Sixty-four of 92 femora are sufficiently preserved to be assessed in a comparative context; the remaining 28 femora (all proximal) are poorly preserved and are not considered further in our descriptions or comparisons. Of the 64 partial femora (62 proximal and two distal fragments) examined herein, 16 are from Lancian assemblages, 27 are from the Lancian/Pu1 mixed assemblages, seven are from Pu1 assemblages, and 14 are from Pu2/3 assemblages (Table S2.1).

3. Methods

3.1. Taxonomic Scope

The extensive dental fossil record from the study area indicates a mammalian fauna of multituberculates, metatherians, and eutherians (e.g., Archibald 1982; Clemens 2002; Wilson 2013). No other major mammalian clades are known from the study area or from contemporaneous faunas in the Western Interior of North America (Cifelli et al. 2004; Lofgren et al. 2004). Thus, we used these major taxa as a starting point for comparative study of our femur specimens.

3.2. Osteological Terminology

Osteological terminology for multituberculate specimens follows Krause and Jenkins (1983), including reference to the femur in dorsal and ventral aspect, rather than 'anterior' and 'posterior', as this better reflects the presumed life position of this element in multituberculates. The osteological terminology of therian specimens follows that of recent papers (e.g., Szalay and Sargis 2001; Chester et al. 2012b), including reference to the femur in anterior and posterior aspects. Although two terminological systems may cause some confusion, we employ both to facilitate comparisons with previously published descriptions of multituberculate and therian femora, respectively (e.g., Matthew 1937; Krause and Jenkins 1983; Kielan-Jaworowska and Gambaryan 1994; Szalay and Sargis 2001; Chester et al. 2012b). We introduce the term *subtrochanteric fossa* to describe a fossa between portions of a proximodistally bisected subtrochanteric tubercle (Fig. 2.2).

3.3. Measurements

Contingent upon specimen completeness, we took 16 measurements on each proximal femur and five measurements on each distal femur (see Figs. 2.2 and S2.1, and Tables 2.1–3 and S2.2–3). All measurements were taken using a Leica MZ9.5 binocular dissecting microscope with a custom measuring stage that has an accuracy of 0.001 mm.

3.4. Morphotype Assignment

We established 16 femoral morphotypes following guidelines from previous studies (e.g., Deischl 1964; Szalay and Sargis 2001; Sargis 2002; Salton and Sargis 2009; Chester et al. 2010, 2012b) after careful consideration of the ontogenetic and intraspecific variation in extant mammalian species (e.g., Szalay and Sargis 2001). Unless otherwise stated, we interpret all fossil specimens with complete fusion of epiphyses to diaphyses as representative of adult individuals. Each femur morphotype was assigned an alphanumeric code (e.g., Mu8), representing an abbreviation of its higher-level taxon assignment (Mu for multituberculate, Eu for eutherian) and its ordinal rank in size (smallest to largest) among all morphotypes in that higher-level taxon, based on the mean size of specimens in the morphotype (using mediolateral proximal or distal shaft widths, FSMLP or FSMLD, respectively, depending on preservation; Table 2.1). Morphotypes were then grouped into six broader size categories (1–6), based on the size of the mediolateral shaft width just distal to the post-trochanteric fossa (see Tables 2.2–3). These size categories are on an ordinal scale, so the difference between successive femur size categories is irregular.

Taxonomic diagnoses of latest Cretaceous and earliest Paleocene mammals are most commonly based on dental features. Although our isolated femur fragments are found in

vertebrate microfossil assemblages with diagnostic dental specimens, the allochthonous nature of the fossils in these deposits means that individual femur specimens cannot be directly associated with individual dental specimens from the same localities. Instead, we constrained the possible taxonomic assignments of our 16 femur morphotypes, using the following procedure. First, we compared our material to published morphological descriptions, photographs, and figures of Late Cretaceous and Paleogene multituberculate and therian femora from North America and Asia; all comparative fossil taxa examined are listed in the Supplementary Information (Table S2.4). Because most of these comparative femora were also found as isolated elements without diagnostic dental fossils, their taxonomic assignments should be considered tentative; we follow Krause and Jenkins (1983) in using a query ('?') to indicate the uncertain taxonomic status of previously published postcranial elements that were not found in direct association with dental material or as part of an articulated skeleton. Additional comparative material of extant therians included descriptions, photographs, and figures of the marsupial *Didelphis virginiana* (Szalay and Sargis 2001), as well as members of the order Scandentia (Sargis 2002). Because higher-level taxa and time intervals are variably represented in the published material, our morphological comparisons with extinct taxa are, in some cases, coarse, uneven across taxa, and only allow family- or genus-level identifications at best.

Second, we refined our taxonomic assignments using faunal lists from the well sampled Lancian, Pu1, and Pu2/3 assemblages in the study area (Archibald 1982; Lofgren 1995; Clemens 2002; Wilson 2005, 2014). We treat dental taxa that are known from the locality that preserved the femur morphotype in question as the most likely candidates for our morphotypes.

Third, we followed previous workers (e.g., Deischl 1964) in using size to discriminate among plausible candidate taxa. For multituberculates, we used the length of the first lower molar (m1 length) as a proxy for size comparisons. To estimate m1 length for our isolated femur specimens, we developed a predictive formula based on linear regressions of log-transformed femur dimensions (head and shaft diameters) and dental dimensions in a comparative dataset. The taxa in the comparative dataset are known from femur and dental specimens that were found in association (e.g., articulated skeleton) or were found in isolation but confidently assigned to the same taxon (Table S2.4–5). The linear regression of mediolateral shaft diameter and m1 length is significant and explained the greatest amount of the variation in the comparative dataset ($R^2 = 0.784$, *p*-value < 0.001; Fig. S2.2). A Percent Prediction Error (%PE), a comparative measure of predictive accuracy for known m1 lengths ([observed – predicted) / predicted] x 100; Table S2.5; Van Valkenburgh 1990), of 30.22% for this material indicates that femur midshaft diameter predicts m1 length well ([%PE] < 40; Van Valkenburgh 1990; Millien 2008; Millien and Bovy 2010; Table S2.5). Thus, we used this formula to predict m1 lengths of the isolated femora in our study sample (Table S2.6) and compared predictions with known m1 lengths of Lancian, Pu1, and Pu2/3 multituberculate taxa from the study area (Wilson et al. 2012). Because descriptions of Pu2/3 dental taxa from the study area are still underway, we broadly compared Puercan femur morphotypes to Pu1 and Pu2/3 dental taxa. Note that Wilson et al. (2012) found that larger multituberculates have relatively larger molars for their body mass. We similarly found that the predicted m1 lengths of larger femur specimens are smaller than expected for large taxa (Tables S2.5–6). This scaling issue likely

only affects our largest multituberculate femora (e.g., UCMP 153091, MOR 802), and in those cases we expanded our candidate pool to include larger multituberculate taxa.

3.5. Analyses

We assessed taxonomic diversity and body size changes through time according to biozone and taxon. We calculated morphotype turnover across biozone boundaries by dividing the number of morphotypes surviving in the subsequent interval by the total morphotypes in the preceding interval and compared these femora patterns to dental patterns from the same area to (Wilson 2014). We assessed changes in femur size (a proxy for body size) by calculating the range of femur sizes (a measure of disparity) and the mean individual femur size in our sample, using membership in size categories 1–6 (Tables 2.2, S2.7). Because the difference between successive femur size categories is irregular and generally increases from size 1 to size 6, our approach tends to underestimate changes in body size. We analyzed these data for gross patterns as well as for multituberculates specifically, to control for the small number of therian specimens.

We also parsed the data to investigate finer patterns seen in the dental data that are obscured by grouping all specimens together. We used our morphotype taxonomic attributions and designated resident or immigrant status according to Clemens (2002) and Wilson (2013). We first performed F tests to compare variance, and then pairwise Welch's t-tests (using either equal or unequal variances, as appropriate) to compare the difference in femur size of residents and immigrants within a single biozone (e.g., Pu1 residents compared to Pu1 immigrants), as well as residents and immigrants grouped for all Puercan

samples (e.g., Pu1 and Pu2/3 residents, compared to Pu1 and Pu2/3 immigrants; Table S2.8).

All analyses were conducted in R version 2.15.2 (R Development Core Team 2012).

4. Descriptions of Femora

4.1. Multituberculate Femora

Relative to therian femora of similar size, multituberculate femora are stout in overall appearance, with straight and wide shafts, heads that are offset from the shaft, and distal ends that are less developed (Simpson 1926; Kielan-Jaworowska and Gambaryan 1994). They also have a subtrochanteric tubercle on the dorsal aspect and a post-trochanteric fossa on the ventral aspect, both synapomorphies among multituberculates (Simpson and Elftman 1928; Krause and Jenkins 1983; Kielan-Jaworowska and Gambaryan 1994). Additional features common among multituberculate femora include proximal femora with: (i) a greater than hemispherical articular head surface; (ii) an elongate neck that is cylindrical in cross section; (iii) a greater trochanter that is aligned with the shaft, extends beyond the head, is dorsally recumbent as well as curved medially, and exhibits a large rugose area for muscle attachment on the lateral surface; (iv) a lesser trochanter that is located on the ventral aspect of the shaft and is bulbous, convex proximolaterally, concave mediodistally, and that terminates abruptly rather than passing into a ridge as in most mammals; (v) a straight shaft that is elliptical in cross section, larger mediolaterally; (vi) a lack of third trochanter; as well as distal femora with: (vii) a distal epiphysis that has a broad intercondylar notch: (viii) small articular surfaces on the condyles; and (ix) a larger lateral epicondyle than medial epicondyle (Simpson and Elftman 1928; Clemens and Kielan-Jaworowska 1979; Krause and Jenkins 1983). In contrast to Krause and Jenkins (1983), who considered the presence of the *fovea capitis* on the femoral head as diagnostic for multituberculates, the multituberculate femora studied herein lack this feature,

affirming the observations of other researchers (e.g., Granger and Simpson 1929; Kielan-Jaworowska and Gambaryan 1994).

4.1.1. Proximal femur morphotype Mu1 (Fig. 2.3A–D)

Morphotype description.—The 31 femora assigned to this group include the smallest in our collection (relative size category 1, hereafter referred to as size 1; see Table 2.2). This morphotype is characterized by a greater trochanter with a prominent rugose area that is bisected in dorsal and proximal aspects, and has a dorsolateral margin that overhangs the shaft, creating a shallow fossa (Fig. 2.3A). It additionally exhibits the following features: (i) a subtrochanteric tubercle bisected by a subtrochanteric fossa, most often with the medial portion of the tubercle larger than the lateral portion, that is flanked by a flat area laterally (Fig. 2.3A); (ii) a lesser trochanter that is triangular to hemispherical at the junction with the shaft, with a convex or pointed proximolateral margin and a mediodistal margin that ranges from concave to flat; and (iii) a post-trochanteric fossa with a lateral margin (i.e., greater trochanteric crest distal extent) that has a slight lateral bulge; a deep trochanteric fossa that extends as a groove one-fifth to one-fourth of the way up the distal part of the greater trochanter and that narrows proximally. Some specimens in this morphotype exhibit a somewhat inflated lesser trochanter proximomedial margin at the junction with the shaft. In medial view, specimens with nearly complete lesser trochanters exhibit hook-like profiles (somewhat visible on the partial lesser trochanter of UCMP 192554; Fig. 2.3C). This morphotype represents a more generalized and typical small multituberculate femur. Some morphotypes described below may share features with this Mu1 morphotype; we highlight those aspects of the morphology that differ.

Remarks.—Two additional specimens, UCMP 196965 and 196967 from loc. V70201, McCone County, MT, strongly resemble morphotype Mu1 (e.g., UCMP 192554; Fig. 2.3). However, because they do not preserve the greater trochanter, where several diagnostic features are located, they are only tentatively assigned to this morphotype.

4.1.2. Proximal femur morphotype Mu2 (Fig. 2.4A–D)

Morphotype description.—This group is represented by one size 1 specimen (Table 2.2). Diagnostic features of Mu2 include: (i) a ridge extending distally from the subtrochanteric tubercle area (Fig. 2.4A); (ii) a concave area lateral to the subtrochanteric tubercle and associated ridge, and (iii) a shallower post-trochanteric fossa than in Mu1. This morphotype is similar in size and in ventral morphology to Mu1, however, the diagnostic features support the erection of separate morphotypes; we acknowledge that additional, better-preserved specimens may later reveal these morphotypes to be within the range of variation of a single morphotype.

4.1.3. Proximal femur morphotype Mu3 (Fig. 2.5A–D)

Morphotype description.—This group is represented by two size 1 specimens (Table 2.2). Diagnostic features of Mu3 include: (i) a slightly longer femoral neck relative to that of Mu1; (ii) an undivided subtrochanteric tubercle (Fig. 2.5A); (iii) an intratrochanteric ridge that is straight (not curved) at the junction with the lesser trochanter (Fig. 2.5C); and (iv) a large trochanteric fossa. The neck of the lesser trochanter in Mu3 specimens appears less constricted than it is in other morphotypes (e.g., Mu2), though this might be due to

breakage (Fig. 2.5B). This morphotype is generally similar in size and morphology to Mu1, however, the diagnostic features currently support the erection of a separate morphotype.

4.1.4. Proximal femur morphotype Mu4 (Fig. 2.6A–D)

Morphotype description.—This morphotype is represented by one size 1 specimen (Table 2.2); the shaft was regrettably broken during the course of study (after the images in Fig. 2.6 were taken). Diagnostic features of Mu4 include: (i) a depressed and rugose area proximal and medial to the subtrochanteric tubercle (itself not a tubercle but rather a raised plane) that is between two ridges, one extending from the greater trochanter and one from the femur head and neck (Fig. 2.6A); (ii) an intertrochanteric ridge that is more shallow and curved at the junction with the lesser trochanter than in other morphotypes of this size (Mu1 and Mu3; Fig. 2.6B); (iii) a long neck that with the head forms a greater angle with the shaft than seen in other morphotypes of similar size (e.g., Mu1–Mu3); and (iv) a lesser trochanter that has a convex margin proximomedially (Fig. 2.6B). UCMP 174494 additionally has a deep trochanteric fossa that extends proximally as a narrow groove onto the greater trochanter (Fig. 2.6D).

4.1.5. Proximal femur morphotype Mu5 (Fig. 2.7A–E)

Morphotype description.—This group is represented by two size 2 specimens (Table 2.2). Diagnostic features of Mu5 include: (i) a very long neck, absolutely longer than in specimens with even larger shaft sizes (e.g., Mu6 and Mu7); (ii) a more obtuse angle formed between the head/neck and the greater trochanter/shaft than in other morphotypes (e.g.,

Mu4); and (iii) a steep, straight intertrochanteric ridge at the junction with the lesser trochanter (Fig. 2.7B).

One specimen in this morphotype (UCMP 196964) additionally has a series of parallel marks, each mark ~1 mm long, on the dorsal aspect of the femur neck (Fig. 2.7A). These marks are perpendicular to the long axis of the femoral neck and appear to be organized into pairs that are ~0.5 mm wide. In a study of Puercan faunas from the San Juan Basin in New Mexico, Sinclair and Granger (1914) indicated that up to one-quarter of specimens showed gnawing traces, which Simpson and Elftman (1928) later attributed to *Eucosmodon* supplementing its "vegetable" diet by gnawing on the bones from multituberculate carcasses. More recently, Longrich and Ryan (2010) described pairs of parallel gnaw-marks on dinosaur bone from Cretaceous deposits that they argued were made by a multituberculate. We hypothesize that the shallow marks on our Mu5 specimen are the result of an animal having made multiple, overlapping bites. The straight and parallel nature of the marks, consistent pattern of the marks being deeper dorsally and shallower ventrally, and the absence of other markings on the bone suggest mammalian gnaw marks rather than root traces, sediment abrasion, or insect damage (Roberts et al. 2007; Britt et al. 2008). If the marks on UCMP 196964 were indeed made by a small multituberculate, they would represent the earliest evidence of a multituberculate feeding on another multituberculate.

4.1.6. Proximal femur morphotype Mu6 (Fig. 2.8A–D)

Morphotype description.—This group is represented by two size 2 specimens (Table 2.2). The diagnostic features of Mu6 include: (i) a post-trochanteric fossa that is much

deeper than in all other morphotypes and that wraps around the lateral margin of the lesser trochanter (Fig. 2.8B); (ii) a lateral margin of the post-trochanteric fossa that is raised, extends mediodistally, and terminates distal to the lesser trochanter (Fig. 2.8B); (iii) an intertrochanteric ridge that is curved at the junction with the lesser trochanter (Fig. 2.8B); (iv) a stout cylindrical neck; (v) a very deep trochanteric fossa; (vi) a subtrochanteric tubercle, bisected by a small and shallow subtrochanteric fossa, that has a larger medial portion than lateral portion (Fig. 2.8A); and (vii) a lesser trochanter that has an inflated medial border at the junction with the shaft.

4.1.7. Proximal femur morphotype Mu7 (Fig. 2.9A–E)

Morphotype description.—This group is represented by two size 3 specimens (Table 2.2). Diagnostic features of Mu7 include: (i) a raised and pronounced subtrochanteric tubercle bisected by relatively deep fossa (Fig. 2.9A), which results in (ii) a straight shaft that is rhomboidal in cross-section proximally (Fig. 2.9C) and elliptical distally, wider mediolaterally (preserved on UCMP 195977 from loc. V65127, not figured); and (iii) a short, deep post-trochanteric fossa with a bulging lateral margin (Fig. 2.9C).

4.1.8. Proximal femur morphotype Mu8 (Fig. 2.10A–D)

Morphotype description.—This group is represented by 10 specimens (sizes 3–4, see Table 2.2). Diagnostic features of Mu8 include: (i) a head with approximately equal volume proximal and distal to the junction with the neck (Fig. 2.10B); (ii) a flat area extending laterally from the subtrochanteric tubercle to meet the gluteal crest; (iii) a narrow subtrochanteric fossa that bisects the subtrochanteric tubercle (Fig. 2.10A); (iv) a greater

trochanter rugosity that has a dorsal fossa, similar to that seen in Mu1 (Fig. 2.10A); (v) a rugosity distal to the post-trochanteric fossa extending the length of the preserved lateral edge of the ventral shaft; and (vi) a deep trochanteric fossa that extends up to one-third the length of the greater trochanter. Some specimens differentially exhibit a convex lesser trochanter proximomedial border.

Remarks.—Three additional size 2 specimens, UCMP 127383 (loc. V88007 from Carter Co., MT), UCMP 195980 (loc. V65127 from McCone Co., MT), and UCMP 195966 (loc. V72137 from Garfield Co., MT) are assigned to this morphotype based on morphological similarity to other Mu8 specimens but we prefer to remain tentative in this case for the following reasons: (i) no articular surfaces are preserved to assess ontogenetic stage, but they may indeed represent individuals of younger age, as they are the smallest specimens in this morphotype; and (ii) these specimens appear to lack a bisected subtrochanteric tubercle; however, this may be due to pitting, abrasion, and/or root etching.

4.1.9. Proximal femur morphotype Mu9 (Fig. 2.11A–D)

Morphotype description.—This morphotype is represented by one size 3 specimen (Table 2.2). Diagnostic features of Mu9 include: (i) a post-trochanteric fossa that is much wider mediolaterally and shallower than in any other specimen studied (Fig. 2.11B); (ii) a prominent ridge that extends distally from the subtrochanteric tubercle area (broken, Fig. 2.11A); (iii) a pronounced flat area lateral to the subtrochanteric tubercle (Fig. 2.11A); (iv) a lesser trochanter that is proximally displaced relative to the condition in other morphotypes (Fig. 2.11B); and (v) a large, deep trochanteric fossa.

4.1.10. Proximal femur morphotype Mu10 (Fig. 2.12A–D)

Morphotype description.—This group is represented by one size 5 specimen, and is the second largest multituberculate specimen described herein (Table 2.2). The diagnostic features of Mu10 include: (i) a lesser trochanter that is convex on both the proximal and distal surfaces, resulting in a circular cross-section at the junction with the shaft, rather than triangular or hemispherical as seen in all other multituberculate morphotypes and comparative material (Fig. 2.12B); (ii) an extremely tall and robust greater trochanter that appears to extend well beyond the inferred extent of the head, and that has a very large rugose area proximolaterally (Fig. 2.12A,B); (iii) a subtrochanteric tubercle that is bisected by an expanded and shallow subtrochanteric fossa and that has a larger medial tubercle portion than lateral portion (Fig. 2.12A); and (iv) a deep post-trochanteric fossa (Fig. 2.12B).

4.1.11. Proximal femur morphotype Mu11 (Fig. 2.13A–D)

Morphotype description.—This group is represented by one size 5 specimen (Table 2.2), and is the largest multituberculate specimen described herein. This proximal fragment of a right femur (MOR 882) was previously described and attributed to *Meniscoessus robustus* by Hunter et al. (1997). It preserves a nearly complete head and shaft, and partial greater and lesser trochanters; the shaft expands at the distal end of this fragmentary specimen, suggesting that only the distal epiphysis is missing (Fig. 2.13A–C). Compared to the robust Mu10 morphotype, Mu11 is more gracile. Diagnostic features of this morphotype include: (i) a relatively long neck; (ii) a very deep trochanteric fossa (Fig. 2.13D); (iii) a subtrochanteric tubercle that is more pointed than in other morphotypes,

with a ridge extending distally (Fig. 2.13A), similar to that seen in Mu2 and Mu9; (iv) a pronounced gluteal crest that extends distally along the lateral edge of the specimen to beyond the approximate mid-point of the shaft (Fig. 2.13C); (v) a crest extending from the lesser trochanter that angles more medially as it extends distally towards the mid-point of the shaft (Fig. 2.13C); (vi) a deep post-trochanteric fossa; and (vii) a shaft that is curved dorsally in lateral aspect (Fig. 2.13B).

4.1.12. Multituberculate distal femur (Fig. 2.14A–E)

Morphotype description.—UCMP 174391 is a distal fragment of a size 2–3 right femur (Table 2.2), which preserves complete condyles and more shaft proximally on the lateral side than the medial. The dorsal aspect has a clearly marked junction between the shaft and distal epiphysis (Fig. 2.14A). The patellar groove is shallow and is offset more medially relative to the mid-width of the specimen. The lateral condyle extends slightly more distally than the medial condyle; the lateral epicondyle is larger, and more rugose and well developed relative to the medial epicondyle (Fig. 2.14C,D). In distal view, the medial condyle is taller dorsoventrally and wider mediolaterally relative to the lateral condyle (Fig. 2.14E). In ventral aspect, the articular condyles are separated by a broad intercondylar fossa (or popliteal notch; Deischl 1964), and the medial condyle is wider than the lateral condyle (Fig. 2.14B). As with other multituberculate distal femora, the distal epiphysis twists laterally relative to the shaft (Fig. 2.14A; Kielan-Jaworowska and Gambaryan 1994).

4.2. Eutherian Femora

We distinguished femora of therians from those of multituberculates based on several morphological features. Most notably, in therians the femoral head is less medially offset from the longitudinal axis of the femur than in multituberculates (Clemens and Kielan-Jaworowska 1979). The third trochanter is absent in multituberculates, and varies greatly among eutherian taxa with respect to presence/absence, morphology, and position (Sargis 2002). Although metatherians are abundant in Lancian dental assemblages, we find exclusively multituberculates represented among our Lancian sample. We find therians represented among our Puercan sample and conclude these are exclusively eutherian after comparisons with extant and extinct metatherian and eutherian femora (e.g., Matthew 1937; Muizon 1998; Szalay and Sargis 2001), and because metatherians are far less abundant than eutherians in Puercan assemblages based on dental remains.

4.2.1. Proximal femur morphotype Eu1 (Fig. 2.15A–D)

Morphotype description.—This group is represented by one size 2 specimen (Table 2.2) that is approximately the size of Mu5 and Mu6 and is much smaller than the other eutherian femora described herein. UCMP 195935 has a partial head and greater and lesser trochanters, as well as an anteroposteriorly compressed shaft. Overall this specimen is poorly preserved (Fig. 2.15A–B), however, because its morphology is unique within our sample, we place it in its own morphotype. Diagnostic features of Eu1 include: (i) a lesser trochanter that is located more medially and protrudes much more from the shaft than in other eutherian morphotypes (Eu2 and Eu3; Fig. 2.15A–B); (ii) in anterior view, the medial margin of the shaft is semicircular between the head/neck and the lesser trochanter (Fig. 2.15A); and (iii) a wider, shallower trochanteric fossa than in Eu2 and Eu3 (Fig. 2.15B).

4.2.2. Proximal femur morphotype Eu2 (Fig. 2.16A–D)

Morphotype description.—This group is represented by one size 4 left proximal femur (Table 2.2) that preserves the greater trochanter, head, neck, and third trochanter, and part of the lesser trochanter. The specimen is broken just distal to the third trochanter. Diagnostic features of Eu2 include: (i) a greater trochanter that is robust and aligned with the shaft and that extends just beyond the level of the head (Fig. 2.16A); (ii) the articular surface of the head extends onto the neck dorsolaterally (Fig. 2.16A,B,D); (iii) the lesser trochanter is located on the posteromedial surface of the shaft (Fig. 2.16B); and (iv) the trochanteric fossa is large and proximodistally elongate, and shallows distally to meet the distal extent of the lesser trochanter (Fig. 2.16B). This specimen also has a greater trochanter with a large and prominent rugose area laterally (Fig. 2.16A). In posterior aspect, the articular surface of the head is directed more dorsally than in multituberculate femora. The head is hemispherical and preserves the fovea capitis on its posteromedial surface (Fig. 2.16C). The border between the head and neck is well defined (Fig. 2.16A,B); the neck is short and elliptical in cross-section, with the major axis in the dorsolateral-ventromedial direction. The lesser trochanter is elongate and extends dorsomedially to ventrolaterally (Fig. 2.16B). The third trochanter is prominent and anteriorly recumbent, and extends laterally from the shaft just below the distal end of the lesser trochanter (Fig. 2.16A,B). The shaft has an elliptical cross-section, wider mediolaterally.

4.2.3. Proximal femur morphotype Eu3 (Fig. 2.17A–D)

Morphotype description.—This group is represented by one size 4 proximal fragment of a left femur, which is slightly larger in size than Eu2 (UCMP 192674, from loc. V87076, see Table 2.2, Figs. 2.16–17). This specimen preserves the greater trochanter and neck, part of the lesser trochanter, and the proximal aspect of the third trochanter. The diagnostic features of Eu3 include: (i) a greater trochanter that is robust, triangular, and that extends beyond the head, and with greater separation between the greater trochanter and the head (Fig. 2.17A), and a lateral margin that is straighter and mediolaterally thicker than seen in Eu2 (Fig 2.17B); (iii) a head with an articular surface that does not extend laterally onto the neck (Fig. 2.17D); (iv) a neck that is, in dorsal view, thinner in cross-section anteroposteriorly than in Eu2, both absolutely and relative to specimen size (Fig. 2.17D); and (v) a trochanteric fossa with a less pronounced distal margin than in Eu2 (Fig. 2.17B). Other features of this morphotype include: a short neck, elliptical in cross-section, widest in the proximolateral to mediodistal direction; and a lesser trochanter that is morphologically similar to but shorter than in Eu2 (possibly an artifact of the greater breakage in Eu2). Based on a widening at the distal extent of the specimen, we infer that this specimen had a third trochanter (Fig. 2.17B). Where the shaft is broken, it has a triangular cross-section with a flat anterior surface.

4.2.4. Distal femur morphotype Eu4 (Fig. 2.18A–D)

Morphotype description.—This group is represented by one size 6 distal epiphysis of a femur (UCMP 145607, from loc. V73080, see Table 2.2), representing an individual that was approximately an order of magnitude larger than the next largest individuals represented in this study (e.g., Mu11, Eu2, or Eu3). It preserves nearly complete condyles

and is partially embedded in siltstone, which obscures the specimen in anterior and proximal views. In distal view, the lateral condyle is slightly wider mediolaterally than the medial condyle (Fig. 2.18A), but the condyles are more symmetrical than seen in most eutherians. There is a moderately deep patellar groove that is offset laterally and extends from the intercondylar fossa dorsally into the encasing siltstone matrix; the lateral ridge on the patellar groove is more prominent than the medial one (Fig. 2.18A). There is a clearly delineated fossa on the lateral surface of the medial condyle, within the intercondylar fossa (Fig. 2.18B). The medial epicondyle is large and well developed (Fig. 2.18D).

5. Taxonomic Affinities

5.1. Multituberculate Femora

Mu1 is the most abundant of our morphotypes, represented in Lancian, Pu1, and Pu2/3 assemblages. It has a fairly generalized multituberculate morphology and is most similar in size to femora attributed to ?*Cimexomys minor* and ?*Mesodma* sp. (Deischl 1964; Krause and Jenkins 1983). Femora of ?*C. minor* (Deischl 1964) appear stouter than our Mu1 femora, whereas those of ?*Mesodma* sp. (e.g., UMVP 1423, MCZ 20775 and 20776; Krause and Jenkins 1983: fig. 21) from the Bug Creek Anthills are similar to Mu1 femora in size and morphology, including the diagnostic features of the subtrochanteric tubercle. The predicted m1 lengths for Mu1 specimens (1.54–2.39 mm) overlap in size with m1s of small-bodied multituberculates, including *M. hensleighi*, *M. formosa*, *Microcosmodon harleyi*, *Mi. arcuatus*, *C. minor*, and smaller individuals of *Paracimexomys priscus* and *M. thompsoni* (Wilson et al. 2012; see Fox 2005 for a discussion of *Mi. harleyi* and *Mi. arcuatus* taxonomic affinities). Because *Mesodma* typically has a greater relative abundance than *Cimexomys, Paracimexomys*, and *Microcosmodon* in Lancian, Pu1, and Pu2/3 dental assemblages from the study area (Weil 1998; Wilson 2005, 2014), we suggest that Mu1 specimens are likely referable to one or more species of *Mesodma*.

Lancian Mu2 broadly resembles Mu1 in morphology (see attribution of Mu1 for details and taxa), and ?*Mesodma* sp. and ?*Cimexomys minor* in size (Deischl 1964; Krause and Jenkins 1983). However, the diagnostic feature for Mu2, a 2-mm long crest that extends distally from the subtrochanteric tubercle, is absent in descriptions and figures of similarly-sized specimens from the Bug Creek Anthills locality that have been attributed to the small-

bodied ?*M. formosa*, ?*M. thompsoni*, ?*C. minor* (Deischl 1964), and ?*Mesodma* sp. (Krause and Jenkins 1983). The predicted m1 length for Mu2 (1.91 mm) is nearest to the published range of m1 lengths of *M. hensleighi* (1.80–1.84 mm; Lillegraven 1969; Wilson et al. 2012) and is smaller than the m1 lengths of all other Lancian multituberculate taxa from the area. Based on its small size, we tentatively refer Mu2 to *M. hensleighi*.

Lancian Mu3 overlaps in size with Mu1 and Mu2 and is slightly smaller than Mu4. Mu3 resembles ?*Mesodma formosa* and ?*Cimexomys minor* (Deischl 1964) in size and overall morphology, but lacks the bisected subtrochanteric tubercle of ?*M. formosa* and the stout appearance and short neck of ?*C. minor*. It also resembles the Late Cretaceous djadochtatherioid *Nemegtbaatar gobiensis* in morphology, but is about half the size (Kielan-Jaworowska and Gambaryan 1994). The range of predicted m1 lengths of Mu3 (1.60–2.44 mm) encompasses the ranges of small Lancian multituberculates, including *M. hensleighi*, *M. formosa*, *C. minor*, and smaller individuals within *Paracimexomys priscus* and *M. thompsoni* (Wilson et al. 2012). Until more morphological information is available for this morphotype and the candidate taxa, we refrain from referring Mu3 to a lower-level taxon.

Lancian Mu4 is most similar to the Asian djadochtatherioid *Nemegtbaatar gobiensis* in head and shaft morphology and somewhat similar to that taxon in subtrochanteric tubercle morphology (ZPAL MgM-I/81; Kielan-Jaworowska and Gambaryan 1994: fig. 16). It is also similar to the djadochtatheriid *Catopsbaatar catopsaloides* (PM 120/170; Hurum and Kielan-Jaworowska 2008: fig. 8) in head/neck angle. Published North American latest Cretaceous and earliest Paleogene femora that are most similar to Mu4 are attributed to ?*Cimexomys minor* (Deischl 1964), although an image or figure capturing the subtrochanteric tubercle, a critical component for diagnosing Mu4, was not available to us.

The predicted m1 length for this specimen (2.33 mm) is within the ranges of *Mesodma formosa*, *C. minor* and *Paracimexomys priscus* (Wilson et al. 2012), however, Mu4 differs from specimens of ?*Mesodma* sp. (Deischl 1964; Krause and Jenkins 1983) in both neck and subtrochanteric tubercle morphology. Based on size and robustness, we suggest that Mu4 may be referable to the "*Paracimexomys*" group.

Mu5 is represented in the Lancian and Lancian/Pu1 mixed assemblages. We know of no published specimens that are similar in size to Mu5 specimens and have long necks and wide neck angles (e.g., the djadochtatheriid *Catopsbaatar catopsaloides* has a wide neck angle, but the femur is about twice the size of Mu5; Hurum and Kielan-Jaworowska 2008). Predicted m1 lengths of Mu5 specimens (2.84 mm) are similar to m1 lengths of *Mesodma thompsoni* (2.39–2.90 mm) and *Parectypodus foxi* (2.98 mm), and slightly larger than those of *Paracimexomys priscus* (2.30–2.80; Wilson et al. 2012). Despite the fragmentary state of Mu5 specimens, the preserved morphology differs from smaller femora attributed to ?*Mesodma* sp. Until the morphology of Mu5 and candidate taxa are better known, we refrain from attributing Mu5 to a lower-level taxon (but see discussion of taxonomic affinity of a distal femur specimen, below).

Pu2/3 Mu6 differs from all other morphotypes in this study and from all comparative specimens in the curvature of the post-trochanteric fossa and the robust gluteal crest distal and lateral to the post-trochanteric fossa. Predicted m1 lengths of Mu6 specimens (3.48–3.60 mm) place this taxon intermediate in size to the Puercan *Cimexomys gratus* (3.43 mm) and *Stygimys kuszmauli* (4.44 mm; Wilson et al. 2012). The post-trochanteric fossa of Mu6 is more similar to descriptions of the strongly developed post-trochanteric fossa of the smaller ?*C. minor* than to the short and straight fossa of ?*S.*

kuszmauli (Deischl 1964). If a strongly developed post-trochanteric fossa is diagnostic of *Cimexomys*, then Mu6 might represent the femur of *C. gratus*.

Mu7 is present in the Lancian/Pu1 mixed assemblage and the Pu1 assemblage. It has a subtrochanteric tubercle morphology that is unique relative to other morphotypes described herein and comparative specimens. In overall size, Mu7 overlaps with Mu8. Mu7 specimens are morphologically most similar to a femur attributed to ?*Stygimys kuszmauli* (Deischl 1964) in exhibiting a short, deep post-trochanteric fossa. Mu7 is also morphologically similar to the femur of the djadochtatherioid *Nemegtbaatar gobiensis* (Kielan-Jaworowska and Gambaryan 1994: fig. 16C) in possessing a greater trochanter that is only slightly dorsally recumbent. In contrast, the femora of North American ptilodontoids *Ptilodus kummae* and ?*Mesodma* sp. and eucosmodontid ?*Eucosmodon* sp. (Krause and Jenkins 1983) have a greater trochanter that is more dorsally recumbent than seen in Mu7. The predicted m1 length of the only measurable Mu7 specimen (4.66 mm) is nearest to the m1 length of *S. kuszmauli* (4.44 mm; Wilson et al. 2012). The second Mu7 specimen, too fragmentary to measure a shaft diameter, is smaller than the other Mu7. Because both these Mu7 specimens resemble the specimen attributed to ?*S. kuszmauli* by Deischl (1964), and the m1 length estimates for these specimens are similar to that of *S. kuszmauli* (Wilson et al. 2012), we suggest Mu7 possibly represents ?*S. kuszmauli*, a Pu1 taxon that is dentally abundant at this Mu7 locality (UCMP locality V74111, "Worm Coulee 1"; Table S2.1).

Mu8 occurs in Lancian through Pu2/3 assemblages. These specimens are similar in morphology and size to the North American ptilodontid ?*Ptilodus montanus* (Gidley 1909); they are smaller than, but similar in morphology, to the ptilodontoid *P. kummae* (Krause and Jenkins 1983) and the eucosmodontid ?*Eucosmodon* sp. (Granger and Simpson 1929;

Krause and Jenkins 1983). The range of predicted m1 lengths of Mu8 (2.85–5.83 mm) is broad, possibly indicating that this morphotype includes multiple taxa. *Mesodma thompsoni* (Lancian–Pu2/3), *Cimexomys gratus* (Pu1–Pu2/3), and ?*Stygimys kuszmauli* (Pu1–Pu2/3) have m1 lengths and temporal ranges that overlap with those of Mu8, respectively (Wilson et al. 2012). Other taxa that fall within the range of predicted m1 lengths of Mu8 and occur in one interval zone in the study area, include (in order of increasing m1 length; Clemens 2002; Wilson et al. 2012; Wilson 2014): the Lancian *Parectypodus foxi*, *Cimolodon nitidus*, and *Cimolomys gracilis*; and the Pu2/3 *S. camptorhiza* and *E. americanus*. Morphological similarities with ?*Eucosmodon.* sp. (Granger and Simpson 1929; Krause and Jenkins 1983) suggest that some Pu2/3 specimens of Mu8 might be attributable to *E. americanus*; we are unable to compare Mu8 to Lancian candidate taxa because femora for these taxa have not been reported. Mu8 has a fairly generalized morphology and specimens in this morphotype are likely representative of one or more of the medium-sized multituberculate taxa listed above.

Lancian Mu9 is most similar in size to Mu7 and Mu8, and despite the fragmentary state of this specimen, but its morphology is unique relative to previously published K-Pg multituberculate femora. The predicted m1 length of this morphotype (4.33 mm) is within the size range of smaller individuals of *Cimolodon nitidus* and *Cimolomys gracilis* (Wilson et al. 2012). Because the relative abundance of *C. nitidus* is greater than that of *C. gracilis* in most Lancian assemblages from the study area, we speculate that Mu9 is more likely referable to *C. nitidus* than to *C. gracilis*.

Mid/late Puercan (Pu2/3) Mu10 is larger than all multituberculate specimens studied herein excepting Mu11. It is similar in size and morphology to femora of the Pu1

taeniolabidids ?*Catopsalis joyneri* (UMVP 1427; Deischl 1964: fig. 29) and ?*C. alexanderi* (UCM 43554; Middleton 1982: fig. 6), and similar in size to that of ?*Eucosmodon* (Granger and Simpson 1929; Krause and Jenkins 1983). Mu10 is only ~40% of the size of the femur attributed to ?*Taeniolabis taoensis* (AMNH 3036; Sloan 1981: fig. 6.15; comparison of FSMLD, see Tables 2.1–2); AMNH 3036 also lacks a greater trochanter and the description lacks a figure of the specimen in dorsal view; as a result, morphological comparisons with Mu10 are limited. In Mu10, the lesser trochanter is circular rather than triangular in cross section and it possesses a faint crest that extends distally; this differs from the condition in ?*C. joyneri* but is similar to ?*C. alexanderi*. The predicted m1 length of Mu10 (6.33 mm) is larger than the range of m1 lengths in the eucosmodontid *E. americanus* (5.60 mm), and smaller than in *C. alexanderi* (8.20–9.30 mm) and the larger taeniolabidids (including *C. joyneri*, *C. foliatus* and the much larger *Taeniolabis* sp.; Wilson et al. 2012). Because the shaft width measurement used in the formula to predict m1 length is a minimum estimate of size in this broken specimen and because our predictive formula likely underestimates m1 length for larger-bodied taxa (see Materials and Methods), Mu10 is more likely from a taxon that is larger than *Eucosmodon* but probably not as large as *Taeniolabis* sp. Thus, we suggest that Mu10 may be attributable to *Catopsalis* sp., a taxon that is recorded in the Pu2/3 assemblages from the study area.

The Mu11 specimen is the largest multituberculate in our studied collection. This specimen's provenance is not well known, but available locality information indicates that it is from the Hell Creek Formation and is Lancian in age (Hunter et al. 1997). This specimen was previously attributed to *Meniscoessus robustus* based on its large size (Hunter et al. 1997). Our predictive formula based on shaft width likely underestimates m1

length for larger femora, so the m1 length for Mu11 is potentially larger than the predicted value of 6.68 mm. This morphotype is nearest in size to the largest Lancian multituberculates in our study area, the cimolomyids *M. robustus* and *Essonodon browni*. Thus, this specimen is potentially referable to either taxon. However, because *M*. *robustus* is more abundant than *E*. *browni* in Lancian assemblages in our study area (e.g., Wilson 2005, 2014), we see no reason to change the taxonomic assignment given by Hunter et al. (1997).

Our distal femur of a Lancian multituberculate (UCMP 174391) overlaps in shaft size with the Lancian morphotype Mu5. UCMP 174391 most closely resembles ?*Mesodma* sp. (UMVP 1424 and MCZ 20777; Deischl 1964; Krause and Jenkins 1983) in nearly all respects except that it is ~20–30% larger and lacks the extension of the patellar groove proximally beyond the epiphyseal junction, a feature that is seen in small specimens of ?*Mesodma* sp. (Krause and Jenkins 1983). We suggest that this distal femur fragment is referable to Mu5 and possibly to the larger *M. thompsoni*.

5.2. Eutherian Femora

Pu2/3 Eu1 is much smaller than our other eutherian morphotypes and bears greater morphological resemblance to femora of extant taxa (e.g., *Ptilocercus*; Sargis 2002) than to older eutherian femora from the Coniacian of Uzbekistan (Averianov 2000; Chester et al. 2012b), or younger eutherian femora, e.g., Paleocene archaic ungulates and leptictids from the San Juan Basin, New Mexico (Matthew 1937). Eu1 is morphologically similar to femora of Paleocene "plesiadapiform" archaic primates (Bloch et al. 2007), including the paromomyid *Ignacius clarkforkensis* (Bloch et al. 2007), the carpolestid *Carpolestes simpsoni* (Bloch and Boyer 2002), and the plesiadapids ?*Nannodectes gidleyi* (=*Plesiadapis*

gidleyi; Simpson 1935), *Plesiadapis cookei* (Bloch et al. 2007), and *P. tricuspidens* (Szalay et al. 1975). Specifically, Eu1 possesses the following "plesiadapiform" features: (i) an enlarged lesser trochanter that protrudes medially, likely subequal to the head (in contrast to e.g., leptictids; Matthew 1937; Szalay et al. 1975; Rose 1999); (ii) a trochanteric fossa that is well marked and deep (Szalay and Delson 1979); and based on preservation proximal to the breakage, we speculate that Eu1 would have possessed (iii) a smaller area for quadratus femoris attachment on the posterior surface between the greater and lesser trochanters (Beard 1993); and (iv) a third trochanter that was proximally overlapped by the lesser trochanter (Szalay et al. 1975; Szalay and Delson 1979). This combination of features is consistent with referral of Eu1 to a "plesiadapiform" taxon. Dental specimens of the purgatoriid *Purgatorius* are abundant in the Pu2/3 assemblage that preserved the Eu1 specimen (UCMP loc. V99438; Clemens 2002, 2004; Wilson 2014). *Pandemonium dis* is another "plesiadapiform" that is present but less abundant in this assemblage (Clemens 2002; Wilson 2014). However, we caution that very little is known about the postcrania of Paleocene small-bodied eutherians, so broad taxonomic comparisons are not yet possible.

Pu1 Eu2 resembles larger specimens attributed to Paleocene and Eocene archaic ungulates. Specifically, Eu2 is morphologically most similar to the periptychid *Ectoconus ditrigonus*, although *E. ditrigonus* has a proximal end that is mediolaterally wider, a neck that is longer and more slender, and a head diameter that is approximately six-times larger than Eu2 (Matthew 1937). Eu2 also morphologically resembles arctocyonid femora of the Paleocene *Arctocyon primaevus* (Russell 1964: fig. 38; Argot 2013: fig. 13) and the Eocene *Chriacus* sp. (Rose 1987), although femora from both taxa are approximately three-times larger than Eu2, and *A. primaevus* differs in posterior aspect. Of all comparative material

examined, arctocyonids *Chriacus* sp. and *A. primaevus* are morphologically the most similar to Eu2. Smaller species of *Chriacus* spp., including some present in eastern Montana, are within the size range to be candidate taxa for Eu2, however, *Chriacus* spp. appears in the study area later in the Paleocene (middle/late Puercan and early Torrejonian) than the material in our study (Clemens and Wilson 2009). Of the archaic ungulates present in Montana during the Pu1 interval zone, three periptychids (*Mimatuta minuial*, *M*. *morgoth*, and Periptychidae sp. A; Wilson 2014) are represented, as well as four early arctocyonids (*Baioconodon engdahli*, *B*. *nordicum, Oxyprimus erikseni*, and *Protungulatum donnae*; Wilson 2014). The small size of Eu2 is more likely representative of the small archaic ungulates *Mimatuta*, *Oxyprimus*, and *Protungulatum*, rather than the much larger *Baioconodon* spp. (Clemens 2002; Wilson 2013).

Pu1 Eu3 is slightly larger than Eu2, larger than all multituberculates except Mu10 and Mu11, but much smaller than the distal femur of Eu4. Despite having a taller greater trochanter and a head more medially offset from the shaft than in comparative archaic ungulate taxa, this Pu1 specimen most closely resembles femora of Paleocene periptychids *Ectoconus ditrigonus* (Matthew 1937), *Mithrandir gillianus* (=*Gillisonchus gillianus*; Rigby 1981), and *Periptychus carinidens* (=*P. rhabdodon*; Matthew 1937). Although the resemblance to the above periptychids (and a comparative lack of resemblance to the arctocyonid *Chriacus* sp.; Rose 1987) tentatively suggests Eu3 is from a Pu1 periptychid, we acknowledge that with our small sample size of comparative femora we cannot eliminate Paleocene arctocyonids as candidate taxa. Periptychid taxa in Pu1 assemblages from our study area include *Mimatuta minuial*, *M*. *morgoth*, and Periptychidae sp. A, with *Mimatuta* spp. being the most common; Pu1 arctocyonid taxa include *Baioconodon engdahli*, *B*.

nordicum, Oxyprimus erikseni, and *Protungulatum donnae* (Wilson 2014). *Baioconodon* spp. are too large to be candidate taxa for Eu3. Thus, at present, Eu3 is attributed to a Pu1 archaic ungulate, possibly within the Periptychidae.

Pu2/3 Eu4 is substantially larger than any other specimen described in this study. Based on dental evidence, several larger-bodied mammals occur in Pu2/3 assemblages of northeastern Montana (e.g., Maas and Krause 1994; Clemens 2002), including two triisodontids *Eoconodon hutchisoni* and *E. nidhoggi*, a taeniodont cf. *Wortmania* (Clemens 2013), an unnamed pantodont, and possibly an unnamed oxyaenid creodont (Clemens unpublished results; Wilson 2014). Descriptions of early Paleocene eutherian femora in this size range are rare and nearly all descriptions are of fragmentary specimens from the San Juan Basin (Matthew 1937; Schoch 1986; Standhardt 1986). A femoral head of ?*Eoconodon coryphaeus* was described by Standhardt (1986). Its diameter suggests that the femur of ?*E. coryphaeus* was larger than Eu4. The m1s of *E. hutchinsoni* and *E. nidhoggi* are smaller than ?*E. coryphaeus* and thus *Eoconodon* is still a plausible candidate taxon for Eu4 (Clemens 2011). Although our comparisons are admittedly constrained by the taxa with preserved femora, Eu4 appears morphologically similar to the San Juan Basin pantodont *Pantolambda bathmodon* (Matthew 1937) and the taeniodonts *Psittacotherium* and *Ectoganus* (Schoch 1986); however, the distal epiphysis of Eu4 is smaller than in those taxa, and Eu4 lacks the condylar asymmetry seen in those taeniodont taxa. We were unable to make morphological comparisons with the beaver-sized taeniodont *Wortmania otariidens* because the San Juan Basin specimen lacks a distal end (Matthew 1937; Schoch 1986), but *W. otariidens* appears to be larger than Eu4 (Matthew 1937). Thus, Eu4 represents a large-bodied eutherian from the Pu2/3 interval whose distal femur has not been previously

described. Until more relevant material is available, we refrain from assigning Eu4 to a lower-level taxon.

6. Discussion

The K-Pg boundary marked the beginning of a major episode of taxonomic and ecomorphologic diversification in mammals (e.g., Alroy 1999; Smith et al. 2010). Previous analyses of diversity across this boundary have relied mostly on dental data aggregated over coarse geographic and temporal scales (e.g., regional or continental, 1–2 myr time bins; Lillegraven 1972; Alroy 1999; Maas and Krause 1994). The large mammalian fossil database and high-resolution chronostratigraphic framework from our study area (Archibald, 1982; Lofgren 1995; Clemens 2002; Wilson 2005, 2013, 2014) have helped refine our understanding of community-scale patterns of diversity across a 3-myr interval spanning the K-Pg boundary. Analyses of dental data show changes in taxonomic diversity (richness and relative abundances), body size, and ecomorphological diversity (dental shape/feeding ecology) leading up to, across, and following the K-Pg boundary that have implications for the causal mechanisms of the K-Pg mass extinction, extinction selectivity, survivorship, and the timing, composition, and mode of the recovery (Archibald 1983; Clemens 2002; Wilson 2005, 2013, 2014; Calede and Wilson 2011; Wilson and Self 2011). These changes appear to be independent of differences in depositional environments among the fossil localities. For example, in eastern Garfield and western McCone counties, Puercan (Pu1) dental assemblages that are derived from the uppermost Hell Creek Formation do not differ compositionally from Pu1 assemblages that are derived from the lowermost Tullock Formation (Lofgren 1995; Clemens 2002). Likewise, Lancian dental assemblages from our study area (Hell Creek Fm) are comparable to Lancian assemblages from further east in southwestern North Dakota that derive from deposits equivalent to the

lowermost Tullock Formation (Bercovici et al. 2009). Conversely, Pu2/3 assemblages from our study system are compositionally distinct from Pu1 assemblages, despite both being derived from channel lag deposits within the Tullock Formation (Clemens 2002). Given that our postcranial specimens derive from these same deposits, we argue that stratigraphic patterns in our femoral assemblages reflect evolutionary and paleoecological changes rather than differences in depositional environment.

Below, we compare our femur-based estimates of diversity (morphotype richness, ecomorphological) and taxonomic composition from the same study area with patterns generated from a dental dataset (Wilson 2014). Given their uncertain age (Lancian or Puercan), we exclude the Bug Creek assemblages. Because of a lack of associated high-resolution stratigraphic data for some Lancian localities, we aggregate all Lancian specimens into one temporal bin; thus, finer scale faunal change within the Hell Creek Formation that has been documented in the dental dataset (Wilson 2014) could not be independently tested in the femoral dataset. In light of the small, fragmentary nature of our dataset, we felt statistical analyses of these changes in diversity were premature. Therefore, we stress that these temporal patterns of the femoral dataset should be cautiously interpreted relative to the dental dataset.

6.1. Richness and Taxonomic Composition Across the K-Pg Boundary

Femur morphotype richness in our sample is greater in the Lancian than in all other time bins, both absolutely (eight morphotypes versus five and six in the Pu1 and Pu2/3, respectively) and relative to sample size (n = 16; Table 2.2; Fig. 2.19). All Lancian morphotypes represent multituberculates, whereas therian taxa are absent from the

Lancian assemblage. Small sample sizes possibly explain the lack of eutherians, which in the dental dataset make up only ~11.5% of the Lancian specimens (Wilson 2014). In contrast, ~43% of all Lancian specimens in the dental dataset are metatherians (Wilson 2014); thus, the absence of metatherians in the femur sample points to a possible preservational bias, perhaps relating to a lack of durability of metatherian femora that stems from their pattern of ossification (Werning, 2012). Among the Lancian multituberculate femora, our results suggest members of all four major groups occur in the dental dataset: the Cimolodontidae (Mu9, ?*Cimolodon nitidus*), Cimolomyidae (Mu11, ?*Meniscoessus robustus*), Neoplagiaulacidae (Mu2, ?*Mesodma hensleighi*; Mu5, ?*M. thompsoni*; Mu1, ?*Mesodma* sp.), and "*Paracimexomys*" group (Mu4, possibly ?*Paracimexomys priscus*). Of the eight Lancian morphotypes, only two to four (depending on the age of the Bug Creek specimens) cross the K-Pg boundary (50–75% disappearance; Fig. 2.19), a proportional rate that is comparable to that of the dental dataset (Wilson 2014).

Femur morphotype richness is lowest in the early Puercan (Pu1) both overall (five) and for multituberculates specifically (three), although we note our sample size is smallest for the Pu1 (n = 7; Table 2.2; Fig. 2.19). The Neoplagiaulacidae (Mu1, Mu8) and "*Paracimexomys*" group (Mu6) persist across the K-Pg boundary into the Puercan, and a possible representative of the Eucosmodontidae (Mu7, ?*Stygimys kuszmauli*), an immigrant to the region, makes its first local appearance in the Pu1 (see Clemens 2002, 2010; Donohue et al. 2013; Wilson 2013, 2014 for discussion of the role of immigrants in early Paleocene faunas). Notably absent are the Taeniolabididae, Microcosmodontidae, and Ptilodontidae, all of which occur but are relatively uncommon in Pu1 dental assemblages

(Wilson 2014). The two Pu1 eutherian morphotypes (Eu3 and Eu2) represent archaic ungulates (?Periptychidae and possibly ?Arctocyonidae, respectively), both of which are immigrants to the study area (Clemens 2002, 2010; Archibald et al. 2011; Wilson 2013, 2014). Metatherians are absent from the Pu1 sample as are the eutherian Cimolestidae, Palaeoryctidae, and Leptictidae, despite the presence of these taxa in the Pu1 dental assemblages (Wilson 2014).

From the early (Pu1) to the middle/late Puercan (Pu2/3), there is a pronounced increase from 18 Pu1 species to 40+ Pu2/3 species in the dental dataset (Wilson 2014). Our femur data show a more subtle increase from five to six morphotypes (n = 14; Table 2.2; Fig. 2.19). This change in richness involves the disappearance of three morphotypes (Mu7, Eu2, Eu3) by the end of Pu1 (60% disappearance) and four to five first appearances (Mu6, Mu10, Eu1, Eu4, and possibly a new taxon represented by Mu8 specimens) in the Pu2/3 (Fig. 2.19). The first appearances include a possible new member of the "*Paracimexomys*" group (Mu6; ?*Cimexomys gratus*) as well as a Puercan immigrant from the Taeniolabididae (Mu10; ?*Catopsalis* sp.), and possibly from the Eucosmodontidae (one Mu8 specimen; ?*Eucosmodon americanus*; Clemens 2002, 2010; Wilson 2014). The middle/late Puercan (Pu2/3) eutherian femur morphotypes include a larger-bodied taxon (Eu4; a triisodontid, pantodont, or taeniodont) and a possible "plesiadapiform" (Eu1).

6.2. Ecomorphological Diversity

Studies of ecomorphological selectivity across the K-Pg boundary and expansion following the K-Pg boundary have mostly focused on changes in body size and feeding ecology, as inferred from fossil teeth (Alroy 1999; Calede and Wilson 2011; Smith et al.

2010; Wilson 2013; Wilson and Self 2011; Wilson et al. 2012; but see Borths and Hunter 2008). Postcranial data provide an opportunity to investigate ecomorphological changes along another axis (i.e., locomotion). We used our Lancian and Puercan femur samples to develop a preliminary assessment of changes in body size, and, from the better preserved femur morphotypes (Mu1, Mu8, Mu10, Mu11, Eu1), changes in locomotor ecology across the K-Pg boundary. Our ecomorphological diversity results should be considered preliminary, given that small sample sizes preclude tests for alternate hypotheses for patterns of body size, or morphological and locomotor diversity.

6.2.1. Body Size

Mean femur size in the Lancian sample is smaller (2.00) than in any other temporal bin in our study, the result of a large number of specimens in small morphotypes (e.g., Mu1–Mu5; Table S2.7). Lancian femur size ranges from size 1 to size 5. Across the K-Pg boundary in the early Puercan, mean individual femur size increased to 2.71, the highest value of any temporal bin in our study. The increase in mean size is the result of fewer small (multituberculate) morphotypes, and the appearance of new medium to large morphotypes (size 4), specifically two morphotypes (Eu2 and Eu3) attributed to archaic ungulate immigrants (Clemens 2002, 2010; Archibald et al. 2011); we note that the Pu1 biozone contains the fewest specimens (n = 7). Despite the small sample size, this Pu1 increase in mean individual femur size, a pattern for all femora as well as multituberculate femora specifically, parallels an increase in body size based on the dental record (Wilson 2013). In contrast, the range of Pu1 femur size decreases (specifically, maximum femur size decreases from size 5 to size 4 overall, and from size 5 to size 3 for multituberculates).

Although in the middle/late Puercan mean individual femur size decreased to 2.07 (Table S2.7), the maximum femur size actually increased to size 6 with appearance of a very large eutherian (Eu4). A decrease in Pu2/3 mean femur size is seen for taxon-specific analyses of multituberculate femora, but not for eutherian femora (Table S2.7). Both multituberculate and eutherian femora increase the range of size in the Pu2/3, to size 5 and size 6, respectively (Fig. 2.19; Table S2.7). The increase in maximum eutherian femur size in the Pu2/3 sample is parallel to the pattern from the dental dataset (e.g., Archibald, 1983; Maas and Krause 1994; Clemens 2002; Wilson 2004). Differences in specimen mean size among Lancian, Pu1, and Pu2/3 biozones are not statistically significant, likely due to small sample sizes (Table S2.8) and due to our ordinal method for size analysis, which underestimates differences in size.

Rather than coordinated size increases among all early Paleogene mammal taxa, dental patterns suggest increases in body size in the early Puercan are driven specifically by immigrant taxa. Thus, we additionally explored changes in femur size after the K-Pg mass extinction with respect to "resident" or "immigrant" status (Clemens 2002; Wilson 2013, 2014). Our results suggest Puercan immigrant morphotypes are significantly larger than Lancian and Puercan resident morphotypes ($p < 0.005$; Table S2.8), and Puercan resident morphotypes are significantly smaller than Lancian morphotypes ($p < 0.05$; Table S2.8). Despite small sample sizes, we conducted separate analyses of resident and immigrant status for the Pu1 and Pu2/3 interval zones, to parse patterns of mass extinction survival and subsequent immigration (i.e., Pu1) from possible evolution (e.g., Pu2/3). These results suggest Pu1 immigrants are significantly smaller than Pu1 residents ($p < 0.05$; Table S2.8); Pu2/3 residents are similarly smaller than Pu2/3 immigrants, although

this pattern is insignificant (p = 0.120; Table S2.8). These patterns suggesting body-size extinction selectivity and significantly larger Pu1 immigrants mirror dental results from the study area (Wilson 2013).

6.2.2. Locomotor Diversity

Here, we interpret the locomotor ecology of select femur morphotypes on the basis of previous functional morphological studies of multituberculate (Simpson and Elftman 1928; Krause and Jenkins 1983; Kielan-Jaworowska and Gambaryan 1994) and eutherian femora (Szalay and Sargis 2001; Sargis 2002; Elissamburu and Vizcano 2004), as well as functional interpretations based on other parts of the skeleton for taxa we infer to be closely related to our morphotypes (e.g., Miao 1988; Kielan-Jaworowska and Qi 1990; Meng and Wyss 1995). We acknowledge that locomotor inferences based on forelimb morphology can differ from those based on hind limb morphology.

Most of our multituberculate femur morphotypes exhibit features consistent with a crouching stance, in which the femur was highly mobile, held nearly horizontally with an outward rotation (Krause and Jenkins 1983; Kielan-Jaworowska and Gambaryan 1994). Among these crouching morphotypes, the morphology and relative size of the greater trochanter in Mu1, Mu8, and Mu11 is comparable to that seen in the Late Cretaceous *Nemegtbaatar* and Paleocene ?*Eucosmodon*, two taxa that were purportedly capable of leaping and "sudden movements" (Simpson and Elftman 1928; Kielan-Jaworowska and Gambaryan 1994). In addition, these morphotypes also possess a large trochanteric fossa and a deep post-trochanteric fossa for insertion of hip flexor muscles, which together suggest an arboreal lifestyle and at minimum the ability to climb (e.g., Krause and Jenkins

1983). Among small mammals especially, arboreal and terrestrial locomotion effectively require the same locomotor function (Jenkins 1974), and some small mammals could therefore lack any musculoskeletal differences indicative of differing substrates and associated locomotor types (Krause and Jenkins 1983), and/or the femur could lack robust indicators of locomotor mode that are seen among other postcranial elements or more complete skeletons (e.g., Szalay and Decker 1974; Kielan-Jaworowska and Gambaryan 1994; Argot 2013). Additionally, recognizing that it is difficult to reconstruct the locomotor mode for mammals with dubious modern analogs and that we are limited to one element and a few preserved features, we preliminarily classify these multituberculate morphotypes as terrestrial/saltatorial or arboreal rather than choosing between these locomotor alternatives.

Morphotype Mu10, which we suggest represents a Pu2/3 taeniolabidid (?*Catopsalis* sp.), is one of the largest multituberculates in our sample and is morphologically distinct from all other multituberculate morphotypes. The robust and tall greater trochanter and a relatively wide shaft are features that are associated with fossorial locomotion in rodents (Stein 2000; Elissamburu and Vizcano 2004; Samuels and Van Valkenburgh 2008). Additionally, its comparatively large lesser trochanter, with a more circular shape at the junction with the femur shaft, differs from the other multituberculate femur morphotypes. The lesser trochanter is the insertion for hip flexors and lateral rotators (psoas major and iliacus, on the medial border of the lesser trochanter; Simpson and Elftman 1928; Kielan-Jaworowska and Gambaryan 1994) and an additional hip extensor (quadratus femoris, on the lateral border of the lesser trochanter; Simpson and Elftman 1928; Kielan-Jaworowska and Gambaryan 1994). We contend that the morphology of Mu10 is consistent with

habitual flexion and external rotation associated with a crouching stance, both of which are more suggestive of fossoriality than saltatorial locomotion (Kielan-Jaworowska and Gambaryan 1994). Other Paleocene taeniolabidids, such as the Asian *Lambdopsalis*, have also been interpreted as fossorial but on the basis of features of the skull, cervical vertebrae, and humerus (Miao 1988; Kielan-Jaworowska and Qi 1990; Meng and Wyss 1995).

The more limited preservation of eutherian femora in our sample makes functional interpretations difficult. Nevertheless, morphotype Eu1, a possible "plesiadapiform," has a relatively small greater trochanter and very large lesser trochanter that protrudes medially beyond the extent of the head, which together indicate strong hip flexors, greater lateral rotation, and generally more arboreal than terrestrial locomotion (e.g., Szalay et al. 1975; Szalay and Sargis 2001; Sargis 2002). Additionally, a distally displaced third trochanter suggests a less rapid, but more powerful, extension of the thigh, in contrast to a more proximally placed third trochanter that is associated with greater speed and leaping among euprimates (Szalay et al. 1975; Salton and Sargis 2009). Other "plesiadapiforms" have been interpreted as arboreal (e.g., Szalay et al. 1975; Bloch and Boyer 2002; Bloch et al. 2007). Most recently, *Purgatorius*, a candidate taxon for Eu1, was interpreted as arboreal on the basis of tarsal morphology (Chester et al. 2012a). Thus, the available morphological evidence is consistent with Eu1 possessing arboreal capabilities, although this should be tested with additional and better-preserved material.

Although the functional interpretations above should be regarded as working hypotheses, they may support a pattern of increasing locomotor diversity following the K-Pg mass extinction. The Lancian sample contains somewhat more morphologically

conservative forms than those seen in younger Puercan samples, with arboreal and/or terrestrial/saltatorial locomotion suggested by nearly all morphotypes that preserve sufficient morphology for preliminary functional inference. Admittedly our Lancian sample is composed exclusively of multituberculates; as Borths and Hunter (2008) reported that an ulna attributed to the Lancian metatherian *Didelphodon* had features that may imply a semiaquatic mode, the discovery of Lancian therian femora should increase locomotor diversity in the Cretaceous. Within our study, it is not until the middle/late Puercan (Pu2/3) that we first detect ecomorphological diversification into a fossorial multituberculate form and potentially an arboreal eutherian form (Mu10 and Eu1, respectively). Although in general multituberculate femora are fairly morphologically conservative, we detect a greater number of Paleocene morphotypes and inferred locomotor types than previously recognized among North American multituberculates (Krause and Jenkins 1983).

7. Conclusion

Study of latest Cretaceous and early Paleogene mammals of North America has almost entirely focused on dental fossils. The 64 partial femora described in this study substantially increase our knowledge of postcrania from this critical interval in mammalian evolutionary history. Our morphologically and taxonomically diverse sample of femora from eastern Montana is tied into a well-constrained chronostratigraphic framework across the K-Pg boundary from which there is also a substantial mammalian dental fossil record. Our morphological and functional analysis of the femur sample reveals several key findings.

1. There is a greater diversity of multituberculate femur morphotypes present in North America than previously recognized (e.g., Gidley 1909; Deischl 1964; Krause and Jenkins 1983), especially in the latest Cretaceous sample.
2. Despite the high relative abundance of metatherians in the Lancian dental assemblages from the study area (Wilson 2014), they are absent from our Lancian and Puercan femur samples.
3. Femur morphotype richness decreased slightly across the K-Pg boundary, but was replenished by the appearance of immigrant taxa, namely two archaic ungulates and one eucosmodontid multituberculate in the early Puercan, as well as a taeniolabidid multituberculate, a very large eutherian (a taeniodont, pantodont, or triisodontid), and a possible “plesiadapiform” primate in the middle/late Puercan.
4. The Lancian assemblage of multituberculates was composed of small-bodied taxa, and early Paleocene immigrant taxa contributed to an increase in mean specimen

sizes in the Pu1 and Pu2/3, and a large increase in maximum specimen size in the Pu2/3. Specimens of Puercan resident or "survivor" taxa are significantly smaller than Puercan immigrant taxa, and these survivors are significantly smaller than the Lancian taxa present before the K-Pg mass extinction.

5. Locomotor diversity expanded from mainly arboreal and/or terrestrial/saltatorial multituberculates in the Lancian to include a fossorial multituberculate and potentially an arboreal eutherian in the middle/late Puercan.

The limited fossil sample sizes in our study caution against overinterpretation of our results; nevertheless, with the exception of a possible metatherian preservational bias, the overall trends in the femoral dataset are largely consistent with those from analyses of the extensive dental fossil record from the study area (Wilson 2013, 2014). We stress that because isolated postcrania and isolated teeth and jaws are collected via the same methods (hand-quarrying and underwater screenwashing), additional postcranial specimens likely exist in museum collections but have been overlooked in favor of the larger samples of more taxonomically informative dental specimens. As we continue to uncover more postcranial specimens in the field and in museum collections, we aim to independently test hypotheses about the K-Pg mass extinction, recovery, and Paleocene radiation of mammals and to highlight isolated postcrania as a valuable source of taxonomic and ecomorphological data.

8. Acknowledgements

We are indebted to the many individuals whose 60+ years of field and laboratory work led to the recovery and curation of the fossils in this study. For the more recently collected material, we thank G. Bennett III, M. Chen, B. Chowdhury, W. A. Clemens, D. DeMar, Jr., S. Smith, S. Wang, and M. Washington. For access to collections, we thank W. A. Clemens and P. Holroyd (UCMP), J. R. Horner and H. Woodward (MOR), and C. Sidor and R. Eng (UWBM). We are grateful for special use permits from the United States Bureau of Land Management, the Charles M. Russell National Wildlife Refuge, the Montana Department of Natural Resources and Conservation, and for access to private lands granted by the Engdahl, McKeever, Twitchell, Olsen, and Strohs families. We thank S. Chester, W. A. Clemens, D. Lofgren, E. Nesbitt, P. D. Polly, E. Sargis, C. Sidor, and C. Strömberg for valuable suggestions and discussion and S. Park for assistance with imaging. This manuscript was greatly improved upon thanks to comments from J. Calede, M. Chen, D. DeBey, D. DeMar, Jr., and S. Smith, and two anonymous reviewers. Funding for this project was provided to LBD by the National Science Foundation Gradate Research Fellowship, the Evolving Earth Foundation, the Doris O. and Samuel P. Welles Fund, the Montana Bureau of Land Management, and the University of Washington Graduate and Professional Student Senate and Department of Biology. Funding for this project was provided to GPW by the University of Washington Department of Biology.

References Cited

Alroy, J. 1999. The fossil record of North American mammals: evidence for a Paleocene evolutionary radiation. Systematic Biology 48: 107–118.

Archibald, J.D. 1982. A study of Mammalia and geology across the Cretaceous-Tertiary boundary in Garfield County, Montana. University of California Publications in Geological Sciences 122: 1–286.

Archibald, J.D. 1983. Structure of the K-T mammal radiation in North America: speculations on turnover rates and trophic structure. Acta Palaeontologica Polonica 28: 7–17.

Archibald, J.D., Y. Zhang, T. Harper, and R.L. Cifelli. 2011. *Protungulatum*, confirmed Cretaceous occurrence of an otherwise Paleocene Eutherian (Placental?) mammal. Journal of Mammalian Evolution 18: 153–161.

Argot, C. 2013. Postcranial analysis of a Carnivoran-like archaic ungulate: the case of *Arctocyon primaevus* (Arctocyonidae, Mammalia) from the Late Paleocene of France. Journal of Mammalian Evolution 20: 83–114.

Averianov, A.O. 2000. Mammals from the Mesozoic of Kirgizstan, Uzbekistan, Kazakhstan and Tadzhikistan, in: M.J. Benton, M.A. Shishkin, D.M. Unwin, and E.N. Kurochkin (Eds.), The Age of Dinosaurs in Russia and Mongolia. Cambridge University Press, Cambridge, pp. 627–652.

Beard, K.C. 1993. Phylogenetic systematics of the Primatomorpha, with special reference to Dermoptera, in: F. S. Szalay, M.J. Novacek, and M.C. McKenna (Eds.), Mammal Phylogeny: Placentals. Springer-Verlag, New York, pp. 129-150.

Bercovici, A., D. Pearson, D. Nichols, and J. Wood. 2009. Biostratigraphy of selected K/T boundary sections in southwestern North Dakota, USA: toward a refinement of palynological identification criteria. Cretaceous Research 30: 632–658.

Bloch, J.I. and D.M. Boyer. 2002. Grasping primate origins. Science 298: 1606–1610.

Bloch, J.I., M.T. Silcox, D.M. Boyer, and E.J. Sargis. 2007. New Paleocene skeletons and the relationship of plesiadapiforms to crown-clade primates. Proceedings of the National Academy of Sciences 104: 1159–1164.

Borths, M. and J. Hunter. 2008. Gimme shelter? Locomotor trends and mammalian survivorship at the K-Pg Boundary. Journal of Vertebrate Paleontology 28: 3A.

Britt, B.B., R.D. Scheetz, and A. Dangerfield. 2008. A suite of dermestid beetle traces on dinosaur bone from the Upper Jurassic Morrison Formation, Wyoming, USA. Ichnos 15, 59–71.

Calede, J.J., and G.P. Wilson. 2011. The last supper before the impact: Mammalian diets across the Cretaceous-Paleogene boundary. Journal of Vertebrate Paleontology 31 (supplement to 3), 82A.

Chester, S.G.B., E.J. Sargis, F.S. Szalay, J.D. Archibald, and A.O. Averianov. 2010. Mammalian distal humeri from the Late Cretaceous of Uzbekistan. Acta Palaeontologica Polonica 55: 199–211.

Chester, S.G.B., J.I. Bloch, and W.A. Clemens. 2012a. Tarsal morphology of the oldest plesiadapiform *Purgatorius* indicates arboreality in the earliest primates. Journal of Vertebrate Paleontology, 77A.

Chester, S.G.B., E.J. Sargis, F.S. Szalay, J.D. Archibald, and A.O. Averianov. 2012b. Therian femora from the Late Cretaceous of Uzbekistan. Acta Palaeontologica Polonica 57: 53–64.

Cifelli, R.L., J.J. Eberle, D.L. Lofgren, J.A. Lillegraven, and W.A. Clemens. 2004. Mammalian biochronology of the latest Cretaceous, in: M.O. Woodburne (Ed.), Late Cretaceous and Cenozoic Mammals of North America: Biostratigraphy and Geochronology. Columbia University Press, New York, pp. 21-42.

Clemens, W.A. 2002. Evolution of the mammalian fauna across the Cretaceous-Tertiary boundary in northeastern Montana and other areas of the Western Interior, in: J.H. Hartman, K.R. Johnson, and D.J. Nichols (Eds.), The Hell Creek Formation and the Cretaceous-Tertiary Boundary in the Northern Great Plains: An Integrated Continental Record of the End of the Cretaceous. Geological Society of America Special Paper 361, Boulder, pp. 217–245.

Clemens, W.A. 2004. *Purgatorius* (Plesiadapiformes, Primates?, Mammalia), a Paleocene immigrant into northeastern Montana: stratigraphic occurrences and incisor proportions. Bulletin of Carnegie Museum of Natural History 36: 3–13.

Clemens, W.A. 2010. Were immigrants a significant part of the earliest Paleocene mammalian fauna of the North American Western Interior? Vertebrata PalAsiatica 48: 285–307.

Clemens, W.A. 2011. *Eoconodon* ("Triisodontidae," Mammalia) From the Early Paleocene (Puercan) of Northeastern Montana, U.S.A. Palaeontologia Electronica 22: 1–22.

Clemens, W.A. 2013. Cf. *Wortmania* from the early Paleocene of Montana and an evaluation of the fossil record of the initial diversification of the Taeniodonta (Mammalia). Canadian Journal of Earth Sciences 50: 341–354.

Clemens, W.A. and J.H. Hartman. 2014. From *T. rex* to asteroid impact: Early studies (1901–1980) of the Hell Creek Formation in its type area, in: G.P. Wilson, W.A. Clemens, J.R. Horner, and J.H. Hartman (Eds.), Through the End of the Cretaceous in the Type Locality of the Hell Creek Formation in Montana and Adjacent Areas. Geological Society of America Special Paper 503, Boulder, pp. 1–87.

Clemens, W.A. and Z. Kielan-Jaworowska. 1979. Multituberculata, in: J.A. Lillegraven, Z. Kielan-Jaworowska, and W.A. Clemens (Eds.), Mesozoic Mammals: the First Two-Thirds of Mammalian History, University of California Press, Berkeley, pp. 99–149.

Clemens, W.A. and G.P. Wilson. 2009. Early Torrejonian mammalian local faunas from Northeastern Montana, U.S.A., in: L.B. Albright III (Ed.), Papers on Geology, Vertebrate Paleontology, and Biostratigraphy in Honor of Michael O. Woodburne. Museum of Northern Arizona Bulletin, Flagstaff, Arizona, 1–48.

Deischl, D.G. 1964. The Postcranial Anatomy of Cretaceous Multituberculate Mammals, unpublished M.Sc. thesis, University of Minnesota, Minneapolis, 85 pp.

Donohue, S.L., G.P. Wilson, and B.H. Breithaupt. 2013. Latest Cretaceous multituberculates of the Black Butte Station local fauna (Lance Formation, southwestern Wyoming), with implications for compositional differences among mammalian local faunas of the Western Interior. Journal of Vertebrate Paleontology 33: 677–695.

Elissamburu, A. and S.F. Vizcano. 2004. Limb proportions and adaptations in caviomorph rodents (Rodentia: Caviomorpha). Journal of Zoology 262: 145–159.

Fastovsky, D.E. 1987. Paleoenvironments of vertebrate-bearing strata during the Cretaceous-Paleogene transition, eastern Montana and western North Dakota. PALAIOS 2: 282–295.

Fox, R.C. 2005. Microcosmodontid multituberculates (Allotheria, Mammalia) from the Paleocene and Late Cretaceous of western Canada. Palaeontographica Canadiana 23: 1–109.

Gidley, J.W. 1909. Notes on the fossil mammalian genus *Ptilodus*, with descriptions of new species. Proceedings of the United States National Museum 36: 611–627.

Granger, W. and G.G. Simpson. 1929. A revision of the Tertiary Multituberculata. Bulletin of the American Museum of Natural History 56: 601–676.

Hunter, J.P., J.H. Hartman, and D.W. Krause. 1997. Mammals and mollusks across the Cretaceous-Tertiary boundary from Makoshika State Park and vicinity (Williston Basin), Montana. University of Wyoming Contributions to Geology 32: 61–114.

Hurum, J.H. and Z. Kielan-Jaworowska. 2008. Postcranial skeleton of a Cretaceous multituberculate mammal *Catopsbaatar*. Acta Palaeontologica Polonica 53: 545–566.

Jenkins, F.A. and D.W. Krause. 1983. Adaptations for climbing in North American multituberculates (Mammalia). Science 220: 712–715.

Ji, Q., Z.-X. Luo, C.-Z. Yuan, J.R. Wible, J.-P. Zhang, and J.A. Georgi. 2002. The earliest known eutherian mammal. Nature 416: 816–822.

Kielan-Jaworowska, Z. 1977. Evolution of the therian mammals in the Late Cretaceous of Asia. Part II. Postcranial skeleton in *Kennalestes* and *Asioryctes*. Palaeontologia Polonica 37: 65–83.

Kielan-Jaworowska, Z. 1979. Pelvic structure and nature of reproduction in Multituberculata. Nature 299: 402–403.

Kielan-Jaworowska, Z. and P.P. Gambaryan. 1994. Postcranial anatomy and habits of Asian multituberculate mammals. Fossils and Strata 36: 1–92.

Kielan-Jaworowska, Z. and T. Qi. 1990. Fossorial adaptations of a Taeniolabidoid Multituberculate mammal from the Eocene of China. Vertebrata PalAsiatica 28: 81–94.

Krause, D.W. and F.A. Jenkins Jr. 1983. The postcranial skeleton of North American multituberculates. Bulletin of the Museum of Comparative Zoology 150: 199–246.

LeCain, R., W.C. Clyde, G.P. Wilson, and J. Riedel. 2014. Magnetostratigraphy of the Hell Creek and lower Fort Union Formations in northeastern Montana, in: G.P. Wilson, W.A. Clemens, J.R. Horner, and J.H. Hartman (Eds.), Through the End of the Cretaceous in the Type Locality of the Hell Creek Formation in Montana and Adjacent Areas. Geological Society of America Special Paper 503, Boulder, pp. 137–147.

Lillegraven, J.A. 1969. Latest Cretaceous mammals of upper part of Edmonton Formation of Alberta, Canada, and review of marsupial-placental dichotomy in mammalian evolution. University of Kansas Paleontological Contributions 50: 1–122.

Lillegraven, J.A. 1972. Ordinal and familial diversity of Cenozoic mammals. Taxon 21: 261–274.

Lofgren, D.L. 1995. The Bug Creek Problem and the Cretaceous-Tertiary transition at McGuire Creek, Montana. University of California Publications in Geological Sciences 140: 1–185.

Lofgren, D.L., J.A. Lillegraven, W.A. Clemens, P.D. Gingerich, and T.E. Williamson. 2004. Paleocene biochronology: The Puercan through Clarkforkian land mammal ages, in:

M.O. Woodburne (Ed.) Late Cretaceous and Cenozoic Mammals of North America: Biostratigraphy and Geochronology. Columbia University Press, New York, pp. 43–105.

Longrich, N.R. and M.J. Ryan. 2010. Mammalian tooth marks on the bones of dinosaurs and other Late Cretaceous vertebrates. Palaeontology 53: 703–709.

Luo, Z.-X. 2007. Transformation and diversification in early mammal evolution. Nature 450: 1011–1019.

Luo, Z.-X., Q. Ji., J.R. Wible, and C.-X. Yuan. 2003. An Early Cretaceous tribosphenic mammal and metatherian evolution. Science 302: 1934–1940.

Luo, Z.-X., C.-X. Yuan, Q.-J. Meng, and Q. Ji. 2011. A Jurassic eutherian mammal and divergence of marsupials and placentals. Nature 476: 442–445.

Maas, M.C. and D.W. Krause. 1994. Mammalian turnover and community structure of the Paleocene of North America. Historical Biology 8: 91–128.

Matthew, W.D. 1937. Paleocene faunas of the San Juan Basin, New Mexico. Transactions of the American Philosophical Society 30: 1–523.

Meng, J., and A.R. Wyss. 1995. Monotreme affinities and low-frequency hearing suggested by multituberculate ear. Nature 377: 141–144.

Miao, D., D.W. Boyd, and J.A. Lillegraven. 1988. Skull morphology of *Lambdopsalis bulla* (Mammalia, Multituberculata) and its implications to mammalian evolution. Contributions to Geology, University of Wyoming, Special Paper 4: 1–104.

Middleton, D. 1982. A new species and additional material of *Catopsalis* (Mammalia, Multituberculata) from the Western Interior of North America. Journal of Paleontology 56: 1197–1206.

Millien, V. 2008. The largest among the smallest: the body mass of the giant rodent *Josephoartigasia monesi*. Proceedings of the Royal Society B: Biological Sciences 275: 1953–1955.

Millien, V. and H. Bovy. 2010. When teeth and bones disagree: body mass estimation of a giant extinct rodent. Journal of Mammalogy 91: 11–18.

Moore, J.R., G.P. Wilson, M. Sharma, H.R. Hallock, D.R. Braman, and P. Renne. 2014. Assessing the relationships of the Hell Creek–Fort Union contact, Cretaceous-Paleogene boundary, and Chicxulub impact ejecta horizon at the Hell Creek Formation lectostratotype, Montana, USA, in: G.P. Wilson, W.A. Clemens, J.R. Horner, and J.H. Hartman (Eds.), Through the End of the Cretaceous in the Type Locality of the Hell Creek Formation in Montana and Adjacent Areas. Geological Society of America Special Paper 503, Boulder, pp. 123–136.

Muizon, C. 1998. *Mayulestes ferox*, a bohyaenoid (Metatheria, Mammalia) from the early Palaeocene of Bolivia. Phylogenetic and palaeobiologic implications. Geodiversitas 20: 19–142.

Novacek, M.J., G.W. Rougier, J.R. Wible, M.C. McKenna, D. Dashzeveg, and I. Horovitz. 1997. Epipubic bones in eutherian mammals from the Late Cretaceous of Mongolia. Nature 389: 483–486.

R Core Team. 2012. *R: A language and environment for statistical computing.* Version 2.15.2 http://www.R-project.org/

Renne, P.R., G. Balco, K.R. Ludwig, R. Mundil, and K. Min. 2011. Response to the comment by W.H. Schwartz et al. on "Joint determination of ^{40}K decay constants and ^{40}Ar*/^{40}K for the Fish Canyon sanidine standard, and improved accuracy for the ^{40}Ar/^{39}Ar

geochronology" by P.R. Renne et al. (2010). Geochimica et Cosmochimica Acta 75: 5097–5100.

Renne, P.R., A.L. Deino, F.J. Hilgen, K.F. Kuiper, D.F. Mark, W.S. Mitchell III, L.E. Morgan, R. Mundil, and J. Smit. 2013. Time scales of critical events around the Cretaceous-Paleogene boundary. Science 339: 684–687.

Rigby Jr., J.K. 1981. A skeleton of *Gillisonchus gillianus* (Mammalia; Condylarthra) from the Early Paleocene (Puercan) Ojo Alamo Sandstone, San Juan Basin, New Mexico, with comments on the local stratigraphy of Betonnie Tsosie Wash, in: S.G. Lucas, J.K. Rigby Jr., and B.S. Kues. (Eds.), Advances in San Juan Basin Paleontology. University of New Mexico Press, Albuquerque, pp. 89–126.

Roberts, E.M., R.R. Rogers, and B.Z. Foreman. 2007. Continental insect borings in dinosaur bone: examples from the Late Cretaceous of Madagascar and Utah. Journal of Paleontology 81: 201–208.

Robertson, D.S., M.C. McKenna, O.B. Toon, S. Hope, and J.A. Lillegraven. 2004. Survival in the first hours of the Cenozoic. Geological Society of America Bulletin 116: 760–768.

Rose, K.D. 1987. Climbing adaptations in the early Eocene mammal *Chriacus* and the origin of Artiodactyla. Science 236: 314–316.

Rowe, T. 1988. Definition, diagnosis, and origin of Mammalia. Journal of Vertebrate Paleontology 8: 241–264.

Russell, D.E. 1964. Les mammifères paléocènes d'Europe. Mémoires du Muséum National D'Histoire Naturelle, Série C. Sciences de la Terre 13: 1–324.

Salton, J.A. and E.J. Sargis. 2009. Evolutionary morphology of the Tenrecoidea (Mammalia) hindlimb skeleton. Journal of Morphology 270: 367–387.

Samuels, J.X., and B. Van Valkenburgh. 2008. Skeletal indicators of locomotor adaptations in living and extinct rodents. Journal of Morphology 269: 1387–1411.

Sargis, E.J. 2002. Functional morphology of the hindlimb of tupaiids (Mammalia, Scandentia) and its phylogenetic implications. Journal of Morphology 254: 149–185.

Schoch, R.M. 1986. Systematics, functional morphology and macroevolution of the extinct mammalian order Taeniodonta. Peabody Museum of Natural History, Yale University Bulletin 42: 1–307.

Simpson, G.G. 1926. Mesozoic Mammalia. IV. The multituberculates as living animals. American Journal of Science 2: 228–250.

Simpson, G.G. 1935. The Tiffany Fauna, Upper Paleocene II.–Structure and relationships of *Plesiadapis*. American Museum Novitates 816: 1–30.

Simpson, G.G. and H.O. Elftman. 1928. Hind limb musculature and habits of a Paleocene Multituberculate. American Museum Novitates 333: 1–19.

Sinclair, W.J. and W. Granger. 1914. Palaeocene deposits of the San Juan Basin, New Mexico. Bulletin of the American Museum of Natural History 33: 297–316.

Sloan, R.E. 1981. Systematics of Paleocene multituberculates from the San Juan Basin, New Mexico, in: S.G. Lucas, J.K. Rigby, Jr., and B.S. Kues (Eds.), Advances in San Juan Basin Paleontology. University of New Mexico Press, Albuquerque, pp. 127–160.

Sloan, R.E. and L. Van Valen. 1965. Cretaceous mammals from Montana. Science 148: 220–227.

Smith, F.A., A.G. Boyer, J.H. Brown, D.P. Costa, T. Dayan, S.K.M. Ernest, A.R. Evans, M. Fortelius, J.L. Gittleman, M.J. Hamilton, L.E. Harding, K. Lintulaakso, S.K. Lyons, C. McCain, J.G. Okie, J.J. Saarinen, R.M. Sibly, P.R. Stephens, J. Theodor, and M.D. Uhen.

2010. The evolution of maximum body size of terrestrial mammals. Science 330: 1216–1219.

Standhardt, B.R. 1986. Vertebrate paleontology of the Cretaceous/Tertiary transition of Big Bend National Park, Texas, Ph.D. dissertation. Louisiana State University and Agricultural and Mechanical College, Baton Rouge, 299 pp.

Stein, B.R. 2000. Morphology of subterranean rodents, in: E.A. Lacey, J.L. Patton, and G.N. Cameron (Eds.), Life Underground: the Biology of Subterranean Rodents. University of Chicago Press, Chicago, pp. 19–61.

Swisher, C.C, L. Dingus III, and R.F. Butler. 1993. 40Ar/39Ar dating and magnetostratigraphic correlation of the terrestrial Cretaceous-Paleogene boundary and Puercan mammal age, Hell Creek–Tullock formations, eastern Montana. Canadian Journal of Earth Sciences 30: 1981–1996.

Szalay, F.S. 1994. Evolutionary History of the Marsupials and an Analysis of Osteological Characters, Cambridge University Press, New York.

Szalay, F.S. and and R.L. Decker. 1974. Origins, evolution, and function of the tarsus in Late Cretaceous Eutheria and Paleocene primates, in: F.A. Jenkins Jr. (Ed.), Primate Locomotion. Academic Press, Inc., New York, pp. 223–259.

Szalay, F.S. and E. Delson. 1979. Evolutionary History of the Primates, Academic Press, New York.

Szalay, F.S. and E.J. Sargis. 2001. Model-based analysis of postcranial osteology of marsupials from the Palaeocene of Itaborai (Brazil) and the phylogenetics and biogeography of Metatheria. Geodiversitas 23: 139–302.

Szalay, F.S., I. Tattersall, and R.L. Decker. 1975. Phylogenetic relationships of *Plesiadapis*-postcranial evidence. Contributions to Primatology 5: 136–166.

Weil, A. 1998. A new species of *Microcosmodon* (Mammalia: Multituberculata) from the Paleocene Tullock Formation of Montana, and an argument for the Microcosmodontinae. PaleoBios 18: 1–15.

Werning, S. 2012. How does a "typical" mammal grow? Sampling and the interpretation of fossil bone tissue. Journal of Vertebrate Paleontology 32: 192A.

Wilson, G.P. 2004. A quantitative assessment of evolutionary and ecological change in mammalian faunas leading up to and across the Cretaceous-Tertiary boundary in northeastern Montana. Unpublished Ph.D. dissertation, University of California Berkeley, Berkeley, 412 pp.

Wilson, G.P. 2005. Mammalian faunal dynamics during the last 1.8 million years of the Cretaceous in Garfield County, Montana. Journal of Mammalian Evolution 12: 53–75.

Wilson, G.P. 2013. Mammals across the K/Pg boundary in northeastern Montana, U.S.A.: dental morphology and body-size patterns reveal extinction selectivity and immigrant fueled ecospace filling. Paleobiology 39: 429–469.

Wilson, G.P. 2014. Mammalian extinction, survival, and recovery dynamics across the Cretaceous-Paleogene boundary in northeastern Montana, in: G.P. Wilson, W.A. Clemens, J.R. Horner, and J.H. Hartman (Eds.), Through the End of the Cretaceous in the Type Locality of the Hell Creek Formation in Montana and Adjacent Areas. Geological Society of America Special Paper 503, Boulder, pp. 365–392.

Wilson, G.P. and C. Self. 2011. Mammalian dental complexity across the Cretaceous-Paleogene boundary with implications for ecological recovery and expansion. Journal of Vertebrate Paleontology 31 (supplement to 3): 215A.

Wilson, G.P., A.R. Evans, I.J. Corfe, P.D. Smits, M. Fortelius, and J. Jernvall. 2012. Adaptive radiation of multituberculate mammals before the extinction of dinosaurs. Nature 483: 457–460.

Figures

Figure 2.1. Map showing Montana and the four counties where the Cretaceous and Paleogene femora included in this study were recovered. Modified from Wilson (2005).

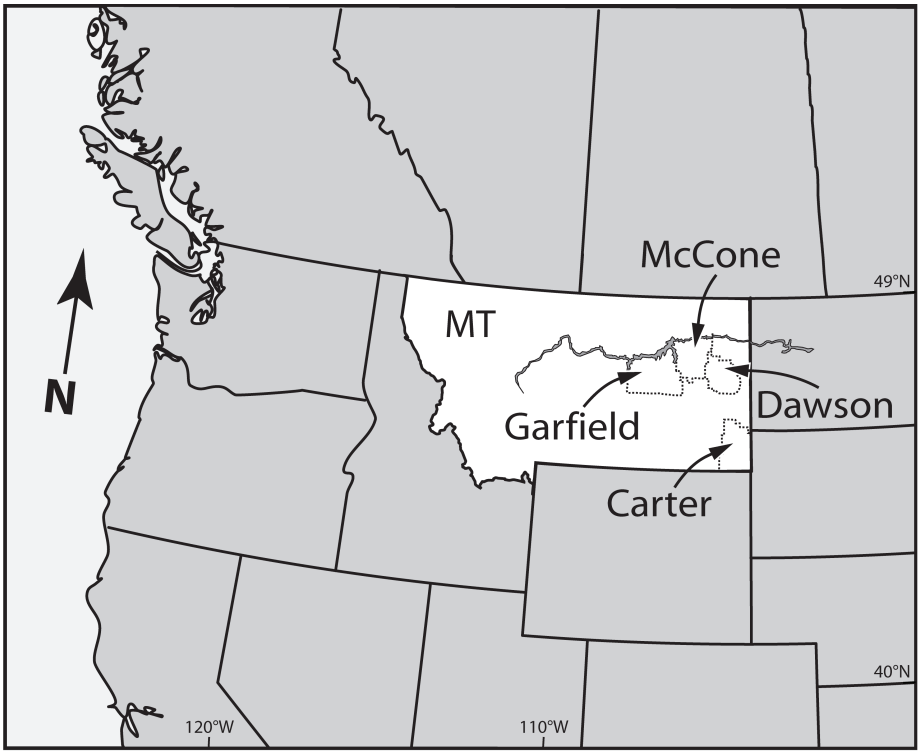

Figure 2.2. Schematic of femur measurements shown on a left proximal fragment in ventral (**A**) and dorsal (**B**) views and on a distal fragment in ventral (**C**), dorsal (**D**), and distal (**E**) views. Abbreviations: FDED, distal end depth; FDEW, distal end width; FGTL, greater trochanter length; FHL, head length; FHW, head width; FICNW, intercondylar notch width; FLCW, lateral condyle width; FMCW, medial condyle width; FLTLW, lesser trochanter lateral width; FMNW, minimum neck width; FNL, neck length; FPEW, proximal end width; FSMLD, shaft mediolateral width (distal); FSMLP, shaft mediolateral width (proximal). See Table 2.1 for measurement details.

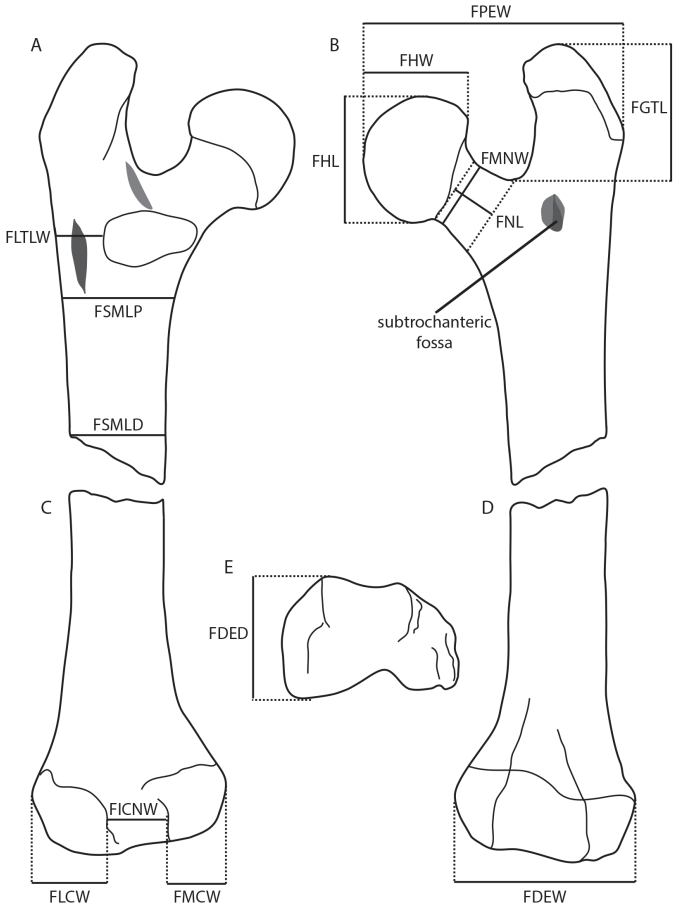

Figure 2.3. Left proximal femur (UCMP 192554 from loc. V77128) representative of multituberculate morphotype Mu1 from the Hell Creek and Tullock formations (Lancian–Pu2/3) of eastern Montana, in stereo dorsal (**A**) and ventral (**B**) views, and medial (**C**) and proximal (**D**) views. Abbreviations: gt, greater trochanter.

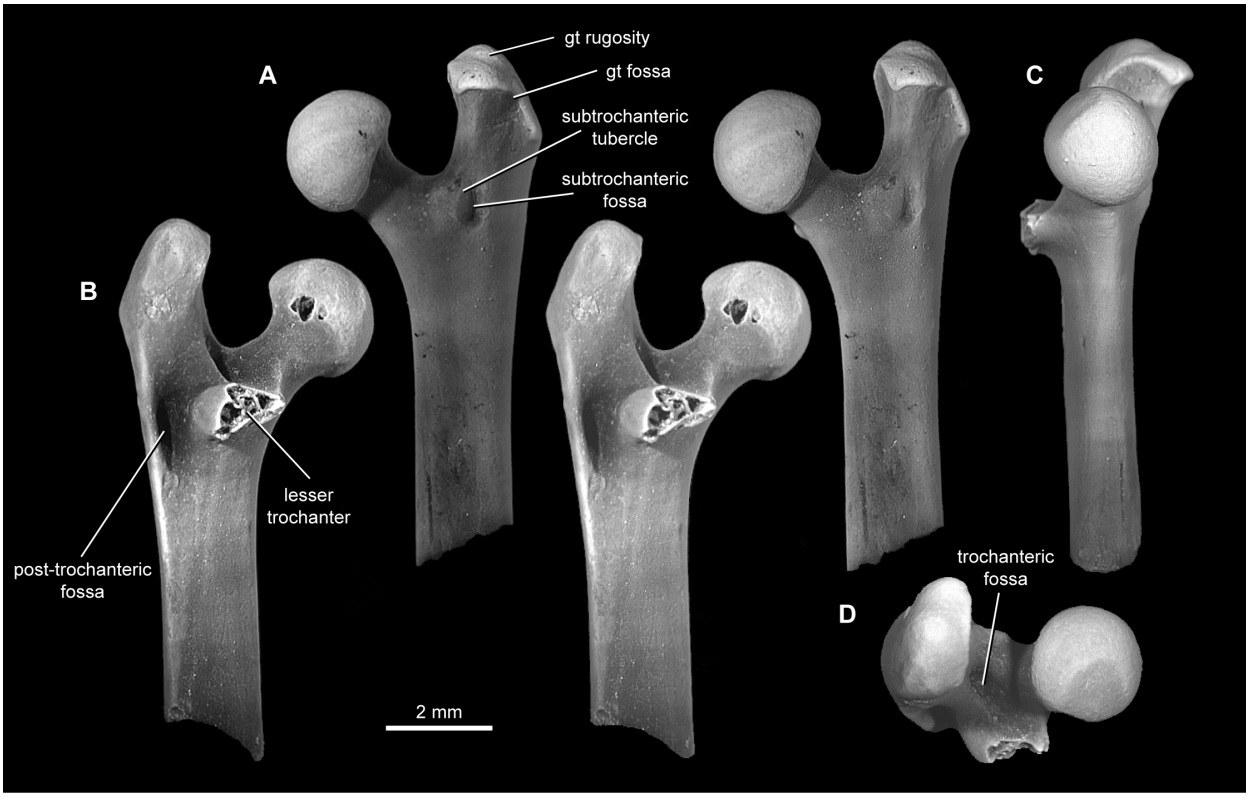

Figure 2.4. Left proximal femur (UCMP 127392 from loc. V88009) representative of multituberculate morphotype Mu2 from the Hell Creek Formation (Lancian) of eastern Montana, in stereo dorsal (**A**) and ventral (**B**) views, and medial (**C**) and proximal (**D**) views.

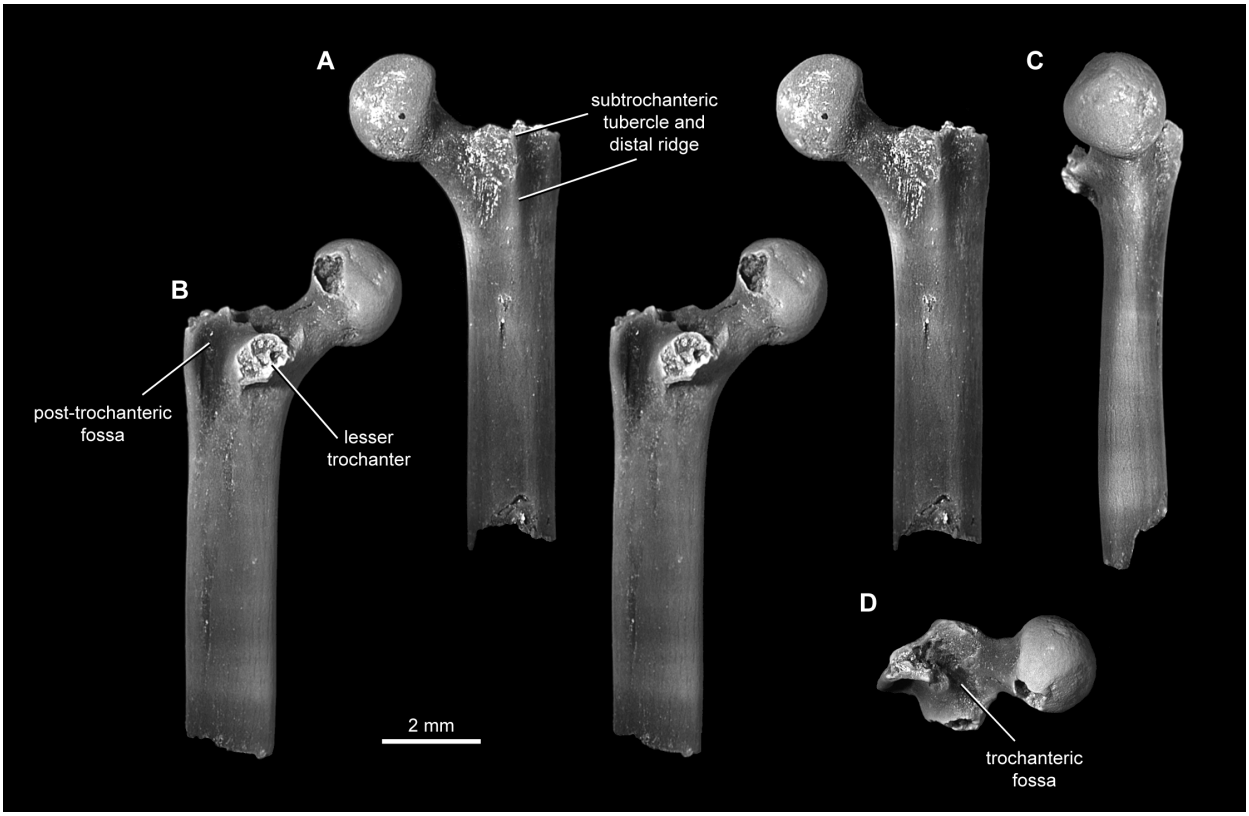

Figure 2.5. Right proximal femur (UCMP 127382 from loc. V88007) representative of multituberculate morphotype Mu3 from the Hell Creek Formation (Lancian) of eastern Montana, in stereo dorsal (**A**) and ventral (**C**) views, and medial (**B**) and proximal (**D**) views.

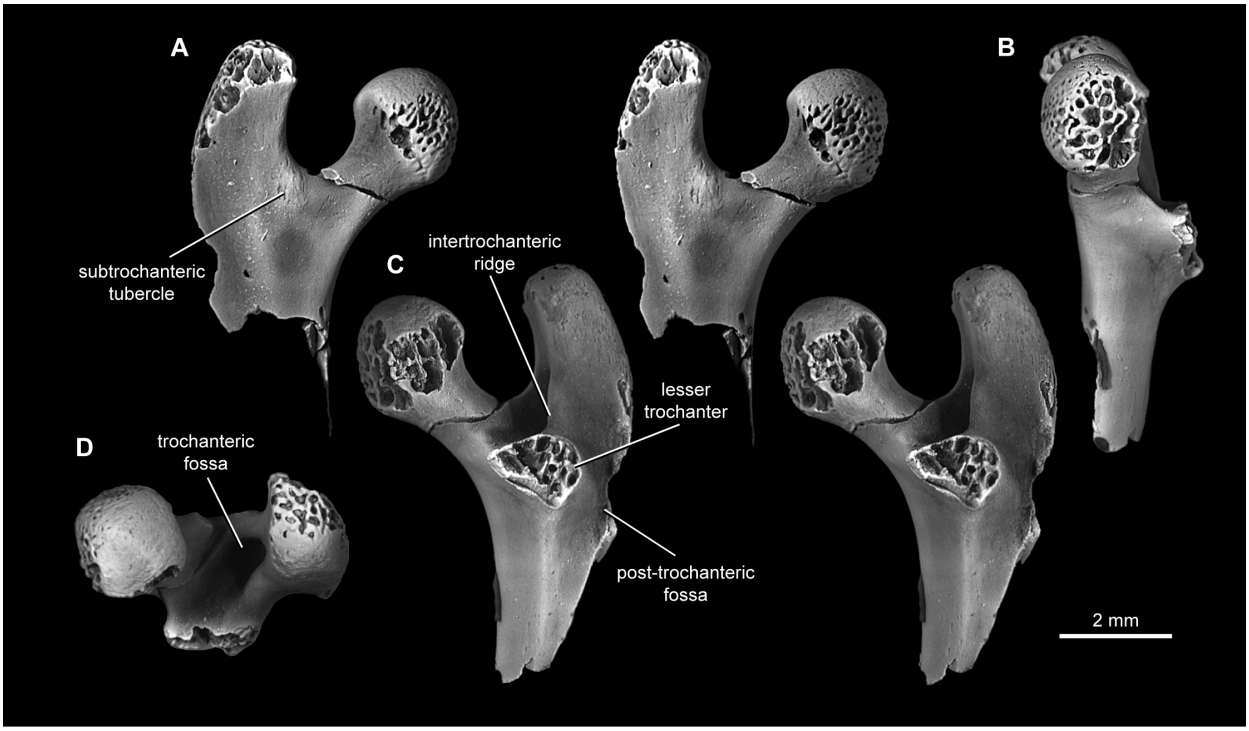

Figure 2.6. Left proximal femur (UCMP 174494 from loc. V75173) representative of multituberculate morphotype Mu4 from the Hell Creek Formation (Lancian) of eastern Montana in stereo dorsal (**A**) and ventral (**C**) views, and medial (**B**) and proximal (**D**) views.

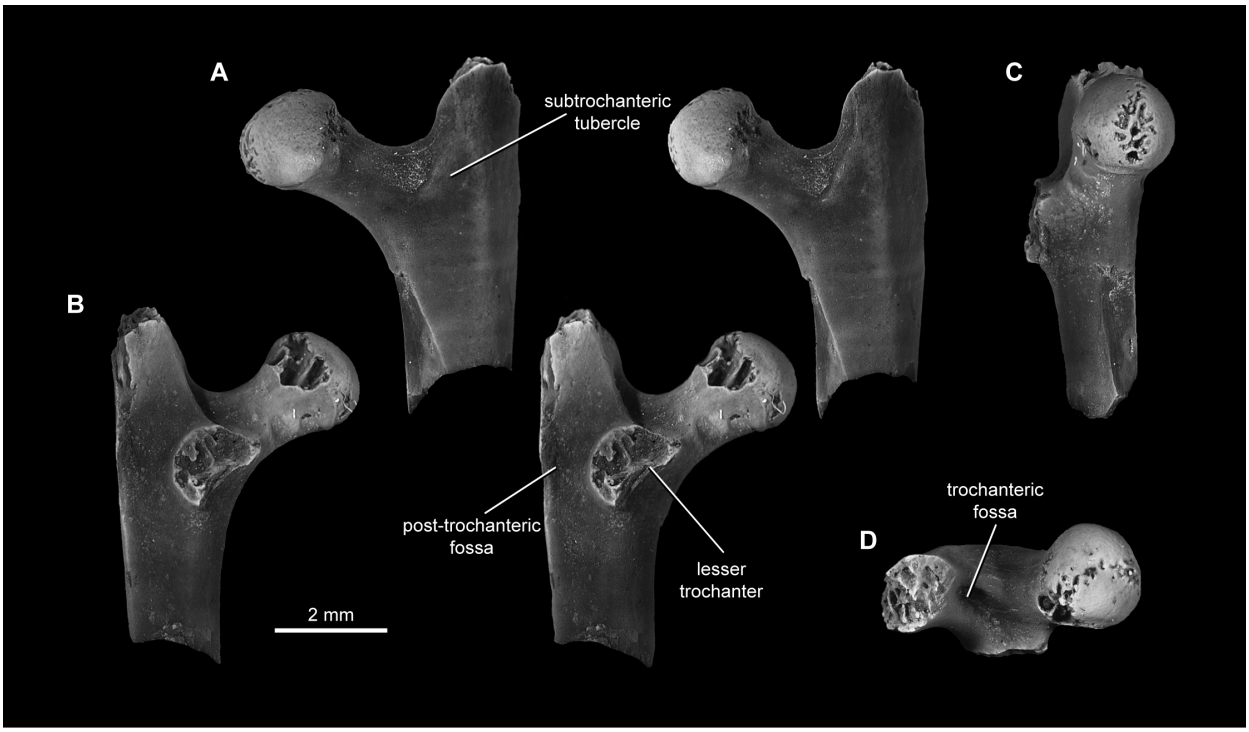

Figure 2.7. Proximal femora (**A–D**: UCMP 196964 from loc. V70201; **E**: UCMP 174343 from loc. V84148) representative of multituberculate morphotype Mu5 from Hell Creek Formation (Lancian) and lower Tullock Formation (mixed Lancian-Pu1) of eastern Montana in stereo dorsal (**A**) and ventral (**C**) views, and medial (**B**), proximal (**D**), and dorsal (**E**) views. See Section 4.1.5 in the text for more description of the gnaw marks in dorsal view (A).

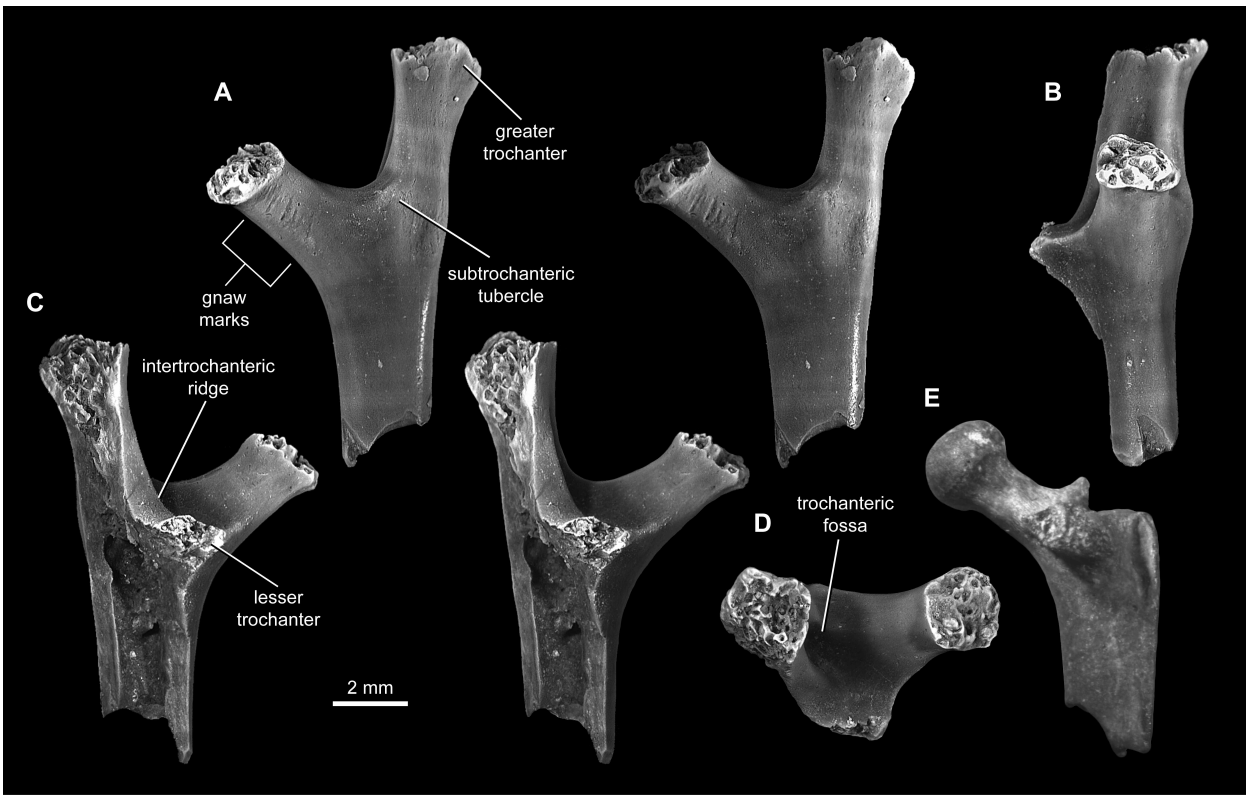

Figure 2.8. Right proximal femur (UCMP 153092 from loc. V99438) representative of multituberculate morphotype Mu6 from the middle Tullock Formation (Pu2/3) of eastern Montana in stereo dorsal (**A**) and ventral (**B**) views, and medial (**C**) and proximal (**D**) views.

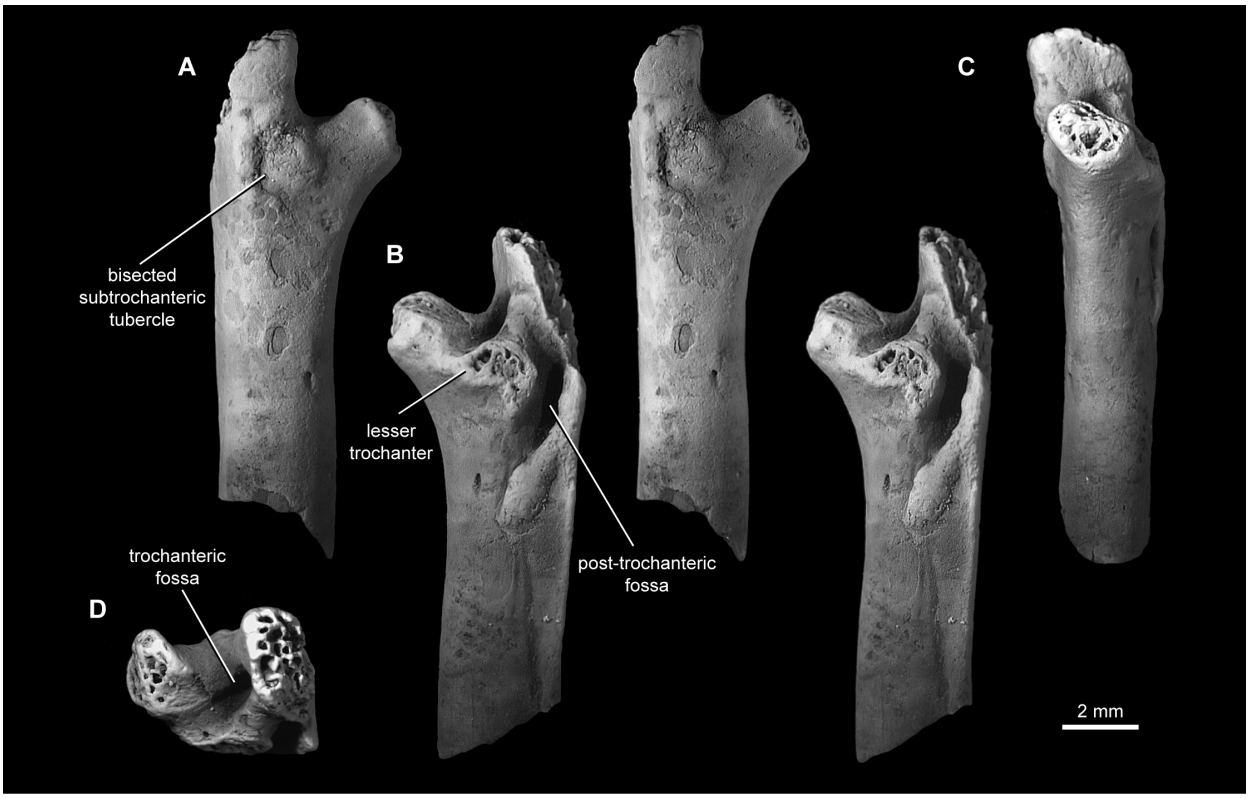

Figure 2.9. Right proximal femur (UCMP 194860 from loc. V74111) representative of multituberculate morphotype Mu7 from the lower Tullock Formation (mixed Lancian-Pu1 and Pu1) of eastern Montana in stereo dorsal (**A**) and ventral (**D**) views, and proximal (**B**), distal (**C**), and medial (**E**) views; dorsal side up and lateral to the left in (**C**).

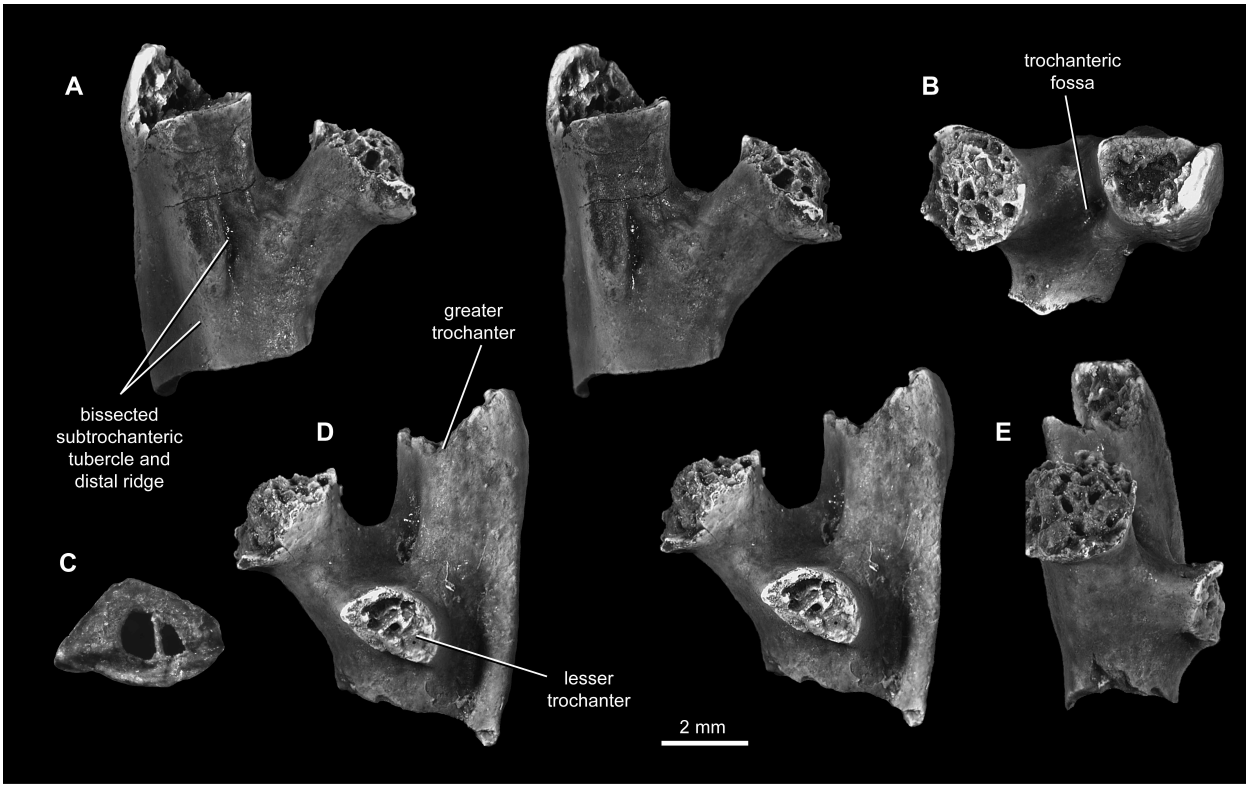

Figure 2.10. Left proximal femur (UCMP 102444 from loc. V70201) representative of multituberculate morphotype Mu8 from Hell Creek and Tullock formations (Lancian–Pu2/3) of eastern Montana in stereo dorsal (**A**) and ventral (**B**) views, and medial (**C**) and proximal (**D**) views.

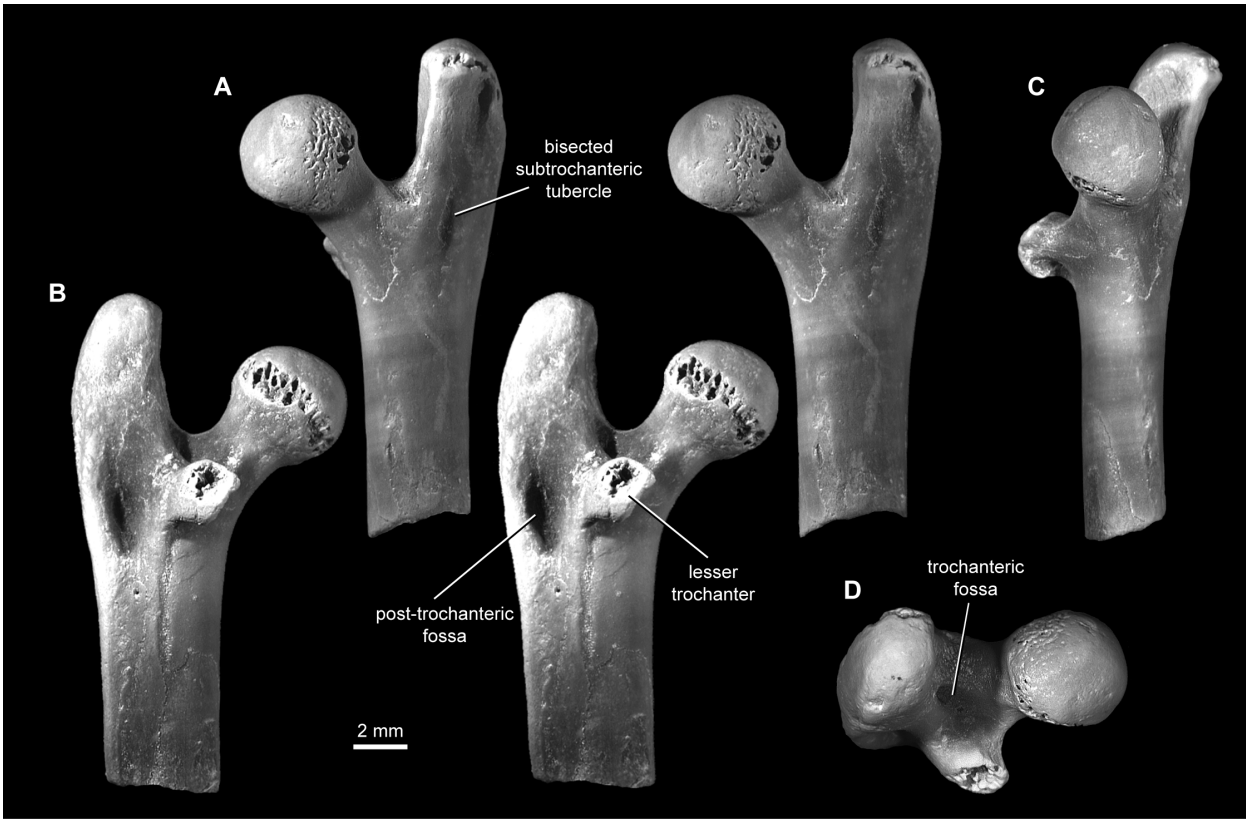

Figure 2.11. Left proximal femur (UCMP 174532 from loc. V73102) representative of multituberculate morphotype Mu9 from the Hell Creek Formation (Lancian) of eastern Montana, in stereo dorsal (**A**) and ventral (**B**) views, and medial (**C**) and proximal (**D**) views.

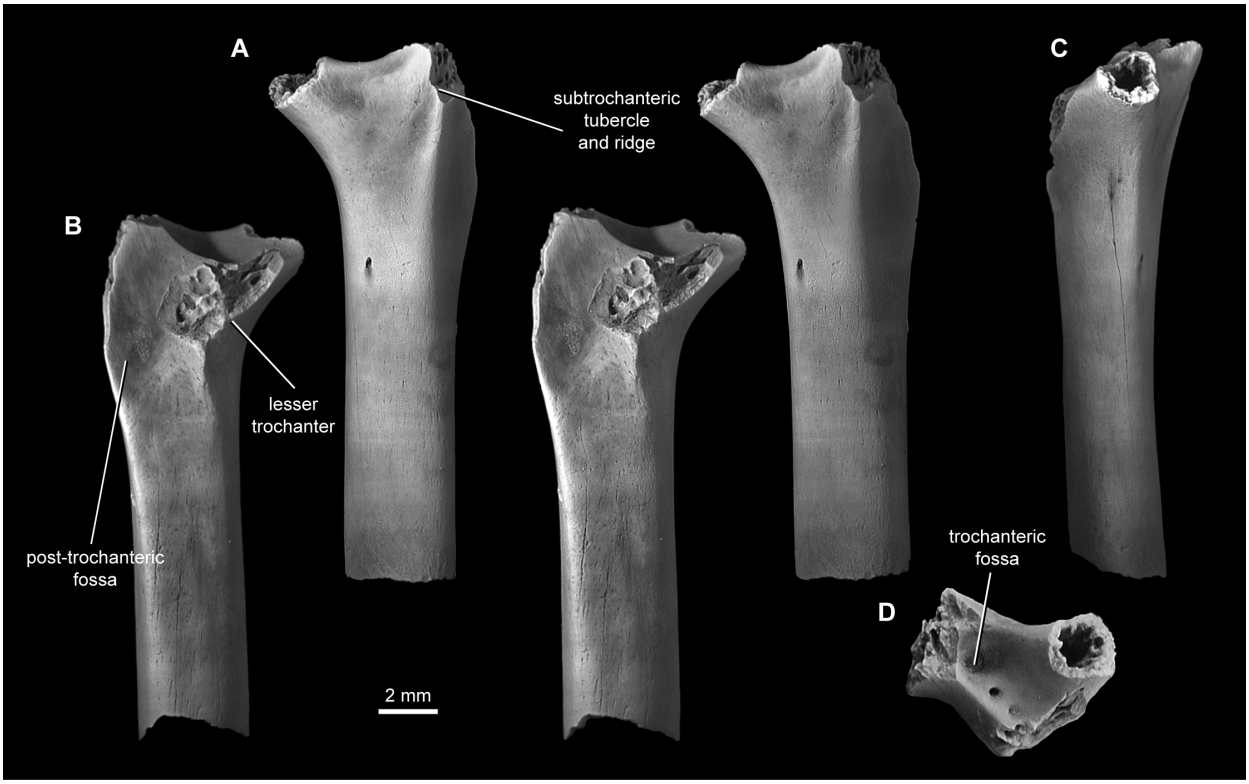

Figure 2.12. Left proximal femur (UCMP 153091 from loc. V99438) representing multituberculate morphotype Mu10 from the middle Tullock Formation (Pu2/3) of eastern Montana, in stereo dorsal (**A**) and ventral (**B**) views, and medial (**C**) and proximal (**D**) views.

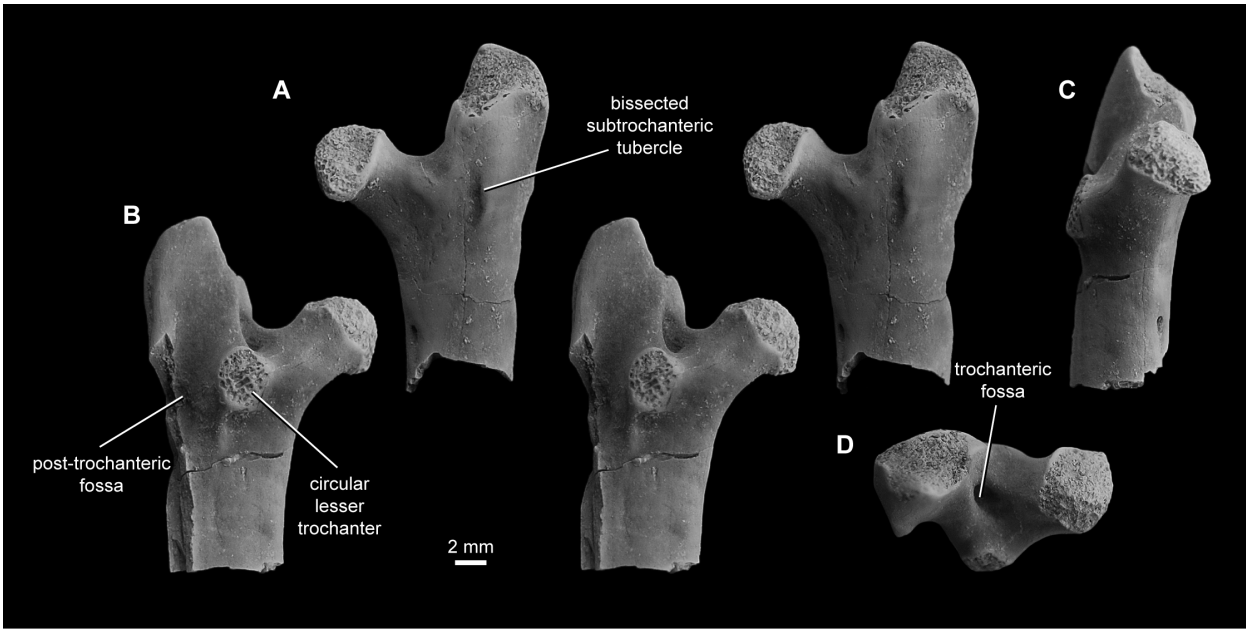

Figure 2.13. Right proximal femur (MOR 882) representing multituberculate morphotype Mu11 from an unknown locality the Hell Creek Formation (Lancian) of eastern Montana, stereo dorsal (**A**), and ventral (**C**) views, and medial (**B**), and proximal (**D**) views.

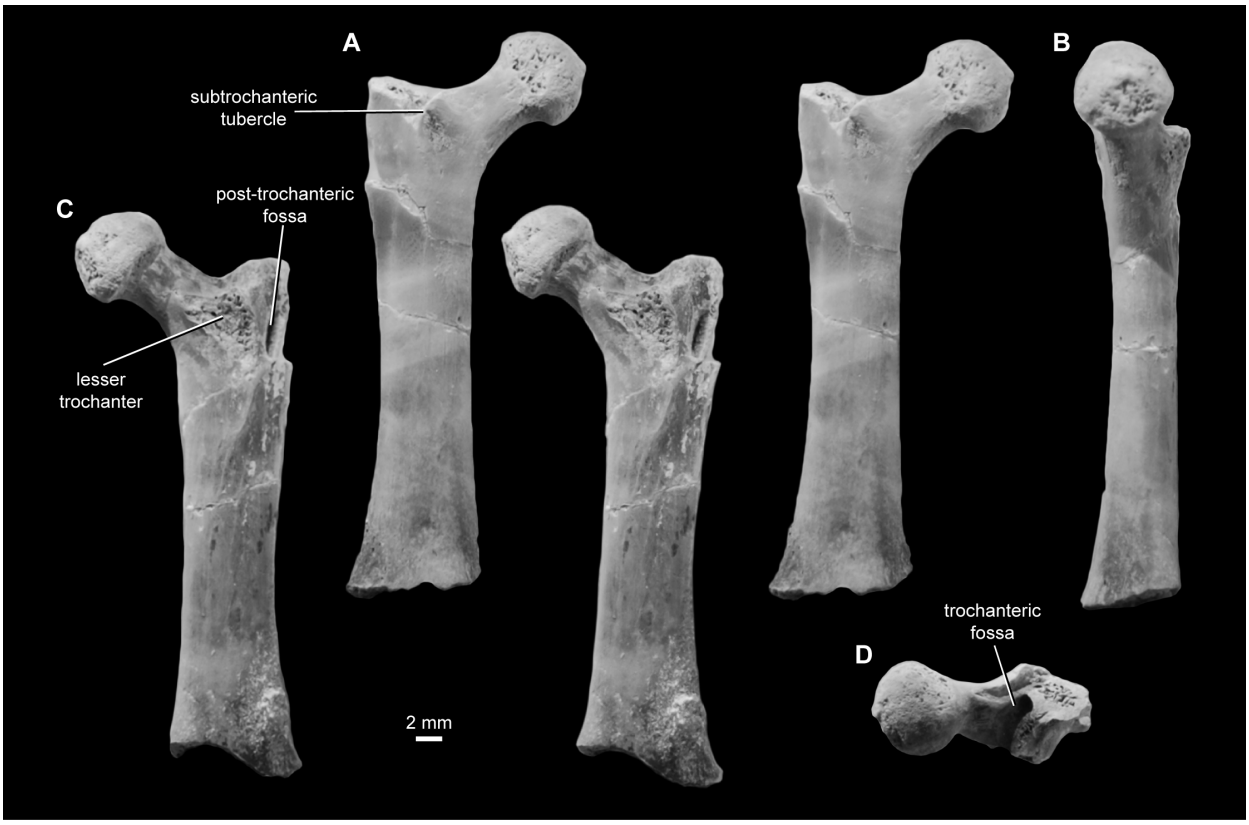

Figure 2.14. Multituberculate right distal femur (UCMP 174391 from loc. V91051) from the Hell Creek Formation (Lancian) of eastern Montana, in stereo dorsal (**A**), ventral (**B**), and distal (**E**) views, and medial (**C**) and proximal (**D**) views. Abbreviations: **icf**, intercondylar fossa; **lc**, lateral condyle; **le**, lateral epicondyle; **mc**, medial condyle; me, medial epicondyle; **pg**, patellar groove.

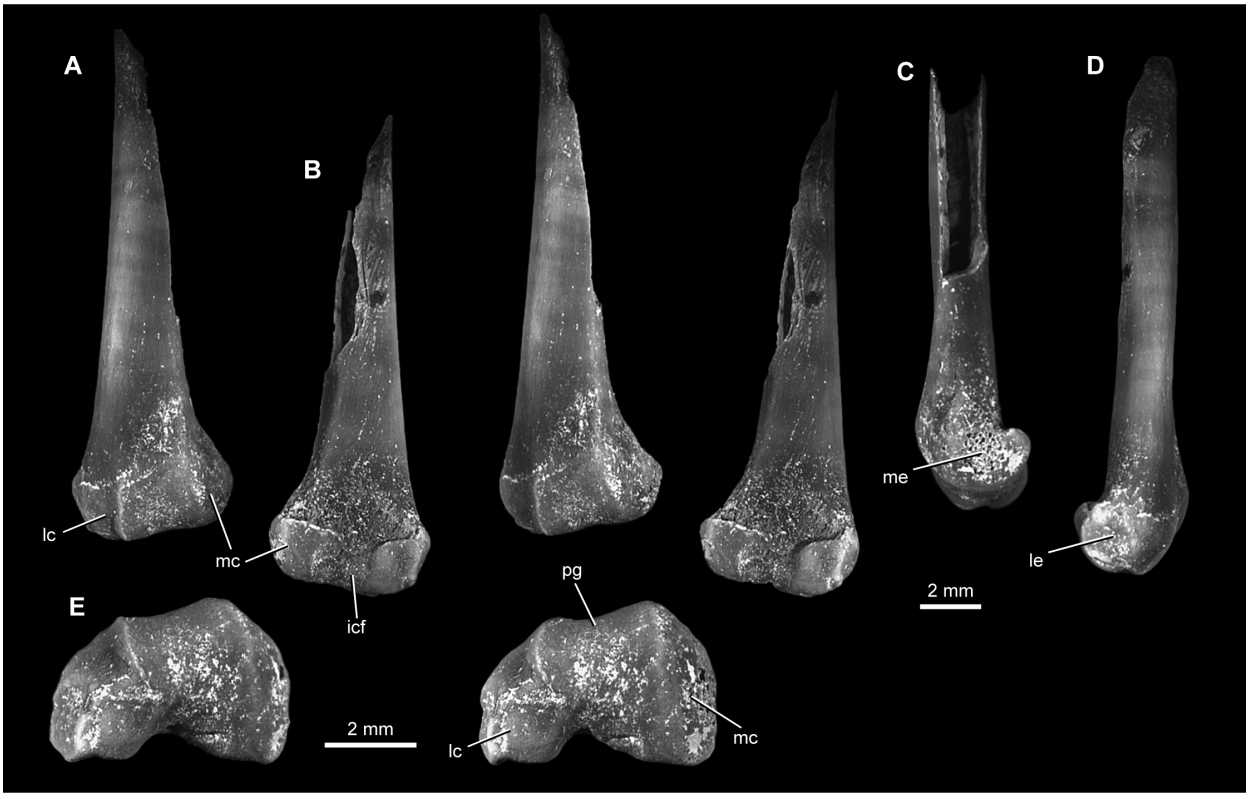

Figure 2.15. Left proximal femur (UCMP 195935 from loc. V99438) representing eutherian morphotype Eu1 from the middle Tullock Formation (Pu2/3) of eastern Montana, in stereo anterior (**A**) and posterior (**B**) views, and medial (**C**) and proximal (**D**) views.

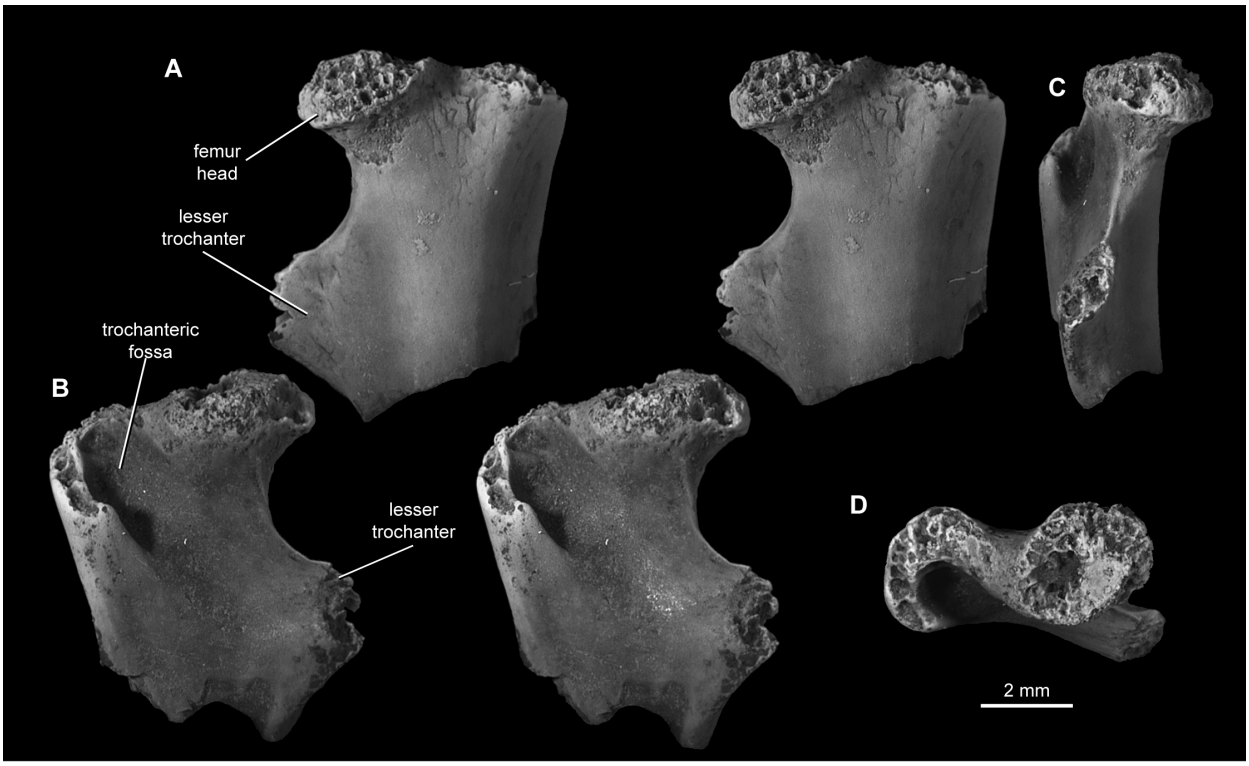

Figure 2.16. Left proximal femur (UCMP 152004 from loc. V87095) representative of eutherian morphotype Eu2 from the lower Tullock Formation (Pu1) of eastern Montana, in stereo anterior (**A**) and posterior (**B**) views, and medial (**C**) and proximal (**D**) views.

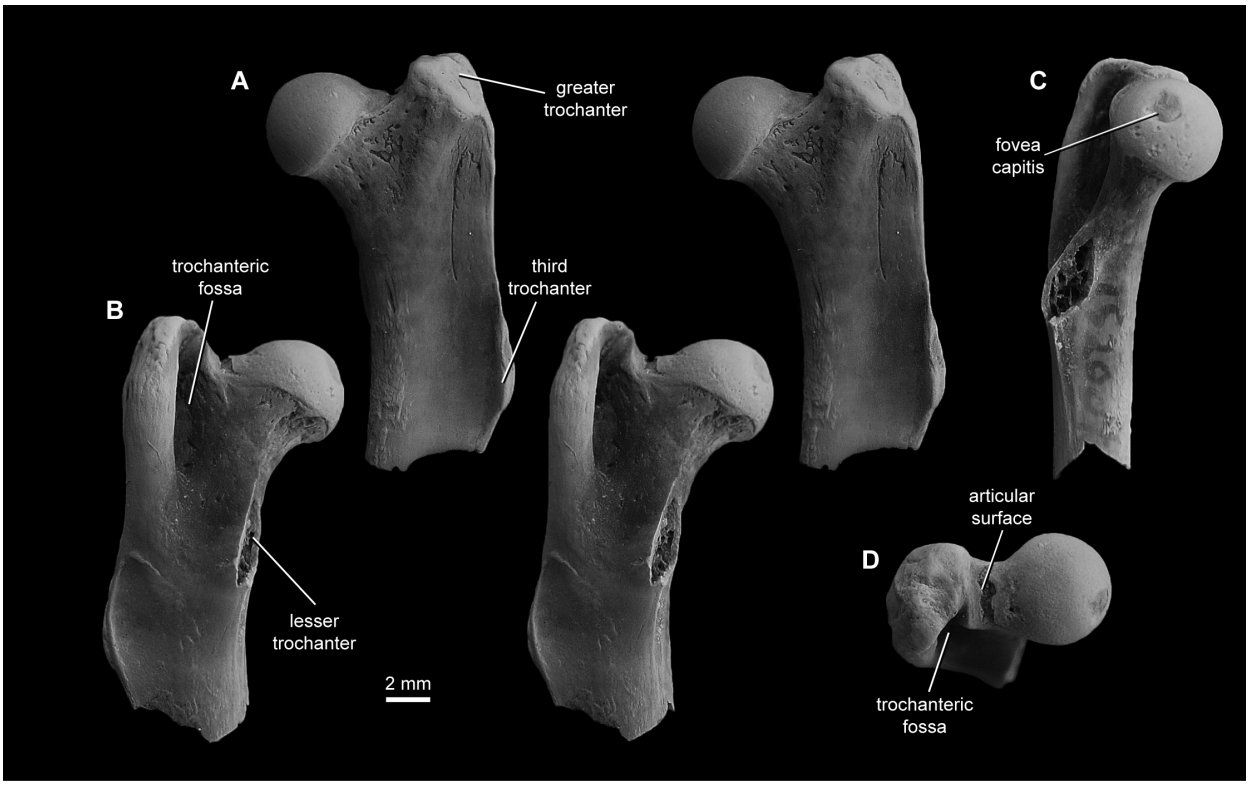

Figure 2.17. Left proximal femur (UCMP 192674 from loc. V87086) representing eutherian morphotype Eu3 from the lower Tullock Formation (Pu1) of eastern Montana, in stereo anterior (**A**) and posterior (**B**) views, and medial (**C**) and proximal (**D**) views.

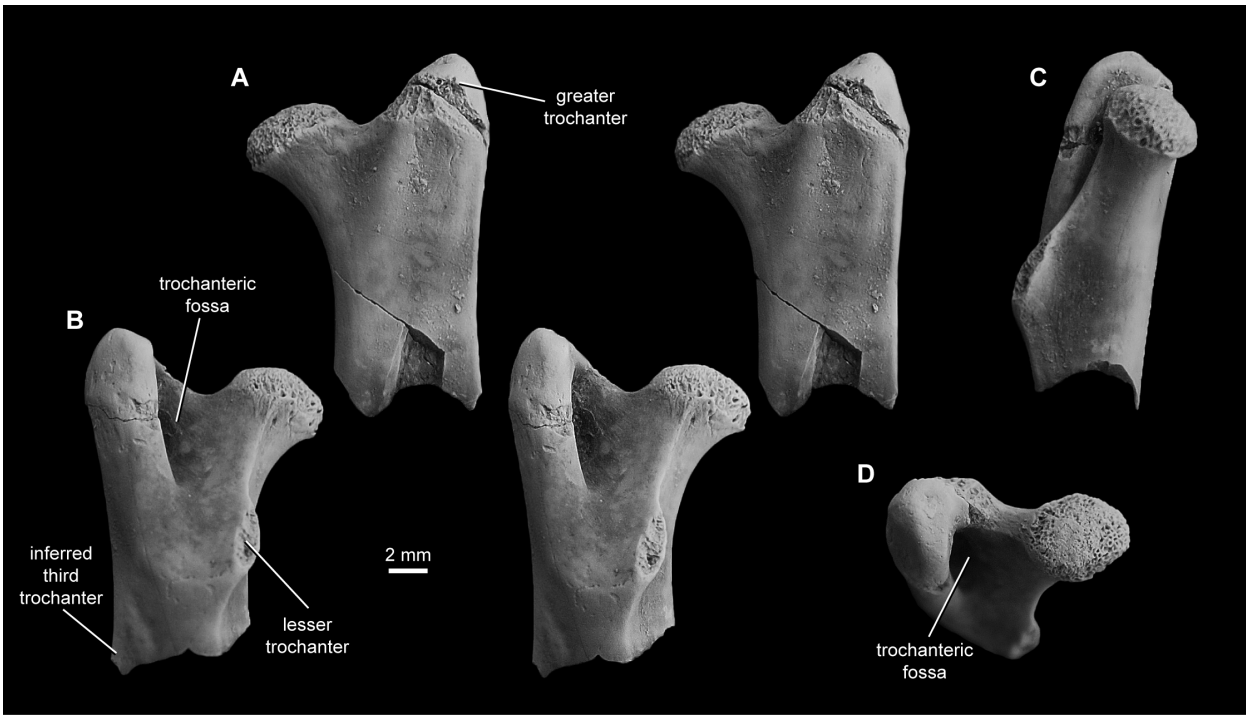

Figure 2.18. Right distal femur (UCMP 145607 from loc. V73080) representing eutherian morphotype Eu4 from the middle Tullock Formation (Pu2/3) of in eastern Montana, in stereo distal (**A**) and posterior (**B**) views, and lateral (**C**) and medial (**D**) views.

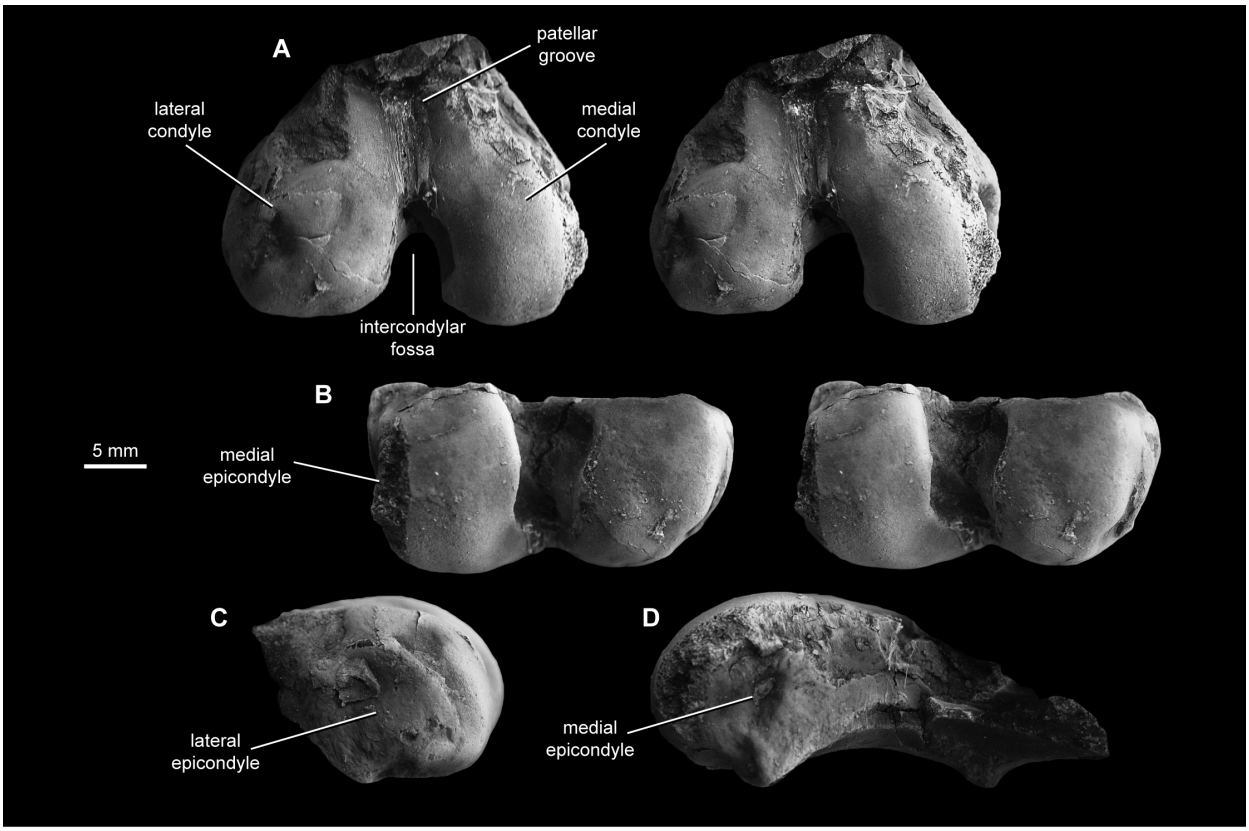

Figure 2.19. Femur morphotypes and relative sizes through the Hell Creek and Tullock formations of eastern Montana. (**A**) Multituberculate morphotypes are shown as black bars and eutherians as white bars. Numbers within the bars indicate the morphotype sample size for each temporal bin. Morphotypes are horizontally arranged according to ordinal size categories (size 1–6) with the scaled outlines showing representative specimens for each size category (size 1 = Mu1; size 2 = Mu6; size 3 = small Mu8; size 4 = large Mu8; size 5 = Mu10; size 6 = Eu4; see text for specimen numbers and localities). The black gradient for Mu5 and Mu7 indicates those multituberculate morphotypes were present in the time-averaged Bug Creek Anthills assemblages, and the morphotype range may extend into the Pu1 and the Lancian, respectively. Ages for the K-Pg boundary and within the Tullock Formation are based on radiometric age determinations of tuffs within lignites, whereas the age for the base of the Hell Creek Formation is based on linear extrapolation of sedimentation rate (Swisher et al. 1993; Renne et al. 2011, 2013; Wilson 2014). Abbreviations: Fm, formation; NALMA, North American Land Mammal "age"; Pu1, early Puercan; Pu2/3, middle/late Puercan. (**B**) Mean femur size throughout the study section with 95% confidence intervals, see text for details, and Tables S2.7, S2.8 for means and t-tests of significance. All Lancian taxa are assumed to be resident taxa; Pu1 and Pu2/3 taxa are separated by resident (open bars) and immigrant taxa (hashed bars), according to morphotype taxonomic attributions (see Discussion) and Clemens (2002). Asterisk indicates the size of Pu1 resident taxa is significantly different from the size of Pu1 immigrants.

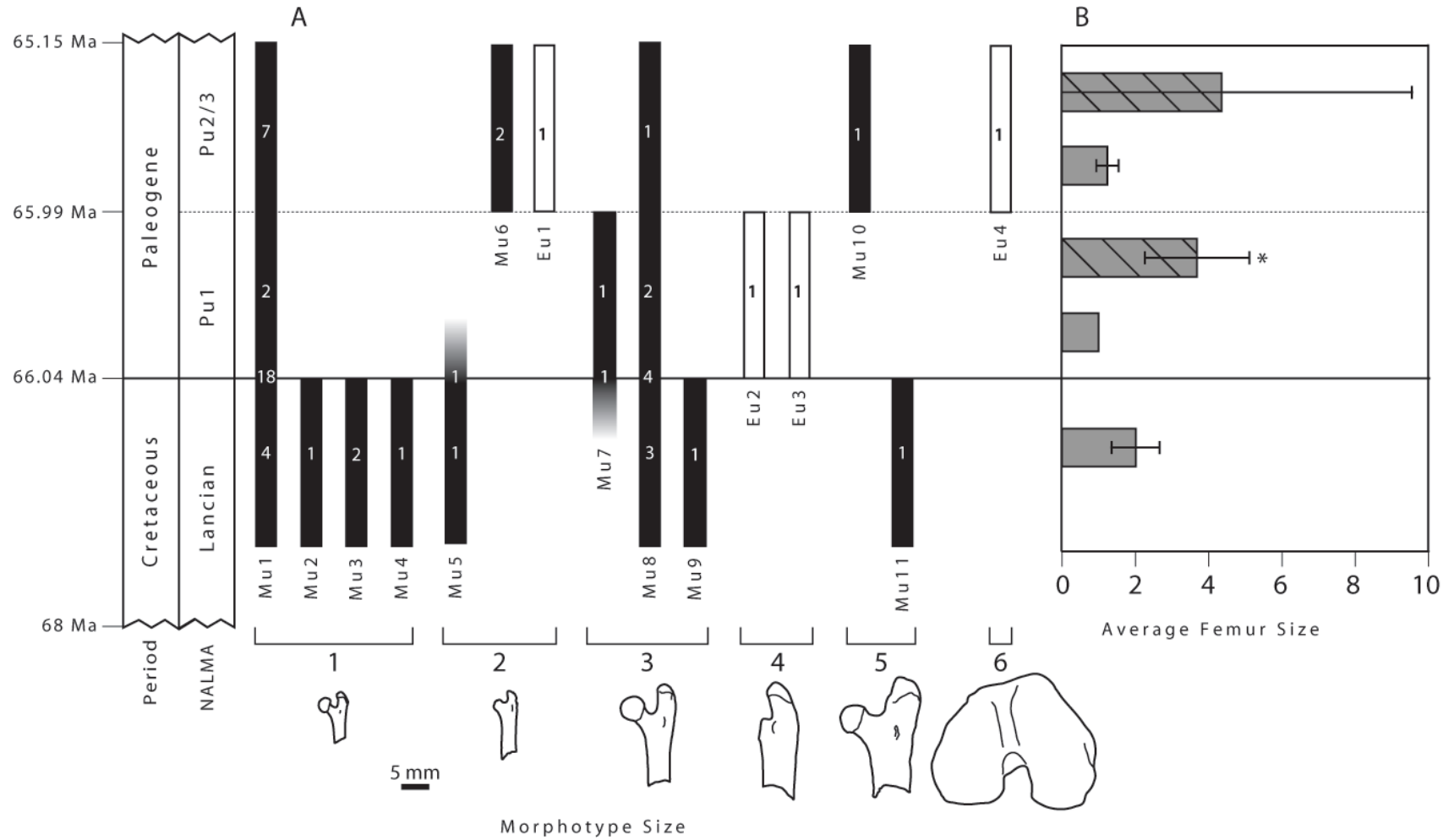
A
B
65.15 Ma
65.99 Ma
66.04 Ma
68 Ma
Paleogene
Cretaceous
Pu2/3
Pu1
Lancian
Period
NALMA
Mu1
Mu2
Mu3
Mu4
Mu5
Mu6
Eu1
Mu7
Mu8
Mu9
Eu2
Eu3
Mu10
Mu11
Eu4
7
2
18
4
1
2
1
1
1
1
2
1
1
1
1
1
1
1
2
4
3
1
1
1
1
1
1
2
3
4
5
6
5 mm
Morphotype Size
0
2
4
6
8
10
Average Femur Size
*

Tables

Table 2.1. Descriptions of proximal and distal femur measurements. Measurements FGTL, FHL, FHW, FLTD, FDEW, FMCW, FLCW, FICNW are modeled after measurements 12, 10, 11, 27, 19, 22, 23, and 26, respectively, in Sargis (2002); FSMLD and FSAP are modified from measurements 15 and 16, respectively, in Sargis (2002); FPEW and FDED are from Chester et al. (2012b). The anatomical view from which the measurement was taken (as it relates to multituberculate femora, see text for more details) is indicated in parentheses.

Proximal Femur Measurements		
Measurements		**Description**
FPEW	Femur Proximal End Width	Medial edge of femoral head to lateral edge of greater trochanter (dorsal)
FGTL	Femur Greater Trochanter Proximal Extension	Proximal edge of greater trochanter to point on femur where the greater trochanter meets the femoral neck and where the greater trochanter begins to protrude proximally (dorsal)
FHL	Femur Head Length	Proximal edge of head to distal edge (dorsal)
FHW	Femur Head Width	Medial edge of head to lateral edge (dorsal)
FMNW	Femur Minimum Neck Width	Minimum neck width, measured from the proximolateral to mediodistal neck margin (dorsal)
FNL	Femur Neck Length	Distance between the base of the head articular surface and the junction of the neck with the greater trochanter/shaft, perpendicular to the neck width, FMNW, measurement (dorsal)
FLTLW	Femur Lesser Trochanter Lateral Width	Distance between the lateral margin of the lesser trochanter and the lateral edge of the specimen (ventral)
FSMLP	Femur Shaft Mediolateral width (proximal)	Distance between the medial and lateral edges of shaft, at posttrochanteric fossa distal extent (ventral)
FSMLD	Femur Shaft Mediolateral width (distal)	Distance between the medial and lateral edges of shaft, at most distal point (breakage point) on the specimen (ventral)
FSAP	Femur Shaft Dorsoventral width	Shaft width from the dorsal to the ventral edge of the shaft, taken at the most distal point (breakage) of the specimen (medial)
Distal Femur Measurements		
Measurements		**Description**
FDEW	Femur Distal End Width	Medial edge of medial condyle to lateral edge of lateral condyle (dorsal)
FDED	Femoral Distal End Depth	Most ventral edge of condyles to most dorsal edge of patellar ridges (distal)
FMCW	Femoral Medial Condyle Width	Medial edge to lateral edge (ventral)
FLCW	Femoral Lateral Condyle Width	Medial edge to lateral edge (ventral)
FICNW	Femoral Intercondylar Notch Width	Lateral edge of medial condyle to medial edge of lateral condyle (ventral)

Table 2.2. Measurements of proximal femur specimens. See Table 2.1 for measurement descriptions; measurements taken in dorsal (multituberculates) or anterior (eutherians) view include FPEW, FGTL, FHL, FHW, FMNW, and FNL; measurements in ventral (multituberculates) or posterior (eutherians) view include: FLTLW, FSMLP, and FSMLD; FSAP was taken in medial view. All measurements are in millimeters. Abbreviations: Fm, Formation; HC, Hell Creek; Morph., Morphotype; Tu, Tullock. Locality numbers follow the system of each institution; those beginning with "V" are UCMP localities; those beginning with "C" are UWBM localities. The locality data for specimen MOR 882 is unknown. Parentheses indicate that the assignment to morphotype is tentative, due to incomplete preservation; see text for more details. Asterisks indicate minimum size values, where preserved morphology was measured but the full measurement was not possible, due to specimen breakage; "A" indicates an inferred size measurement; "B" indicates that the specimen was broken and shaft measurements were taken proximal to the breakage and the re-glued portion; "C" indicates that the specimen has exceptional shaft preservation, such that the "distal" mediolateral shaft width of other specimens was better approximated by an approximate "mid-shaft" mediolateral width; "–" indicates specimen was broken; "NA" indicates non-applicable measurements, as eutherian femora lack post-trochanteric fossae. The UCMP locality V75178 (Wild Horse Basin) is of somewhat questionable age, with all material suggestive of a Lancian age except for one tooth of a Pu1 eutherian taxon; we interpret the locality (and our multituberculate femur) as Lancian in age, although our results are not affected by the biozone age of this specimen.

Specimen	Locality	Fm	Biozone	Morph.	Relative Size	Dorsal							Ventral		Medial
						FPEW	FGTL	FHL	FHW	FMNW	FNL	FLTLW	FSMLP	FSMLD	FSAP
174448	V84043	HC	Lancian	Mu1	1	–	2.360	–	–	–	–	0.770	–	–	–
127394	V88006	HC	Lancian	Mu1	1	4.095	–	1.895	1.680	1.140	0.875	0.565*	1.865	–	1.180
127387	V88007	HC	Lancian	Mu1	1	5.480	2.450	2.355	2.210	1.400	1.255	0.830	2.315	1.890	–
555982	V99369	HC	Lancian	Mu1	1	–	–	–	–	–	–	0.805*	2.185	1.955	1.290
195979	V65127	Tu	mixed	Mu1	1	–	1.940	–	–	–	–	0.650	1.865	1.760	1.280
195981	V65127	Tu	mixed	Mu1	1	–	–	–	–	1.260*	0.630*	0.560*	2.110	–	–
195985	V65127	Tu	mixed	Mu1	1	–	–	–	–	1.090*	0.960*	0.855	1.810	1.715	1.435
196965	V70201	Tu	mixed	Mu1	1	–	–	–	–	1.075	1.030*	0.660	2.080	1.765	1.215
196967	V70201	Tu	mixed	Mu1	1	4.705*	–	2.030*	1.935	1.360	1.030	0.725	2.200	1.945	1.420
196969	V70201	Tu	mixed	Mu1	1	3.115*	–	1.490	1.310	0.860	0.745	0.455*	1.490	1.290	0.095
196975	V70201	Tu	mixed	(Mu1)	1	–	–	–	–	1.280	–	1.045*	1.690	1.755	1.185
196976	V70201	Tu	mixed	Mu1	1	–	1.885*	–	–	–	–	0.505*	1.970	1.650	1.440
196977	V70201	Tu	mixed	(Mu1)	1	3.620*	–	1.775*	1.275*	1.185	0.825	0.620	1.770	–	1.160
196978	V70201	Tu	mixed	Mu1	1	–	–	–	–	0.995	1.085*	0.540*	1.740	1.635	1.035
195986	V65127	Tu	mixed	Mu1	1	4.110*	–	1.755	1.405*	1.120	1.100	0.680*	1.815	–	1.120
196961	V70201	Tu	mixed	Mu1	1	–	1.735*	–	–	–	–	0.715*	1.910	–	1.350
196966	V70201	Tu	mixed	Mu1	1	–	–	–	–	–	–	0.690	1.935	1.785	1.235
196970	V70201	Tu	mixed	Mu1	1	–	–	–	–	1.225	0.835*	0.685	2.170	1.865	1.425
196972	V70201	Tu	mixed	Mu1	1	–	–	–	–	0.930	0.830*	0.835	1.625	1.510	1.285*
196974	V70201	Tu	mixed	Mu1	1	–	–	1.885*	1.250*	1.145	0.970	0.875	1.675	–	1.930*
70535	C0338	Tu	mixed	Mu1	1	3.170	2.235	1.905	1.735	1.205	1.095	0.830	2.030	1.760	1.295
70536	C0338	Tu	mixed	Mu1	1	4.885*	–	2.255	1.935	1.180	0.960	0.880	2.375	2.025	1.400
70974	C0338	Tu	mixed	Mu1	1	4.435	–	1.720	1.655	1.130	0.975*	0.670	2.220	1.945	1.190
94267	C0338	Tu	mixed	Mu1	1	–	–	–	–	1.125	1.155*	0.760	–	–	–
192554	V77128	Tu	Pu1	Mu1	1	4.845	2.475	2.310	2.045	1.265	0.905	1.100	2.205	1.855	1.375
153040	V84193	HC	Pu1	Mu1	1	–	2.465	–	–	1.175*	–	–	–	–	–
195963	V72128	Tu	Pu2/3	Mu1	1	–	–	–	–	1.160*	0.745*	0.620*	2.010	1.660	1.210*
195902	V73080	Tu	Pu2/3	Mu1	1	–	–	–	–	1.040	0.670*	0.790*	1.890	1.670	1.190
557503	V74122	Tu	Pu2/3	Mu1	1	3.290*	–	1.495	1.450	0.950	0.800	–	–	–	–
153093	V99438	Tu	Pu2/3	Mu1	1	–	2.160	–	–	–	–	0.870*	–	–	–
153094	V99438	Tu	Pu2/3	Mu1	1	–	–	–	–	2.740	0.950	0.820	–	–	1.080
557505	V99438	Tu	Pu2/3	Mu1	1	–	–	1.755	1.625	0.945	1.035	–	–	–	–

557506	V99438	Tu	Pu2/3	Mu1	1	–	1.595	–	–	–	–	0.595*	1.445	1.235	0.975
127392	V88009	HC	Lancian	Mu2	1	0.205*	–	2.055	1.720	1.100	1.015	1.095	1.845	1.735	1.230
127382	V88007	HC	Lancian	Mu3	1	2.335*	2.485	2.050	1.800*	1.130	1.650	–	2.195	–	1.385
127388	V88007	HC	Lancian	Mu3	1	4.655*	–	2.035A	1.655*	1.020	1.375	0.730*	1.725	1.450	–
174494	V75173	HC	Lancian	Mu4	1	5.430	1.880*	2.045	1.860	1.495	1.415	1.165	2.300	2.030	1.095
174343	V84148	HC	Lancian	Mu5	2	6.210*	–	2.340	2.010	1.555	1.67*	0.650	2.880	2.590	1.670
196964	V70201	Tu	mixed	Mu5	2	–	3.840*	–	–	1.735	2.360	–	–	–	–
195901	V73080	Tu	Pu2/3	Mu6	2	–	–	–	–	1.795	1.365	1.215	3.625	3.230	2.350
153092	V99438	Tu	Pu2/3	Mu6	2	–	–	–	–	1.770*	1.480*	1.160*	3.770	3.475B	2.150B
195977	V65127	Tu	mixed	Mu7	3	–	–	–	–	2.310	1.625*	1.925*	5.045	4.105	2.670
194860	V74111	Tu	Pu1	Mu7	3	–	3.660*	–	–	2.225	1.695*	1.600	–	4.095*	2.605*
117602	V73097	HC	Lancian	Mu8	4	–	6.770	–	–	–	–	2.370	6.505	6.100	4.055
174544	V75178	HC	Lancian	Mu8	3	7.695	4.725	3.090	2.785*	2.035	2.285	1.500	–	–	–
174397	V87080	HC	Lancian	Mu8	3	–	–	–	–	2.585	1.620*	1.975	4.600	4.260	2.645
127383	V88007	HC	Lancian	(Mu8)	2	–	–	–	–	1.430	1.085*	1.405	2.890	2.720	2.010
195980	V65127	Tu	mixed	(Mu8)	2	–	–	–	–	1.915	1.755*	1.370*	–	–	2.090
153000	V65127	Tu	mixed	Mu8	3	–	–	–	–	2.320*	2.075*	2.150	4.245	4.040	2.725
195972	V65127	Tu	mixed	Mu8	3	–	–	–	–	2.100*	1.165*	2.205	4.245	3.870	2.600
102444	V70201	Tu	mixed	Mu8	3	9.930	5.180	4.250	4.130	2.715	1.770	2.890	5.010	4.295	3.095
196971	V70201	Tu	mixed	Mu8	3	–	–	–	–	–	–	1.980	5.085	4.625	2.700
187551	V96268	HC	Pu1	Mu8	3	–	–	–	–	2.805	1.500	2.865	4.825	4.370	2.845
195966	V72137	Tu	Pu2/3	(Mu8)	2	–	–	–	–	1.995	1.700*	1.730*	3.355	2.940	2.225
152997	V73080	Tu	Pu2/3	Mu8	3	–	4.990	–	–	2.345	1.225*	1.710	3.800*	–	2.240
152996	V91002	Tu	Pu1	Mu8	3	–	–	–	–	2.345	2.630	–	4.105	3.485	2.840
174532	V73102	HC	Lancian	Mu9	3	–	–	–	–	2.350*	1.725*	2.395*	4.645	3.825	3.215
153091	V99438	Tu	Pu2/3	Mu10	5	14.145*	6.995	4.595*	4.135*	4.460	2.440	3.365*	7.145*	6.840*	5.480
882	unknown	HC	Lancian	Mu11	5	16.060*	–	6.770	5.910*	4.685	4.670	2.795*	7.595*	6.705C	4.46C
195935	V99438	Tu	Pu2/3	Eu1	2	4.810*	–	1.350*	2.100*	2.135	0.835	–	NA	–	–
152004	V87095	HC	Pu1	Eu2	4	9.845	1.595	4.365	4.295	4.805	1.190	4.705	NA	5.265	3.385
192674	V87076	HC	Pu1	Eu3	4	1.965*	3.655	3.490*	4.640*	4.535	1.540	4.955	NA	7.055	4.840

Table 2.3. Measurements of distal femur specimens. See Table 2.1 for measurement descriptions. All measurements are in millimeters. All measurements on the multituberculate femur were taken in dorsal view; those on the eutherian femur were taken in anterior view. Abbreviations: Fm, Formation; HC, Hell Creek; Tu, Tullock. Asterisk indicates that the measurement was taken in distal view.

						Dorsal	Distal	Ventral		
Specimen	**Locality**	**Locality**	**Biozone**	**Morphotype**	**Relative Size**	**FDEW**	**FDED**	**FMCW**	**FLCW**	**FICNW**
174391	V91051	HC	Lancian	(Mu5)	2–3	5.375	3.495	2.030	2.425	0.885
145607	V73080	Tu	Pu2/3	Eu4	6	32.765*	–	–	–	–

SUPPLEMENTARY MATERIAL FOR

Mammalian Femora from across the Cretaceous-Paleogene Boundary in eastern Montana

1. Additional Descriptive Information for Multituberculate Femur Morphotypes

*Referenced figures and section numbers match those in the text.

3.1.1. Proximal femur morphotype Mu1 (Fig. 2.3A–D)

Referred specimens.—Lancian: UCMP 174448, from loc. V84043 (Hell Creek Fm., McCone Co., MT); UCMP 127394, from loc. V88006 (Hell Creek Fm., Carter Co., MT); UCMP 127387, from loc. V88007 (Hell Creek Fm., Carter Co., MT); and UCMP 555982, from loc. V99369 (Hell Creek Fm., Garfield Co., MT). Lancian/Pu1 mixed: UCMP 195979, 195981, 195985, and 195986, from loc. V65127 (Tullock Fm., McCone Co., MT); UCMP 196961, 196966, 196969, 196970, 196972, 196974, 196976, and 196978, from loc. V70201 (Tullock Fm., McCone Co., MT); and UWBM 70535, 70536, 70974, and 94267, from loc. C0338 (Tullock Fm., McCone Co., MT); Pu1: UCMP 192554 (Fig. 2.3), from loc. V77128 (Tullock Fm., Garfield Co., MT); and UCMP 153040, from loc. V84193 (Hell Creek Fm., McCone Co., MT). Pu2/3: UCMP 195963, from loc. V72128 (Tullock Fm., Garfield Co., MT); UCMP 195902, from loc. V73080 (Tullock Fm., Garfield Co., MT); UCMP 557503, from loc. V74122 (Tullock Fm., Garfield Co., MT); and UCMP 153093, 153094, 557505, and 557506, from loc. V99438 (Tullock Fm., Garfield Co., MT).

Tentatively referred specimens.—Lancian/Pu1 mixed: UCMP 196975, and 196977, from loc. V70201 (Tullock Fm., McCone Co., MT).

Additional morphological features.—Specimens within this morphotype also exhibit the following features that are common among multituberculate femora: a spherical

(greater than hemispherical) head with more volume displaced proximally than distally relative to the clear junction with the cylindrical neck; a greater trochanter that is aligned with the shaft, dorsally recumbent, and curved medially toward the head, and that exhibits an inflated, rugose area proximally and laterally; and a straight shaft that is elliptical, wider mediolaterally, in cross section.

3.1.2. Proximal femur morphotype Mu2 (Fig. 2.4A–D)

Referred specimen.—Lancian: UCMP 127392 (Fig. 2.4), from loc. V88009 (Hell Creek Fm., Carter Co., MT).

Additional morphological features.—Specimens within this morphotype also exhibit the following features that are common among multituberculate femora: a spherical head with more volume displaced proximal to the junction with the cylindrical neck; a bulbous and hemispherical lesser trochanter that is approximately one-fifth of the size of the head; and a shaft that is elliptical in cross-section, wider mediolaterally.

3.1.3. Proximal femur morphotype Mu3 (Fig. 2.5A–D)

Referred specimens.—Lancian: UCMP 127382 (Fig. 2.5) and 127388, from loc. V88007 (Hell Creek Fm., Carter Co., MT).

Additional morphological features.—Specimens in Mu3 also exhibit several traits that are common among multituberculates, including: a spherical head with more volume proximal than distal to the junction with the cylindrical neck; a greater trochanter that extends beyond the head, is aligned with the shaft, is dorsally recumbent, curved medially,

and preserves a rugose area laterally; and a lesser trochanter that is convex proximolaterally and concave mediodistally.

3.1.4. Proximal femur morphotype Mu4 (Fig. 2.6A–D)

Referred specimen.—Lancian: UCMP 174494, from loc. V75173 (Hell Creek Fm., Garfield Co., MT).

Additional morphological features.—The specimen within this morphotype also exhibits the following features that are common among multituberculate femora: a greater trochanter that is aligned with the shaft and extends beyond the head; and a hemispherical lesser trochanter that is concave distally and is approximately half the size of the head. The head of Mu4 is similar in size to those of Mu1–Mu3, and Mu4 has a shaft cross-sectional diameter that is near the upper size range of shafts in Mu1 (see Table 2.2).

3.1.5. Proximal femur morphotype Mu5 (Fig. 2.7A–E)

Referred specimens.—Lancian: UCMP 174343 (Fig. 2.7E), from loc. V84148 (Hell Creek Fm., Garfield Co., MT). Lancian/Pu1 mixed: UCMP 196964 (Fig. 2.7A–D), from loc. V70201 (Tullock Fm., McCone Co., MT).

Additional morphological features.—The specimens within this morphotype also exhibit features that are common among multituberculate femora, specifically: UCMP 174343 has a spherical head, and a hemispherical lesser trochanter that is approximately equal in size to the head and has a hook-like profile in distal view; and UCMP 196964 has a greater trochanter that is aligned with the shaft and extends beyond the inferred head height.

3.1.6. Proximal femur morphotype Mu6 (Fig. 2.8A–D)

Referred specimens.—Pu2/3: UCMP 195901, from loc. V73080 (Tullock Fm., Garfield Co., MT); and UCMP 153092 (Fig. 2.8), from loc. V99438 (Tullock Fm., Garfield Co., MT).

Additional morphological features.—The specimens in Mu6 also exhibit the following features common among multituberculate femora: a lesser trochanter that is lunate to hemispherical in shape at the junction with the shaft.

3.1.7. Proximal femur morphotype Mu7 (Fig. 2.9A–E)

Referred specimens.—Lancian/Pu1 mixed: UCMP 195977, from loc. V65127 (Tullock Fm., McCone Co., MT). Pu1: UCMP 194860 (Fig. 2.9), from loc. V74111 (Tullock Fm., Garfield Co., MT).

Additional morphological features.—Specimens in this morphotype exhibit features common among other multituberculates, including: a cylindrical neck; a greater trochanter that is aligned with the shaft and appears to extend beyond the head, is dorsally recumbent, and has a rugose area laterally; and a lesser trochanter that is hemispherical and has a distal hook.

3.1.8. Proximal femur morphotype Mu8 (Fig. 2.10A–D)

Referred specimens.—Lancian: UCMP 117602, from loc. V73097 (Hell Creek Fm., Garfield Co., MT); UCMP 174397, from loc. V87080 (Hell Creek Fm., McCone Co., MT); and UCMP 174544, from loc. V75178 (Hell Creek Fm., Garfield Co., MT). Lancian/Pu1 mixed: UCMP 153000, and 195972, from loc. V65127 (Tullock Fm., McCone Co., MT); UCMP

102444 (Fig. 2.10) and 196971, from loc. V70201 (Tullock Fm., McCone Co., MT). Pu1: UCMP 187551, from loc. V96268 (Hell Creek Fm., Garfield Co., MT); and UCMP 152996, from UCMP V91002 (Tullock Fm., McCone Co., MT). Pu2/3: UCMP 152997, from loc. V73080 (Tullock Fm., Garfield Co., MT).

Tentatively referred specimens.—Lancian: UCMP 127383, from loc. V88007 (Hell Creek Fm., Carter Co., MT). Lancian/Pu1 mixed: 195980, from loc. V65127 (Tullock Fm., McCone Co., MT). Pu2/3: UCMP 195966, from loc. V72137 (Tullock Fm., Garfield Co., MT).

Additional morphological features.—Specimens in Mu8 exhibit features common among multituberculates, including: a nearly spherical head, with an articular surface oriented proximomedially; a cylindrical neck; a greater trochanter that is aligned with the shaft and extends beyond the head, is dorsally recumbent, and has a well defined margin dorsal to the rugose area; a lesser trochanter that is triangular to hemispherical, has a constricted neck at the junction with the shaft, and a hook-shaped distal end; and a straight shaft that is elliptical in cross-section, wider mediolaterally.

3.1.9. Proximal femur morphotype Mu9 (Fig. 2.11A–D)

Referred specimen.—Lancian: UCMP 174532, from loc. V73102 (Hell Creek Fm., Garfield Co., MT).

Additional morphological features.—Mu7 also exhibits the following features that are common among multituberculates: a cylindrical neck; and a straight shaft that is elliptical in cross-section, wider mediolaterally.

3.1.10. Proximal femur morphotype Mu10 (Fig. 2.12A–D)

Referred specimen.—Pu2/3: UCMP 153091, from loc. V99438 (Tullock Fm., Garfield Co., MT).

Additional morphological features.—This morphotype exhibits the following features common among other multituberculates: a cylindrical neck; a greater trochanter that is aligned with the shaft and is slightly dorsally recumbent; and a shaft that has an elliptical cross-section, wider mediolaterally.

3.1.11. Proximal femur morphotype Mu11 (Fig. 2.13A–D)

Referred specimen.—Lancian: MOR 882, specific locality unknown (Makoshika State Park; Hell Creek Fm., Dawson Co., MT).

Additional morphological features.—This morphotype exhibits the following features common among other multituberculates: a spherical head; cylindrical neck; and a shaft that has an elliptical cross-section, wider mediolaterally.

2. Supplementary Tables and Figures

Table S2.1. Femur specimen localities. All localities are located in Montana, in Garfield, McCone, or Carter counties (one specimen additionally comes from an unknown locality in Dawson county). Locality numbers that begin with "V" are UCMP localities; those beginning with "C" are UWBM localities. Abbreviations: Fm, Formation; HC, Hell Creek; Tu, Tullock; Pu1, Puercan 1; Pu2/3, Puercan 2/3 undifferentiated biozone; n, number of femur specimens.

Locality Number	Locality Name	County	Fm	Biozone	n
V65127	Bug Creek Anthills General	McCone	Tu	mixed	8
V70201	Bug Creek Anthills C	McCone	Tu	mixed	15
V72128	Garbani 03-NW Surface	Garfield	Tu	Pu2/3	1
V72137	Garbani 12-Nw Macdonald Ext	Garfield	Tu	Pu2/3	1
V73080	Garbani 13-NW Harley's High	Garfield	Tu	Pu2/3	3
V73097	Brownie Butte	Garfield	HC	Lancian	1
V73102	Didelphodon	Garfield	HC	Lancian	1
V74111	Worm Coulee 1	Garfield	Tu	Pu1	1
V74122	Biscuit Springs	Garfield	Tu	Pu2/3	1
V75173	Billy Creek 2	Garfield	HC	Lancian	1
V75178	Wild Horse Basin	Garfield	HC	Lancian	1
V77128	Morales 1	Garfield	Tu	Pu1	1
V84043	Laurie's Painted Rock	McCone	HC	Lancian	1
V84148	Egg Shell	Garfield	HC	Lancian	1
V84193	Z-Line Quarry	McCone	HC	Pu1	1
V87076	Grass Patch North	McCone	HC	Pu1	1
V87080	Three Buttes 3	McCone	HC	Lancian	1
V87095	Rattlesnake Nest	McCone	HC	Pu1	1
V88006	Johnstone Anthill 7	Carter	HC	Lancian	1
V88007	Spigot Bottle	Carter	HC	Lancian	4
V88009	Spigot Gary's Spot	Carter	HC	Lancian	1
V91002	Coal Bank Coulee West 3	McCone	Tu	Pu1	1
V96268	Constenius Locality	Garfield	HC	Pu1	1
V99369	Celeste's Magnificent Microsite	Garfield	HC	Lancian	1
V99438	Garbani Sandy Channel	Garfield	Tu	Pu2/3	7
C0338	Bug Creek A	McCone	Tu	mixed	4

Figure S2.1. Additional measurements taken on proximal femur specimens in ventral (A) and dorsal (B) views. Abbreviations: FHMLD, head mediolateral depth; FHSID, head superoinferior diameter; FLTD, lesser trochanter distal extent; FLTH, lesser trochanter height; FLTM, lesser trochanter maximum; FLTP, lesser trochanter proximal extent; FLTW, lesser trochanter width. See Tables S2.2 and S2.3 for descriptions and measurements, respectively.

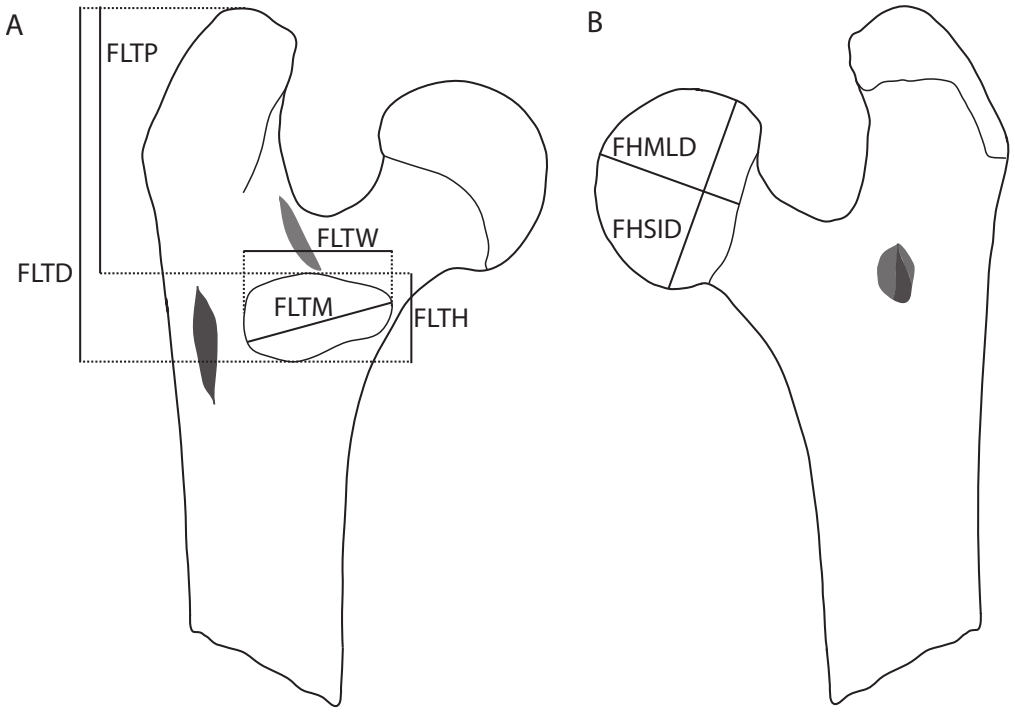

Table S2.2. Descriptions of additional proximal femur measurements. The view from which the measurements was taken is in parentheses. FSID and FHMLD are measurements SI and ML, respectively, in Egi (2001).

Proximal Femur Measurements		
Measurements		**Description**
FHSID	Femur Head Superoinferior Diameter	Maximum head diameter, from the proximolateral to distomedial margin (dorsal)
FHMLD	Femur Head Mediolateral Depth	Head depth from midpoint at the base of head to proximomedial head extent (dorsal)
FLTP	Femur Lesser Trochanter Proximal Extent	Proximal edge of greater trochanter to proximal edge of lesser trochanter (ventral)
FLTD	Femur Lesser Trochanter Distal Extent	Proximal edge of greater trochanter to distal margin of lesser trochanter, aligned to the shaft (ventral)
FLTH	Femur Lesser Trochanter Height	Height of the lesser trochanter from proximal margin to distal margin (ventral)
FLTW	Femur Lesser Trochanter Width	Width of the lesser trochanter from medial margin to lateral margin (ventral)
FLTM	Femur Lesser Trochanter Maximum	Largest dimension of lesser trochanter at its junction with shaft (ventral)

Table S2.3. Additional measurements of proximal femur specimens, see Table S2.2 for measurement descriptions; taken in dorsal (multituberculates) and anterior (eutherians) view include FHSID and FHMLD; measurements in ventral (multituberculate) and posterior (eutherian) view include: FLTP, FLTD, FLTH, FLTW, and FLTM. All measurements are in millimeters. Abbreviations: Fm, Formation; HC, Hell Creek; Tu, Tullock. Locality numbers that begin with "V" are UCMP localities; those beginning with "C" are UWBM localities. The locality data for specimen MOR 882 is unknown. Parentheses indicate that the assignment to morphotype is tentative, due to incomplete preservation. Asterisks indicate minimum size values, where preserved morphology was measured but the full measurement was not possible, due to specimen breakage; "A" indicates potential overestimates of size due to breakage; "–" indicates specimen was broken.

					Dorsal		Ventral				
Specimen	**Locality**	**Fm**	**Biozone**	**Morphotype**	**FHSID**	**FHMLD**	**FLTP**	**FLTD**	**FLTH**	**FLTW**	**FLTM**
174448	V84043	HC	Lancian	Mu1	–	–	3.060	4.180	0.700	1.395	1.635
127394	V88006	HC	Lancian	Mu1	2.010	1.480	–	–	0.655	1.150	1.375
127387	V88007	HC	Lancian	Mu1	2.520	1.855	2.975	4.250	0.825	1.445	1.800
555982	V99369	HC	Lancian	Mu1	–	–	2.955	4.205	0.700	1.325	1.425
195979	V65127	Tu	mixed	Mu1	–	–	2.565	3.835	0.730	1.135	1.400
195981	V65127	Tu	mixed	Mu1	–	–	–	–	0.905	1.310	1.715
195985	V65127	Tu	mixed	Mu1	–	–	–	–	1.965	1.120	1.440
196965	V70201	Tu	mixed	Mu1	–	–	–	–	0.525	1.125	1.330
196967	V70201	Tu	mixed	Mu1	2.340	1.650	–	–	0.670	1.135	1.715
196969	V70201	Tu	mixed	Mu1	1.520	1.130	–	–	0.470	0.860	1.035
196975	V70201	Tu	mixed	(Mu1)	–	–	–	–	0.920	1.165	1.375
196976	V70201	Tu	mixed	Mu1	–	–	2.560*	3.630*	0.730	1.235	1.480
196977	V70201	Tu	mixed	(Mu1)	1.840*	1.300*	–	–	0.765	1.220	1.695
196978	V70201	Tu	mixed	Mu1	–	–	–	–	0.775	1.100	1.360
195986	V65127	Tu	mixed	Mu1	1.870*	1.345*	–	–	0.900	1.180	–
196961	V70201	Tu	mixed	Mu1	–	–	2.275*	3.400*	0.885	1.435	1.610
196966	V70201	Tu	mixed	Mu1	–	–	2.460	3.540	0.785	1.365	1.605
196970	V70201	Tu	mixed	Mu1	–	–	–	–	0.600	1.765	1.870
196972	V70201	Tu	mixed	Mu1	–	–	–	–	0.975	1.205	1.545
196974	V70201	Tu	mixed	Mu1	–	1.380*	–	–	0.810	1.210	1.540
70535	C0338	Tu	mixed	Mu1	1.350	1.335*	2.790	3.895	0.770	1.445	1.575

70536	C0338	Tu	mixed	Mu1	2.285	1.685	–	–	0.575	1.280	1.410
70974	C0338	Tu	mixed	Mu1	1.725	1.550	–	–	1.050	1.310	1.720
94267	C0338	Tu	mixed	Mu1	–	–	–	–	0.560	1.140	1.540
192554	V77128	Tu	Pu1	Mu1	2.345	1.735	3.210	4.275	0.710	1.540	1.750
153040	V84193	HC	Pu1	Mu1	–	–	2.950	3.990	0.730	1.005	1.475
195963	V72128	Tu	Pu2/3	Mu1	–	–	–	–	0.610	1.075	1.385
195902	V73080	Tu	Pu2/3	Mu1	–	–	1.835	2.710	0.620	1.265	1.465
557503	V74122	Tu	Pu2/3	Mu1	1.545	1.155	–	–	0.545	0.865	1.230
153093	V99438	Tu	Pu2/3	Mu1	–	–	2.595	–	–	–	–
153094	V99438	Tu	Pu2/3	Mu1	–	–	–	–	0.645	1.435	1.490
557505	V99438	Tu	Pu2/3	Mu1	1.905	1.285	–	–	0.600	1.180	1.385
557506	V99438	Tu	Pu2/3	Mu1	–	–	1.955	2.880	0.425	0.945	1.085
127392	V88009	HC	Lancian	Mu2	2.100	1.330	–	–	0.425	0.925	1.125
127382	V88007	HC	Lancian	Mu3	2.080	1.405	3.010	4.245	0.830	1.300	1.710
127388	V88007	HC	Lancian	Mu3	–	1.775	2.550*	3.830*	0.785	1.535	1.885
174494	V75173	HC	Lancian	Mu4	2.245	1.785	2.585*	4.315*	1.215	1.355	1.950
174343	V84148	HC	Lancian	Mu5	4.590	1.535*	–	–	1.035	2.185	2.345
196964	V70201	Tu	mixed	Mu5	–	–	4.840*	–	–	–	–
195901	V73080	Tu	Pu2/3	Mu6	–	–	–	–	0.850	2.015	2.070
153092	V99438	Tu	Pu2/3	Mu6	–	–	–	–	0.970	1.745	1.800
195977	V65127	Tu	mixed	Mu7	–	–	–	–	1.615	2.395	3.110
194860	V74111	Tu	Pu1	Mu7	3.250*	–	4.660*	6.445*	1.210	2.220	2.545
117602	V73097	HC	Lancian	Mu8	–	–	9.000	11.540	1.855	2.760	3.380
174544	V75178	HC	Lancian	Mu8	3.095*	2.045	6.025	8.235	1.815	2.175	2.835
174397	V87080	HC	Lancian	Mu8	–	–	–	–	1.240	2.310	2.480
127383	V88007	HC	Lancian	(Mu8)	–	–	–	–	0.970	0.985	1.720
195980	V65127	Tu	mixed	(Mu8)	–	–	–	–	–	–	–
153000	V65127	Tu	mixed	Mu8	–	–	–	–	1.330	2.255	2.175
195972	V65127	Tu	mixed	Mu8	–	–	–	–	1.090	2.200	2.300
102444	V70201	Tu	mixed	Mu8	4.320	3.635	6.760	8.870	1.995	2.485	3.000
196971	V70201	Tu	mixed	Mu8	–	–	–	–	1.280	2.885	3.055
187551	V96268	HC	Pu1	Mu8	3.665*	–	–	–	1.690	2.495	3.150
195966	V72137	Tu	Pu2/3	(Mu8)	–	–	–	–	1.385	2.125	2.145
152997	V73080	Tu	Pu2/3	Mu8	–	–	5.965	7.815	1.270	1.850	2.015
152996	V91002	Tu	Puercan	Mu8	–	–	–	–	1.550	2.895	3.560
174532	V73102	HC	Lancian	Mu9	–	–	–	–	–	–	–
153091	V99438	Tu	Pu2/3	Mu10	5.075*	3.525*	8.870*	12.810*	2.510	3.025	4.145
882	unknown	HC	Lancian	Mu11	7.207	4.785	–	–	5.71A	5.305A	7.035A
195935	V99438	Tu	Pu2/3	Eu1	–	–	–	–	3.350	–	–
152004	V87095	HC	Pu1	Eu2	5.050	3.400	7.220	12.115	4.955	1.410	5.040
192674	V87076	HC	Pu1	Eu3	5.055*	1.640*	9.305	15.135	6.385	2.015	5.555

Table S2.4. List of fossil specimens used for comparative study. Question marks indicate that the specimen was not associated with diagnostic dental material and thus is only tentatively assigned to taxon. Multituberculate taxonomy follows Kielan-Jaworowska et al. (2004). Age data for Late Cretaceous and Paleogene North American taxa are given as NALMAs, and those for European, Asian, and earlier North American taxa are given as geologic stages. Specimens from the Bug Creek Anthills localities (Deischl 1964) are given a "Lancian-Pu1 mixed" age. See text for explanation of museum abbreviations. Note: UALVP 9001 is UA 9001 of Krause and Jenkins (1983).

Specimen Number	Taxon Name	Superfamily/ Suborder	Family	Age	Location	References
	Multituberculata					
UALVP 9001	*Ptilodus kummae*	Ptilodontoidea	Ptilodontidae	Tiffanian	North America	Krause and Jenkins 1983
USNM 6076	*Ptilodus montanus*	Ptilodontoidea	Ptilodontidae	Torrejonian	North America	Gidley 1909
UMVP 1422	?*Mesodma formosa*	Ptilodontoidea	Neoplagiaulacidae	Lancian-Pu1 mixed	North America	Deischl 1964
ANMH 77178	?*Mesodma primaeva*	Ptilodontoidea	Neoplagiaulacidae	Judithian	North America	Sahni 1972
UMVP 1423–1424	?*M. thompsoni*	Ptilodontoidea	Neoplagiaulacidae	Lancian-Pu1 mixed	North America	Deischl 1964
MCZ 20775–20778	?*Mesodma* sp.	Ptilodontoidea	Neoplagiaulacidae	Lancian-Pu1 mixed	North America	Krause and Jenkins 1983
BT03049	*Ectypodus* sp.	Ptilodontoidea	Neoplagiaulacidae	Tiffanian	North America	Minjin 2008
UMVP 1426	?*Stygimys kuszmauli*	Djadochtatherioidea	Eucosmodontidae	Lancian-Pu1 mixed	North America	Deischl 1964
AMNH 16325	?*Eucosmodon* sp.	Djadochtatherioidea	Eucosmodontidae	Puercan	North America	Granger and Simpson 1929; Krause and Jenkins 1983
ZPAL MgM-I/110; ZPAL MgM-I/81	*Nemegtbaatar gobiensis*	Djadochtatherioidea		Campanian	Asia	Kielan-Jaworowska and Gambaryan 1994
ZPAL MgM-I/41	*Kryptobaatar dashzevegi*	Djadochtatherioidea	Djadochtatheriidae	Santonian and/or early Campanian	Asia	Kielan-Jaworowska and Gambaryan 1994; Minjin 2008
PM 120/107	*Catopsbaatar catopsaloides*	Djadochtatherioidea	Djadochtatheriidae	?late Campanian	Asia	Hurum and Kielan-Jaworowska 2008
CCMGE 104/12455	*Uzbekbaatar kizylkumensis*			Santonian and/or early Campanian	Asia	Kielan-Jaworowska and Nessov 1992
UCM 43554	?*Catopsalis alexanderi*	Taeniolabidoidea	Taeniolabididae	Puercan	North America	Middleton 1982
UMVP 1427	?*Catopsalis joyneri*	Taeniolabidoidea	Taeniolabididae	Lancian-Pu1 mixed	North America	Deischl 1964
AMNH 3036	?*Taeniolabis taoensis*	Taeniolabidoidea	Taeniolabididae	Puercan	North America	Sloan 1981

UMVP 1421	?*Cimexomys minor*	"*Paracimexomys*" group		Lancian-Pu1 mixed	North America	Deischl 1964
PU 21451	Multituberculata indet.			Maestrichtian	New Jersey, North America	Krause and Baird 1979
	Eutheria					
AMNH 16748	*Prodiacodon puercensis*	Leptictida	Leptictidae	Puercan	North America	Matthew 1937
AMNH 16011	*Prodiacodon puercensis*, formerly *Palaeolestes*	Leptictida	Leptictidae	Puercan	North America	Matthew 1937
UM 88105	cf. *Prodiacodon tauricinerei*	Leptictida	Leptictidae	Wasatchian	North America	Rose 1999
DMNH 29264	*Palaeictops*, cf. *P. bridgeri*	Leptictida	Leptictidae	Bridgerian	North America	Rose 1999
CR71–72, CR742	*Arctocyon primaevus*		Artocyonidae	Thanetian	Europe	Russell 1964; Argot 2013
USGS 2353	*Chriacus* sp.		Artocyonidae	Wasatchian	North America	Rose 1987
AMNH 16343	*Loxolophus hyattianus*		Artocyonidae	Puercan	North America	Matthew 1937
USGS 2352	*Diacodexis metsiacus*		diacodexid	Wasatchian	North America	Rose 1985
AMNH 16500	*Ectoconus ditrigonus (=Ectoconus majusculus)*		Periptychidae	Puercan	North America	Matthew 1937
UNM-B029	*Mithrandir gillianus* (=*Gillisonchus gillianus)*		Periptychidae	Puercan	North America	Rigby 1981
AMNH 837	?*Periptychus carinidens* (=*P. rhabdodon)*		Periptychidae	Torrejonian	North America	Matthew 1937
AMNH 16368	?*Oxyacodon apiculatus*		Periptychidae	Puercan	North America	Matthew 1937
UM 108210 and 82606	*Ignacius clarkforkensis*	"Plesiadapiformes"	Paramomyidae	Clarkforkian	North America	Bloch et al. 2007
UM 101963	*Carpolestes simpsoni*	"Plesiadapiformes"	Carpolestidae	Clarkforkian	North America	Bloch and Boyer 2002
AMNH 17379	*?Nannodectes gidleyi (=Plesiadapis gidleyi)*	"Plesiadapiformes"	Plesiadapidae	Tiffanian	North America	Simpson 1935
UM 87990	*Plesiadapis cookei*	"Plesiadapiformes"	Plesiadapidae	Clarkforkian	North America	Bloch et al. 2007
MNHN R444 and R450	*P. tricuspidens*	"Plesiadapiformes"	Plesiadapidae	Thanetian	Europe	Szalay et al. 1975
AMNH 16663	*Pantolambda bathmodon*	Pantodonta		Torrejonian	North America	Matthew 1937
AMNH 3405	*Onychodectes*	Taeniodonta	Conoryctidae	Puercan	North America	Schoch 1986
USNM no number	*Ectoganus gliriformis*	Taeniodonta	Stylinodontidae	Wasatchian	North America	Schoch 1986
AMNH 16560 and TMM 41364-1	*Psittacotherium multifragum*	Taeniodonta	Stylinodontidae	Torrejonian	North America	Schoch 1986
AMNH 3394	*Wortmania otariidens*	Taeniodonta	Stylinodontidae	Puercan	North America	Matthew 1937; Schoch 1986
LSUMG V-1159	*Eoconodon coryphaeus*		Triisodontidae	Puercan	North America	Standhardt 1986

Table S2.5. Multituberculate taxa and measurements used in the linear regression analysis of m1 length and femur dimensions. All dental measurements are from Wilson et al. (2012) and the references therein, except for cases in which m1 length and femur shaft width was available from the same specimen (*Ptilodus montanus* [Gidley 1909], *Catopsbaatar* [Hurum and Kielan-Jaworowska 2008], and *Ectypodus* sp. [Minjin 2008]). We used the m1 length for *Eucosmodon americanus* (Wilson et al. 2012) for the femur attributed to ?*Eucosmodon* sp. Femur shaft diameter is FSMLP (see Table 2.1 for measurement description, and text and Table S2.4 for additional information). The linear model $y = 0.8836x + 0.1082$, where x and y are log-transformed FSMLP and m1 length, respectively, best explained the relationship between femur and tooth size ($R^2 = 0.787$, $p < 0.001$). We used this formula to predict m1 length for this dataset (Model m1 length) and found the average absolute percent prediction for the linear model is 30.22%; we also report the individual Percent Prediction Error (%PE; Van Valkenburgh 1990; Millien 2008; Millien and Bovy 2010). All measurements are in millimeters.

Specimen	Taxon	FSMLP	m1_length	Model m1 length	%PE
UMVP 1422	?*Mesodma formosa*	1.6	2.29	1.69	35.44
UMVP 1421	?*Cimexomys minor*	1.95	2.36	2.01	17.16
UMVP 1423	?*Mesodma thompsoni*	2.7	2.68	2.68	0.09
UMVP 1426	?*Stygimys kuszmauli*	3.4	4.44	3.29	35.13
UMVP 1427	?*Catopsalis joyneri*	8	9.70	7.00	38.60
AMNH 16325	?*Eucosmodon sp.*	9.58	5.60	8.21	31.77
UALVP 9001 +11301 composite	?*Ptilodus kummae*	4.7	3.30	4.37	24.67
MOR 882	?*Meniscoessus robustus*	7	8.12	6.22	30.61
AMNH 3036	?*Taeniolabis taoensis*	10.67	19.80	9.03	119.34
USNM 6076	*Ptilodus montanus*	4.7	3.30	4.37	24.56
PM 120/107	*Catopsbaatar catopsaloides*	5.6	5.80	5.11	13.58
ZPAL MgM-I/41	*Kryptobaatar dashzevegi*	2	2.20	2.06	7.01
ZPAL MgM-I/81	*Nemegtbaatar gobiensis*	3.75	3.11	3.58	13.20
BT0349	*Ectypodus sp.*	1.4	1.98	1.50	31.99

Table S2.6. Predicted lower first molar (m1) length for multituberculate femur morphotypes in this study. We predicted m1 lengths for isolated femora in our study using the formula from Table S2.5 and Fig. S2.1. We report the mean, maximum, minimum, and 95% confidence interval of predicted m1 length for each morphotype containing more than one specimen (Mu1, Mu3, Mu6, and Mu8). The predicted m1 length for a morphotype with a single representative specimen is listed in the "mean" column. All measurements are in millimeters.

Morphotype	Mean	Maximum	Minimum	CI
Mu1	1.998	2.393	1.543	0.086
Mu2	1.914			
Mu3	2.018	2.232	1.804	0.419
Mu4	2.326			
Mu5	2.838			
Mu6	3.539	3.600	3.477	0.120
Mu7	4.657			
Mu8	4.137	5.829	2.846	0.472
Mu9	4.329			
Mu10	6.333			
Mu11	6.685			

Table S2.7. Specimen size through time. We determined maximum and mean size for all biozones and for taxonomic and immigrant/resident status within biozones. All Lancian specimens are multituberculates; we calculated maxima and means for Pu1 and Pu2/3 biozones for all specimens as well as for multituberculates specifically. We used our morphotype taxonomic assignments for Pu1 and Pu2/3 morphotypes and Clemens (2002) to determine a morphotype's status as either an "immigrant" or "resident" taxon. We determined 95% confidence limits (CL) using a t-distribution (appropriate for samples of estimated standard deviations). Abbreviations: n, number of femur specimens; Max, maximum specimen size; SD, standard deviation.

Biozone	Sample	n	Max	Mean	SD	95% CL
Lancian	all	16	3	2.000	1.265	1.326–2.674
Pu1	all	7	4	2.714	1.254	1.555–3.874
Pu1	multituberculates	5	3	2.200	1.095	0.840–3.560
Pu1	eutherians	2	4	4.000	NA	NA
Pu2/3	all	14	6	2.071	1.592	1.152–2.990
Pu2/3	multituberculates	12	5	1.750	1.215	0.978–2.522
Pu2/3	eutherians	2	6	4.000	NA	NA
Puercan	residents	11	2	1.182	0.405	0.910–1.454
Puercan	immigrants	6	6	4.000	1.414	2.516–5.484
Pu1	residents	2	1	1.000	NA	NA
Pu1	immigrants	3	4	3.667	0.577	2.232–5.101
Pu2/3	residents	9	2	1.222	0.441	0.883–1.561
Pu2/3	immigrants	3	6	4.333	2.082	-0.838–9.504

Table S2.8. Results of pairwise Welch's Two-Sample t-tests for size differences between biozones. We conducted F tests for equal variances of the two sample populations (F indicates F-statistic, and asterisk indicates equal variances), and then conducted t-tests with either equal or unequal variances, as appropriate. The t-statistic (t) is negative if the mean of Sample 1 is smaller than that of Sample 2. See Table S2.7 for sample means, sample size, and standard deviations. Additional abbreviations: df, degrees of freedom. Biozones with significantly different sizes ($p < 0.05$) are highlighted in bold.

Sample 1	**Sample 2**	**F**	**t**	**df**	***p*-value**
Lancian	Pu1	1.018*	-1.249	21	0.225
Pu1	Pu2/3	0.620*	0.930	19	0.364
Lancian	Puercan immigrants	0.800*	-3.204	20	**0.004**
Lancian	Puercan residents	9.778	2.414	19.16	**0.026**
Puercan residents	Puercan immigrants	0.082	-4.776	5.45	**0.004**
Pu1 residents	Pu1 immigrants	0.000	-8.000	2	**0.015**
Pu2/3 residents	Pu2/3 immigrants	0.045	-2.570	2.06	0.120

Figure S2.2. Linear regression of first molar length (m1) and femur shaft width (FSMLP) in comparative multituberculate taxa. Axes are log transformed. Circles indicate measurements for specimens with both the m1 and femur preserved; crosses are for inferred associations between femora and m1 lengths based on published taxonomic attributions made for isolated femora (see Tables S2.4 and S2.5 for taxa and measurements).

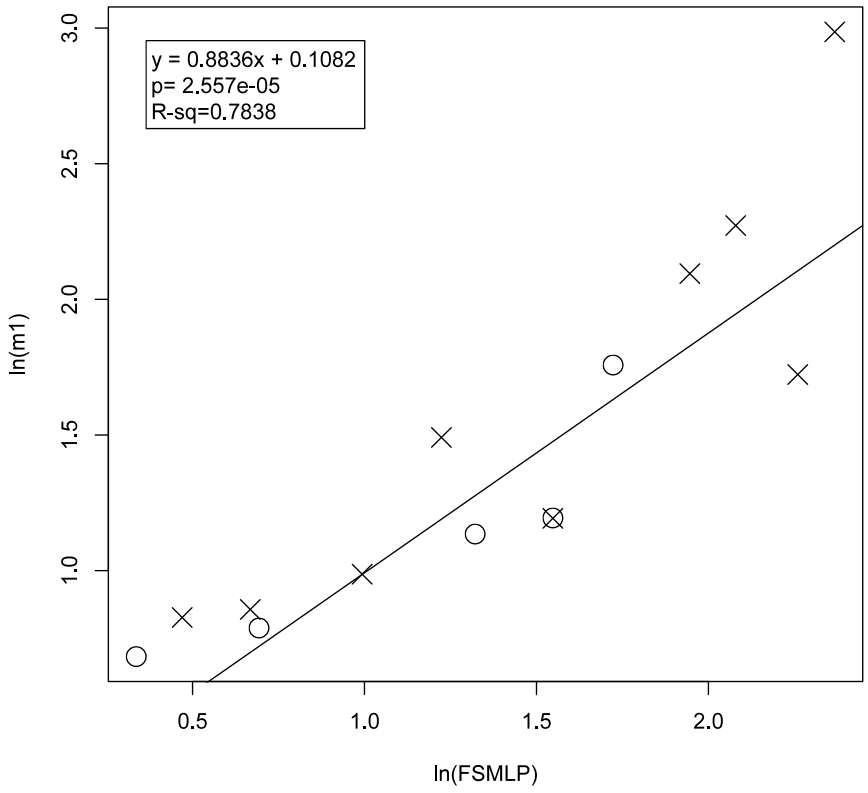

Supplementary References

Argot, C. 2013. Postcranial analysis of a Carnivoran-like archaic ungulate: the case of *Arctocyon primaevus* (Arctocyonidae, Mammalia) from the Late Paleocene of France. Journal of Mammalian Evolution 20: 83–114.

Bloch, J.I. and D.M. Boyer. 2002. Grasping primate origins. Science 298: 1606–1610.

Bloch, J.I., M.T. Silcox, D.M. Boyer, and E.J. Sargis. 2007. New Paleocene skeletons and the relationship of plesiadapiforms to crown-clade primates. Proceedings of the National Academy of Sciences 104: 1159–1164.

Deischl, D.G. 1964. The Postcranial Anatomy of Cretaceous Multituberculate Mammals, unpublished M.Sc. thesis, University of Minnesota, Minneapolis, 85 pp.

Egi, N. 2001. Body mass estimates in extinct mammals from limb bone dimensions: the case of North American Hyaenodontids. Palaeontology 44: 497–528.

Gidley, J.W. 1909. Notes on the fossil mammalian genus *Ptilodus*, with descriptions of new species. Proceedings of the United States National Museum 36: 611–627.

Granger, W. and G.G. Simpson. 1929. A revision of the Tertiary Multituberculata. Bulletin of the American Museum of Natural History 56: 601–676.

Hurum, J.H. and Z. Kielan-Jaworowska. 2008. Postcranial skeleton of a Cretaceous multituberculate mammal *Catopsbaatar*. Acta Palaeontologica Polonica 53: 545–566.

Kielan-Jaworowska, Z. and L.A. Nessov. 1992. Multituberculate mammals from the Cretaceous of Uzbekistan. Acta Paleontologica Polonica 37: 1–17.

Kielan-Jaworowska, Z. and P.P. Gambaryan. 1994. Postcranial anatomy and habits of Asian multituberculate mammals. Fossils and Strata 36: 1–92.

Kielan-Jaworowska, Z., R. Cifelli, and Z.-X. Luo. 2004. Mammals from the Age of Dinosaurs: Origins, Evolution, and Structure. Columbia University Press, New York.

Kielan-Jaworowska, Z., J.H. Hurum, and A.V. Lopatin. 2005. Skull structure in *Catopsbaatar* and the zygomatic ridges in multituberculate mammals. Acta Palaeontologica Polonica 50: 487–512.

Krause, D.W. and D. Baird. 1979. Late Cretaceous mammals east of the North American Western Interior Seaway. Journal of Paleontology 53: 562–565.

Krause, D.W. and F.A. Jenkins Jr. 1983. The postcranial skeleton of North American multituberculates. Bulletin of the Museum of Comparative Zoology 150: 199–246.

Matthew, W.D. 1937. Paleocene faunas of the San Juan Basin, New Mexico. Transactions of the American Philosophical Society 30: 1–523.

Middleton, D. 1982. A new species and additional material of *Catopsalis* (Mammalia, Multituberculata) from the Western Interior of North America. Journal of Paleontology 56: 1197–1206.

Millien, V. 2008. The largest among the smallest: the body mass of the giant rodent *Josephoartigasia monesi*. Proceedings of the Royal Society B: Biological Sciences 275: 1953–1955.

Millien, V. and H. Bovy. 2010. When teeth and bones disagree: body mass estimation of a giant extinct rodent. Journal of Mammalogy 91: 11–18.

Minjin, B. 2008. A phylogenetic study of the postcranial anatomy of Multituberculata (Mammalia, Synapsida) and descriptions of three new specimens, unpublished Ph.D. dissertation. City University of New York, New York.

Rigby, J.K. Jr.. 1981. A skeleton of *Gillisonchus gillianus* (Mammalia; Condylarthra) from the Early Paleocene (Puercan) Ojo Alamo Sandstone, San Juan Basin, New Mexico, with comments on the local stratigraphy of Betonnie Tsosie Wash, in: S.G. Lucas, J.K. Rigby Jr., and B.S. Kues. (Eds.), Advances in San Juan Basin Paleontology. University of New Mexico Press, Albuquerque, pp. 89–126.

Rose, K.D. 1985. Skeleton of *Diacodexis*, oldest known Artiodactyl. Science 216: 621–623.

Rose, K.D. 1987. Climbing adaptations in the early Eocene mammal *Chriacus* and the origin of Artiodactyla. Science 236: 314–316.

Russell, D.E. 1964. Les mammifères paléocènes d'Europe. Mémoires du Muséum National D'Histoire Naturelle, Série C. Sciences de la Terre 13: 1–324.

Sahni, A. 1972. The vertebrate fauna of the Judith River Formation, Montana. Bulletin of the American Museum of Natural History 147: 323–412.

Schoch, R.M. 1986. Systematics, functional morphology and macroevolution of the extinct mammalian order Taeniodonta. Peabody Museum of Natural History, Yale University Bulletin 42: 1–307.

Simpson, G.G. 1935. The Tiffany Fauna, Upper Paleocene II.–Structure and relationships of *Plesiadapis*. American Museum Novitates 816: 1–30.

Sloan, R.E. 1981. Systematics of Paleocene multituberculates from the San Juan Basin, New Mexico, in: S.G. Lucas, J.K. Rigby, Jr., and B.S. Kues (Eds.), Advances in San Juan Basin Paleontology. University of New Mexico Press, Albuquerque, pp. 127–160.

Standhardt, B.R. 1986. Vertebrate paleontology of the Cretaceous/Tertiary transition of Big Bend National Park, Texas, Ph.D. dissertation. Louisiana State University and Agricultural and Mechanical College, Baton Rouge, 299 pp.

Szalay, F.S., I. Tattersall, and R.L. Decker. 1975. Phylogenetic relationships of *Plesiadapis*-postcranial evidence. Contributions to Primatology 5: 136–166.

Wilson, G.P., A.R. Evans, I.J. Corfe, P.D. Smits, M. Fortelius, and J. Jernvall. 2012. Adaptive radiation of multituberculate mammals before the extinction of dinosaurs. Nature 483: 457–460.

CHAPTER 3:

HUMERI MORPHOTYPE DIVERSITY AND LOCOMOTOR FUNCTION IN LATEST CRETACEOUS AND EARLY PALEOGENE MAMMALS FROM EASTERN MONTANA

Abstract

Mammal postcrania from latest Cretaceous and earliest Paleocene (K-Pg) assemblages of the Western Interior of North America are relatively rare and usually found as isolated elements, however this material can provide powerful and novel insight for body size and locomotor ecologies and can supplement taxonomic patterns derived from the well-sampled local dental record. The humerus in particular plays a key role in locomotion, is strongly correlated to locomotor and substrate preference in a wide range of mammals, and is a relatively common element in K-Pg mammal postcranial assemblages. This study describes 50 distal humeri from K-Pg deposits in northeastern Montana from the Hell Creek (Upper Cretaceous) and Tullock formations (lower Paleogene), representing Lancian and Puercan North American Land Mammal Ages, respectively. Humeri were assigned to morphotypes and quantitatively and qualitatively assessed for body size and locomotor mode diversity through time. Three-dimensional geometric morphometrics (3D GM) was used to assess locomotor mode in select, exceptionally preserved fossil specimens via comparison to a phylogenetically broad sample of humeri from extant mammals of known locomotion.

Taxonomically, these Lancian and Puercan samples record all of the major groups of mammals alive at the time (multituberculates, metatherians, and eutherians). The Lancian sample includes mostly multituberculates as well as humeri from a small therian and small eutherian, and a humerus from the largest Cretaceous metatherian, *Didelphodon vorax*. Eutherians are more abundant in the Puercan samples; among these we identified large and small archaic ungulates, a possibly leptictid, a much larger mammal (possibly

representing a taeniodont, triisodontid, or pantodont), and a possible “plesiadapiform” primate. Humerus size implies a decrease in mean body size following the K-Pg mass extinction, and a subsequent increase in the mid-late Puercan, a trend that is also supported by the dental record. Maximum size is relatively small for Lancian and early Puercan samples, but greatly increases in the mid-late Puercan, with multiple specimens suggestive of body sizes an order of magnitude larger than the next largest specimens in the study. Despite phylogenetic influence, 3D GM results show distal humerus morphology is a strong predictor locomotor mode. Using this extant model, combined results from quantitative and qualitative analyses suggest K-Pg humeri included: largely arboreal Cretaceous and Paleogene multituberculates, one latest Cretaceous arboreal or semifossorial eutherian, an early Puercan (Pu1) semifossorial leptictid and terrestrial small archaic ungulate, and a later Puercan (Pu3) arboreal ?plesiadapiform primate and large scansorial archaic ungulate. Functional results increase ecomorphological diversity beyond that previously recognized among K-Pg postcrania. This foundational work improves our ability to test ecological hypotheses of extinction and recovery, and to refine our understanding of locomotor patterns among K-Pg mammals.

1. Introduction

The Cretaceous-Paleogene (K-Pg) mass extinction was a watershed event in mammalian history. Research on K-Pg mammals has yielded important insights regarding changes in taxonomic and morphological diversity, diet, and body size across mass extinction events; however, the majority of these patterns are based on dental fossil material (e.g., Alroy 1999; Smith et al. 2010; Wilson et al. 2012; Wilson 2013, 2014; O'Leary et al. 2013; Raia et al. 2013). With a few exceptions (Borths and Hunter 2008; DeBey and Wilson 2014), postcranial patterns of extinction and recovery and hypotheses for locomotor-related extinction selectivity (e.g., the Sheltering Hypothesis; Robertson et al. 2004) remain largely unexplored. Here, we use fossil humeri from extremely well-sampled and well-studied localities in eastern Montana to document richness, body size, and locomotor patterns among assemblages of latest Cretaceous and earliest Paleogene mammals.

Research to date on K-Pg mammalian postcrania has mostly focused on a particular taxon (i.e., multituberculates, archaic primates; Deischl 1964; Krause and Jenkins 1983; Szalay 1994; Borths and Hunter 2008; Chester et al. 2015) or on a single assemblage (e.g., Deischl 1864; Sloan and Van Valen 1965; Szalay and Decker 1975). More temporally and taxonomically comprehensive research has been hindered by low sample sizes of postcranial fossils, which is likely a function of the rarity of these elements (and extreme rarity of skeletons) relative to the thousands of mammalian teeth known from these deposits (e.g., Sloan and Van Valen 1965; Archibald 1982; Lofgren 1995; Clemens 2002; DeBey and Wilson 2014; Wilson 2014). Despite small sample sizes, recent analyses on

femora in our study area demonstrate isolated postcranial elements can be used to evaluate patterns of change in taxonomic richness, body size, and locomotor ecology across the K-Pg boundary (DeBey and Wilson 2014).

The humerus plays a key role in locomotion and is a relatively common element in fossil assemblages of mammalian postcrania. Morphology of the humerus is strongly correlated to locomotor and substrate preference in a wide range of mammals (e.g., Smith and Savage 1956; Brown and Yalden 1973; Hildebrand 1985; Van Valkenburgh 1987; Janis and Figueirido 2014; Chen and Wilson 2015; Fabre et al. 2015). Functional morphological analyses of the humerus have been performed in the context of the appendicular skeleton, the forelimb (e.g., Iwaniuk et al. 1999; Argot 2001; Janis and Figueirido 2014; Chen and Wilson 2015; Fabre et al. 2015), and as an isolated element (e.g., Milne et al. 2009; Steiner-Souza et al. 2010; Morgan and Alvarez 2013). These analyses used more traditional, comparative anatomical methods (e.g., Szalay and Dagosto 1980; Argot 2001), as well as linear measurements or indices (e.g., Van Valkenburgh 1987; Argot 2001; Samuels and Van Valkenburgh 2008; Janis and Figueirido 2014; Chen and Wilson 2015), and two- and three-dimensional geometric morphometrics (e.g., Schutz and Guranlick 2007; Milne et al. 2009; Steiner-Souza et al. 2010; Morgan and Alvarez 2013; Fabre et al. 2015). Here, we infer locomotion and quantify morphospace occupation of fossil taxa using two-dimensional geometric morphometrics (2D GM) because it confers several benefits over traditional morphometric analysis. First, geometric morphometrics enables a quantitative comparison of shape across fossil and modern specimens independent of size (e.g., Polly 2008). Second, it allows a more comprehensive investigation and visualization of the particular areas of

the distal humerus that are hypothesized as driving the variation in the sample (e.g., Zelditch et al. 2004).

Previous research on fossil humeri from our study area is largely limited to more qualitative assessment of morphological variation of material from the Bug Creek Anthills localities (e.g., Deischl 1964; Krause and Jenkins 1983; Szalay and Dagosto 1980), which unfortunately preserve a time-averaged assemblage of latest Cretaceous and earliest Paleogene material (Lofgren 1995; Clemens 2002). We expand upon these studies to include humeri specimens from well-sampled and stratigraphically well-constrained localities in the Hell Creek and the Tullock formations (e.g., Archibald 1982; Lofgren 1995; Wilson 2005), in addition to the Bug Creek Anthills material. Our study represents the first quantitative assessment of postcrania for a taxonomically diverse, succession of mammalian assemblages across the K-Pg boundary.

Specifically, we describe and morphotype 50 partial mammalian humeri from 25 localities in the Hell Creek and Tullock formations of eastern Montana. We then (1) assess humeral morphotype richness through the latest Cretaceous and earliest Paleogene of our study area; (2) quantitatively and qualitatively constrain taxonomic affinities of humeral morphotypes on the basis of size and abundance; (3) infer body size changes across and following the K-Pg boundary; and (4) constrain morphofunctional affinities of select, well-preserved latest Cretaceous and earliest Paleogene humeri on the basis of a geometric morphometric analysis of a broad sample of extant, small-bodied mammals of diverse locomotor function. Our results highlight changes in mean body size (i.e., decreases among multituberculates and increases among eutherians) across the K-Pg boundary, and suggest

we can infer locomotor mode in these Cretaceous and Paleogene mammals using qualitative and quantitative methods.

Institutional abbreviations.—**AMNH**, American Museum of Natural History, New York, New York, U.S.A.; **FMNH**, Field Museum of Natural History, Chicago, Illinois, U.S.A.; **GISPS**, Geological Institute, Section of Palaeontology and Stratigraphy the Academy of Sciences of the Mongolian People's Republic, Ulanbaataar, Mongolia; **IVPP**, Institute of Vertebrate Paleontology and Paleoanthropology, Beijing, China; **LSUMG**, Louisiana State University Museum of Geoscience (now the LSU Museum of Natural History), Baton Rouge, Louisiana, U.S.A.; **MCZ**, Museum of Comparative Zoology, Harvard University, Cambridge, Massachusetts, U.S.A.; **MHNC**, Museo de Historia Natural de Cochabamba, Cochabamba, Bolivia; **MNHN**, Musée National d'Histoire Naturelle, Paris, France; **NMMNH**, New Mexico Museum of Natural History and Science, Albuquerque, New Mexico, U.S.A.; **PM**, Paleontological Center of the Mongolian Academy of Sciences, Ulaanbaatar, Mongolia; **PSS-MAE**, Paleontology Section, Mongolian Academy of Sciences, Ulaanbaatar, Mongolia; **PU**, Princeton University, Princeton, New Jersey, U.S.A.; **TMM**, Texas Memorial Museum, Austin, Texas, U.S.A.; **UA**, University of Alberta, Edmonton, Alberta, Canada; **UALVP**, University of Alberta, Edmonton, Alberta, Canada; **UCMP**, University of California Museum of Paleontology, Berkeley, California, U.S.A.; **UMVP**, University of Minnesota, Minneapolis, Minnesota, U.S.A.; **UM**, University of Michigan Museum of Paleontology, Ann Arbor, Michigan, U.S.A.; **UNM**, Department of Geology, University of New Mexico, Albuquerque, New Mexico, U.S.A.; **URBAC**, Uzbek–Russian–British–American–Canadian Joint Paleontological Expedition (specimens currently housed at San Diego State University, San

Diego, California, U.S.A); **USGS**, U.S. Geological Survey, Denver, Colorado, U.S.A.; **USNM**, United States National Museum, Washington, D.C., U.S.A.; **UWBM**, University of Washington Burke Museum of Natural History and Culture, Seattle, Washington, U.S.A.**; YPM**, Yale Peabody Museum of Natural History, Yale University, New Haven, Connecticut, U.S.A.; **YPFB**, Yacimentos Petroliferos Fiscales Bolivianos, Santa Cruz, Bolivia.

Other abbreviations.—**Eu**, Eutherian; **Mu**, Multituberculate; **NALMA**, North American Land Mammal "age"; **La**, Lancian NALMA; **Pu1**, early Puercan NALMA; **Pu3**, middle-late Puercan NALMA; **SD**, standard deviation.

2. Materials

2.1. Study Area and Specimens

Fossil specimens used in this study are from Cretaceous- and Paleogene-age deposits in the Williston Basin. We include material from eastern Montana, specifically in Carter, Fallon, Garfield, and McCone counties (Fig. 3.1), as well as from one locality in Niobrara County, Wyoming (see Table S3.1 for locality information). Our eastern Montana study area is tied into a high-resolution chronostratigraphic framework that spans ca. 3.2 Ma across the K-Pg boundary (Archibald 1982; Swisher et al. 1993; Lofgren 1995; Clemens 2002; Renne et al. 2013; Wilson 2005, 2014; LeCain et al. 2014; Moore et al. 2014; Sprain et al. 2015). In the Western Interior of North America, the K-Pg boundary is approximately coincident with the boundary between the Lancian and Puercan North American Land Mammal "ages" (NALMAs; Cifelli et al. 2004; Lofgren et al. 2004; Sprain et al. 2015; but see Fox 1989 and Kelly 2014). Our specimens are from the Hell Creek and Tullock formations, except three specimens from the Lancian Formation of Wyoming (UCMP loc. V5620). Hell Creek specimens are largely Lancian in age (ca. 68–66.04 Ma; Swisher et al. 1993; Renne et al. 2011, 2013; Wilson 2014; Sprain et al. 2015); all Lance Formation specimens are Lancian in age. In eastern Garfield County and western McCone County, some localities from the uppermost Hell Creek Formation are earliest Paleogene (Puercan) in age; we include two specimens from two of these localities (UCMP loc. V84162 in Garfield County and V84193 in McCone County; Lofgren 1995; Sprain et al. 2015). Specimens from the lowermost Tullock Formation are early Puercan (Pu1 interval zone, ca. 66.04–65.97 Ma), whereas those from the middle part of the Tullock Formation are late Puercan (Pu3

interval zone, ca. 65.74–65.12 Ma; Swisher et al. 1993; Renne et al. 2011, 2013; Wilson 2014; Sprain et al. 2015). Our study also includes specimens from the temporally mixed Bug Creek Anthills assemblages, which greatly increase our sample sizes, but are composed of both Lancian and earliest Puercan specimens (Lancian-Pu1 mixed; Lofgren 1995). Local faunas in our study area referable to the Pu2 interval zone (65.97–65.74 Ma; Sprain et al. 2015) have yet to be found or described (e.g., Clemens 2015).

Fifty distal humeri fragments from 25 localities preserve sufficient morphology to be assessed in a comparative context. Of these, 14 specimens are from 10 Lancian localities, six specimens are from four Pu1 localities, seven specimens are from five Pu3 localities, and an additional 23 are from six Lancian–Pu1 mixed-age localities (e.g., Bug Creek Anthills; Tables 3.2–3, S3.1; Fig. S3.1).

3. Methods

3.1. Taxonomic Scope

The large, well studied Lancian and Puercan mammalian dental assemblages consist of multituberculates, metatherians, and eutherians (e.g., Archibald 1982; Lofgren 1995; Clemens 2002; Wilson 2014). On this basis, our comparative analyses and taxonomic designations of humeral morphotypes begin with dental taxa known from these deposits (e.g., Clemens 2002; Wilson 2014).

3.2. Osteological Terminology

Proposed differences in forelimb posture of multituberculates and therians (e.g., Kielan-Jaworowska and Hurum 2006) dictates that we use different anatomical directional terms for humeri of these taxa. Following Krause and Jenkins (1983) and Kielan-Jaworowska and Gambaryan (1994), the dorsal and ventral aspects of the multituberculate humerus correspond to the posterior and anterior aspects of the therian humerus. Osteological terminology follows Krause and Jenkins (1983) for multituberculates, Szalay and Sargis (2001) for metatherians, and Szalay and Dagosto (1980) and Boyer et al. (2010) for eutherians.

3.3. Morphotype Assignment

We assign our specimens to 15 morphotypes based on morphology and size, and after comparison with published specimens of similar age and/or related taxa, following guidelines from other studies that employ morphotype 'parataxonomy' for analysis of

isolated proximal limb elements (e.g., Deischl 1964; Chester et al. 2010; 2012; DeBey and Wilson 2014; Szalay and Sargis 2001). We assign an alphabetical code (e.g., EuA) to each morphotype to designate higher-level taxonomic assignment (i.e., eutherian) and size rank among all morphotypes in that higher-level taxon (ranked smallest to largest, based on measured or inferred mean Total Distal Width, TDW; Fig. 3.2; Tables 3.1–3).

Following the methodology of DeBey and Wilson (2014), we constrain the possible taxonomic assignments of our 15 humerus morphotypes by first using published morphological descriptions, photographs, and figures of Late Cretaceous and Paleogene multituberculate and therian humeri from North America and Asia, including material found in our study area; all comparative fossil taxa examined are listed in the Supplementary Information (Tables S3.2–3). Because most of these comparative humeri were also found as isolated elements unassociated with diagnostic dental fossils, their taxonomic assignments should be considered tentative; we follow Krause and Jenkins (1983) in using a query ('?') to indicate the uncertain taxonomic status of previously published postcranial elements that were not found in direct association with dental material or as part of an articulated skeleton. Second, we examined comparative material of extant therians, including specimens, descriptions, photographs, and figures (e.g., *Caluromys*, *Didelphis*, *Oryzorictes*, *Rhyncholestes*, *Tenrec*; Szalay and Sargis 2001; Argot 2001; Sargis 2002; Salton and Sargis 2008; Flores 2009). Third, we compared sizes among our humeri to taxa known from the same time and area (based on dental material), and use relative size to distinguish amongst candidate taxa (Wilson et al. 2012; Wilson 2013, 2014).

3.4. Linear Measurements

Contingent upon completeness, we took 10 measurements on each specimen (see Fig. 3.2, Tables 3.1–3). Measurements are identical to or slightly modified from those in previous studies, and are correlated with body size or locomotor function (Deischl 1964; Szalay and Dagosto 1980; Argot 2001; Szalay and Sargis 2001; Boyer et al. 2010). All measurements were taken using a Leica MZ9.5 binocular dissecting microscope with a custom measuring stage that has an accuracy of 0.001 mm.

Because of the variable completeness of specimens in our sample, we were unable to collect all of the measurements on all of our specimens; thus, we opted to explore differences among morphotypes and across biozones using univariate rather than multivariate analyses of the data. Our univariate analyses include comparisons of all measurements (excluding minimum values; Tables 3.1–3), which are largely informative of specimen size. Because we used morphology exclusively to assign specimens to morphotypes, we explored size differences across morphotypes using one-way ANOVAs. For any ANOVAs with significant differences among morphotypes, we conducted Tukey honest significant difference (HSD) post-hoc tests to determine which specific variables (i.e., particular morphotypes) were significantly different from one another. To increase sample size, we included the mixed-age assemblages of the Bug Creek Anthills (BCA) in these calculations; however, we omitted any specimens only tentatively attributed to morphotype. Because we only used qualitative features to morphotype our material and we did not use geologic age information (i.e., biozones) to separate morphotypes, inclusion of BCA specimens should not affect a quantitative assessment of differences across morphotypes. Additionally, to compare with dental- and femur-based body-size patterns (Archibald 1982; Maas and Krause 1994; Clemens 2002; Wilson 2005, 2013; DeBey and

Wilson 2014), we tested for significant changes in body size through our study section, using humeri measurements. Specifically, we conducted one-way ANOVAs of these measurements grouped by biozones, followed by Tukey HSD post-hoc tests to identify which biozones were significantly different from one another. As with our ANOVAs on morphotype size, we include BCA material in all calculations, but assign the BCA assemblages to "Lancian-Pu1 mixed" rather than to either Lancian or Pu1 biozones. Including this material in our analyses does not affect the pattern or interpretation of Lancian and Pu1 sizes; however, the "Lancian-Pu1 mixed" size likely averages the Lancian and Pu1 signals.

Multituberculate humeri are the most abundant and best-preserved specimens in our assemblage. To graphically represent the shape of these humeri in multivariate space, we conducted principal components analyses (PCA) of their measurement data. To control for size, all measurements were standardized to radial condyle width (RCW); as a result, the dataset was reduced to specimens in which the RCW could be measured. We acknowledge problems with using RCW, a potentially functionally informative measurement, to standardize for size; however, this measurement was the best preserved among our material, and were we to use more conventional measurements for standardization (e.g., total distal width) we would have unduly decreased our sample size further.

We performed three PCAs, each of which used different permutations of the dataset. The first PCA used nearly the full set of variables (i.e., measurements), excluding AW, TLW, and TDW, which are not independent of other measurements (six variables; Fig. 3.2; Tables 3.1–2). Because some measurements could not be taken on some specimens (incomplete

preservation), those specimens were excluded from this PCA (n = 10). The second PCA used a reduced set of variables (five measurements) that enabled us to increase the number of specimens included (n = 11). The third PCA used a further reduced set of variables (four measurements) and included additional specimens that were measured from published figures (n = 9 specimens from our sample, and n = 7 specimens from the published literature; see Table S3.2 for specimens). We added these published specimens to increase sample size and to examine where our specimens plotted in the PCA morphospace relative to specimens that have previously been described and attributed to taxon.

3.5. Geometric Morphometrics

To quantitatively compare morphology and to infer locomotion, we applied geometric morphometrics to select, well-preserved therian distal humeri from our K-Pg samples and to humeri of extant, small-bodied mammals of known locomotor mode. Our extant sample consists of (1) a subset of that used in Chen and Wilson (2015), which broadly samples taxonomic and locomotor-mode diversity (Table 3.4); (2) five UWBM specimens that further expand our sampling of taxa and locomotor modes; and (3) photographs of 15 species of didelphids and tenrecs that were figured in distal view in Argot (2001) and Salton and Sargis (2008), respectively (Table 3.4). Our modern dataset samples a total of 109 individuals and 71 species from nearly half of all mammalian orders.

Each extant species was assigned to one of eight locomotor modes [arboreal (A), fossorial (F), gliding (G), saltatorial (S), semi-aquatic (Sa), scansorial (Sc), semi-fossorial (Sf), or terrestrial (T)] on the basis of natural history compendia and the primary literature

(Nowak 1999; Argot 2001; Salton and Sargis 2008; as used by Chen and Wilson 2015; Table 3.4). Due to specimen availability, our database is predominantly composed of carnivorans, rodents, primates, and afrosoricids. We photographed and digitized one adult male and female of each species, unless otherwise indicated (Table 3.4). Some major taxa in our dataset (e.g., primates) only sample one locomotor mode (e.g., arboreal), possibly confounding functional morphology with phylogenetic relatedness; this issue was also discussed in Chen and Wilson (2015).

All specimens were photographed using a Nikon D80 Digital SLR camera with an interchangeable Quantaray AF LD 70-300 mm 1:4–5.6 Tele-macro lens. Rather than choose between the anterior or posterior view for our geometric morphometrics analyses, we chose to photograph specimens in distal view, which captures gross articular shape about the axis of the elbow joint. Specimens were consistently oriented in three dimensions: the medial to lateral axis was aligned along a horizontal line in the camera view and a plane horizontal with the stage, and the proximal-to-distal axis was aligned perpendicular to the stage. A millimeter scale bar was included in all images to enable rescaling in the geometric morphometric analyses. We reflected all right humeri about a vertical axis to appear as left humeri during post-processing of photographs.

We chose morphologically and functionally informative landmarks (LMs) that define articular surfaces and muscle attachment sites in distal view (Zelditch et al. 2004). Most of our LMs were Type II (i.e., tip of structure, local maxima or minima of a curve); a few were Type III (e.g., furthest extent measurement; Bookstein 1991; Zelditch et al. 2004). All of our LMs are based on LMs in comparable studies (Table 3.5; Schutz and Guralnick 2007; Milne et al. 2009; Steiner-Souza et al. 2010). We digitized six LMs (Fig. 3.3A; Table 3.5) on each

specimen image using tpsDig version 2.17 (Rohlf 2013a). We acknowledge that plotting landmarks on a two-dimensional (2D) picture of a three-dimensional structure may result in a loss of information and a degree of inaccuracy (Cardini 2014); however, 2D approximation should be sufficient to capture morphological variation because the landmarks are approximately coplanar (Cardini et al. 2015). All of the digitizing was done by one of us (L.B.D.).

We also used semilandmarks (SLMs), evenly spaced along a curve or surface, to characterize aspects of shape not readily captured by LMs (Zelditch et al. 2004). Although an individual SLM might not be homologous across taxa, the curve or surface as a whole may be (Gunz and Mitteroecker 2013; Wilson 2013). We traced three curves on distal humeri (Fig. 3.3B) using the pencil tool in tpsDig; the resultant curve was resampled for a specific number of points that were equally distributed by length (Fig. 3C). Points along the curve were initially converted to LMs in tpsUtil version 1.58 (Rohlf 2013b), but were later designated as SLMs (see below).

We performed Procrustes generalized least squares (GLS) superimpositions (Rohlf and Slice 1990; Zelditch et al. 2004) on our combined dataset of digitized extant and fossil specimens to remove any differences in size, translation, and rotation so that only shape differences remained (Kendall 1977). To avoid excessive weighting of curves in the analyses, every other point along a curve was designated as a helper point and was used only for superimposition (Fig. 3C; Wilson 2013). Remaining points along the curve were designated as sliders (Fig. 3.3C), which minimize Procrustes distances during superimposition by allowing some SLMs (i.e., sliders) of one specimen to slide between helper points, initially with respect to those of another (arbitrary) specimen (Gunz and

Mitteroecker 2013). Procrustes superimposition from these slid coordinates results in a mean shape, and subsequently all SLMs are allowed to slide with respect to the mean Procrustes shape (Gunz and Mitteroecker 2013). After superimposition, we deleted curve helper points, and designated SLMs (i.e., curve slider points) as separate from LMs (Fig. 3.3D). The resultant dataset contained six LMs and 14 SLMs (Fig. 3.3D). We then converted LMs and SLMs to partial warp scores for use in subsequent analyses.

We used principal components analysis (PCA) to visualize the morphospace occupancy of the extant mammalian taxa and where our morphotypes plot within that morphospace. Specifically, we calculated a mean (or consensus) shape for all specimens, and subtracted this from the Procrustes superimposed dataset to produce Procrustes residuals (Polly and MacLeod 2008; Wilson 2013). We conducted PCAs on the covariance matrix of the residuals of the extant specimens only, and used singular value decomposition to calculate the eigenvectors for the extant dataset (Polly and MacLeod 2008). We determined the PCA scores for fossil specimens by calculating the dot product of the eigenvectors and the Procrustes residuals of the fossil specimens. We plotted the PC1–3 scores for fossil specimens to interpret their placement within the morphospace defined by the extant specimens (Wilson 2013). We also used linear discriminant analysis (LDA) to maximize differences among a priori groups and predict locomotor groups based on distal humerus shape (Mitteroecker and Bookstein 2011). LDA is an ordination method that uses principal components and an external variable (i.e., locomotor function), predicts a locomotor mode for each specimen, and measures the percentage of specimens correctly assigned in our extant mammal dataset. We then used this LDA to rank predicted locomotor modes for K-Pg fossil specimens used in the 2D GM analysis.

To assess intraobserver error, one of us (L.B.D.) digitized LMs on a set of 25 images that consisted of five randomly arranged copies of five specimen images. The five specimens sample the taxonomic range (e.g., one each of Metatheria, Lagomorpha, Carnivora, and two within Rodentia) and the morphologic variation in the dataset (i.e., at the maxima and minima of our PC1 and PC2; Boyer and Seiffert 2013). For each LM on each specimen, we calculated the digitizing variance across all trials by calculating the mean of the Euclidean distance between each digitized point and the centroid for that LM (Table S3.4). Digitizing error, or variance across trials, was extremely low for each LM, and low for mean variances across LMs and across specimens (Table S3.4). We also conducted F-tests, which compare equivalences among variances, to examine whether digitizing some LMs resulted in different variances than for other LMs (i.e., digitizing had variable precision across LMs; Table S3.5). Some LMs had significantly greater variance than others (e.g., LM6 for *Lepus americanus* and *Dipodomys deserti*; Table S3.5); however, this was not consistent for any LM across all specimens. Thus, there was not strong justification for excluding any of the LMs from our analyses.

All analyses were preformed in RStudio version 0.98.1062 (RStudio 2012) in R version 3.1.2 (R Core Team 2014). Specifically, Procrustes superimpositions (including designation of helper and slider points, and LMs and SLMs), intraobserver error assessments, and all PCA analyses were preformed using the 'geomorph' package in R (Adams and Otarola-Castillo 2013). LDA analyses were performed using the 'lda' function from the 'MASS' package in R (Venables and Ripley 2002).

4. Descriptions of Humeri

4.1. Multituberculate humeri

Multituberculates first appear in the Middle Jurassic (160 Mya) of China (Clemens and Kielan-Jaworowska 1979), are abundant in the Mesozoic and early Paleogene, and go extinct in the late Eocene (Clemens and Kielan-Jaworowska 1979; Weil and Krause 2008). In our sample of Cretaceous and Paleogene distal humeri, multituberculates are the most abundant higher-level taxon (60% of total specimens), and are recognized in every time interval of this study. Here, we describe 10 Lancian, four Pu1, and three Pu3 multituberculate specimens, as well as 12 specimens of mixed age (Lancian-Pu1 time-averaged from the Bug Creek Anthills assemblages; Table 3.2).

Multituberculate humeri are easily recognizable, with a stout shaft, proximal and distal ends that are twisted relative to one another (Jenkins 1973; Szalay and Dagosto 1980; Kielan-Jaworowska and Qi 1990), a mediolaterally wide distal end, and a distal articular surface that is much narrower mediolaterally, compared to therians (Krause and Jenkins 1983; Szalay and Dagosto 1980; Kielan-Jaworowska et al. 2004). Multituberculate distal humeri strongly differ from therian distal humeri in the morphology of the articular condyles. Specifically, (i) the multituberculate ulnar condyle is more bulbous, proximodistally elongate and mediolaterally compressed, with a sharp medial keel (Fig. 3.2; Kielan-Jaworowska and Dashzeveg 1978; Clemens and Kielan-Jaworowska 1979; Szalay and Dagosto 1980; Weil and Krause 2008); (ii) the radial condyle is very large and spherical, rather than slight and only somewhat rounded as in most therian mammals, and has a lateral capitular tail (Deischl 1964; Szalay and Dagosto, 1980; Weil and Krause 2008);

(iii) the intercondylar groove (trochlea) separating the ulnar and radial condyles is a wide, deep, and sharply concave notch (Deischl 1964; Kielan-Jaworowska and Dashzeveg 1978; Kielan-Jaworowska 1990); (iv) the entepicondyle, much larger than the ectepicondyle, is a broad, dorsoventrally compressed flange that is pierced by the entepicondylar foramen (Jenkins 1973; Krause and Jenkins 1983; Weil and Krause 2004); (v) the ectepicondyle is more pronounced than that of generalized therian mammals (Deischl 1964; Krause and Jenkins 1983); and (vi) both the radial and ulnar condyles extend from the ventral to the dorsal surface of the distal surface (Gambaryan and Kielan-Jaworowska, 1997). The distal humeri described here all have expanded distal ends, as in North American ptilodontoid and taeniolabidoid multituberculates (Krause and Jenkins 1983; Kielan-Jaworowska and Gambaryan 1994).

4.1.1. Distal humerus morphotype MuA (Fig. 3.4)

Morphotype description.—The eight humeri assigned to this morphotype are among the smallest in our sample (TDW mean = 3.9 mm, SD = 0.19 mm). Diagnostic features of this morphotype include: (i) a transverse depression at the blunt proximal termination of the ventral surface of the ulnar condyle; (ii) a broad, shallow separation dorsally between the entepicondyle and ulnar condyle; and (iii) an inflated appearance, especially on the condyles and entepicondyle, but otherwise with proportions and morphology that generally resemble larger multituberculate morphotypes MuE and MuC. We note one additional specimen attributed to this morphotype despite a much smaller size (UCMP 195998 from loc. V5620, preserved TDW = 2.2 mm, 80% complete); this specimen was

excluded from calculations of average measurements of the MuA morphotype, and we discuss this further in the following paragraph.

This morphotype greatly resembles Bug Creek Anthills material previously attributed to ?*Mesodma* sp., ?*M. thompsoni*, and ?*M. formosa* (Deischl 1964; Krause and Jenkins 1983). That most of our MuA specimens are from Bug Creek Anthills localities and that they do not resemble any other comparative material (Table S3.3), we find it likely they are from the same or closely related taxa. We prefer a more conservative attribution of MuA to ?*Mesodma* sp.

Among the two humeri tentatively attributed to this morphotype, one is missing the area proximal to the ulnar condyle and portions of the entepi- and ectepicondyles, key features for diagnosing this morphotype. The other (UCMP 195998 from Lancian loc. V5620) greatly resembles the other MuA specimens in morphology but is much smaller. Perhaps this specimen is attributable to the smallest of the Lancian species of *Mesodma*, *M. hensleighi*, a taxon that is also known from this specimen's locality (Clemens 1963, 2002; Wilson et al. 2012; Wilson 2014).

4.1.2. Distal humerus morphotype MuB (Fig. 3.5)

Morphotype description.—The humerus assigned to this morphotype is among the smallest in our assemblage. Diagnostic features of this morphotype include: (i) an entepicondyle, ulnar condyle, and radial and olecranon fossae that are small relative to specimen size; (ii) a relatively large supinator crest lateral to the radial and olecranon fossae; (iii) a mediolaterally wide ulnar condyle with a shallow dimple proximally on the ventral surface; and (iv) an even more inflated appearance than in MuA.

The specimen in this morphotype is quite small, but is comparable in size to some MuA specimens. Despite its poor preservation (i.e., missing the radial condyle and ectepicondyle), diagnostic features separate it from all comparative material that we studied (e.g., ?*Mesodma* sp., ?*Meniscoessus sp.*, *Microcosomodon conus*, ?*Ptilodus montanus*, ?*Stygimys kuszmauli*; Cope 1884; Marsh 1889; Gidley 1909; Deischl 1964; Sahni 1972; Krause and Jenkins 1983; Fox 2005). We suggest that this morphotype represents one of the many small multituberculates from the Pu3 in our study area (e.g., ?*Xyronomys*, *Microcosmodon harleyi*, *M. arcuatus*, *Mesodma garfieldensis*, in increasing size order; Clemens 2002; Wilson et al. 2012; Wilson 2014). However, UCMP 195933 does not share the distal, especially articular, morphology of similarly sized humeri attributed to the late Paleocene *Microcosmodon conus* (Fox 2005). Thus, until we have more comparative material representing small multituberculates, we do not attribute MuB to taxon.

4.1.3. Distal humerus morphotype MuC (Fig. 3.6)

Morphotype description.—The seven specimens in this morphotype are larger (TDW > 6.5 mm) than the smallest multituberculate morphotypes (MuA, MuB), and smaller than MuE and MuF. Diagnostic features of this morphotype include: (i) a deeper separation between the ulnar condyle and entepicondyle dorsally; (ii) a larger ectepicondyle lateral to the capitular tail; and (iii) a shallow, transverse dimple proximal to the ulnar condyle on the ventral surface.

Specimens in this morphotype are morphologically very similar to specimens in MuE and those attributed to ?*Stygimys kuszmauli*, differing only in the dorsal morphology between the entepicondyle and ulnar condyle, and in size (MuC is approximately 0.8x the

size of MuE and ?*Stygimys kuszmauli*; Deischl 1964; Krause and Jenkins 1983). Similarly, specimens in MuC are morphologically similar to, but approximately 1.5–1.6x the size of specimens in the smallest morphotypes (e.g., MuA) and those attributed to ?*Mesodma* sp. and ?*M. thompsoni* (Deischl 1964, Krause and Jenkins 1983); among the 87 distal humeri from the mixed-age Bug Creek Anthills that were examined by Deischl (1964), none are in the size range occupied by our MuC specimens. MuC differs from smaller, late Paleocene specimens attributed to ?*Microcosmodon conus* in having a much more laterally projecting ectepicondyle (Fox 2005), and from select Asian multituberculates in having a larger and more bulbous radial condyle than the slightly smaller Late Cretaceous *Kryptobaatar* (formerly *Tugrigbaatar*; Kielan-Jaworowska and Dashzeveg 1978). MuC differs from larger humeri attributed to Eocene ?*Lambdopsalis bulla* in having a mediolaterally larger, but dorsoventrally less robust entepicondyle (Kielan-Jaworowska and Qi 1990). The specimens in MuC are representative of Lancian, Pu1, and Pu3 taxa that are likely larger than *Microcosmodon conus*, and smaller than *Stygimys kuszmauli* and *Cimolodon nitidus*. Although we do not attribute this morphotype to taxon at this time, we note that candidate taxa known from our study area in this size range include the Lancian *Parectypodus foxi* and Pu1–Pu3 *Cimexomys gratus* (Clemens 2002; Wilson et al. 2012; Wilson 2014).

4.1.4. Distal humerus morphotype MuD (Fig. 3.7)

Morphotype description.—The humerus assigned to this morphotype greatly resembles the slightly larger specimens in MuE in morphology (MuD TDW = 7.3 mm). We specifically highlight features where this morphotype differs from MuE. Diagnostic features of this morphotype include: (i) a radial condyle dorsally that is quite reduced; (ii) a more

bulbous ulnar condyle dorsally; and (iii) a relatively smaller radial fossa, both mediolaterally and proximodistally. This specimen lacks a dimple proximal to the ulnar condyle.

UCMP 195990 in many ways resembles specimens that we attribute to MuE and specimens that others attributed to *Stygimys kuszmauli* (Deischl 1964; Krause and Jenkins 1983). However, the eucosmodontid *Stygimys* has not been reported from the Cretaceous of the Western Interior (but see Lillegraven 1972 for a Cretaceous occurrence in Baja California); in our study area, the earliest occurrence of *Stygimys* is Pu1 (Clemens 2002; Wilson 2014). Along with this temporal incongruity, the slight differences in size and morphology suggest that MuD represents a different taxon. If we assume that the body size of individuals in MuD is slightly smaller than that of *Stygimys* (ca. 210 g), MuD might be attributable to the Lancian cimolodontid *Cimolodon nitidus* (ca. 180 g; Wilson et al. 2012). This taxon is known from this formation and from this locality specifically (Clemens 1964).

4.1.5. Distal humerus morphotype MuE (Fig. 3.8)

Morphotype description.—The five humeri assigned to this morphotype are among the medium-sized humeri in our sample (TDW mean = 8.31 mm, SD = 0.25 mm). Diagnostic features of this morphotype include: (i) an ulnar condyle that tapers proximally on the ventral surface (i.e., mediolaterally narrows at the proximal ulnar condyle extent); (ii) an ulnar condyle that terminates in a small pit or dimple; (iii) a stout distal shaft; and (iv) a deep olecranon fossa.

These humeri are nearly identical to specimens from the Bug Creek Anthills attributed to ?*Stygimys kuzsmauli* (mean TDW = 8.18 mm, SD = 0.64 mm; Deischl 1964;

Krause and Jenkins 1983). The Bug Creek Anthills are composed of stratigraphically mixed Lancian and Pu1 assemblages (Lofgren 1995; Clemens 2002). *Stygimys kuszmauli* is the only Pu1 taxon in this size range (body mass estimate = 210 g), with the next closest candidate being the smaller *Cimexomys gratus* (body mass estimate = 110 g); the only Lancian taxa in this approximate size range is the slightly smaller *Cimolodon nitidus* (180 g; Wilson et al. 2012). Thus, we attribute these Pu1 and mixed-age MuE specimens to *Stygimys kuszmauli* (Deischl 1964; Krause and Jenkins 1983).

4.1.6. Distal humerus morphotype MuF (Fig. 3.9)

Morphotype description.—The six specimens in this morphotype are among the largest in our sample of K-Pg multituberculate humeri (mean TDW = 13.9 mm, SD = 0.23 mm). Diagnostic features of this morphotype include: (i) a large, spherical radial condyle with a prominent, ventrolaterally flaring capitular tail that extends to nearly the lateral edge of the specimen; (ii) a small entepicondylar foramen relative to specimen size; (iii) a rugosity on the dorsomedial surface of the entepicondyle; and (iv) a pronounced, sharp medial margin of the ulnar condyle dorsally. Larger specimens in this morphotype (e.g., UCMP 174232) generally appear more robust, and specifically have a more rugose proximal surface of the olecranon fossa, which we attribute to differences in size. One specimen (UCMP 127384; Fig. 3.9) has a pronounced distolaterally facing notch with a sharp proximal border proximal to the ulnar condyle on the ventral surface of the specimen (i.e., the location of the ulnar condyle dimple in MuB, MuC, MuE, and transverse depression in MuA). Because another specimen (UCMP 174400) has a slight depression in this same area, we suggest that this represents morphological variation of this feature within MuF.

These specimens are morphologically generalized and closely resemble humeri attributed to ?*Stygimys kuszmauli* from the Bug Creek Anthills, but are twice as large (Deischl 1964; Krause and Jenkins 1983). They also closely resemble the more fragmentary Lancian specimens attributed to ?*Meniscoessus conquistus* (Cope 1884; Deischl 1964) and ?*Meniscoessus robustus* (formerly ?*Dipriodon lunatus*; Marsh 1889). The cimolomyid *Meniscoessus robustus* and ?cimolomyid *Essonodon browni* are the two largest multituberculate taxa present in Lancian deposits in our study area (Clemens 2002; Wilson et al. 2014). We tentatively attribute these MuF specimens to the most abundant of these large Lancian multituberculates, *Meniscoessus robustus* (e.g., Wilson 2005, 2014). A femur from eastern Montana (Museum of the Rockies specimen MOR882, locality unknown), which is comparable in size to these MuF humeri, was previously attributed to this species (Hunter et al. 1997; DeBey and Wilson 2014).

4.2. Therian humeri

Therian distal humeri are characterized by a trochlear articular surface, as opposed to the bulbous, condylar articular surface morphology of multituberculate humeri. Although in some more derived therians the entepi- and ectepicondyles are reduced and the entepicondylar foramen lost (e.g., Rowe 1988; Ji et al. 2002), our latest Cretaceous and earliest Paleogene therian specimens retain a substantial entepi- and ectepicondyle and an entepicondylar foramen. Here, we attribute one Lancian fragmentary distal humerus to Theria; all other specimens are attributed to Metatheria or Eutheria.

4.2.1. Distal humerus morphotype ThA (Fig. 3.10)

Morphotype description.—This morphotype contains one fragmentary specimen, a very small left humerus that preserves only the entepicondyle and entepicondylar foramen, trochlea, and partial radial and olecranon fossae (minimum TDW = 4.9 mm). Diagnostic features of this morphotype include: (i) a relatively large entepicondyle with a large elliptical entepicondylar foramen; (ii) a posterior surface between the entepicondyle and trochlea that is flat and lacks a dorsoepitrochlear fossa; and (iii) an olecranon and radial fossae that is inferred as shallow.

This very small Lancian specimen, although fragmentary, is morphologically unique among our specimens. The preserved entepicondylar and trochlear morphology indicate that this specimen is not a multituberculate. The absence of a proposed metatherian synapomorphy (presence of a capitular tail; O'Leary et al. 2013), and other features common among Cretaceous and Paleogene metatherian humeri (e.g., spherical capitulum, zona conoidea articulation with the ulna, well-developed ectepicondylar crest; Szalay and Dagosto 1980; Szalay and Trofimov 1996; Szalay and Sargis 2001; Argot 2001; Chester et al. 2010) are missing in this specimen due to breakage and cannot be evaluated. The greater abundance of metatherians relative to eutherians in the Lancian (Clemens et al. 1979; Wilson 2014) suggests a metatherian identity for this specimen, but we provisionally attribute it to Theria indet. until more material can be recovered and examined.

4.3. Metatherian humeri

Metatherian distal humeri are characterized by a relatively large, spherical capitulum with a capitular tail, a trochlea that is separated from the capitulum, and a relatively large and well-developed supinator crest with a sigmoid profile (Szalay and

Dagosto 1980; Szalay and Trofimov 1996; Argot 2001; Szalay and Sargis 2001; Luo et al. 2003; Chester et al. 2010; O'Leary et al. 2013; Williamson et al. 2014). Here, we attribute one Lancian humerus to Metatheria.

4.3.1. Distal humerus morphotype MeA (Fig. 3.11)

Morphotype description.—This morphotype contains one left humerus of a relatively large metatherian (minimum TDW = 18.2 mm). Proximally this specimen preserves the narrowest portion of the mid-shaft and the distal extent of the deltopectoral shelf; distally this specimen preserves 80–90% of the supinator crest, the proximal portion of the entepicondylar foramen, and the proximal extent of the olecranon fossa; this specimen lacks the distal epiphysis, entepicondyle, and the lateral, natural edge of the supinator crest. The diagnostic feature for this morphotype is a very pronounced, laterally extensive supinator crest that is sigmoid in profile and that contains a hypertrophied process on the proximal margin.

Relative to extant material, this specimen broadly resembles *Didelphis* spp. in morphology and size. However, this specimen differs from *Didelphis* in being more squat (proximodistally compressed), and differs from *Didelphis* and other extant marsupial taxa in having a larger, more robust, and more medially extensive supinator crest (e.g., Argot 2001; Szalay and Sargis 2001; Flores 2009). The proximal process of the supinator crest of this specimen is much more developed than it is in *Didelphis*, more closely resembling other didelphids, such as *Monodelphis* and *Caluromys* (Fig. 3.11; Argot 2001; Szalay and Sargis 2001; Flores 2009). This specimen is the largest Lancian humerus in our sample; it has a TDW more than 1.5x that of the largest Lancian multituberculate. The only mammal

in this size range is *Didelphodon vorax*, the largest Cretaceous metatherian (Clemens 2002; Wilson 2014). Marsh (1889: plate V: figs. 5–6) reported a distal humerus from the latest Cretaceous of Wyoming (Lance Formation) that he tentatively attributed to *Didelphodon vorax* (Table S3.3). However, our specimen greatly differs from the published image in the shape of the supinator crest proximally, as well as in overall size; the TDW (~8–10 mm) that we estimated from the figure is half the size of our specimen, but we are not confident that the listed scaling factor is correct (x2, Marsh 1889). If the specimen figured by Marsh (1889) is in fact *Didelphodon vorax*, then we suggest that it could be from an immature individual, and/or broken at the proximal supinator crest, or there could be sexual dimorphism of size and distal humerus shape in this species (personal observation, Wilson 2015) such that there is a real discrepancy in morphology and size between our MeA specimen and the specimen figured. Regardless of Marsh's attribution, the large size of the specimen warrants an attribution of this morphotype to ?*Didelphodon*.

4.4. Eutherian humeri

We compared our material with a broad sample of extant eutherians and with Cretaceous, Paleocene, and Eocene fossil taxa. Postcranial synapomorphies for eutherians are not well defined; however, there are some features that are generally shared among eutherians, including a single, continuous articular surface (in contrast to the separated trochlea and capitulum in metatherians) and the presence of a dorsoepitrochlear pit (i.e., in some archaic ungulates and early primates; Szalay et al. 1975; Szalay and Dagosto 1980; Horovitz 2003; Luo et al. 2003; Boyer et al. 2010; Chester et al. 2010; Hooker et al. 2014). Here, we describe and attribute to Eutheria one Lancian, one Pu1, and four Pu3 specimens,

as well as 11 specimens from deposit of Lancian-Pu1 mixed-age (from the Bug Creek Anthills; Table 3.3).

4.4.1. Distal humerus morphotype EuA (Fig. 3.12)

Morphotype description.—The specimen in this morphotype is among the smaller eutherian specimens described herein (minimum TDW = ~6.4 mm); it preserves the complete distal surface (except the medial extent of the entepicondyle) and a substantial portion of the shaft. Diagnostic features of this morphotype include: (i) the presence of a small and relatively shallow dorsoepitrochlear fossa (especially compared to e.g., EuC); (ii) a trochlea and capitulum that are separated by a deep zona conoidea, and that are approximately equal in the mediolateral width (trochlea slightly narrower); (iii) a spherical capitulum with a capitular tail; (iv) a large, circular entepicondylar foramen (mediolaterally wider than in EuB); (v) a shallow border separating the radial fossa from the entepicondyle (proximal to the trochlea); (vi) a large and posteriorly projecting supinator crest; (vii) a trochlea that is proximodistally short and mediolaterally narrow posteriorly; and (viii) a proximodistally tall, shallow olecranon fossa.

This specimen resembles plesiadapiform and early euprimate distal humeri more closely than it does any published archaic ungulate, "insectivoran," or larger mammalian humeri from the Paleocene of North America (Matthew 1937; Szalay and Dagosto 1980; Rigby 1981; Schoch 1986; Boyer et al. 2010; Kondrashov and Lucas 2012; Argot 2013; Table S3.3). In anterior view, the dorsal trochlea morphology, spherical capitulum, relative proportions of the trochlea and capitulum, and extended entepicondyle all resemble Paleocene plesiadapiforms more than larger specimens from our study area attributed to

?*Protungulatum* and ?*Procerberus* (Simpson 1935; Szalay et al. 1975; Szalay and Dagosto 1980; Bloch et al. 2007; Boyer et al. 2010; Table S3.3). Similarly, in posterior view, the short and narrow trochlea, dorsoepitrochlear foramen, and olecranon fossa more closely resemble Paleocene plesiadapiforms than specimens attributed to ?*Protungulatum* and ?*Procerberus* (Simpson 1935; Szalay et al. 1975; Szalay and Dagosto 1980; Bloch et al. 2007; Boyer et al. 2010; Table S3.3). We suggest humerus morphotype EuA is a plesiadapiform primate, possibly attributable to one of three plesiadapiform taxa described from the Pu3 area: *Purgatorius unio*, *Purgatorius janisae*, and *Pandemonium dis*. We further suggest EuA is attributable to *Purgatorius* sp., the most abundant plesiadapiform in these Pu3 deposits (Clemens 2002, 2004; Wilson 2014). This is consistent with the presence of teeth and isolated tarsals that have been found at this locality and attributed to *Purgatorius* (Clemens 2002, 2004; Wilson 2014; Chester et al. 2015).

4.4.2. Distal humerus morphotype EuB (Fig. 3.13)

Morphotype description.—This morphotype is represented by one small distal humerus specimen that is ~80–90% complete, missing only the terminal ends of the medial entepicondyle and lateral ectepicondyle (minimum TDW = 8.53 mm; Fig. 3.13). The diagnostic features of this morphotype are (i) a rugosity medial to the trochlea on the anterior surface, which has three ridges that extend from the medial edge of the trochlea on to the entepicondyle, each ridge with a pock-like, indented texture; (ii) a very large entepicondyle, with a more exaggerated medial extent than in other eutherian specimens (apparent even in this broken state); (iii) a distal concavity on the posterior surface, that extends medially from the entepicondyle and that becomes less pronounced and ultimately

disappears laterally; (iv) a bulbous trochlea (anteriorly) that is approximately 50–60% of the capitulum width, and is therefore larger (mediolaterally and proximodistally) than in other eutherians in our sample (e.g., EuA and EuD); (v) a trochlea (posteriorly) that is mediolaterally narrow relative to specimen distal width; and (vi) a shallow, proximodistally short olecranon fossa that is not perforated. The specimen lacks a dorsoepitrochlear fossa. We note the medial extent of the entepicondylar rugosity cannot be determined due to specimen breakage.

The Lancian morphotype EuB differs greatly from published humeri material, especially in the expanded entepicondyle and morphology of the olecranon fossa, from the study area (e.g., Bug Creek Anthills material attributed to ?*Protungulatum donnae* and ?*Procerberus formicarum*; Szalay and Dagosto 1980; Boyer et al. 2010; Table S3.3), younger "insectivoran" material (e.g., leptictid cf. *Prodiacodon tauricinerei*; Rose 1999; Table S3.3), and older eutherian material (e.g., *Barunlestes*, *Ukhaatherium*; Horovitz 2003; Kielan-Jaworowska 2009; Chester et al. 2010). Unfortunately, there are no other latest Cretaceous eutherian humeri for comparisons. UWBM 97114 does not possess a capitular tail, a synapomorphy of Metatheria (O'Leary 2013; Williamson et al. 2014); the morphology of its entepicondyle, trochlea, and capitulum also differs greatly from the Paleocene *Mayulestes* and *Pucadelphys* as well as some extant marsupials, including didelphids (*Caluromys*, *Chironectes*, *Didelphis, Metachirus*), the microbiotherian *Dromiciops*, and the caenolestid *Rhyncholestes* (Marshall et al. 1995; Muizon 1998; Argot 2001; Szalay and Sargis 2001; Flores 2009; Chester et al. 2010). Superficially, EuB most closely resembles extant semi-fossorial tenrecs *Oryzorictes* sp. in the extreme medial extension of the entepicondyle; however, breakage in EuB prevents comparison with the bulbous nature of the

entepicondyle medial extent in *Oryzorictes* sp. (Salton and Sargis 2008). Among small eutherian taxa present in the Lancian of our study area, two species of *Gypsonictops*, and five species of cimolestid *Cimolestes* are plausible candidate taxa; the small palaeoryctid *Batodon tenuis* is too small to be a candidate taxon for this morphotype (Clemens 2002; Wilson 2014).

4.4.3. Distal humerus morphotype EuC (Fig. 3.14)

Morphotype description.—Specimens in this morphotype (TDW = 9.52 mm) have a large and robust entepicondyle, a deep olecranon fossa, proximodistally tall articular surface (in posterior view), and a spindle-shaped capitulum that is approximately three times wider than the mediolaterally narrow trochlea. Diagnostic features of this morphotype include: (i) a pronounced, deep, and round dorsoepitrochlear fossa on the posterior surface; (ii) a prominent medial trochlear keel and proximomedial trochlear lip on the anterior surface; (iii) a sharp and prominent crest extending proximally from the medial edge of the trochlea, delineating the boundary between the radial fossa medially and the entepicondylar foramen laterally; (iv) an entepicondylar foramen that does not extend distally beyond the proximal extent of the capitulum; (v) an entepicondyle that is larger anteroposteriorly in distal view than in morphotype EuD; and (vi) a humerus shaft that has a supinator crest that displays undulation of the lateral margin (preserved in specimen UCMP 151991; Fig. 3.14).

Of all comparative material we examined, the specimens in this morphotype exactly match those attributed to ?*Protungulatum donnae* (Szalay and Dagosto, 1980; Boyer et al. 2010; Table S3.3). However, dental specimens of four other archaic ungulates that are

similar in size and dental morphology to *Protungulatum donnae* are known from similarly aged deposits in this area: *Protungulatum gorgun*, two species of the periptychid *Mimatuta* (*M. morgoth* and *M. minuial*), and the arctocyonid *Oxyprimus erikseni* (Luo 1991; Wilson 2004, 2013, 2014). In fact, *Protungulatum* and *Mimatuta* are both known from the mixed and early Puercan localities where these humeri were found (from UCMP locs. V71203 and V74111, respectively; Archibald, 1982; Wilson 2004, 2014). As such, the rationale is unclear for why so many specimens that resemble EuC were attributed to ?*Protungulatum* rather than some combination of these five archaic ungulate species (Rigby 1981). It might point to identification bias that stemmed from one or more factors: (1) *Protungulatum* was the first genus of archaic ungulate named from the early Puercan (Sloan and Van Valen 1965), whereas *Mimatuta* and *Oxyprimus* were named over a decade later (Van Valen 1978); (2) many institutions contain older collections from Pu1 assemblages in which specimens were attributed to *Protungulatum*, and (3) *Protungulatum*, on the basis of dental material, was the most abundant of these three taxa (Wilson 2004). Until a humerus is found in association with dental specimens of one of these five taxa, we recommend that isolated humeri referable to the EuC morphotype be attributed to archaic ungulate indet. rather than to a lower taxon. This logic also applies to other isolated postcranial elements previously attributed to *Protungulatum*.

4.4.4. Distal humerus morphotype EuD (Fig. 3.15)

Morphotype description.—This morphotype is represented by five specimens (plus an additional five specimens tentatively attributed to EuD) from two to three Bug Creek localities with temporally mixed ages (see note below on tentative assignments).

Specimens in this morphotype are approximately the same size as those in EuC (EuD TDW mean = 9.58 mm, SD = 0.50 mm, n = 2; Fig. 3.15). Diagnostic features of this morphotype include: (i) a large and mediolaterally wide entepicondyle that is less robust than in other morphotypes of similar size (i.e., EuC); (ii) a relatively large entepicondylar foramen that is ovoid (rather than long and thin, as in EuC); (iii) a pronounced and rounded supinator crest that is curved posterolaterally and that greatly expands the anteroposterior width of the specimen compared to other morphotypes (e.g., EuC); (iv) a mediolaterally wide but proximodistally short olecranon fossa, resulting in a squat appearance; and (v) an articular surface that is mediolaterally wider and proximodistally shorter than in EuC, and that contains a lateral flange of the capitulum (Boyer et al. 2010). Additionally, the more completely preserved shaft of UCMP 151946 (Fig. 3.15) has two ridges: one dorsal to and continuous with the entepicondyle and a second on the anterior shaft (i.e., the distal extent of the pectoral crest).

Some specimens have all the diagnostic features of the shaft listed above and include the proximal portions of the entepicondylar foramen and olecranon fossa; however, they are missing articular surfaces (and in some cases the entire distal epiphysis). We therefore tentatively assign these to morphotype EuD (Table 3.3).

EuD morphology resembles that of similarly sized humeri attributed to ?*Protungulatum donnae* and ?*Procerberus formicarum* in having a trochlea and capitulum that are continuous and are separated by a wide and shallow margin (Szalay and Dagosto 1980; Boyer et al. 2010; Table S3.3). EuD is more similar to specimens attributed to ?*Procerberus* specifically than to ?*Protungulatum* in the proximodistally short trochlea and in the lack of a dorsoepitrochlear pit (Szalay and Dagosto 1980; Boyer et al. 2010; Table

S3.3). Specimens in this morphotype bear little resemblance to much larger Paleocene taxa from the San Juan Basin (e.g., taeniodonts, tillodonts, periptychids, or arctocyonids, or the larger pantodont *Pantolambda*; Matthew 1937; Schoch 1986; Kondrashov and Lucas 2012; Table S3.3). The EuD specimens generally resemble those of the Eocene leptictid *Prodiacodon* (Rose 1999; Table S3.3), and most closely resemble those attributed to the Pu1 cimolestid *Procerberus formicarum* (Szalay and Dagosto 1980; Boyer et al. 2010; Wilson 2014).

As with morphotype EuC, we caution against attributing this morphotype to cimolestid *Procerberus formicarum* because of the presence of other similarly-sized taxa at the same time and in the same place (Archibald 1982; Lofgren 1995; Wilson 2004, 2013, 2014). This issue is further complicated by the fact that all of our EuD specimens, and all morphologically similar specimens from the literature (Szalay and Dagosto 1980; Boyer et al. 2010; Table S3.3), are from the stratigraphically mixed assemblages of the Bug Creek Anthills; thus, they could be Lancian or Pu1 in age. Eutherian candidate taxa present in the latest our study area include leptictidans *Gypsonictops* sp. (Lancian) and *Prodiacodon* sp. A (Pu1), and cimolestid *Cimolestes* (Lancian and Pu1; Archibald, 1982; Lofgren, 1995; Wilson 2004, 2014; Clemens 2015). In fact, *Gypsonictops*, *Cimolestes*, and *Procerberus* have been found at the Bug Creek Anthills (Archibald and Clemens, 1984). Others have commonly referred specimens matching this morphotype to *Procerberus*, perhaps because (i) *Procerberus* sp. was the first leptictidan named from the study area (Sloan and Van Valen 1965); (ii) humeri specimens were attributed to this taxon in museum collections and the attributions were propagated by subsequent researchers; and (iii) *Procerberus*, on the basis of dental evidence, was the most abundant mammal in Pu1 assemblages (Wilson 2014).

Nevertheless, given the multiple candidate taxa for this morphotype and the lack of associated skeletal and dental material of *Procerberus* (Rigby 1981), we do not assign EuD to a particular taxon.

4.4.5. Distal humerus morphotype EuE (Fig. 3.16)

Morphotype description.—This morphotype is represented by two right humeri that preserve nearly the complete distal surface, missing only the medial extent of the entepicondyle (minimum mean TDW = 16.48 mm, SD = 2.05 mm, n = 2). Diagnostic features of this morphotype include: (i) a large, deep, and circular dorsoepitrochlear fossa; (ii) a large, spindle-shaped capitulum that is ~3x the size of the trochlea; (iii) a large, ellipsoidal entepicondylar foramen with a slightly bulbous appearance at the proximal portion of the thin entepicondylar bridge; (iv) a pronounced proximal border of the trochlea on the posterior surface of the specimen, similar to that in EuF; (v) a mediolaterally and proximodistally large albeit shallow radial fossa, also similar to that of EuF; (vi) a pronounced supinator crest that is reflected more posteriorly than in EuF; and (vii) a moderately deep olecranon fossa that is not perforated. This morphotype is very similar to morphotype EuF; however, because EuE is about half the size of EuF, and many features are differentially preserved, we treat these morphotypes as separate at this time.

Relative to comparative taxa, EuE is morphologically similar to humeri attributed to ?*Protungulatum donnae*, despite the difference in size (i.e., EuE is ~1.5x larger than ?*Protungulatum* specimens; Szalay and Dagosto 1980; Boyer et al. 2010; Table S3.3). Among the diagnostic features of EuE, the very deep dorsoepitrochlear foramen has so far only been observed in specimens attributed to ?*Protungulatum* and early primates (Szalay

and Dagosto 1980; Boyer et al. 2010; Table S3.3). Also, the morphology of the olecranon and radial fossae, articular surface, entepicondyle and ectepicondyle, and entepicondylar foramen closely match specimens attributed to ?*Protungulatum* (Szalay and Dagosto 1980; Boyer et al. 2010; Table S3.3). However, EuE differs from those specimens in having a larger entepicondylar foramen with a narrower entepicondylar bridge, a wider proximal surface of the trochlea, a larger olecranon fossa posteriorly, and a larger and more pronounced fossa laterally on the ectepicondyle surface (Szalay and Dagosto 1980; Boyer et al. 2010). EuE and Paleocene archaic ungulates (e.g., *Arctocyon*, *Periptychus*) share a few general features, including a wide distal end, a proximally extensive anterior trochlear surface, a lateral capitular flange, and a distal notch between the capitulum posterior articular surface and the ectepicondyle (Matthew 1937; Argot 2013; Table S3.3). However, some features distinguish EuE from these comparative taxa. For example, the large, ovoid entepicondylar foramen, larger and more laterally extensive and posteriorly reflected supinator crest, and proximodistally shorter and shallower olecranon fossa of EuE differ from those of many comparative archaic ungulate taxa (e.g., *Loxolophus, Arctocyon*, *Periptychus*, and *Ectoconus*; Matthew 1937; Russell 1964; Argot 2013; Table S3.3). Compared to other large therian candidate taxa, we find EuE bears little resemblance to younger Paleocene tillodont (*Deltatherium*; Matthew 1937; Kondrashov and Lucas 2012), pantodont (*Pantolambda*; Matthew 1937), and taeniodont taxa (e.g., *Onychodectes*, *Ectoganus*, *Lampadophorous*, *Psittacotherium*, *Stylinodon*; Matthew 1937; Schoch 1986; Table S3.3). Based on similarities with archaic ungulate taxa we examined, we suggest that EuE represents an archaic ungulate taxon; given the large size of this specimen, we suggest it is attributable to a large archaic ungulate whose humeri are currently unknown. The only

candidate taxon present in both Pu1 and Pu3, and in this size category is *Baioconodon* sp. (Clemens 2002; Wilson 2014), and thus we tentatively assign this morphotype to *Baioconodon*. We note a lower third molar (m3) tooth attributed to *Baioconodon* (Clemens, personal communication) has also been found at the locality preserving one of these specimens (UCMP 218901).

4.4.6. Distal humerus morphotype EuF (Fig. 3.17)

Morphotype description.—This specimen, a partial right humerus, is the most complete among the larger eutherian distal humeri in our sample (minimum TDW = 19.4 mm; Fig. 3.17). Diagnostic features of this specimen include: (i) a trochlea that is proximodistally tall, distally extensive, with a fairly flat (not especially convex) lateral distal surface; (ii) a very large trochlear keel, with a smooth and concave facet that is oriented anteroposteriorly on the medial surface; (iii) a spindle-shaped capitulum that is proximolaterally bulbous, mediolaterally wide (~3x the width of the trochlea), and has a slight capitular tail; (iii) a very large, deep, and rugose fossa on the posterior aspect of the ectepicondyle; (vi) a pronounced, raised, and rugose margin on the proximal trochlea in posterior view, as in EuE; and (v) a mediolaterally wide, proximodistally short olecranon fossa composed of very thin bone that is perforated in the center.

Among the diagnostic features of EuF, the semilunar-shaped radial fossa is found in smaller humeri specimens that have been attributed to ?*Protungulatum* (Szalay and Dagosto 1980; Boyer et al. 2010); whereas the proximodistally tall olecranon fossa and the small fossa on the medial surface of the trochlea are not found in any of the comparative material that we examined. That said, EuF has a number of features on the distal humerus

in common with younger taxa. Specifically, it resembles the larger arctocyonids *Arctocyon primaevus* and *A. corrugatus* (formerly *Claenodon corrugatus*) in capitulum and trochlear morphology and the presence of a capitular flange; however, EuF has a relatively wider capitulum, with a more shallowly sloping distolateral trochlear margin (Matthew 1937; Russell 1964; Argot 2013; Table S3.3). EuF also shares the relative proportions of capitulum and trochlea in common with some larger archaic ungulate taxa, including the Paleocene periptychids *Periptychus carinidens* and *Ectoconus majusculus*, as well as the smaller Paleocene periptychid *Mithrandir gillianus* and arctocyonid *Chriacus* (Matthew 1937; Rigby 1981; Table S3.3). Although more similar in size, this specimen is less similar in morphology to the Paleocene archaic ungulates *Loxolophus*, *Tetraclaenodon*, and *Protoselene* (Matthew 1937; Kondrashov and Lucas 2012; Table S3.3). Among comparative taeniodonts, EuF has a different morphology from the much larger Paleocene pantodont *Pantolambda,* tillodont *Deltatherium*, and stylinodont taeniodonts, including *Ectoganus* sp., *Stylinodon mirus*, and *Psittacotherium multifragum* (Matthew 1937; Schoch 1986; Kondrashov and Lucas 2012; Table S3.3); we therefore exclude the Pu3 taeniodont cf. *Wortmania* as a candidate taxon. The humerus specimen in morphotype EuF might instead represent a medium- to large-sized Pu3 taxon whose humeri have not yet been published, possibly the triisodontid *Eoconodon nidhoggi* or *E. hutchisoni*. We note an unnamed pantodont and an unnamed oxyaenid creodont could also be candidates for EuF (Clemens 2002, unpublished results; Wilson 2014).

4.4.7. Distal humerus morphotype EuG (Fig. 3.18)

Morphotype description.—This specimen from the left side preserves only the medial aspect of the distal humerus, including the distal entepicondyle and trochlea, and a channel just proximal to these that represents the distal portion of the entepicondylar foramen (Fig. 3.18). Despite its fragmentary state, it is one of the largest distal humeri in our study (e.g., approximately the same size as EuF, and ~3.5x the size of EuC; NCW = 10.3 mm), and is sufficiently unique to describe a new morphotype. Diagnostic features of this specimen include: (i) a shallow but pronounced dorsoepitrochlear fossa on the posterior surface, with an especially rugose mediodistal border; (ii) a shallow notch separating the entepicondyle and trochlea distally; (iii) a distal surface of the trochlea that, in anterior view, has a slope similar to that in EuD, and which is intermediate to the shallow slope in EuB and the steep slope in EuF; (iv) a pinched margin, separating the entepicondylar foramen and the radial fossa, that is not seen in the other large eutherian morohotype (EuF); and (v) a small, medially-facing fossa proximal to the trochlea (posteriorly).

Among the larger-bodied Paleocene taxa that we examined for comparisons with this Pu3 morphotype, the strongest resemblance is to the Torrejonian pantodont *Pantolambda bathmodon* (AMNH 16663; Matthew 1937; Table S3.3). We speculate the distal humerus morphology of an unnamed pantodont from our study area may be morphologically similar to *P. bathmodon* (Clemens, unpublished results; Wilson 2014). Although our specimen is 60–70% of the size of the distal humerus of Torrejonian *P. bathmodon* (Matthew 1937), the morphological similarities are striking. They include the flat, robust distal surface of the entepicondyle, placement of the entepicondylar foramen, and the modest trochlear flange (Osborn and Earle 1895; Matthew 1937). In these features, EuG strongly differs from published specimens of Paleocene Theria indet. (Jenkins 1973;

Standhardt 1986), and from Paleocene and Eocene archaic ungulates (e.g., Matthew 1937; Russell 1964; Rigby 1981; Rose 1987; Kondrashov and Lucas 2012; Argot 2013; Table S3.3). Additionally, none of the known Pu3 archaic ungulates from this area would likely have a humerus as large as EuG (Clemens, 2002; Wilson 2014). The taeniodont cf. *Wortmania* is yet another large-bodied taxon known from this area (Clemens, 2013). Although humeri of *Wortmania* are unknown, EuG strongly differs in trochlea and entepicondyle shape with the humeri of other taeniodont taxa, including the much larger stylinodontid taeniodonts *Psittacotherium*, *Lampadophorus*, *Ectoganus*, or *Stylinodon*, and the similarly sized *Onychodectes tisonensis* (Schoch 1986). It is thus unlikely that EuG represents a taeniodont (Matthew 1937; Schoch 1986; Clemens 2013). Moreover, EuG bears little resemblance to the humerus of the Paleocene tillodont *Deltatherium* (Matthew 1937; Kondrashov and Lucas 2012; Table S3.3). We were unable to compare EuG to other taxa known from this study area and geologic interval, specifically two triisodontids *Eoconodon hutchisoni* and *E. nidhoggi*, and a possible, as yet unnamed oxyaenid creodont, because humeri material attributed to these taxa is currently unknown (Clemens, unpublished results; Clemens 2011; Wilson, 2014). We tentatively attribute EuG to the unnamed pantodont (Pantodonta sp. A; Clemens, unpublished results; Wilson 2014), although we recognize we cannot rule out an attribution to triisodontid *Eoconodon* spp. or an unnamed oxyaenid credont (Clemens, unpublished results; Clemens 2011; Wilson, 2014). This specimen is too small to be part of the same taxon as the largest femur published from this area (morphotype Eu4 of DeBey and Wilson 2014).

5. Results & Discussion

5.1. Quantitative discrimination among morphotypes

We classified our sample of 50 distal humeri from the Lancian- and Puercan-age deposits of eastern Montana into six multituberculate and nine therian morphotypes (Tables 3.2–3, S3.6–7; Fig. 3.19). All morphotypes were based on qualitative characters, but we also tested for quantitative differences among morphotypes using univariate (e.g., ANOVAs) and multivariate statistics (e.g., PCAs).

Multituberculate humeri size varies significantly across morphotypes (Tables S3.6, S3.8). Tukey honest significant difference (HSD) post hoc tests indicate all morphotypes vary significantly from all others for measurements TDW, AW, and TLW ($p < 0.01$; Table S3.9). Most morphotypes vary significantly from one or more morphotypes for the other measurements, a pattern that is especially common among larger morphotypes, MuE and MuF (Table S3.9). As is expected, larger morphotypes have a greater variance across measurements than is seen among the smaller morphotypes (Figs. S3.2–3), so we corrected for size by calculating a coefficient of variation (CV). MuF has the largest coefficient of variation for RCH, UCL, and RCL; MuE has the largest coefficient of variation for UCH; and MuC has the largest coefficient of variation for all other measurements (Table S3.6).

PCA results of the size-standardized, multituberculate measurement data indicate that multituberculate specimens did not cluster together with those from the same morphotype, and separate from other morphotypes. This pattern was consistent across different permutations of the multituberculate datasets (Figs. S3.4–5, Tables S3.10–12), although we note published specimens occupy a greater area of the morphospace than any

of our morphotypes (Fig. S3.6). Most of our measurements of condyle shape consistently load positively on PC1, whereas relative entepicondyle width (relNCW) consistently loads most strongly on PC2 (Figs. S3.4–5, Tables S3.10–12). Relative ulnar condyle width (relUCW) is the only variable that dominantly loads on both PC1 and PC2, and it varies by dataset whether it is loading with or against relNCW; relUCW also loads most strongly on PC3 (Table S3.10–12). We find no quantitative characters (i.e., standardized measurements) that discriminate among multituberculate morphotypes (Figs. S3.4–6, Tables S3.10–12). It is possible our measurements do not capture nuanced differences in multituberculate distal humeri shape, and/or these small sample sizes fail to represent the patterns of morphotype distribution in the morphospace. That relUCW has a different pattern depending on the size and composition of the dataset implies small sample sizes are affecting these results. However, we detect many qualitative differences among our morphotypes, and, although beyond the scope of this project, we expect that a multivariate analysis of shape that included these qualitative characters would better discriminate among our morphotypes.

Therian morphotypes are significantly different from one another with respect to size. All morphotypes vary significantly across all measurements except for TDW (Table S3.13). Tukey HSD tests indicate larger morphotypes EuE, EuF, and EuG differ the most from all other morphotypes (Table S3.14; Figs. S3.7–8). Because metatherian morphotype MeA is poorly preserved (see Table 3.3), we excluded it from these calculations. We suggest that these data should be considered preliminary, as sample sizes are very small among these therians (i.e., six therian morphotypes have n = 1; Table S3.7).

5.2. Morphotype richness and taxonomic composition through the section

Humerus morphotype richness is greatest in the Lancian (n = 14 humeri), both overall (Morphotype richness [M] = 7) and for multituberculates specifically (M = 4; Fig. 3.19). Eutherians and metatherians are also present in the Lancian sample – this contrasts with the sample of femora from this interval, which only included multituberculates (DeBey and Wilson 2014). Lancian multituberculate humeri morphotype richness represents half of the femur morphotype richness previously reported (DeBey and Wilson 2014). Extant mammals whose forelimbs are used for habitat construction or in prey capture and manipulation are often less morphologically diverse than hind limbs (e.g., Szalay and Dagosto 1980; Polly 2007), a trend that may be a factor among these Lancian multituberculate humeri. Among Lancian therians, there is a large form (MeA) that we attribute to the metatherian *Didelphodon vorax*, one of the largest Late Cretaceous mammals (~1.7 kg; Gordon 2003; Wilson 2013, 2014), as well as two small humeri attributed to Theria and Eutheria (ThA and EuB, respectively); these three therian morphotypes are restricted to the Lancian. In our Lancian sample, metatherians and eutherians represent 14% of morphotypes and 7% of specimens respectively; these values differ from the relative abundances based on dental specimens (45% for metatherians, 14% for eutherians; Wilson 2014), but humeral sample sizes are small. Among the multituberculates, MuF is the largest and most abundant Lancian morphotype (43% of specimens). The Lancian sample also includes the only specimen of morphotype MuD, which is from the Lance Formation of Wyoming. Also among the Lancian sample are two specimens in the smallest morphotype, MuA, and two specimens in the medium-sized morphotype MuC (also found in Pu1 and Pu3 localities). Among the taxa to which we

attributed these Lancian morphotypes, ?*Meniscoessus robustus*, ?*Mesodma* sp., and ?*Cimolodon nitidus*, respectively, have also previously been identified among femora from the same study area (Hunter et al. 1997; DeBey and Wilson 2014).

The Bug Creek Anthills (BCA) mixed-age assemblage is our largest sample (n = 23, M = 5; Fig. 3.19), and includes one morphotype, EuD, that has not been found elsewhere in the section. That this eutherian morphotype is the most abundant morphotype (n = 10 humeri) in our entire sample is notable considering that our sample of femora from the BCA contained only multituberculates (DeBey and Wilson 2014). Among BCA material, humeri morphotypes MuA (Lancian), MuC (Lancian and Pu1), MuE (Pu1), and EuC (Pu1) are also present (Fig. 3.19).

Humerus morphotype richness is lowest in the early Puercan (Pu1) both overall (M = 4 or 5) and for multituberculates specifically (M = 2 or 3; Fig. 3.19). This pattern was also found in our sample of femora (DeBey and Wilson 2014) and may be a function of small samples sizes (n = 6 humeri); however, richness relative to sample size is high in this Pu1 assemblage. From this interval, we identify specimens of EuC, EuE, MuC, MuE, and tentatively MuA (Fig. 3.19). Among the taxa to which we attributed these Pu1 morphotypes, femora of ?*Stygimys kuszmauli* (MuE) and ?*Mesodma* sp. (MuA) were found in our study area; however, femora of ?*Protungulatum* (EuC) were not (DeBey and Wilson 2014).

In the Pu3, humerus morphotype richness slightly rebounds (M = 6), and is the highest relative to sample size (n = 7; Fig. 3.19). This Pu3 assemblage includes five eutherian morphotypes and two multituberculate morphotypes. All morphotypes present are restricted to this interval with the exception of morphotypes MuC and EuE. Morphotype MuC occurs in the Lancian through Pu3 in our study area, and the archaic

ungulate EuE appears in Pu1 and Pu3. Among those morphotypes restricted to Pu3, are very small taxa including EuA and MuB, as well as large eutherians EuF and EuG. These richness results mirror results from femora in the presence of small- and medium-sized multituberculates, large eutherians, and postcranial material possibly attributable to plesiadapiforms (Clemens 2002; DeBey and Wilson 2014; Wilson 2014). However, our Pu3 humeri sample lacks a large multituberculate morphotype, and has more large eutherian taxa than were found among femora (Clemens, unpublished results; Clemens 2011; DeBey and Wilson 2014; Wilson 2014).

Overall, our sample contains approximately twice as many specimens of multituberculates as therians among our humeri, but this varies through the section. In the Lancian sample, there are more multituberculates than therians, but in the Pu3 sample more therians than multituberculates (Fig. S3.1; Tables S3.15–16). The Bug Creek Anthills assemblage has the largest sample size for both multituberculates and therians; the smallest sample size for multituberculates is in the Pu1, and in the Pu1 and Lancian (tied) for eutherians (Fig. S3.1; Tables S3.15–16). These patterns are likely some combination of collecting and taphonomic biases, as well as evolutionarily meaningful patterns. For example, the large sample sizes from the BCA assemblage are most likely due the anomalous productivity of the assemblage (e.g., Sloan and Van Valen 1965; Lofgren 1995; Clemens 2002). However, dental material from extensively sampled Pu1 localities indicates a depauperate, "survival" fauna and relative to Lancian and Pu3 assemblages (e.g., Lofgren 1995; Wilson 2014). Despite small sample sizes in our study of humeri, that this dental pattern is also seen among femora from our study area (DeBey and Wilson 2014) suggests it may be biologically meaningful among our sample of humeri.

Although our sample sizes are low, the observed changes in humerus morphotype richness through time are consistent with those from dental and femora data from this study area: high richness of mostly multituberculates in the Lancian, a depauperate Pu1 fauna largely composed of small-bodied multituberculates and eutherians, and rebounding diversity of mostly eutherians in the Pu3 (i.e., Archibald 1982, 1983; Lofgren 1995; Clemens 2002; Wilson 2004, 2005, 2013, 2014; DeBey and Wilson 2014). Our proposed taxonomic assignments of some of the specimens in our humeri sample, if correct, would add to the postcranial record of these taxa and the study area (e.g., Deischl 1964; Szalay et al. 1975; Szalay and Dagosto 1980; DeBey and Wilson 2014; Chester et al. 2015). Specifically, referral of a large, distinctive humerus to the Lancian stagodontid metatherian *Didelphodon vorax* could illuminate an aspect of the locomotor ecology and phylogenetic relationships of this curious taxon (Fox and Naylor 2006); and the two other small Lancian therian humeri, one attributed to Eutheria, would be among the few specimens with which to study the postcranial morphology of small Lancian therians. Similarly, if the three large Pu3 humeri described here represent eutherian taxa distinct from that represented by the large Pu3 femur that was previously reported (DeBey and Wilson 2014), then we would have postcrania from at least four large Pu3 eutherian taxa, approximately one third all large eutherian Pu3 taxa known from our study area.

5.3. Specimen size and changes in body mass through time

Overall, our sample shows a five-fold difference between the smallest and largest specimens of multituberculates and therians (Tables S3.6–7). Results of one-way ANOVAs results (Tables S3.15–16) indicate significant differences through time (Lancian, BCA, Pu1,

Pu3) for multituberculate measurements RCW, UCH, RCH, and UCL (all $p < 0.05$; Table S3.17). These measurements describe the shape of the distal humerus articular surfaces, which is predictive of body mass (e.g., Egi 2001). Post hoc comparisons using the Tukey HSD test indicate that for all measurements Lancian multituberculate specimens are significantly larger than only BCA multituberculates (Table S3.18; Fig. S3.9).

For therians, the small sample sizes across biozones limit the number of measurements that can be compared with ANOVAs (which require at least three biozones). Results from ANOVAs of these measurements indicate a significant difference across biozones for only NCW and TH ($p < 0.01$ and $p < 0.05$, respectively; Table S3.19). Tukey post hoc results indicate Pu3 therian specimens are significantly larger than Lancian, BCA, and Pu1 specimens (for NCW; Fig. S3.10; Table S3.20). Entepicondylar width is a functionally significant measurement and is therefore potentially suboptimal for comparison of size through time (e.g., Argot 2001; Milne et al. 2009; Warburton et al. 2011; Janis and Figueirido 2014); however, in some groups, e.g., fossorial taxa, entepicondyle size is actually more strongly correlated with body mass than are other humerus measures (Elissamburu and Vizcano 2004). Although no other measurements yielded significant ANOVA results across biozones, nearly all measurements exhibited the same pattern of Pu3 specimens being larger than those in the Lancian or BCA bins (Fig. S3.10; Table S3.16); this pattern that might become significant for these measurements with larger sample sizes.

Using humerus size as a proxy for body size, we observe changes in body size through our section that are consistent with those described from our section on the basis of dental (e.g., Archibald 1983; Maas and Krause 1994; Clemens 2002; Wilson 2004, 2005, 2013, 2014) and femoral data (DeBey and Wilson 2014). Specifically, we note (1) a

significant decrease in multituberculate body size across the K-Pg boundary, and (2) an increase in therian body size through the Puercan. This post-K-Pg increase in eutherian body size is also consistent with results from synoptic studies using large temporal bins (i.e., 1 Ma, 2.5 Ma) and at continental and global scales (e.g., Stucky 1990; Alroy 1999; Smith et al. 2010). Additionally, using our taxonomic attributions and the distinction among Pu1 taxa as either "residents" or "immigrants" (Clemens 2002), we find Pu1 residents (MuC, and possibly MuA), are smaller than Pu1 immigrants to the study area (MuC, EuC, EuE, and possibly EuD). Similarly, Pu3 resident taxa are larger than Pu3 immigrants to the study area. These patterns were also seen among femora from the study area.

5.4. Geometric morphometrics results

To test whether the morphology of the distal humerus correlates with locomotor mode, we conducted a 2D GM analysis of extant mammalian humeri. Figure 3.20 shows a plot of the first three principal components (PCs) from the PCA of the partial warps of the 2D GM analyses on the full datasets. We limited our descriptions and interpretations of the morphospace to these PCs because together they comprise a substantial amount of the variance in the dataset (46%, 13%, and 11%, respectively; Table S3.21; Figs. 3.20, S3.11–12). Specimens at the minimum of PC1 are mediodistally wide, anteroposteriorly narrow, and have a large, medially projecting entepicondyle (Fig. 3.20; reversed from Fig. S3.11). In contrast, specimens at the minimum of PC1 are mediolaterally narrow and anteroposteriorly wide, with small entepi- and ectepicondyles, an anteriorly projecting medial trochlear keel, and a posteriorly projecting lateral trochlear margin (Fig. 3.20;

reversed from Fig. S3.11). Specimens at the maximum of PC2 have a wider trochlea posteriorly, in contrast with those at minimum of PC2 have more bulbous articular surfaces and a narrow trochlea posteriorly (Fig. 3.20). Metatherians generally plot higher on PC1 and lower PC2 and PC3 (Figs. 3.20, S3.11–12), and are more restricted in their morphospace occupation than eutherians (Figs. S3.11–12); however, we note that our sample includes 4.5X more eutherian specimens than metatherians (Table 3.4).

Locomotor segregation of locomotor groups on the first three PCs is poor. PC2 generally discriminates between fossorial taxa (positive scores on PC2), and arboreal and scansorial taxa (negative scores on PC2; Fig. 3.20C,D). Semiaquatic and gliding taxa plot in the middle of PC1, and gliding taxa plot in the middle of PC2 (Fig. 3.20C,D). There appears to be a pattern of locomotor placement that is phylogenetically correlated. This pattern of clustering according to ordinal-level taxon is not surprising given the phylogenetically diverse sampling of our dataset (13 mammalian orders across metatherians and eutherians) and the known phylogenetic signal that is preserved in humerus morphology (e.g., Morgan and Álvarez 2013; Fabre et al. 2015).

In this morphospace, the four fossil specimens (Lancian small eutherian EuB; BCA–Pu1 small archaic ungulate EuC; and two specimens of the BCA small "insectivoran" EuD) have high scores on PC1 and are near zero on PC2 (Fig. 3.20A). That is, they have a wider distal humerus than most of our extant specimens, with a moderately bulbous articular surface. In this respect, they most closely resemble didelphimorph and diprotodont metatherians and afrosoricid and cingulatan eutherians (Fig. 3.20A). On PC2 and PC3 the fossil specimens plot nearest to afrosoricids, rodents, scandentians, and one eulipotyphylan (Fig. 3.20B).

To reduce the phylogenetic signal, enhance discrimination among pertinent locomotor groups, and better predict locomotor mode in our fossil specimens, we removed several specimens from subsequent analyses: all metatherians because of their large phylogenetic distance from eutherians (including the fossil morphotypes), and extant eutherians that we deemed as poor functional analogs (i.e., taxa and locomotor groups that plotted very far from our fossil taxa). The latter consist of taxa with extreme cursorial and saltatorial morphological adaptations (i.e., carnivorans and lagomorphs, respectively). Although Mesozoic (and certainly Cretaceous) mammals were ecomorphologically diverse with respect to locomotor function (e.g., Luo 2007; Chen and Wilson 2015), taxa at the extremes of cursorial and saltatorial locomotion, similar to extant carnivorans and lagomorphs, are as yet unknown (Luo 2007; Chen and Wilson 2015). In this reduced dataset of extant taxa, PC1, PC2, and PC3 explain 37%, 19%, and 13% of the total variance, respectively (Table S3.21; Fig. 3.21). The phylogenetic signal in this second analysis is less than in the analysis of the original dataset (Fig. 3.20A,B vs. Fig. 3.21A,B).

As in the first analysis, the specimens distribute along PC1 in this second analysis on the basis of mediolateral width (e.g., entepicondylar and ectepicondylar width) and anteroposterior trochlea height (Fig. 3.21). Specimens at the maximum of PC1 are mediolaterally narrow and anteroposteriorly tall and have a large entepicondyle (Fig. 3.21); however, these patterns are less pronounced relative to those in the first analysis (Fig. 3.20). Similarly, those specimens at the minimum of PC1 are mediolaterally wide and anteroposteriorly short (Fig. 3.21), although not as anteroposteriorly constricted at the trochlea as in the analysis of the full dataset (Fig. 3.20). Variation along PC2 in the analysis of the reduced dataset is also similar to that of the full dataset (Figs. 3.20–21); in this

analysis, specimens at the minimum of PC2 also have a lateral extension of the articular surface beyond the capitulum (Fig. 3.21).

Locomotor discrimination is improved in the analysis of the reduced dataset. PC2 discriminates arboreal, terrestrial, and scansorial taxa (positive on PC2) from fossorial, semifossorial, and semiaquatic taxa (negative on PC2; Fig. 3.21C,D). On PC1, saltatorial and gliding taxa generally have positive scores (Fig. 3.21C). The discrimination of locomotor groups, especially on PC2, is consistent with the morphofunctional continuum found in Chen and Wilson (2015). In this morphospace, all fossil specimens generally plot low on PC1, with mediolaterally wide distal humeri and anteroposteriorly short articular surfaces; the Lancian EuB and BCA "insectivorans" (EuD) plot the lowest on PC1 of our fossil taxa (Fig. 3.21A,C). Lancian EuB and archaic ungulate EuC plot the highest on PC2 and have the most bulbous articular surfaces of our four fossil specimens (Fig. 3.21).

We plotted PC1 vs. PC2 (Fig. 3.22) and PC2 vs. PC3 (Fig. 3.23) separately for each locomotor group to assess how our fossil specimens compare to these groups. Our fossil specimens plot lower on PC1 than all arboreal, gliding, saltatorial, and terrestrial taxa (Fig. 3.22A,C,D,H) because of a mediolaterally wider distal humerus than the species in these extant groups. The only locomotor groups with PC1 and PC2 scores similar to all our fossils are extant species in the semifossorial, fossorial, and semiaquatic groups (Fig. 3.22B,E,G). Specifically, Lancian EuB and one BCA "insectivoran" EuD specimen have the mediolaterally widest distal humeri and the largest entepicondyle, and plot within the semifossorial locomotor group on PC1, PC2, and PC3 (i.e., nearest tenrecs *Hemicentetes* and *Oryzorictes*; Figs. 3.22–23). The other EuD specimen plots on PC1 and PC2 nearest the fossorial dasypodid *Cabassous* and close to the terrestrial tenrec *Microgale* (Fig. 3.22). The

archaic ungulate EuC plots nearest members of fossorial, semiaquatic, scansorial, and terrestrial locomotor groups (i.e., fossorial rodent *Aplodontia*, scansorial and semiaquatic tenrecs *Limnogale* and *Tupaia*, respectively, and terrestrial tenrecs *Setifer*, *Tenrec*, and *Microgale*; Fig. 3.22). Although in this morphospace our fossils specimens plot nearest to a number of afrosoricids (i.e., tenrecs) and rodents, we note arboreal representatives in our sample of these two groups, *Dendrohyrax* and *Sciurus* spp., and the gliding rodent *Glaucomys* spp. do not plot near our eutherian fossils (Fig. 3.22).

To emphasize morphological differences across our locomotor groups and to quantitatively predict locomotor mode among our fossil morphotypes, we conducted a linear discriminant analysis (LDA) of this reduced dataset on locomotor modes and significant principal components (i.e., PCs that explained > 1% of the total variance). Results show that the extant specimens were assigned to locomotor category with 74.19% accuracy (100% of gliding taxa; 93.33% of arboreal taxa; 90.00% of terrestrial taxa; 66.67% of semiaquatic and scansorial taxa; 62.50% of semifossorial taxa; 58.33% of fossorial taxa; and 33.33% of saltatorial taxa; Tables S3.22–23). In total, 16 of 62 specimens were misclassified (Table S3.23) and the majority of misclassified taxa were classified as terrestrial, semifossorial, and fossorial. The LDA predicts that the small Lancian eutherian (EuB) had an overwhelmingly arboreal locomotor mode, given the 99% prediction probability (followed by 0.4% probability of semifossorial locomotor mode). The predictions for EuC are reversed (61% semifossorial, 27% arboreal; Table S3.24). The two EuD specimens are predicted to be fossorial (93% for UCMP 151964) or semifossorial (51% for UCMP 153036; Table S3.24). Although rank among locomotor groups differs for each specimen, we suggest the general assignment to arboreal, semifossorial, and fossorial

locomotor groups for all fossil specimens is reflective of strong grasping muscles on the entepicondyle.

The LDA morphospace, which we defined by LDs 1–3, shows good discrimination of locomotor groups (Fig. 3.24). Arboreal and scansorial taxa plot high on LD1 and separate from semiaquatic and saltatorial taxa (low on LD1; Fig. 3.24). Fossorial taxa plot low on LD2, and terrestrial taxa high on LD2; semifossorial taxa fall between and overlap these two groups (Fig. 3.24). Scansorial and gliding taxa plot between arboreal and terrestrial taxa on LD1 (Fig. 3.24). Among the fossil specimens, EuC projected among arboreal and semifossorial taxa and also near fossorial and saltatorial specimens on LD1 vs. LD2 (Fig. 3.24A); one specimen of EuD falls among the fossorial taxa; and the other EuD specimen and the EuB specimen plot outside the region occupied by extant taxa, but closest to fossorial and arboreal taxa, respectively (Fig. 3.24A).

5.5. Additional comments on geometric morphometrics results

We recognize a disparity in morphospace occupation among some locomotor groups, such that gliding taxa occupying a small area, and saltatorial and semi-aquatic taxa occupying a greater area of the PCA and LDA morphospaces than other locomotor groups. We hypothesize the pattern among gliding taxa here is an artifact of sampling. Although our dataset originally included metatherians and eutherian gliders, the only gliding specimens included in the reduced dataset are males and females of two species of sciurid rodents (*Glaucomys sabrinus* and *G. volans*; Table 3.4). In the original dataset however, eutherian and metatherian gliders plot very near to one another on PC2 and PC3, and are only slightly separated on PC1, with the male and female metatherian sugar gliders (*Petaurus breviceps*,

family Petauridae) located nearest other metatherians (Fig. 3.20). We suggest the low morphological variance of gliders is a biologically meaningful pattern reflecting functional constraints, and we suggest a test of this hypothesis with inclusion of additional and more distantly related gliding taxa (e.g., metatherian *Acrobates pygmaeus*, dermopteran flying lemur *Cyanocephalus* spp., and anomalurid flying squirrels; Nowak 1999). Although our sampling is suboptimal, it is possible that the narrow morphospace occupation of gliders represents a real pattern.

In contrast to the narrow morphospace occupation of gliders, we recognize greater PCA morphospace occupation among humeri of saltatorial taxa and suggest this is also a biologically meaningful pattern. Saltatorial (or richochetal) taxa include species that are more bipedal (e.g., kangaroo rat, jerboas; Nowak 1999), and others that use their forelimbs during saltatorial locomotion (e.g., lagomorphs; Nowak 1999); the latter results in locomotion more similar to cursorial than to bipedal saltatorial taxa (Hildebrand 1988; Polly 2007). Although there are morphologies more characteristic of saltatorial taxa (e.g., narrow distal humerus, deep and constricted trochlea; i.e., Polly 2007), our broad sampling of saltatorial taxa may be introducing enough noise into the system such that we do expect saltatorial taxa to plot near one another in this morphospace (e.g., bipedal, saltatorial *Dipodomys* actually plots nearest semiaquatic *Ondatra* for PC1–3 and is classified as fossorial in the LDA; Figs. S3.10–11; Table S3.23). Rather, we expect saltatorial taxa to be using their forelimbs for other activities (i.e., food manipulation, digging; Hildebrand et al. 1985; Chen and Wilson 2015), and these species may be better categorized for the purpose of this study within a locomotor group whose humerus function is nearest to their own. This pattern was also detected in the whole skeletal analysis of Chen and Wilson (2015).

Semiaquatic species also occupy greater regions of the PCA (and to a lesser extent LDA) morphospaces than other locomotor groups, which we suggest this is a combination of phylogenetic effects and functional differences. Although the rodent and afrosoricid taxa group separately on PC2, afrosoricid taxa themselves group far from one another on PC1 (Figs. 3.20–21). These afrosoricid taxa, the aquatic or web-footed tenrec (*Limnogale mergulus*) and giant otter shrew (*Potamogale velox*; Table 3.4), differ greatly from one another in body size (accounted for in our PCA), but also have different body dimensions and habits. The giant otter shrew is a larger-bodied (300-950 g) animal that superficially resembles the river otter (*Lontra canadensis*) in body proportions, and inhabits slow-moving waters (Nowak 1999). In contrast, the web-footed tenrec is an order of magnitude smaller (40–60 g), with a body shape nearest to other tenrecs (e.g., *Microgale* sp.), and hunts at night in fast-moving streams and spends the day in shallow burrows (Nowak 1999). These two animals, although both semiaquatic tenrecs, swim differently (i.e., via tail propulsion in *Potamogale*, and tail plus hind limb propulsion in *Limnogale*), and additionally use their humeri for other functions (i.e., burrowing in *Limogale*; Nowak 1999). In fact, in our results, *Limnogale* plots nearer to the semifosorial tenrecs than to *Potamogale* (Fig. 3.22), is classified as fossorial in our LDA (Table S3.23), and has a relatively wide distal humeri and large entepicondyle. This is one example of how the use of locomotor categories with substantial functional diversity can reduce the signal-to-noise ratio. However, we argue that the inclusion of this functional diversity better accounts for potential functional diversity in fossil taxa (Chen and Wilson 2015).

We also find examples of similar morphologies mapping to different functions in our analysis of humeri shape and locomotor function. For example, a large entepicondyle is

suggestive of strong wrist and digital flexors, indicative of grasping muscles for use in either climbing or digging (e.g., Taylor 1974; Szalay and Sargis 2001; Salton and Sargis 2008; Flores 2009). We would therefore expect arboreal and fossorial taxa to group near one another in our PCA and LDA morphospaces, and specifically to fall near the extreme of PC1 for mediolaterally wide specimens with large entepicondyles. Although our LDA results are consistent with this prediction (i.e., arboreal, fossorial, and semifossorial specimens have similar morphologies; Table S3.24), and we find considerable overlap between these groups and a gradient from fossorial and semifossorial to arboreal taxa (Fig. 3.21C), it is actually semifossorial taxa that are the most extreme on PC1 and have the mediolaterally widest distal humeri (Fig. 3.21C). Further complicating the signal, in both datasets, fossorial and arboreal taxa separate fairly well on PC2, with semifossorial taxa generally in between (Figs. 3.22–23). Our results suggest arboreal and fossorial taxa could be morphologically and functionally different with respect to patterns of the distal humeri; however, our quantitative study excludes other functionally informative areas of the humerus, i.e., muscle attachments sites on the proximal shaft (e.g., Hildebrand 1988; Polly 2007; Salton and Sargis 2008; Samuels and Van Valkenburgh 2008; Chen and Wilson 2015).

5.6. Functional implications for select morphotypes

We combined the results of 2D GM with our morphotype descriptions to further interpret the functional morphology of the EuB, EuC, and EuD morphotypes, and place these in the context of what is known about K-Pg mammalian postcrania from this area.

***EuB* (the small Lancian "insectivoran")—**The large, medially extensive entepicondyle of this morphotype is associated with well-developed wrist- and digit flexors in extant taxa and implies more powerful grasping, as seen in both climbers and diggers (Taylor 1974; Hildebrand 1985; Szalay and Sargis 2001; Sargis 2002; Salton and Sargis 2008; Flores 2009). We hypothesize the entepicondylar distal rugosity specifically is also for muscle attachment, although we could not find a description of this feature or its function in the literature, and could not validate this in extant comparative specimens. The high PC2 score, bulbous articular surfaces, and spherical capitulum of EuB imply that the animal was capable of more flexible, multi-axial movement at the elbow joint, rather than movement restricted to flexion/extension (Argot 2001; Szalay and Sargis 2001; Sargis 2002; Salton and Sargis 2008; Fabre et al. 2015). The shallow olecranon and radial fossae of EuB indicate habitual, but less extreme flexion (Penkrot et al. 2008; Salton and Sargis 2008; Flores 2009). The functional morphology of EuB therefore implies that the elbow had a habitually flexed stance, had a wide range of motion, and conferred rotational and grasping abilities, consistent with either fossorial or arboreal locomotion. This prediction is consistent with LDA results, which rank locomotor predictions for this specimen as overwhelmingly arboreal (99%), followed by distantly semifossorial (0.44%; Table S3.24). In the 2D GM of the distal humerus, EuB plots near semifossorial taxa, especially *Oryzorictes* sp. and *Hemicentetes semispinosus* (PCs 1–3; Figs. 3.21–22). For PC2 and PC3 specifically, EuB plots nearest to arboreal taxa (i.e., rodent *Sciurus carolinensis* and afrosoricid *Dendrohyrax arboreus*, respectively), and to a fossorial rodent (*Aplodontia rufa*; Fig. 3.22). In anterior and posterior views, EuB most closely resembles *Oryzorictes* sp.

among all extant taxa in our dataset. Taken together, we infer that EuB had strong grasping and rotational abilities that were used in either digging and/or climbing activities.

***EuC* (BCA–Pu1 small archaic ungulate)—**The very deep dorsoepitrochlear fossa of this morphotype is possibly the site of attachment for a ligament binding the humerus with the ulna (cf. medial ligament of Szalay et al. 1975; Szalay and Dagosto 1980); this might suggest a well-developed flexor carpi ulnaris, which acts in flexion/adduction of the hand (Argot 2013). The deep and perforated olecranon fossa, much deeper than in EuB, enables major extension of the forearm and suggests a more upright forelimb posture (Penkrot et al. 2008; Flores 2009). The large entepicondyle of EuC is more robust and proximally extensive than in EuB or EuD, reflecting greater area for muscle attachment, namely for wrist and digit flexors (Taylor 1974; Hildebrand 1985; Szalay and Sargis 2001; Sargis 2002; Salton and Sargis 2008; Flores 2009). Within our 2D GM analysis, EuC plots high on PC2 and has bulbous distal articular surfaces; it also plots low on PC1, but higher than any of our other fossil specimens. Specimens nearest to this morphotype in the PCA morphospace include scansorial and terrestrial taxa (PC1 and PC2), and terrestrial, arboreal, and gliding taxa (PC2 and PC3). The LDA prediction for this specimen is semifossorial followed by arboreal locomotion (61% and 27%, respectively; Table S3.24). We interpret the arboreal, scansorial, and terrestrial PCA predictions, and LDA semifossorial and arboreal predictions, to suggest potential general locomotor activities with strong grasping (i.e., digging and climbing) muscles and an upright posture. We suggest this morphotype was able to exploit many available resources niche in its environment, similar to many extant small mammals (e.g., squirrels; Jenkins 1974; Jenkins and Parrington 1976).

***EuD* (BCA "insectivoran")—**The large entepicondyle of this morphotype might imply that this taxon, like EuB and EuC, had powerful grasping muscles (Taylor 1974; Szalay and Dagosto 1980; Hildebrand 1985; Szalay and Sargis 2001; Salton and Sargis 2008; Flores 2009); however, the entepicondyle of EuD is not as medially extensive as in EuB or as robust as in EuC. The deep radial and olecranon fossae of EuD would enable substantial flexion and extension of the forelimbs (Penkrot et al. 2008; Flores 2009). The lateral extension of the capitulum, where the supinator brevis muscle originates, suggests habitual supination of the manus of EuD (the supinator brevis inserts on the proximal anterior radius; Flores 2009). 2D GM results place the wide distal humerus of EuD near the extreme of PC1, and almost more extreme than any extant taxon. The morphology of EuD most closely resembles that of semifossorial afrosoricids and fossorial cingulatans, and fossorial, semifossorial, and saltatorial rodents (Fig. 3.20C,D). These specimens are all characterized by medially extensive entepicondyles, which may also suggest digging activities among saltatorial rodents. LDA predictions for this morphotype differ between specimens, with one specimen suggestive of fossorial followed by semifossorial locomotion (93% and 6%, respectively; Table S3.24), and the other specimen suggestive of semifossorial locomotion (51%) followed by arboreal and fossorial locomotion (25% and 24%, respectively; Table S3.24). The combined qualitative and quantitative assessments of functional morphology imply EuD had a mobile elbow joint, capable of frequent supination and/or powerful grasping of the hand, and likely was fossorial or semifossorial.

Below, we comment on a few other morphotypes, although they were not preserved well enough to be included in our quantitative analyses. First, the six multituberculate humerus morphotypes, which are remarkably similar to each other in morphology, are

consistent with arboreal locomotor capabilities (e.g., substantial pronation/supination abilities at the radial condyle, large muscle attachment areas on entepicondyle for grasping muscles; Krause and Jenkins 1983). Second, morphotype EuA shares many features with primates that imply an arboreal mode of locomotion; e.g., a wide entepicondyle for attachment of strong grasping muscles, spherical capitulum allowing forearm rotation, and weight-bearing humeroulnar joint (e.g., Szalay et al. 1975; Szalay and Dagosto 1980; Szalay and Lucas 1996; Bloch et al. 2007; Boyer et al. 2010). We interpret this late Puercan (Pu3) ?plesiadapiform primate as a predominantly arboreal taxon, a finding which is also supported by recent analyses of tarsal material from the same assemblage and that was attributed to the plesiadapiform *Purgatorius* (Chester et al. 2015). We also attributed a partial proximal femur from this same locality to the same taxon (DeBey and Wilson 2014). Finally, the large archaic ungulate (EuE) has a humeroulnar joint that does not restrict rotational movement on the posterior trochlea and has broad epicondyles, unlike those found in a cursorial mammal (e.g., Rose 1987; Polly 2007; Argot 2010). The distal humerus morphology of EuE is also similar to that of *Arctocyon primaevus*, which has been interpreted as arboreal/scansorial (Argot 2013). Thus, we tentatively interpret EuE as a Pu3 arboreal/scansorial archaic ungulate.

The functional and locomotor inferences of our humerus morphotypes expand our understanding of the ecologies of K-Pg mammals. Acknowledging the limitations of our data, our working hypotheses are that the Lancian eutherian represented by the EuB morphotype was a semifossorial and/or arboreal taxon; the early Puercan archaic ungulate represented by EuC (previously attributed to ?*Protungulatum*) had a more generalized locomotor mode; and the BCA eutherian represented by EuD (previously attributed to

?*Procerberus*) was a small-bodied, semifossorial or fossorial mammal. These hypotheses complement previous postcranial research suggestive of greater locomotor breadth among K-Pg mammals; for example, semiaquatic habit in the Cretaceous metatherian *Didelphodon* (Longrich 2005; Borths and Hunter 2008), saltatorial or arboreal locomotor mode among Lancian–Pu3 multituberculates (Krause and Jenkins 1983; Kielan-Jaworowska and Gambaryan 1994; DeBey and Wilson 2014), fossoriality in Pu3 multituberculates (DeBey and Wilson 2014), terrestrial locomotor mode in some large Pu3 eutherians (i.e., Matthew 1937; Schoch 1986), and arboreal habits among Pu3 plesiadapiforms (DeBey and Wilson 2014; Chester et al. 2015). Moreover, the arboreal/scansorial interpretations for other Pu3 morphotypes (EuA, EuE) are consistent with a habitat shift from a more open Cretaceous landscape to a more closed, wet, and forested Paleocene landscape (e.g., Fastovsky 1987; Clemens 2002; Wilf et al. 2003; Nichols and Johnson 2008).

6. Conclusion

Recent postcrania research on latest Cretaceous and early Paleogene mammals of North America has allowed us to track the rise of taxonomic, morphological, and ecological diversity associated with the early Paleogene radiation of placental mammals. This has laid a framework for testing ecological components of mass extinction and recovery dynamics beyond the traditional focus on dental fossils. Our study represents the first attempt to quantitatively map morphological and ecomorphological diversity of humeri onto the critical time frame of the Cretaceous-Paleogene mass extinction. Functional results increase ecomorphological diversity beyond that previously recognized among K-Pg postcrania. Future work on additional specimens and other functionally informative elements (e.g., tarsals) will improve our ability to test ecological hypotheses of extinction and recovery and refine our understanding of locomotor patterns among K-Pg mammals.

7. Acknowledgements

We thank the many individuals whose fieldwork and curation efforts have made this work possible, specifically J. D. Archibald, W. A. Clemens, D. Lofgren, and the many UCMP field crews who collected the majority of these specimens, and the many people who sorted, identified, and curated them for study, especially S. Zack and T. Stidham. For the more recently collected material, we thank W. A. Clemens, D. DeMar, Jr., S. Smith, S. Wang, M. Washington, and UW field crews. We thank P. Holroyd and W. A. Clemens (UCMP), and J. Bradley, R. Eng, and C. Sidor (UWBM) for access to collections. We are grateful for special use permits from the United States Bureau of Land Management, the Charles M. Russell National Wildlife Refuge, the Montana Department of Natural Resources and Conservation, and for access to private lands granted by the Engdahl, McKeever, Twitchell, Olsen and Strohs families. We are especially grateful to L. Heilicher for specimen photography, to S. Chester for CT scans of UCMP 153100, and to O. Campos for 3D printing. We thank A. Brannick, J. Calede, M. Chen, S. Chester, W. A. Clemens, D. DeBey, D. DeMar Jr., E. Nesbitt, C. Sidor, S. Smith, and C. Strömberg for valuable suggestions, discussion, and comments on earlier drafts of this manuscript. Funding for this project was provided to LBD by the National Science Foundation Gradate Research Fellowship, Charlotte Cornell Crary Distinguished Teaching Fellowship, Henry and Frances Decker Fellowship, Evolving Earth Foundation, University of California Museum of Paleontology Doris O. and Samuel P. Welles Fund, Montana Bureau of Land Management, and the University of Washington Graduate and Professional Student Senate. Funding for this project was provided to LBD and GPW by the University of Washington Department of Biology and by N. Myhrvold.

References Cited

Adams, D.C. and E. Otarola-Castillo. 2013. Geomorph: an R package for the collection and analysis of geometric morphometric shape data. Methods in Ecology and Evolution 4: 393–399.

Alroy, J. 1999. The fossil record of North American mammals: evidence for a Paleocene evolutionary radiation. Systematic Biology 48: 107–118.

Archibald, J.D. 1982. A study of Mammalia and geology across the Cretaceous-Tertiary boundary in Garfield County, Montana. University of California Publications in Geological Sciences 122: 1–286.

Archibald, J.D. 1983. Structure of the K-T mammal radiation in North America: speculations on turnover rates and trophic structure. Acta Palaeontologica Polonica 28: 7–17.

Archibald, J.D. and W.A. Clemens. 1984, Mammal evolution near the Cretaceous-Tertiary boundary, in: W.A. Berggren and J.A. Van Couvering (Eds.), Catastrophes in Earth History: the New Uniformitarianism. Princeton University Press, Princeton, pp. 339–371.

Argot, C. 2001. Functional-adaptive anatomy of the forelimb in the Didelphidae, and the paleobiology of the Paleocene marsupials *Mayulestes ferox* and *Pucadelphys andinus*. Journal of Morphology 247: 51–79.

Argot, C. 2010. Morphofunctional analysis of the postcranium of *Amphicyon major* (Mammalia, Carnivora, Amphicyonidae) from the Miocene of Sansan (Gers, France) compared to three extant carnivores: *Ursus arctos*, *Panthera leo*, and *Canis lupus*. Geodiversitas 32: 65–106.

Argot, C. 2013. Postcranial analysis of a Carnivoran-like archaic ungulate: the case of *Arctocyon primaevus* (Arctocyonidae, Mammalia) from the Late Paleocene of France. Journal of Mammalian Evolution 20: 83–114.

Bassarova, M., C.M. Janis, and M. Archer. 2009. The calcaneum—on the heels of marsupial locomotion. Journal of Mammalian Evolution 16:1–23.

Bloch, J.I., M.T. Silcox, D.M. Boyer, and E.J. Sargis. 2007. New Paleocene skeletons and the relationship of plesiadapiforms to crown-clade primates. Proceedings of the National Academy of Sciences 104: 1159–1164.

Bookstein, F.L. 1991. Morphometric Tools for Landmark Data: Geometry and Biology. Cambridge University Press, Cambridge.

Borths, M. and J. Hunter. 2008. Gimme shelter? Locomotor trends and mammalian survivorship at the K-Pg boundary. Journal of Vertebrate Paleontology 28: 3A.

Boyer, D.M. and E.R. Seiffert. 2013. Patterns of astragalar fibular facet orientation in extant and fossil primates and their evolutionary implications. American Journal of Physical Anthropology 151: 420–47.

Boyer, D.M., G.V.R. Prasad, D.W. Krause, M. Godinot, A. Goswami, O. Verma, and J.J. Flynn. 2010. New postcrania of *Deccanolestes* from the Late Cretaceous of India and their bearing on the evolutionary and biogeographic history of euarchontan mammals. Naturwissenschaften 97: 365–77.

Brown, J.C. and D.W. Yalden. 1973. Limbs and locomotion of terrestrial mammals. Mammal Review 3: 107–134.

Cardini, A. 2014. Missing the third dimension in geometric morphometrics: How to assess if 2D images really are a good proxy for 3D Structures? Hystrix, the Italian Journal of Mammalogy 25: 73–81.

Cardini, A., K. Seetah, and G. Barker. 2015. How many specimens do I need? Sampling error in geometric morphometrics: testing the sensitivity of means and variances in simple randomized selection experiments. Zoomorphology 134: 149–163.

Chen, M. and G.P. Wilson. 2015. A multivariate approach to infer locomotor modes in Mesozoic mammals. Paleobiology 41: 280–312.

Chester, S.G.B., E.J. Sargis, F.S. Szalay, J.D. Archibald, and A.O. Averianov. 2010. Mammalian distal humeri from the Late Cretaceous of Uzbekistan. Acta Palaeontologica Polonica 55: 199–211.

Chester, S.G.B., E.J. Sargis, F.S. Szalay, J.D. Archibald, and A.O. Averianov. 2012. Therian femora from the Late Cretaceous of Uzbekistan. Acta Palaeontologica Polonica 57: 53–64.

Chester, S.G.B., J.I. Bloch, D.M. Boyer, and W.A. Clemens. 2015. Oldest known euarchontan tarsals and affinities of Paleocene *Purgatorius* to primates. Proceedings of the National Academy of Sciences 112: 1487–1492.

Cifelli, R.L., J.J. Eberle, D.L. Lofgren, J.A. Lillegraven, and W.A. Clemens. 2004. Mammalian biochronology of the latest Cretaceous, in: M.O. Woodburne (Ed.), Late Cretaceous and Cenozoic mammals of North America: biostratigraphy and geochronology. Columbia University Press, New York, pp. 21-42.

Clemens, W.A. 1963. Fossil mammals of the type Lance formation Wyoming; Part I, introduction and Multituberculata. University of California Publications in Geological Sciences 48: 1–105.

Clemens, W.A. 1964. Fossil mammals of the type Lance Formation, Wyoming, Part I. Introduction and Multituberculata. University of California Publications in Geological Sciences 48: 1–105.

Clemens, W.A. 2002. Evolution of the mammalian fauna across the Cretaceous-Tertiary boundary in northeastern Montana and other areas of the Western Interior, in: J.H. Hartman, K.R. Johnson, and D.J. Nichols (Eds.), The Hell Creek Formation and the Cretaceous-Tertiary Boundary in the Northern Great Plains: An Integrated Continental Record of the End of the Cretaceous. Geological Society of America Special Paper 361, Boulder, pp. 217–245.

Clemens, W.A. 2004. *Purgatorius* (Plesiadapiformes, Primates?, Mammalia), a Paleocene immigrant into northeastern Montana: stratigraphic occurrences and incisor proportions. Bulletin of Carnegie Museum of Natural History 36: 3–13.

Clemens, W.A. 2011. *Eoconodon* ("Triisodontidae," Mammalia) From the Early Paleocene (Puercan) of Northeastern Montana, U.S.A. Palaeontologia Electronica 22: 1–22.

Clemens, W.A. 2015. *Prodiacodon crustulum* (Leptictidae, Mammalia) from the Tullock Member of the Fort Union Formation, Garfield and McCone counties, Montana, USA. PaleoBios 32: 1–17.

Clemens, W.A. and Kielan-Jaworowska, Z., 1979. Multituberculata, in: J.A. Lillegraven, Z. Kielan-Jaworowska, and W.A. Clemens (Eds.), Mesozoic Mammals: the First Two-Thirds of Mammalian History, University of California Press, Berkeley, pp. 99–149.

Cope, E.D. 1884. The Tertiary Marsupialia. American Naturalist 18: 686–97.

DeBey, L.B. and G.P. Wilson. 2014. Mammalian femora across the Cretaceous-Paleogene boundary in eastern Montana. Cretaceous Research 51: 361–85.

Deischl, D.G. 1964. The postcranial anatomy of Cretaceous multituberculate mammals, unpublished M.Sc. thesis, University of Minnesota, Minneapolis.

Delciellos, A.C. and M.V. Vieira. 2006. Arboreal walking performance in seven didelphid marsupials as an aspect of their fundamental niche. Austral Ecology 31: 449–457.

Egi, N. 2001. Body mass estimates in extinct mammals from limb bone dimensions: the case of North American Hyaenodontids. Palaeontology 44: 497–528.

Elissamburu, A. and S.F. Vizcano. 2004. Limb proportions and adaptations in caviomorph rodents (Rodentia: Caviomorpha). Journal of Zoology 262: 145–159.

Endo, H., T. Yonezawa, F. Rakotondraparany, M. Sasaki, and M. Hasegawa. 2006. The adaptational strategies of the hindlimb muscles in the Tenrecidae species including the aquatic web-footed tenrec (*Limnogale mergulus*). Annals of Anatomy 188: 383–390.

Fabre, A.-C., M.J. Salesa, R. Cornette, M. Antón, J. Morales, and S. Peigné. 2015. Quantitative inferences on the locomotor behaviour of extinct species applied to *Simocyon batalleri* (Ailuridae, Late Miocene, Spain). The Science of Nature 102: 30.

Fastovsky, D.E. 1987. Paleoenvironments of vertebrate-bearing strata during the Cretaceous-Paleogene transition, eastern Montana and western North Dakota. PALAIOS 2: 282–295.

Flores, D.A. 2009. Phylogenetic analyses of postcranial skeletal morphology in didelphid marsupials. Bulletin of the American Museum of Natural History 320: 1–81.

Fox, R.C. 1989. The Wounded Knee local fauna and mammalian evolution near the Cretaceous-Tertiary boundary, Saskatchewan, Canada. Palaeontographica, Abteilung A. 208: 11–59.

Fox, R.C. 2005. Microcosmodontid multituberculates (Allotheria, Mammalia) from the Paleocene and Late Cretaceous of western Canada. Palaeontographica Canadiana 23: 1–109.

Gambaryan, P.P. and Z. Kielan-Jaworowska. 1997. Sprawling versus parasagittal stance in multituberculate mammals. Acta Palaeontologica Polonica 42: 12–44.

Gidley, J.W. 1909. Notes on the fossil mammalian genus *Ptilodus*, with descriptions of new species. Proceedings of the United States National Museum 36: 611–627.

Gingerich, P.D. 2003. Land-to-sea transition in early whales: evolution of Eocene Archaeoceti (Cetacea) in relation to skeletal proportions and locomotion of living semiaquatic mammals. Paleobiology 29:429–454.

Gordon, C.L. 2003. A first look at estimating body size in dentally conservative marsupials. Journal of Mammalian Evolution 10: 1–21.

Gunz, P. and P. Mitteroecker. 2013. Semilandmarks: a method for quantifying curves and surfaces. Hystrix, the Italian Journal of Mammalogy 24: 103–9.

Heinrich, R. and P. Houde. 2006. Postcranial anatomy of *Viverravus* (Mammalia, Carnivora) and implications for substrate use in basal Carnivora. Journal of Vertebrate Paleontology 26: 422–435

Hildebrand, M. 1985. Digging in quadrupeds, in: M. Hildebrand, D.M. Bramble, K.F. Liem, and D.B. Wake (Eds.), Functional Vertebrate Morphology. Harvard University Press, Cambridge, pp. 89–109.

Hildebrand, M. 1988. Analysis of Vertebrate Structure. Wiley, New York.

Hildebrand, M., D.M. Bramble, K.F. Liem, and D.B. Wake. 1985. Functional Vertebrate Morphology. Harvard University Press, Cambridge.

Hooker, J.J. 2014. New postcranial bones of the extinct mammalian family Nyctitheriidae (Paleogene, UK): primitive euarchontans with scansorial locomotion. Palaeontologia Electronica: 1–82.

Horovitz, I. 2003. Postcranial skeleton of *Ukhaatherium nessovi* (Eutheria, Mammalia) from the Late Cretaceous of Mongolia. Journal of Vertebrate Paleontology 23: 857–68.

Howell, A.B. 1930. Aquatic Mammals. Charles C. Thomas, Springfield, Illinois.

Hunter, J.P., J.H. Hartman, and D.W. Krause. 1997. Mammals and mollusks across the Cretaceous-Tertiary boundary from Makoshika State Park and vicinity (Williston Basin), Montana. University of Wyoming Contributions to Geology 32: 61–114.

Iwaniuk, A.N., S.M. Pellis, and I.Q. Whishaw. 1999. The relationship between forelimb morphology and behavior in North American carnivores (Carnivora). Canadian Journal of Zoology 77: 1064–1074.

Janis, C.M. and B. Figueirido. 2014. Forelimb anatomy and the discrimination of the predatory behavior of carnivorous mammals: the thylacine as a case study. Journal of Morphology 275: 1321–1338.

Jenkins, F.A., Jr. 1973. The functional anatomy and evolution of the mammalian humero-ulnar articulation. American Journal of Anatomy 137: 281–98.

Ji, Q., Z.-X. Luo, C.-Z. Yuan, J.R. Wible, J.-P. Zhang, and J.A. Georgi. 2002. The earliest known eutherian mammal. Nature 416: 816–822.

Kelly, T.S. 2014. Preliminary report on the mammals from Lane's Little Jaw Site Quarry: a Latest Cretaceous (earliest Puercan?) Local Fauna, Hell Creek Formation, southeastern Montana. Paludicola 10: 50–91.

Kendall, D.G. 1977. The diffusion of shape. Advances in Applied Probability 9: 428–430.

Kielan-Jaworowska, Z. and D. Dashzeveg. 1978. New Late Cretaceous mammal locality in Mongolia and a description of a new multituberculate. Acta Paleontologica Polonica 23: 115–130.

Kielan-Jaworowska, Z. and P.P. Gambaryan. 1994. Postcranial anatomy and habits of Asian multituberculate mammals. Fossils and Strata 36: 1–92.

Kielan-Jaworowska, Z. and J.H. Hurum. 2006. Limb posture in early mammals: sprawling or parasagittal. Acta Palaeontologica Polonica 51: 393–406.

Kielan-Jaworowska, Z. and T. Qi. 1990. Fossorial adaptations of a taeniolabidoid multituberculate mammal from the Eocene of China. Vertebrata PalAsiatica 28: 81–94.

Kondrashov, P.E. and S.G. Lucas. 2012. Nearly complete skeleton of *Tetraclaenodon* (Mammalia, Phenacodontidae) from the Early Paleocene of New Mexico: morpho-functional analysis. Journal of Paleontology 86: 25–43.

Körtner, G. and F. Geiser. 2000. Torpor and activity patterns in free-ranging sugar gliders *Petaurus breviceps* (Marsupialia). Oecologia 123: 350–357.

Krause, D.W. and F.A. Jenkins, Jr. 1983. The postcranial skeleton of North American multituberculates. Bulletin of the Museum of Comparative Zoology 150: 199–246.

Lackey, J.A. 1996. *Chaetodipus fallax*. Mammalian Species 517: 1–6.

Lariviére, S. 1999. *Mustela vison*. Mammalian Species 608: 1–9.

Lariviére, S. and M. Pasitschniak-Arts. 1996. *Vulpes vulpes*. Mammalian Species 537: 1–11.

LeCain, R., W.C. Clyde, G.P. Wilson, and J. Riedel. 2014. Magnetostratigraphy of the Hell Creek and lower Fort Union Formations in northeastern Montana, in: G.P. Wilson, W.A. Clemens, J.R. Horner, and J.H. Hartman (Eds.), Through the End of the Cretaceous in the Type Locality of the Hell Creek Formation in Montana and Adjacent Areas. Geological Society of America Special Paper 503, Boulder. pp. 137–147.

Lillegraven, J.A. 1972. Preliminary report on Late Cretaceous mammals from the El Gallo Formation, Baja de California, Mexico, in: W.A. Clemens, R.C. Fox, and D.P. Whistler (Eds.), Contributions in Science, 1–11. Los Angeles County Natural History Museum, Los Angeles.

Lofgren, D.L. 1995. The Bug Creek Problem and the Cretaceous-Tertiary transition at McGuire Creek, Montana. University of California Publications in Geological Sciences 140: 1–185.

Lofgren, D.L., J.A. Lillegraven, W.A. Clemens, P.D. Gingerich, and T.E. Williamson. 2004. Paleocene biochronology: The Puercan through Clarkforkian land mammal ages, in: M.O. Woodburne (Ed.), Late Cretaceous and Cenozoic Mammals of North America: Biostratigraphy and Geochronology. Columbia University Press, New York, pp. 43–105.

Longrich, N. 2005. Aquatic specialization in marsupials from the Late Cretaceous of North America. Cranbrook Institiute of Science Miscellaneous Publications (Evolution of Aquatic Tetrapods Convention Abstracts) V 1: 53.

Luo, Z.-X. 1991. Variability of dental morphology and the relationships of the earliest arctocyonid species. Journal of Vertebrate Paleontology 11: 452–471.

Luo, Z.-X. 2007. Transformation and diversification in early mammal evolution. Nature 450: 1011–1019.

Luo, Z.-X., Q. Ji, J.R. Wible, and C.-X. Yuan. 2003. An Early Cretaceous tribosphenic mammal and metatherian evolution. Science 302: 1934–1940.

Maas, M.C. and D.W. Krause. 1994. Mammalian turnover and community structure of the Paleocene of North America. Historical Biology 8: 91–128.

Marsh, O.C. 1889. Discovery of Cretaceous Mammalia. American Journal of Science 38: 81–92.

Marshall, L.G., C. de Muizon, and D. Sigogneau-Russell. 1995. *Pucadelphys andinus* (Marsupialia, Mammalia) from the Early Paleocene of Bolivia. Mémoires du Muséum National D'Histoire Naturelle 165: 91–164.

Matthew, W.D. 1937. Paleocene faunas of the San Juan Basin, New Mexico. Transactions of the American Philosophical Society 30: 1–523.

Meachen-Samuels, J. 2010. Comparative scaling of humeral cross-sections of felids and canids using radiographic images. Journal of Mammalian Evolution 17: 193–209.

Milne, N., S.F. Vizcaíno, and J.C. Fernicola. 2009. A 3D geometric morphometric analysis of digging ability in the extant and fossil cingulate humerus. Journal of Zoology 278: 48–56.

Mitteroecker, P. and F. Bookstein. 2011. Linear discrimination, ordination, and the visualization of selection gradients in modern morphometrics. Evolutionary Biology 38: 100–114.

Moore, J.R., G.P. Wilson, M. Sharma, H.R. Hallock, D.R. Braman, and P. Renne. 2014. Assessing the relationships of the Hell Creek–Fort Union contact, Cretaceous-Paleogene

boundary, and Chicxulub impact ejecta horizon at the Hell Creek Formation lectostratotype, Montana, USA, in: G.P. Wilson, W.A. Clemens, J.R. Horner, and J.H. Hartman (Eds.), Through the End of the Cretaceous in the Type Locality of the Hell Creek Formation in Montana and Adjacent Areas. Geological Society of America Special Paper 503, Boulder, pp. 123–136.

Morgan, C.C. and A. Álvarez. 2013. The humerus of South American caviomorph rodents: shape, function and size in a phylogenetic context. Journal of Zoology 290: 107–16.

Muizon, C. 1998. *Mayulestes ferox*, a bohyaenoid (Metatheria, Mammalia) from the early Palaeocene of Bolivia. Phylogenetic and palaeobiologic implications. Geodiversitas 20: 19–142.

Nichols, D.J. and K.R. Johnson. 2008. Plants and the K–T Boundary. Cambridge University Press, Cambridge.

Nowak, R.M. 1999. Walker's Mammals of the World. Johns Hopkins University Press, Baltimore.

Nyakatura, J.A., M.S. Fischer, and M. Schmidt. 2008. Gait parameter adjustments of cotton-top tamarins (*Saguinus oedipus*, Callitrichidae) to locomotion on inclined arboreal substrates. American Journal of Physical Anthropology 135: 13–26.

O'Leary, M.A., J.I. Bloch, J.J. Flynn, T.J. Gaudin, A. Giallombardo, N.P. Giannini, S.L. Goldberg, B.P. Kraatz, Z.-X. Luo, J. Meng, X. Ni, M.J. Novacek, F.A. Perini, Z.S. Randall, G.W. Rougier, E.J. Sargis, M.T. Silcox, N.B. Simmons, M. Spaulding, P.M. Velazco, M. Weksler, J.R. Wible, and A.L. Cirranello. 2013. The placental mammal ancestor and the post-K-Pg radiation of placentals. Science 339: 662–67.

Osborn, H.F. and C. Earle. 1895. Fossil mammals of the Puerco beds. Collection of 1892. Bulletin of the American Museum of Natural History 7: 1–70.

Pasitschniak-Arts, M. and S. Lariviére. 1995. *Gulo gulo*. Mammalian Species 499: 1–10.

Penkrot, T.A., S.P. Zack, K.D. Rose, and J.I. Bloch. 2008. Postcranial morphology of *Apheliscus* and *Haplomylus* (Condylarthra, Apheliscidae): evidence for a Paleocene Holarctic origin of Macroscelidea, in: E.J. Sargis and M. Dagosto (Eds.), Mammalian Evolutionary Morphology: a Tribute to Frederick S. Szalay. Springer, Dordrecht, pp. 73-106.

Polly, P.D. 2007. Limbs in mammalian evolution, in: B.K. Hall (Ed.) Fins into Limbs: Evolution, Development, and Transformation. University of Chicago Press, Chicago, pp. 1–24.

Polly, P.D. 2008. Adaptive zones and the pinniped ankle: a 3D quantitative analysis of carnivoran tarsal evolution, in: E. Sargis and M. Dagosto (Eds.), Mammalian Evolutionary Morphology: a Tribute to Frederick S. Szalay. Springer, Dordrecht, pp. 167–196.

Polly, P.D. and N. MacLeod. 2008. Locomotion in fossil Carnivora: an application of eigensurface analysis for morphometric comparison of 3D surfaces. Palaeontologia Electronica 11: 1–13.

R Core Team. 2014. R: A language and environment for statistical computing (Version 3.1.2). R Foundation for Statistical Computing, Vienna, Austria. URL http://www.R-project.org/.

RStudio. 2012. RStudio: Integrated development environment for R (Version 0.98.1062). Boston, MA. URL http://www.rstudio.com/.

Raia, P., F. Carotenuto, F. Passaro, P. Piras, D. Fulgione, L. Werdelin, J. Saarinen, and M. Fortelius. 2012. Rapid action in the Palaeogene, the relationship between phenotypic and taxonomic diversification in Coenozoic mammals. Proceedings of the Royal Society B: Biological Sciences 280: 20122244.

Redford, K.H. and R.M. Wetzel. 1985. *Euphractus sexcinctus*. Mammalian Species 252: 1–4.

Renne, P.R., G. Balco, K.R. Ludwig, R. Mundil, and K. Min. 2011. Response to the comment by W.H. Schwartz et al. on "Joint determination of 40K decay constants and 40Ar*/40K for the Fish Canyon sanidine standard, and improved accuracy for the 40Ar/39Ar geochronology" by P.R. Renne et al. (2010). Geochimica et Cosmochimica Acta 75: 5097–5100.

Renne, P.R., A.L. Deino, F.J. Hilgen, K.F. Kuiper, D.F. Mark, W.S. Mitchell III, L.E. Morgan, R. Mundil, and J. Smit. 2013. Time scales of critical events around the Cretaceous-Paleogene boundary. Science 339: 684–687.

Rigby, J.K. Jr., 1981. A skeleton of *Gillisonchus gillianus* (Mammalia; Condylarthra) from the Early Paleocene (Puercan) Ojo Alamo Sandstone, San Juan Basin, New Mexico, with comments on the local stratigraphy of Betonnie Tsosie Wash, in: S.G. Lucas, J.K. Rigby Jr., and B.S. Kues (Eds.), Advances in San Juan Basin Paleontology. University of New Mexico Press, Albuquerque, pp. 89–126.

Robertson, D.S., M.C. McKenna, O.B. Toon, S. Hope, and J.A. Lillegraven 2004. Survival in the first hours of the Cenozoic. Geological Society of America Bulletin 116: 760–768.

Rohlf, F.J. and D. Slice. 1990. Extensions of the Procrustes method for the optimal superimposition of landmarks. Systematic Zoology 39: 40–59.

Rohlf, F.J. 2013a. tpsDIG Version 2.17. Department of Ecology and Evolution, State University of New York at Stony Brook, New-York.

Rohlf, F.J. 2013b. tpsUtil Version 1.58. Department of Ecology and Evolution, State University of New York at Stony Brook, New-York.

Rose, K.D. 1987. Climbing adaptations in the early Eocene mammal *Chriacus* and the origin of Artiodactyla. Science 236: 314–316.

Rose, K. 1999. Postcranial skeleton of Eocene Leptictidae (Mammalia), and its implications for behavior and relationships. Journal of Vertebrate Paleontology 19: 355–72.

Rowe, T. 1988. Definition, diagnosis, and origin of Mammalia. Journal of Vertebrate Paleontology 8: 241–264.

Russell, D.E. 1964. Les mammifères paléocènes d'Europe. Mémoires du Muséum National D'Histoire Naturelle, Série C. Sciences de la Terre 13: 1–324.

Sahni, A. 1972. The vertebrate fauna of the Judith River Formation, Montana. Bulletin of the American Museum of Natural History 147: 323–412.

Salton, J.A., and E.J. Sargis. 2008. Evolutionary morphology of the Tenrecoidea (Mammalia) forelimb skeleton, in: E.J. Sargis and M. Dagosto (Eds.), Mammalian Evolutionary Morphology: a Tribute to Frederick S. Szalay. Springer, Dordrecht, pp. 51–71.

Samuels, J.X. and B. Van Valkenburgh. 2008. Skeletal indicators of locomotor adaptations in living and extinct rodents. Journal of Morphology 269: 1387–1411.

Sargis, E.J. 2002. Functional morphology of the hindlimb of tupaiids (Mammalia, Scandentia) and its phylogenetic implications. Journal of Morphology 254: 149–185.

Schoch, R.M. 1986. Systematics, functional morphology and macroevolution of the extinct mammalian order Taeniodonta. Peabody Museum of Natural History, Yale University Bulletin 42: 1–307.

Schutz, H., and R.P. Guralnick. 2007. Postcranial element shape and function: assessing locomotor mode in extant and extinct mustelid carnivorans. Zoological Journal of the Linnean Society 150: 895–914.

Simpson, G.G. 1935. The Tiffany Fauna, Upper Paleocene II.–Structure and relationships of *Plesiadapis*. American Museum Novitates 816: 1–30.

Sloan, R.E. and L. Van Valen. 1965. Cretaceous mammals from Montana. Science 148: 220–227.

Smith, F.A., A.G. Boyer, J.H. Brown, D.P. Costa, T. Dayan, S.K.M. Ernest, A.R. Evans, M. Fortelius, J.L. Gittleman, M.J. Hamilton, L.E. Harding, K. Lintulaakso, S.K. Lyons, C. McCain, J.G. Okie, J.J. Saarinen, R.M. Sibly, P.R. Stephens, J. Theodor, and M.D. Uhen. 2010. The evolution of maximum body size of terrestrial mammals. Science 330: 1216–1219.

Smith, J.M. and R.J.G. Savage 1956. Locomotor adaptations in mammals. Zoological Journal of the Linnean Society 42: 603–622.

Smith, M.J. 1973. *Petaurus breviceps*. Mammalian Species 30:1–5.

Sprain, C.J., P.R. Renne, G.P. Wilson, and W.A. Clemens. 2014. High-resolution chronostratigraphy of the terrestrial Cretaceous-Paleogene transition and recovery interval in the Hell Creek region, Montana. Geological Society of America Bulletin. 127: 393–409.

Standhardt, B.R. 1986. Vertebrate paleontology of the Cretaceous/Tertiary transition of Big Bend National Park, Texas, Ph.D. dissertation. Louisiana State University and Agricultural and Mechanical College, Baton Rouge.

Steiner-Souza, F., T.R.O. De Freitas, and P. Cordeiro-Estrela. 2010. Inferring adaptation within shape diversity of the humerus of subterranean rodent *Ctenomys*. Biological Journal of the Linnean Society 100: 353–367.

Stucky, R.K. 1990. Evolution of land mammal diversity in North America during the Cenozoic. Current Mammalogy 2: 375–432.

Swisher, C.C., III, L. Dingus, and R.F. Butler. 1993. 40Ar/39Ar dating and magnetostratigraphic correlation of the terrestrial Cretaceous-Paleogene boundary and Puercan mammal age, Hell Creek–Tullock formations, eastern Montana. Canadian Journal of Earth Sciences 30: 1981–1996.

Szalay, F.S. 1994. Evolutionary History of the Marsupials and an Analysis of Osteological Characters. Cambridge University Press, New York.

Szalay, F.S. and M. Dagosto. 1980. Locomotor adaptations as reflected on the humerus of Paleogene primates. Folia Primatologica 34: 1–45.

Szalay, F.S. and R.L. Decker. 1974. Origins, evolution, and function of the tarsus in Late Cretaceous Eutheria and Paleocene primates, in: F. A. Jenkins Jr. (Ed.), Primate Locomotion. Academic Press, Inc., New York, pp. 223–259.

Szalay, F.S. and S.G. Lucas. 1996. The postcranial morphology of Paleocene *Chriacus* and *Mixodectes* and the phylogenetic relationships of archontan mammals. New Mexico Museum of Natural History and Science Bulletin 7: 1–47.

Szalay, F.S. and E.J. Sargis, 2001. Model-based analysis of postcranial osteology of marsupials from the Palaeocene of Itaborai (Brazil) and the phylogenetics and biogeography of Metatheria. Geodiversitas 23: 139–302.

Szalay, F.S. and B.A. Trofimov. 1996. The Mongolian Late Cretaceous *Asiatherium*, and the early phylogeny and paleobiogeography of Metatheria. Journal of Vertebrate Paleontology 16: 474–509.

Szalay, F.S., I. Tattersall, and R.L. Decker. 1975. Phylogenetic relationships of Plesiadapis-postcranial evidence. Contributions to Primatology 5: 136–166.

Taylor, M.E. 1974. The functional anatomy of the forelimb of some African Viverridae (Carnivora). Journal of Morphology 143: 307–336.

van Staaden, M.J. 1994. *Suricata suricatta*. Mammalian Species 483:1–8.

Van Valen, L.M. 1978. The beginning of the Age of Mammals. Evolutionary Theory 4: 45–80.

Van Valkenburgh, B. 1987. Skeletal indicators of locomotor behavior in living and extinct carnivores. Journal of Vertebrate Paleontology 7: 162–82.

Venables, W.N. and B.D. Ripley. 2002. Modern Applied Statistics with S. Fourth Edition. Springer, New York.

Wade-Smith, J. and B.J. Verts. 1982. *Mephitis mephitis*. Mammalian Species 173:1–7.

Warburton, N.M., K.J. Harvey, G.J. Prideaux, and J.E. O'Shea. 2011. Functional morphology of the forelimb of living and extinct tree-kangaroos (Marsupialia: Macropodidae). Journal of Morphology 272: 1230–44.

Weil, A. and D.W. Krause. 2008. Multituberculata, in: C.M. Janis, G.F. Gunnell, and M.D. Uhen (Eds.) Evolution of Tertiary Mammals of North America Vol. 2. Cambridge University Press, Cambridge, pp. 19–38.

Wilf, P., K.R. Johnson, and B.T. Huber. 2003. Correlated terrestrial and marine evidence for global climate changes before mass extinction at the Cretaceous–Paleogene boundary. Proceedings of the National Academy of Sciences: 599–604.

Wilson, G.P. 2004. A quantitative assessment of evolutionary and ecological change in mammalian faunas leading up to and across the Cretaceous-Tertiary boundary in northeastern Montana. Unpublished Ph.D. dissertation, University of California Berkeley, Berkeley.

Wilson, G.P. 2005. Mammalian faunal dynamics during the last 1.8 million years of the Cretaceous in Garfield County, Montana. Journal of Mammalian Evolution 12: 53–75.

Wilson, G.P. 2013. Mammals across the K/Pg boundary in northeastern Montana, U.S.A.: dental morphology and body-size patterns reveal extinction selectivity and immigrant fueled ecospace filling. Paleobiology 39: 429–469.

Wilson, G.P. 2014. Mammalian extinction, survival, and recovery dynamics across the Cretaceous-Paleogene boundary in northeastern Montana, in: G.P. Wilson, W.A. Clemens, J.R. Horner, and J.H. Hartman (Eds.), Through the End of the Cretaceous in the Type Locality of the Hell Creek Formation in Montana and Adjacent Areas. Geological Society of America Special Paper 503, Boulder, pp. 365–392.

Wilson, G.P., A.R. Evans, I.J. Corfe, P.D. Smits, M. Fortelius, and J. Jernvall. 2012. Adaptive radiation of multituberculate mammals before the extinction of dinosaurs. Nature 483: 457–460.

Wilson, G.P., D.G. DeMar Jr., and G. Carter. 2014. Extinction and survival of salamander and salamander-like amphibians across the Cretaceous-Paleogene boundary in northeastern Montana, in: G.P. Wilson, W.A. Clemens, J.R. Horner, and J.H. Hartman

(Eds.), Through the End of the Cretaceous in the Type Locality of the Hell Creek Formation in Montana and Adjacent Areas. Geological Society of America Special Paper 503, Boulder, pp. 271–297.

Williamson, T.E., S.L. Brusatte, and G.P. Wilson. 2014. The origin and early evolution of Metatherian mammals: the Cretaceous record. ZooKeys 465: 1–76.

Zelditch, M.L., D.L. Swiderski, H.D. Sheets, and W.L. Fink. 2004. Geometric Morphometrics for Biologists: a Primer. Elsevier Academic Press, Amsterdam.

Figures

Figure 3.1. Map of localities in northeastern Montana producing humeri specimens used in this study. Localities span the Lancian biozone (yellow circles), and early and middle Puercan biozones (Pu1 and Pu3, in blue stars and green triangles, respectively), as well as the time-averaged and stratigraphically mixed localities representative of the Bug Creek Anthills fauna (red squares). Most localities are located within Garfield and McCone counties; Fallon and Carter counties each contain one locality, as well as Niobrara County in eastern Wyoming (not pictured). Locality names and details are given in Table S3.1. Map modified from Wilson et al. 2014.

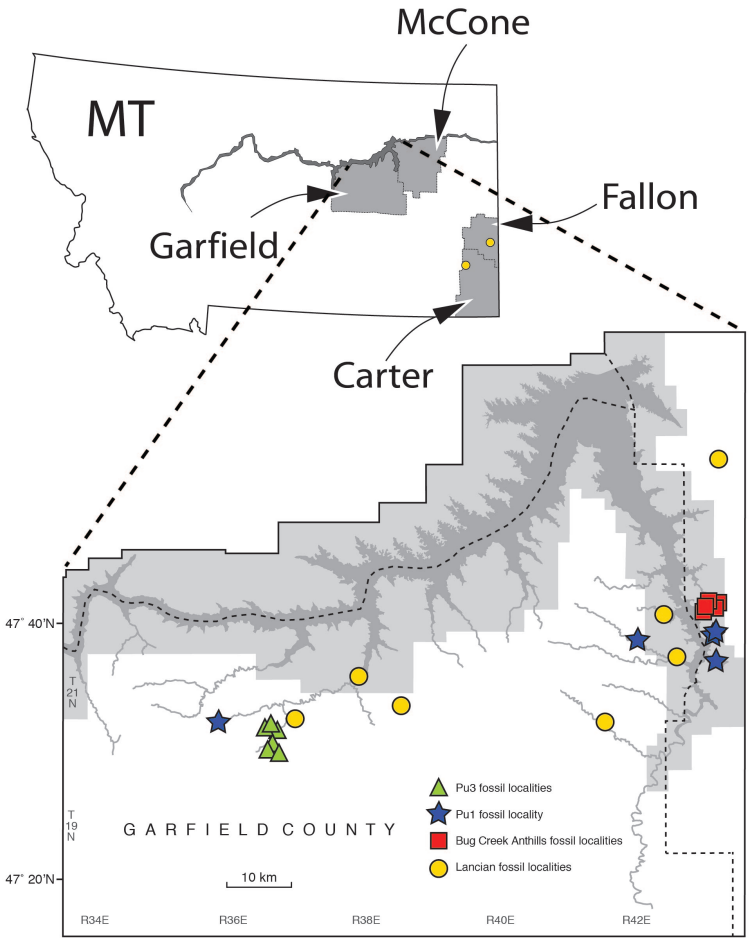

Figure 3.2. Multituberculate and therian measurements used in this study. Multituberculate specimen (UCMP 153039; left) in ventral (**A**), dorsal (**B**), and distal (**C**) views; eutherian specimen (UCMP 151964; right, reversed to appear as left) in anterior (**D**), posterior (**E**), and distal (**F**) views. See Table 3.1 for measurement descriptions. Abbreviations: AW, articular width; C, capitulum; CH, capitulum height; CL, capitulum, length; EC, ectepicondyle; LC, lateral epicondyle (ectepicondyle); MC, medial epicondyle (entepicondyle); NC, entepicondyle; NCW, entepicondylar width; RC, radial condyle; RCH, radial condyle height; RCL, radial condyle length; RCW, radial condyle width; TDW, total distal width; TH, trochlear height; TL, trochlear length; TLW, total lateral width; TW; trochlear width; UC, ulnar condyle; UCH, ulnar condyle height; UCL, ulnar condyle length; UCW, ulnar condyle width; UT, ulnar trochlea.

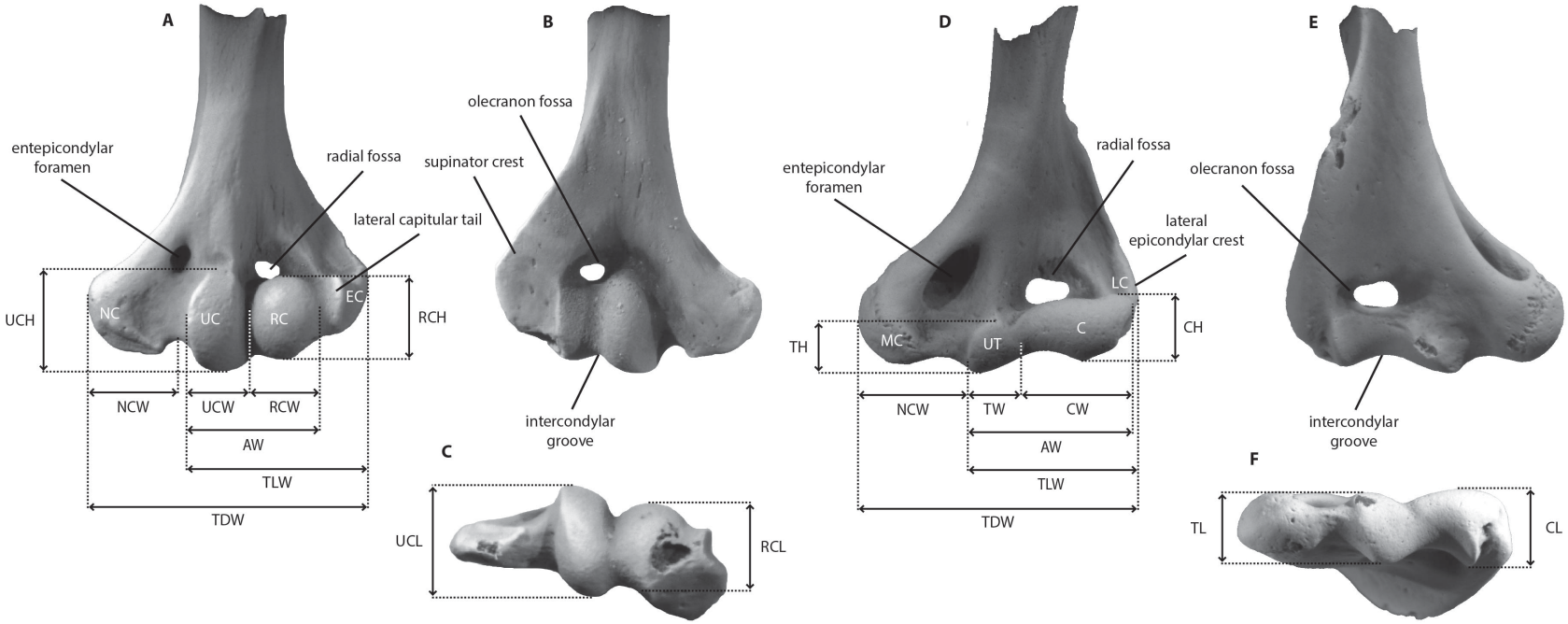

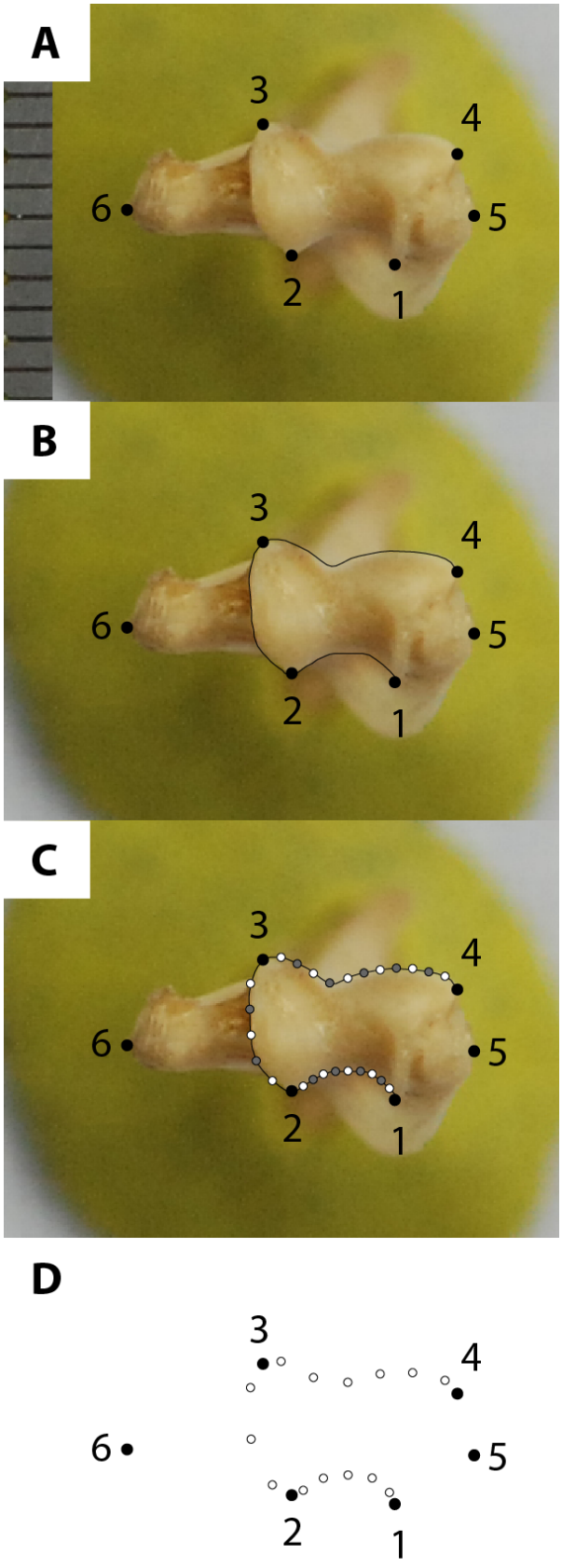

Figure 3.3. Therian left distal humerus (UWBM 20646, *Sciurus carolinensis*) and landmarks (LMs), curves, and semilandmarks (SLMs). All specimens were oriented with anterior up and medial to the left; right specimens were reflected to appear as lefts. Images indicate point placement process. (**A**) LMs 1–6 were plotted (see Table 3.5 for landmark descriptions). (**B**) Curves were traced along the anterior, posterior, and medial borders of the articular surface. (**C**) Curves were re-sampled for equivalent lengths between points, with eleven, nine, and five points describing the anterior, posterior and medial borders of the articular surface, respectively. (**C**) All resampled points and LMs were used for Procrustes superimposition, with sliders (gray) allowed to slide between helper points (white; see Methods). (**D**) Helpers were deleted and all remaining LMs (black) and SLMs (white) were used in PCA analyses.

Figure 3.4. Multituberculate morphotype MuA (UCMP specimen 122045, from locality V70201; right), in ventral (**A**) and dorsal (**B**) stereopair views, and in lateral (**C**), medial (**D**), and distal (**E**) views.

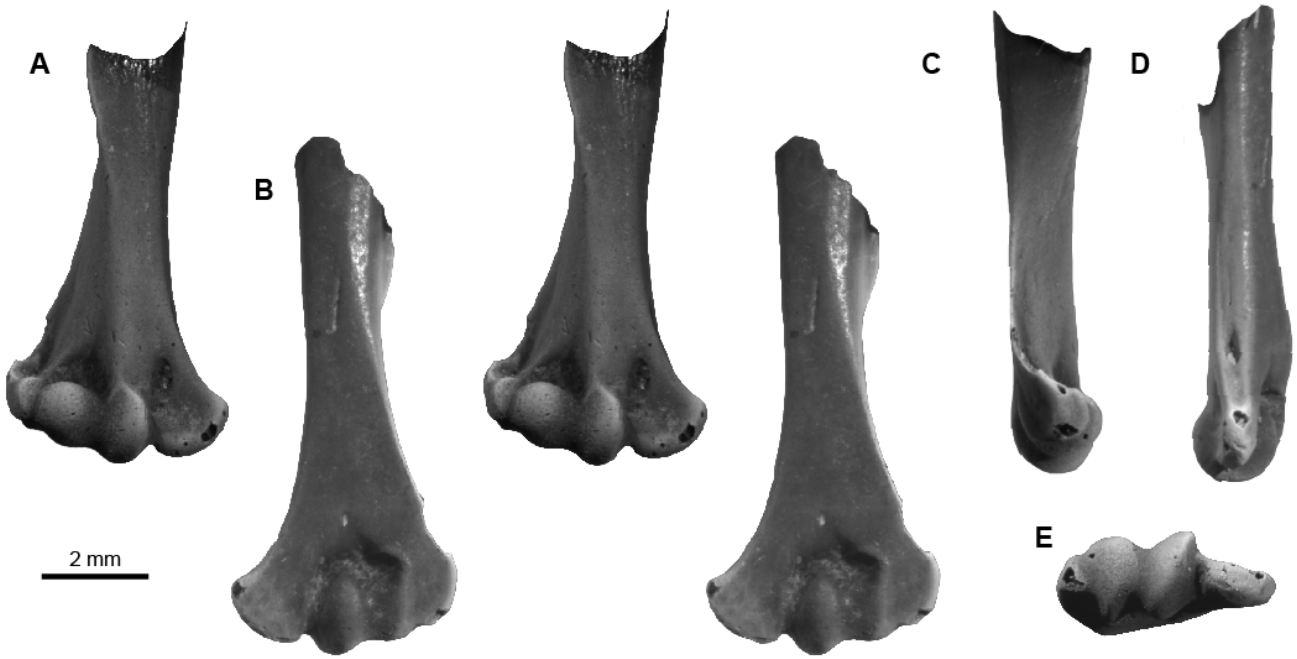

Figure 3.5. Multituberculate morphotype MuB (UCMP specimen 195933, from locality V99438; left), in ventral (**A**) and dorsal (**B**) stereopair views, and in distal (**C**), medial (**D**), and lateral (**E**) views.

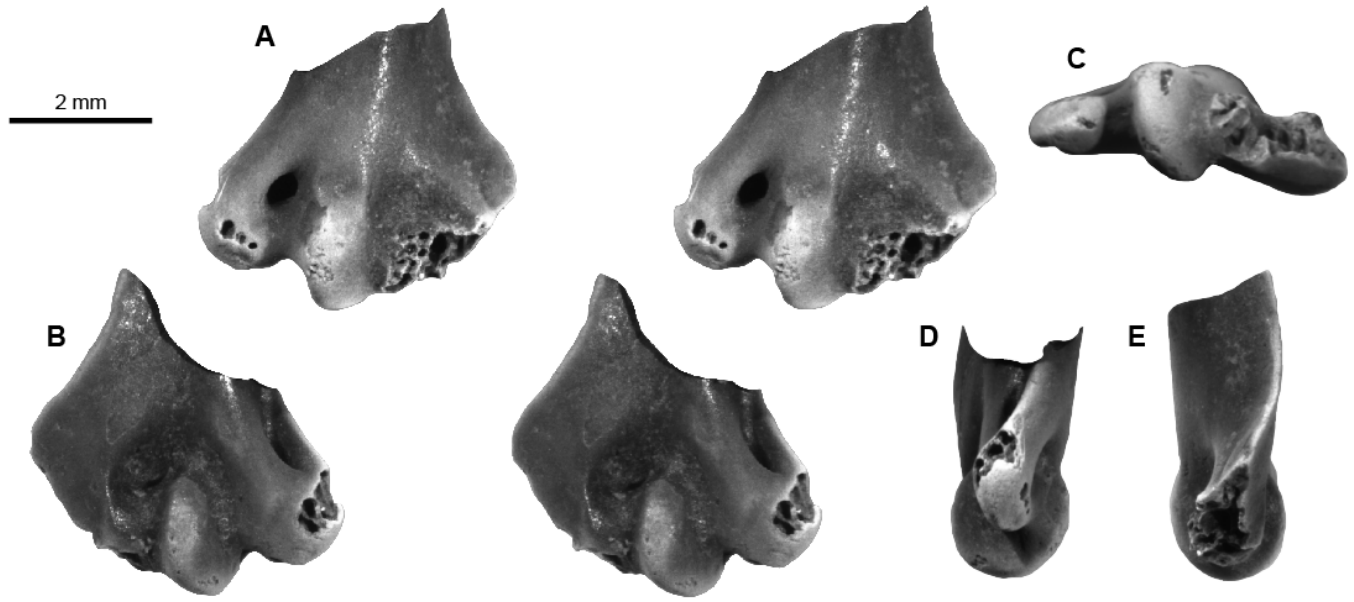

Figure 3.6. Multituberculate morphotype MuC (UCMP specimen 153039, from locality V84193; left), in ventral (**A**) and dorsal (**B**) stereopair views, and in lateral (**C**), medial (**D**), and distal (**E**) views.

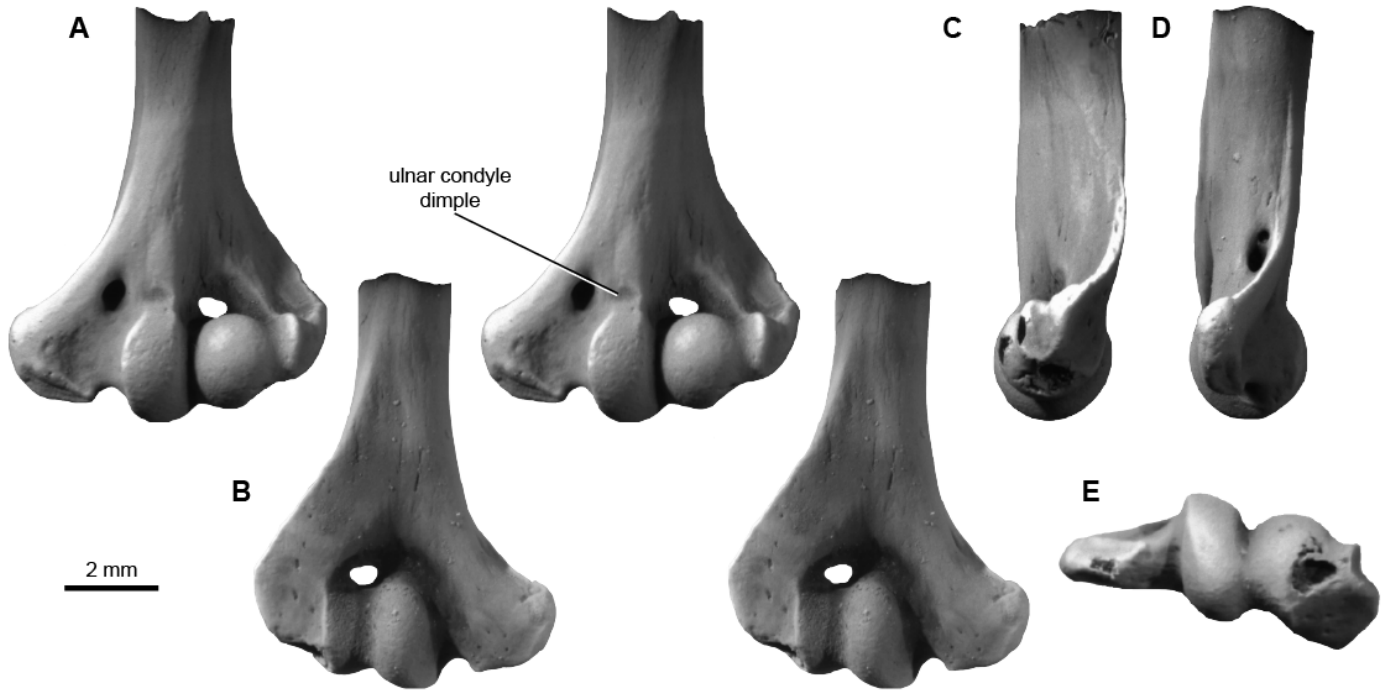

Figure 3.7. Multituberculate morphotype MuD (UCMP specimen 195990, from locality V5620; left), in ventral (**A**) and dorsal (**B**) stereopair views, and in medial (**C**), lateral (**D**), and distal (**E**) views.

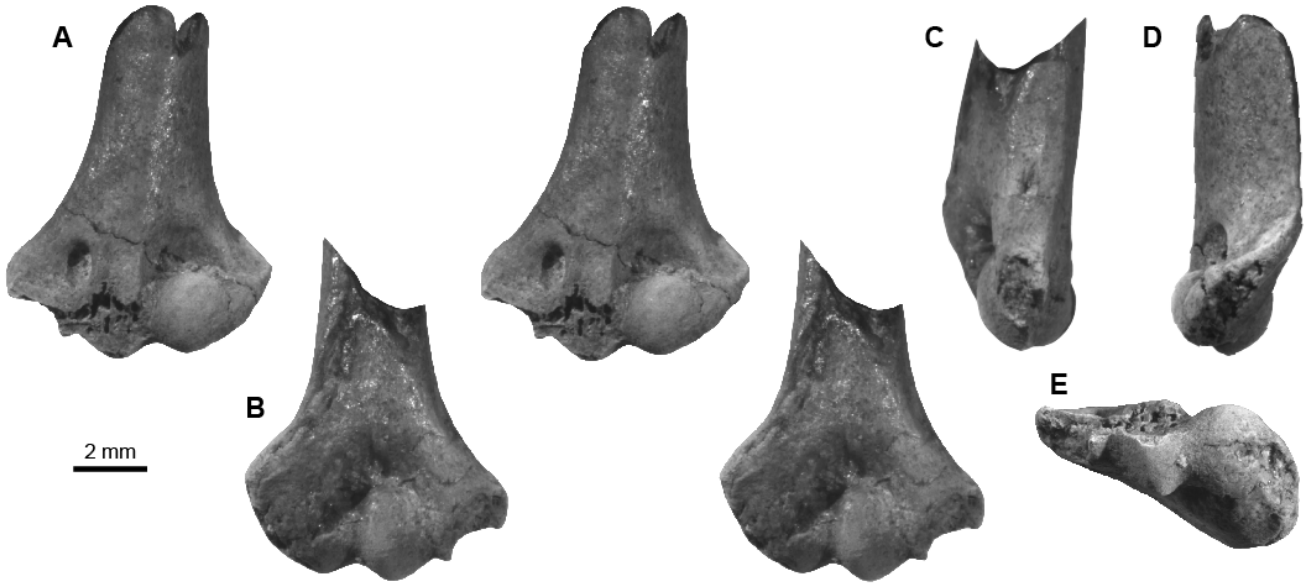

Figure 3.8. Multituberculate morphotype MuE (UWBM specimen 97031, from locality C1845; right), in ventral (**A**) and dorsal (**B**) stereopair views, and in lateral (**C**), medial (**D**), and distal (**E**) views.

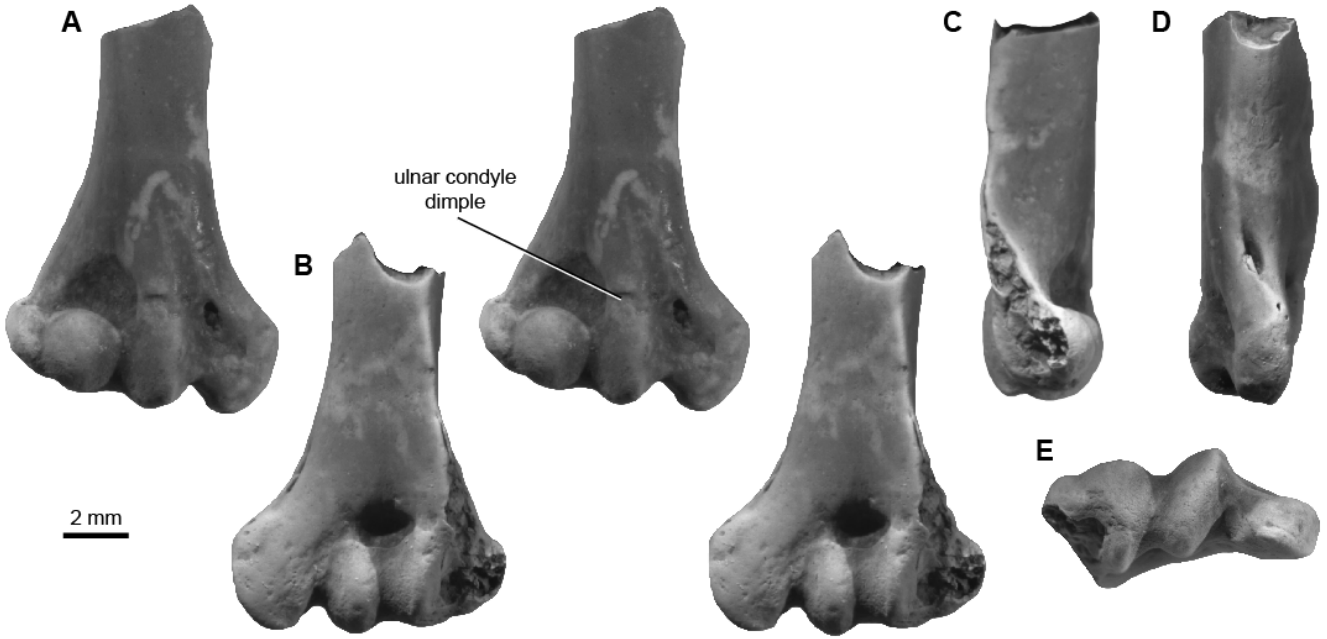

Figure 3.9. Multituberculate morphotype MuF (UCMP specimen 127384, from locality V87001; left), in ventral (**A**) and dorsal (**B**) stereopair views, and in lateral (**C**), medial (**D**), and distal (**E**) views.

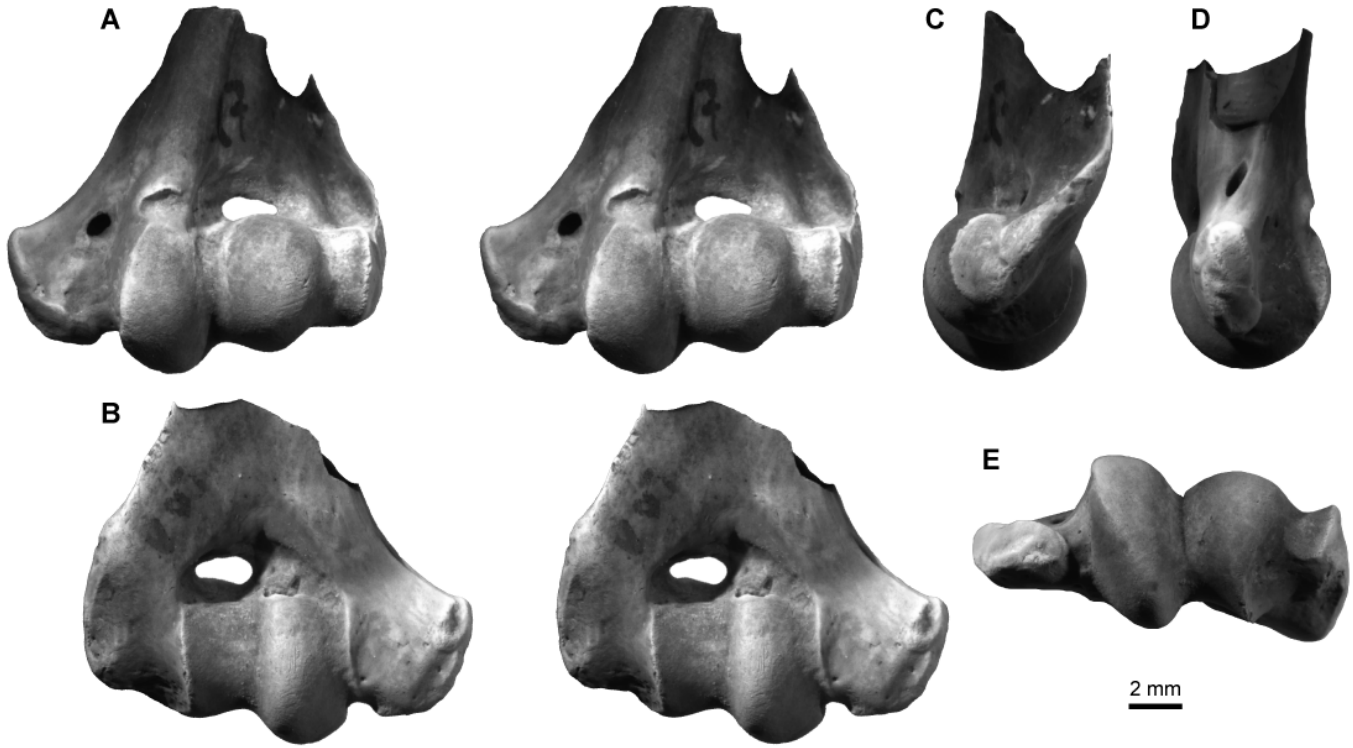

Figure 3.10. Metatherian morphotype ThA (UCMP specimen 127391, from locality V88007; left) in anterior (**A**) and posterior (**B**) stereopair views, and in medial (**C**) view.

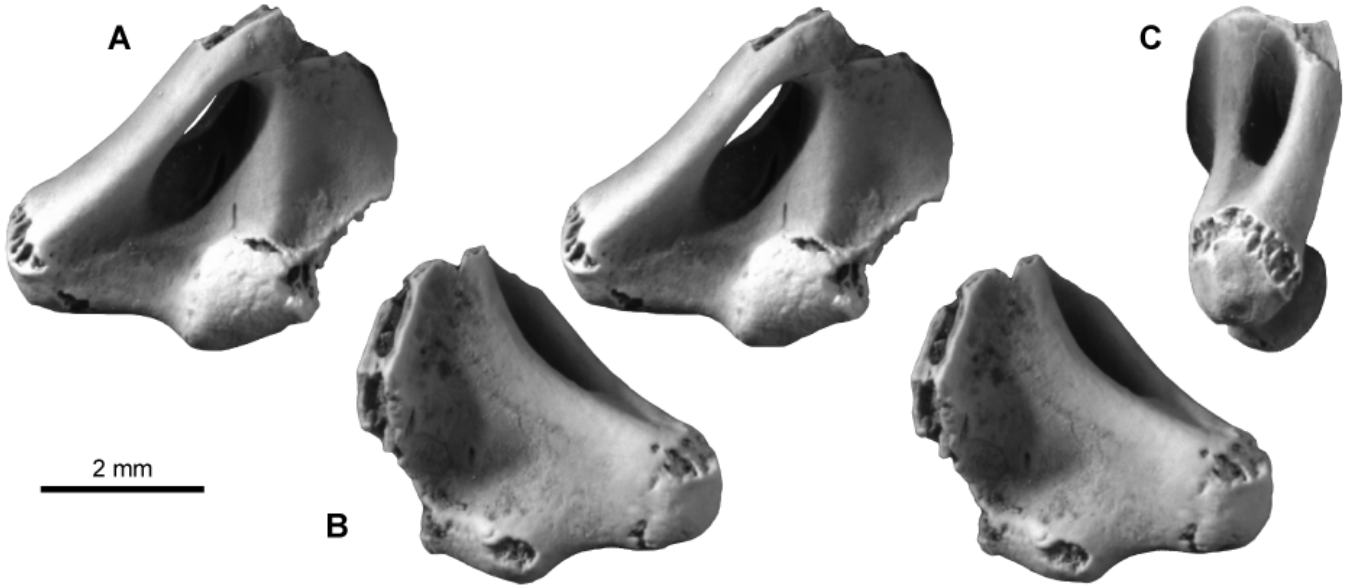

Figure 3.11. Metatherian morphotype MeA (UCMP specimen 152394, from locality V93169; left) in anterior (**A**) and posterior (**B**) stereopair views, and in lateral (**C**), medial (**D**), and distal (**E**) views.

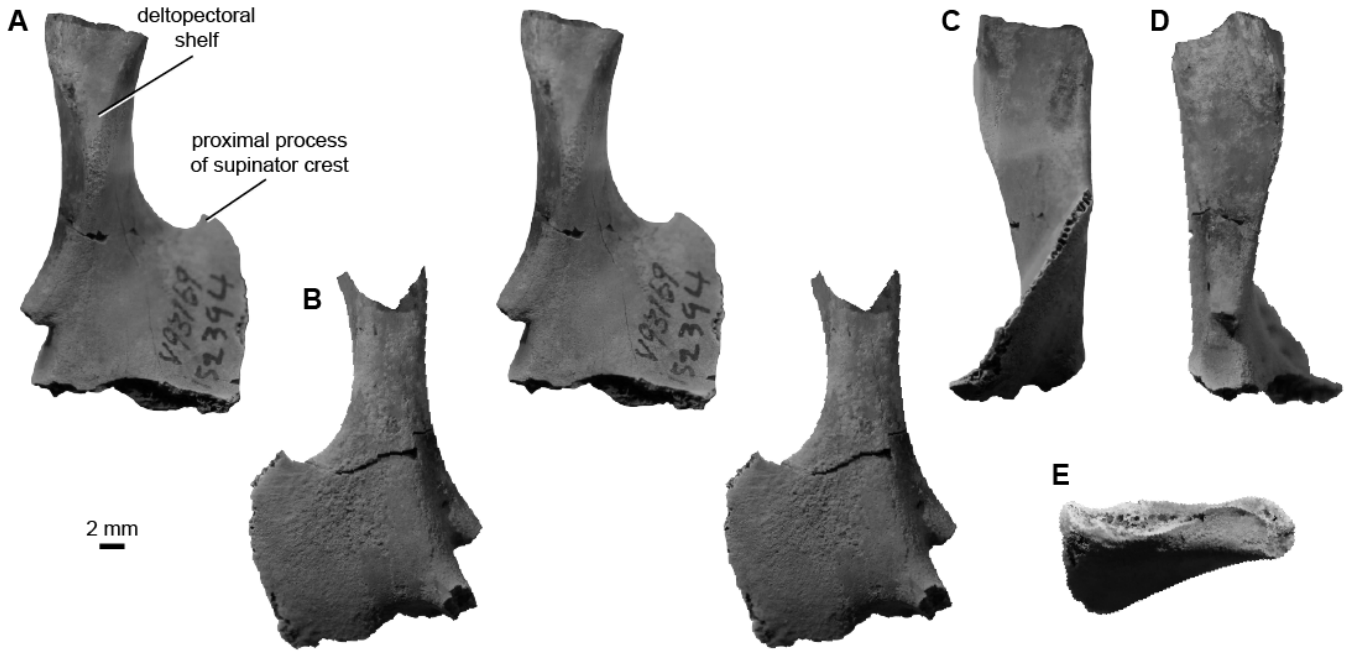

Figure 3.12. Eutherian morphotype EuA (UCMP specimen 153100, from locality V99438; left) in anterior (**A**) and posterior (**B**) stereopair views, and in lateral (**C**), medial (**D**), and distal (**E**) views. Specimen images are CT scan views, not photographs; see Methods for details. Rough patches inside the shaft and within the entepicondylar foramen are the result of sediment infilling, whereas other rough areas (i.e., supinator crest, medial entepicondyle, posterior articular surfaces) indicate specimen breakage.

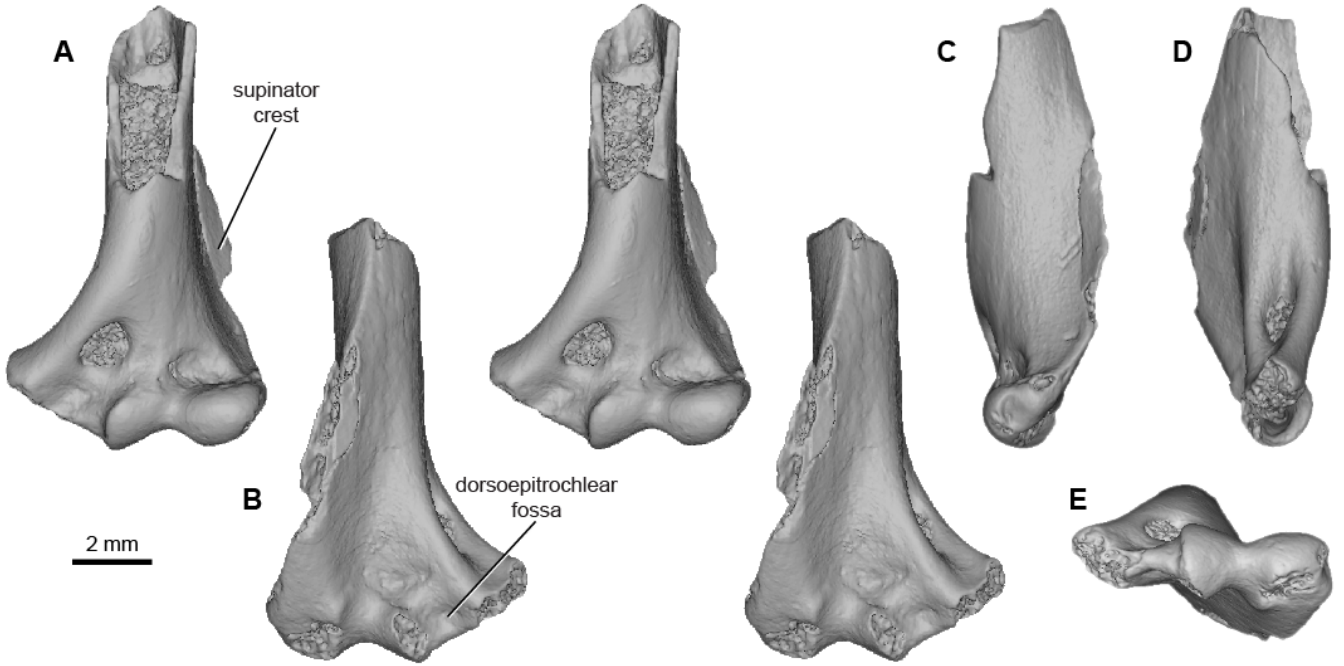

Figure 3.13. Eutherian morphotype EuB (UWBM specimen 97114, from locality C1115; left) in anterior (**A**) and posterior (**B**) stereopair views, and in distal (**C**), lateral (**D**), and medial (**E**) views.

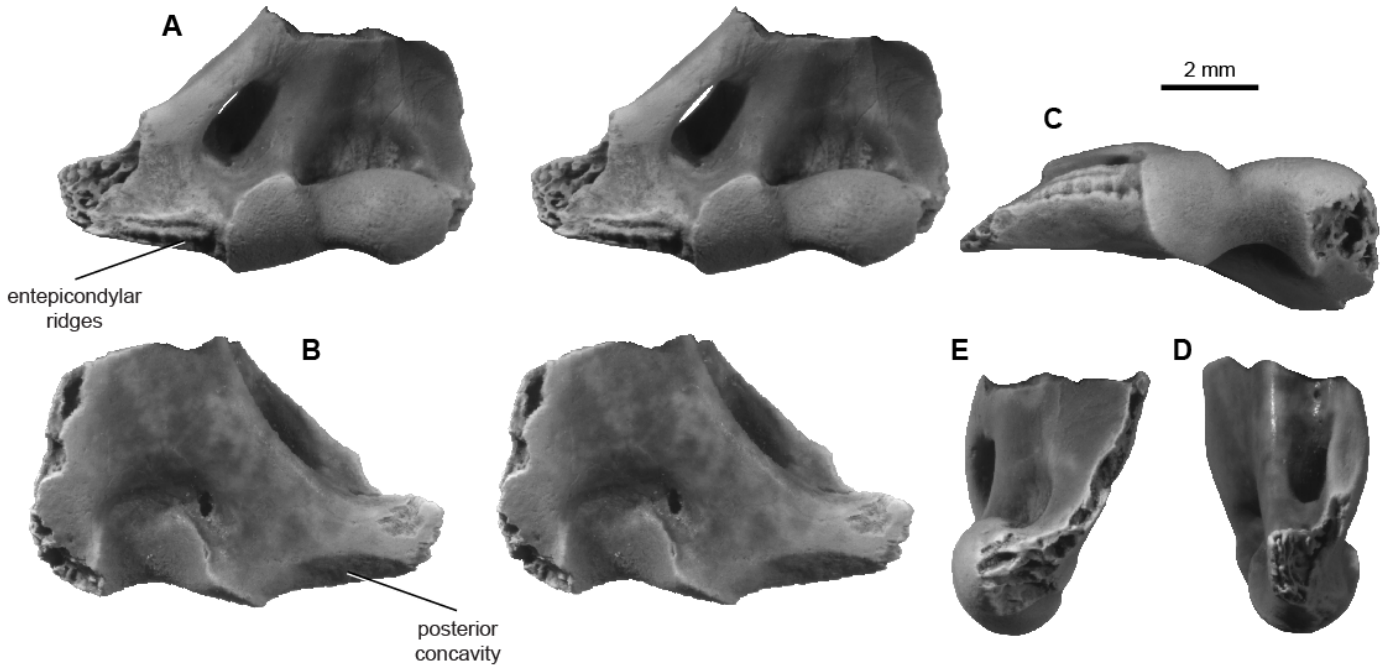

Figure 3.14. Eutherian morphotype EuC (UCMP specimen 151991, from locality V71203; right) in anterior (**A**) and posterior (**B**) stereopair views, and in lateral (**C**), medial (**D**), and distal (**E**) views.

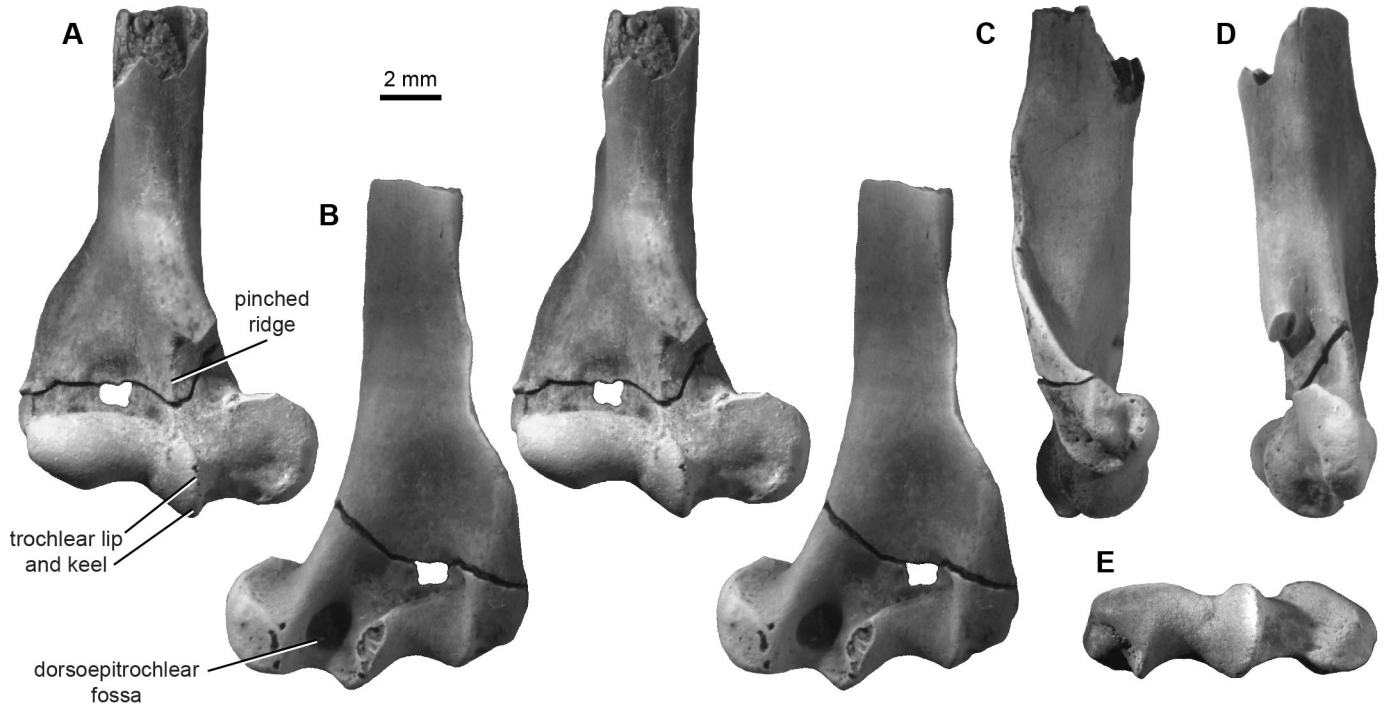

Figure 3.15. Eutherian morphotype EuD (UCMP specimen 151964, from locality V65127; right) in anterior (**A**) and posterior (**B**) stereopair views, and in lateral (**C**), medial (**D**), and distal (**E**) views.

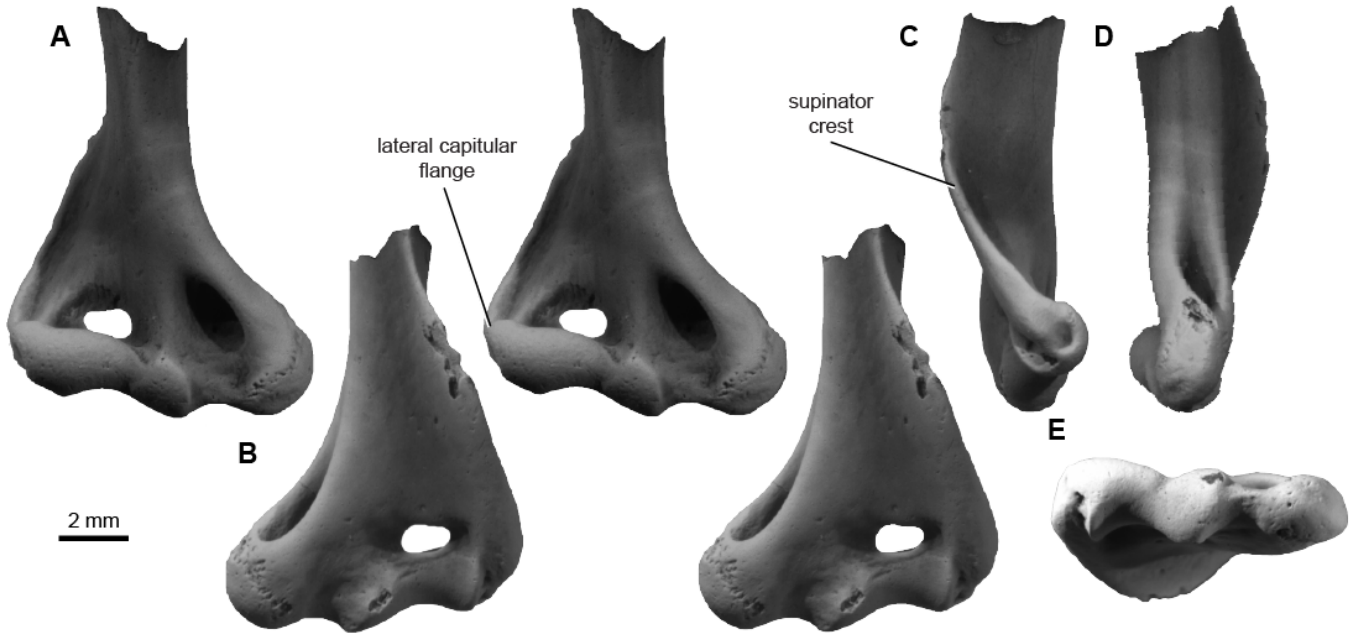

Figure 3.16. Eutherian morphotype EuE (UCMP specimen 218901, from locality V91065; right) in anterior (**A**) and posterior (**B**) stereopair views, and in lateral (**C**), medial (**D**), and distal (**E**) views.

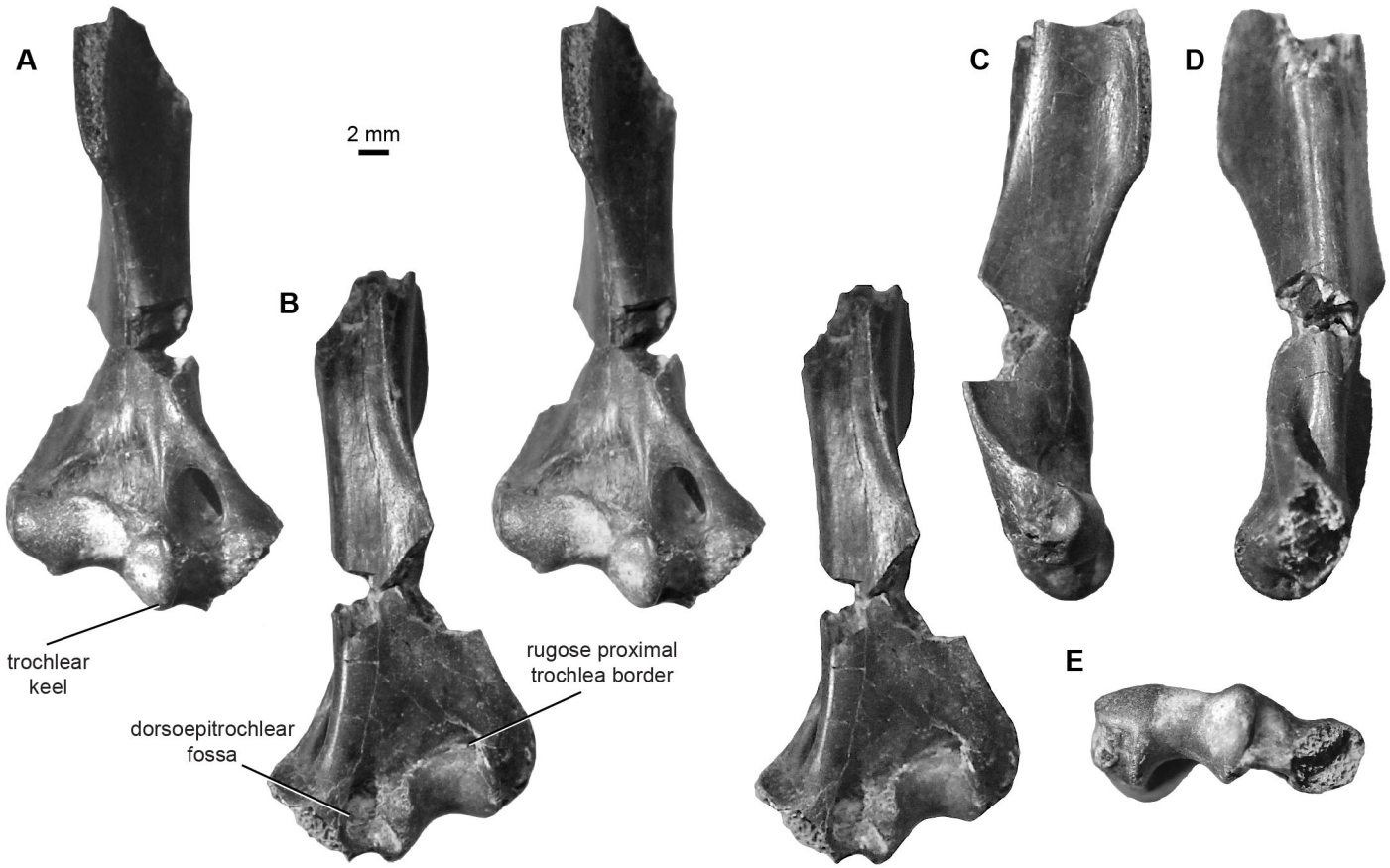

Figure 3.17. Eutherian morphotype EuF (UCMP specimen 92928, from locality V72129; right) in anterior (**A**) and posterior (**B**) stereopair views, and in lateral (**C**), medial (**D**), and distal (**E**) views.

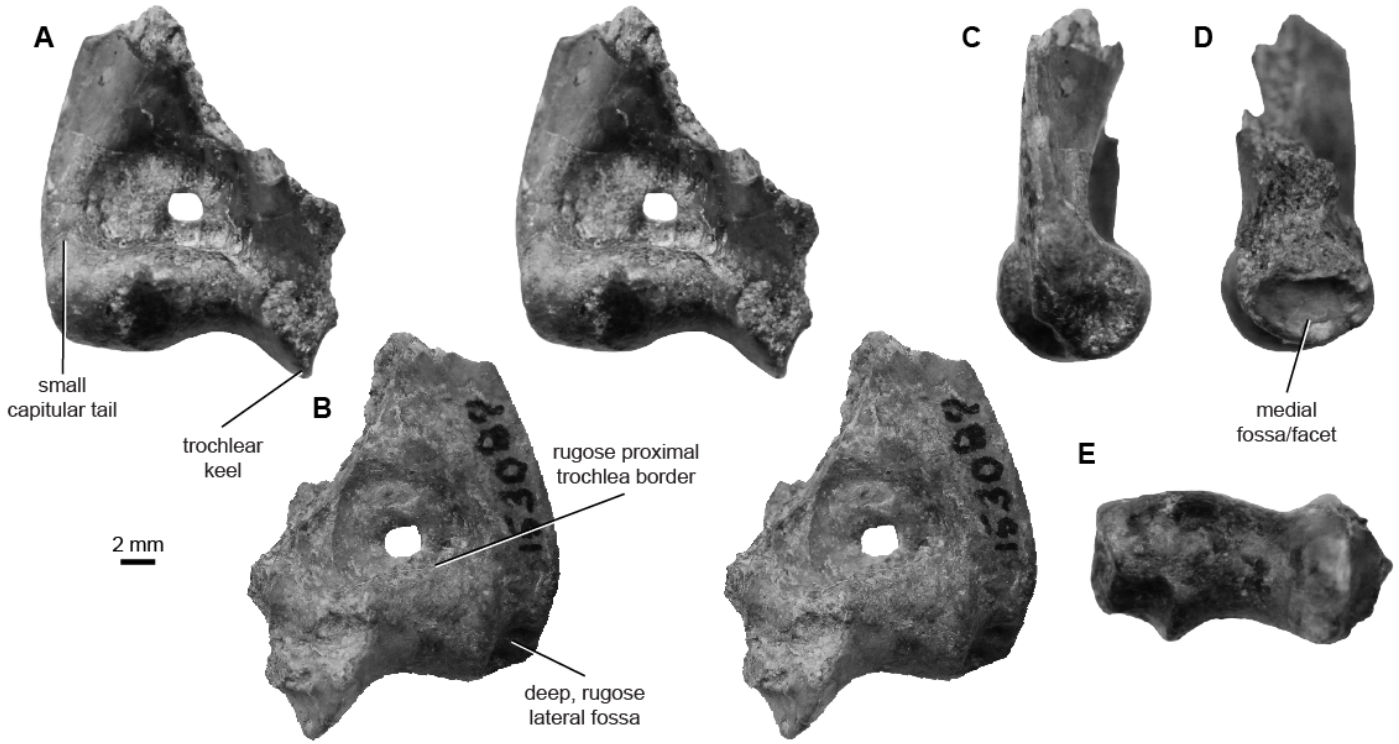

Figure 3.18. Eutherian morphotype EuG (UCMP specimen 192678, from locality V74124; left) in anterior (**A**) and posterior (**B**) stereopair views, and in medial (**C**) and distal (**D**) views.

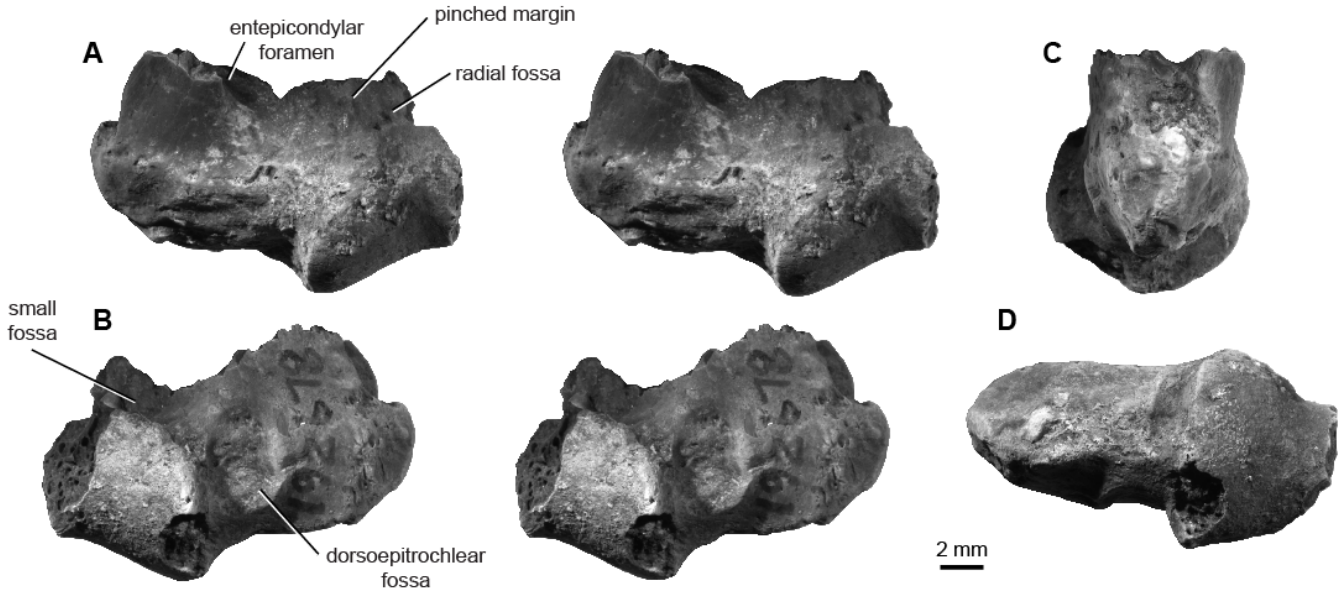

Figure 3.19. Summary of humeri morphotypes and relative sizes through our study area in the Hell Creek and Tullock Formations of eastern Montana. Multituberculate morphotypes are shown as black bars, metatherians as gray bars, and eutherians as white bars. Numbers within the bars indicate the morphotype sample size for each temporal bin. Morphotypes are horizontally arranged according to increasing size (left to right, see text for specimen numbers, localities, and details; Tables S3.6–7 for morphotype mean sizes). Gradients for MuF, EuC, and EuD indicate morphotypes were present in the time-averaged Bug Creek Anthills assemblages, and the morphotype range may extend into the Pu1 and/or the Lancian. Our study area includes Lancian, Pu1, and Pu3 assemblages; Pu2 assemblages are known from the San Juan Basin but not from our study area (hashmarks indicate resultant uncertainty of range-through morphotypes; Clemens 2015). Ages for K–Pg boundary and within the Tullock Formation are based on radiometric age determinations of tuffs within lignites, whereas the age for the base of the Hell Creek Formation is based on linear extrapolation of sedimentation rate (Swisher et al., 1993; Renne et al., 2011, 2013; Wilson, 2014; Sprain et al. 2014); note the temporal axis is not to scale. Figure is modified from Sprain et al. (2014). Abbreviations: Fm, Formation; NALMA, North American Land Mammal "age"; Pu1, early Puercan; Pu3, middle/late Puercan; question marks indicate specimens tentatively attributed to that morphotype, see Methods.

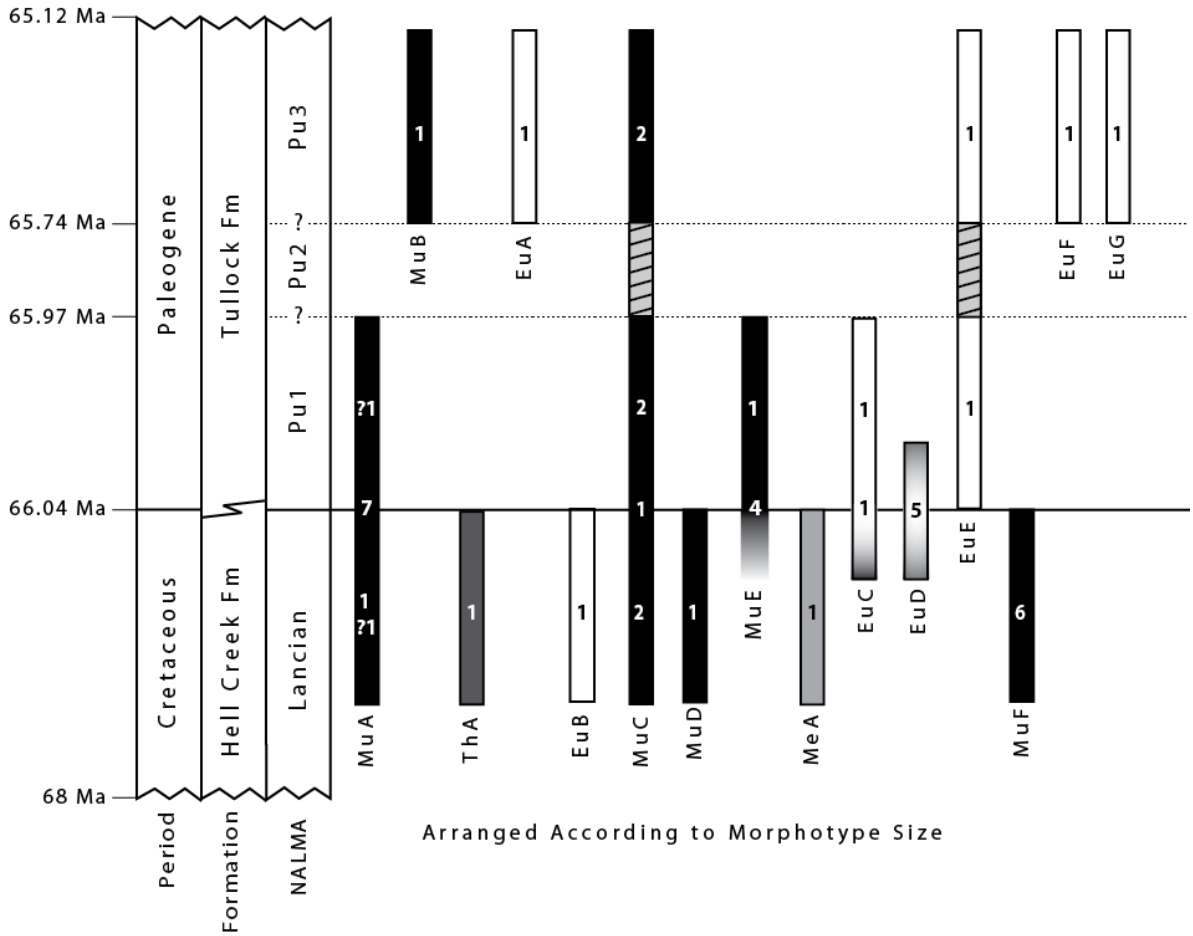
65.12 Ma
65.74 Ma
65.97 Ma
66.04 Ma
68 Ma
Paleogene
Cretaceous
Tullock Fm
Hell Creek Fm
Pu3
Pu2
Pu1
Lancian
?
?
?1
7
1
?1
1
1
2
2
1
2
1
1
1
4
1
1
1
5
1
1
6
1
1
1
MuA
ThA
EuB
MuC
MuD
MuE
MeA
EuC
EuD
EuE
MuF
MuB
EuA
EuF
EuG
Period
Formation
NALMA
Arranged According to Morphotype Size

Figure 3.20. Results of Principal Component Analyses of full dataset color-coded for taxon (top) and locomotor group (bottom), with fossils (open circles) projected into morphospace. We plot PC1 and PC2 (**A**) and PC2 and PC3 (**B**) for all taxa (legend top right), and the same data for locomotor group (**C–D**; legend bottom right). We also include the partial warps for PC1 and PC2 (identical to Figs. S3.11–12).

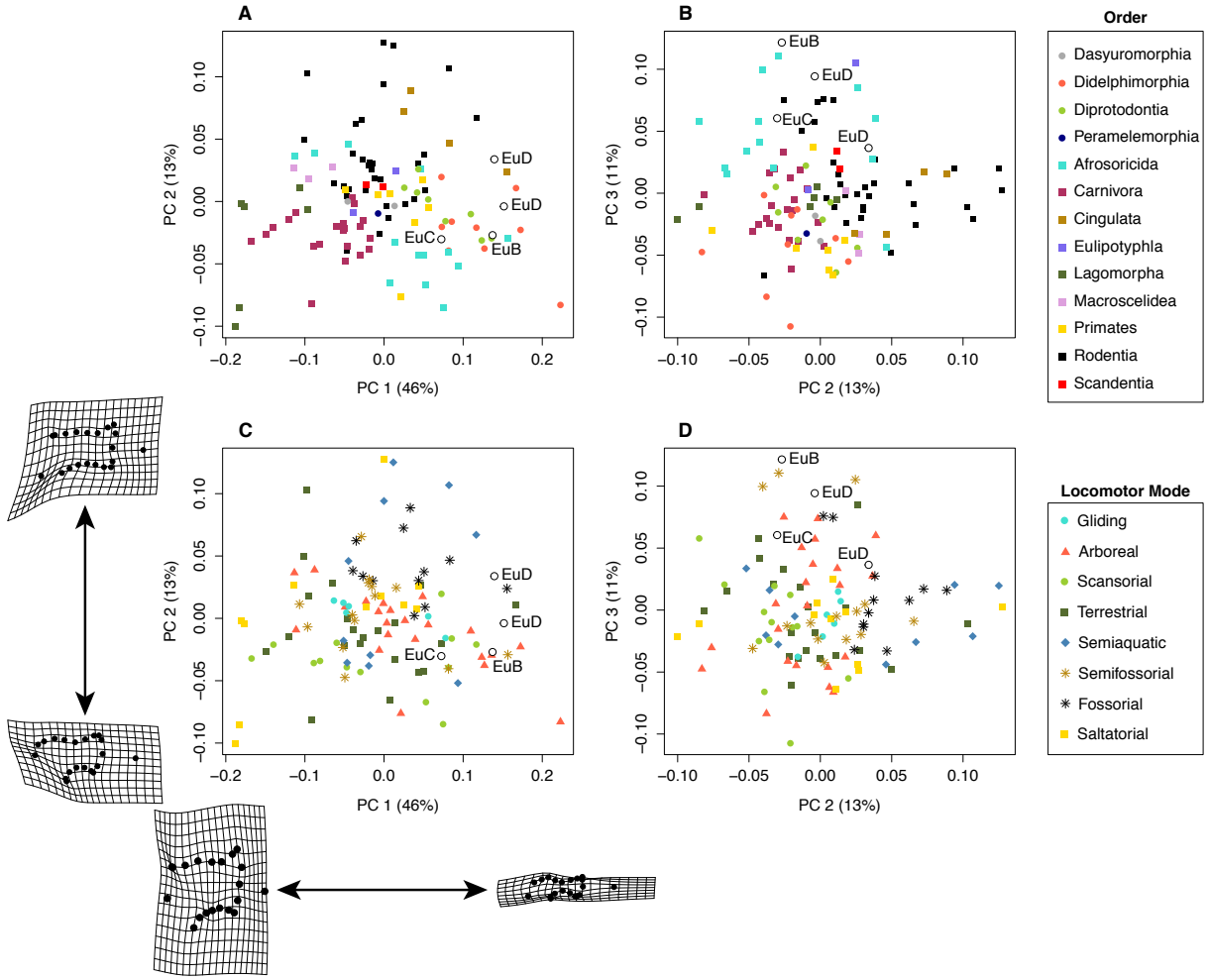

Figure 3.21. Results of Principal Component Analyses of reduced dataset color-coded for taxon (top) and locomotor group (bottom), with fossils (open circles) projected into morphospace. We plot PC1 and PC2 (**A**) and PC2 and PC3 (**B**) for all taxa (legend top right), and the same data for locomotor group (**C–D**; legend bottom right). We also include the reduced dataset partial warps for PC1 and PC2.

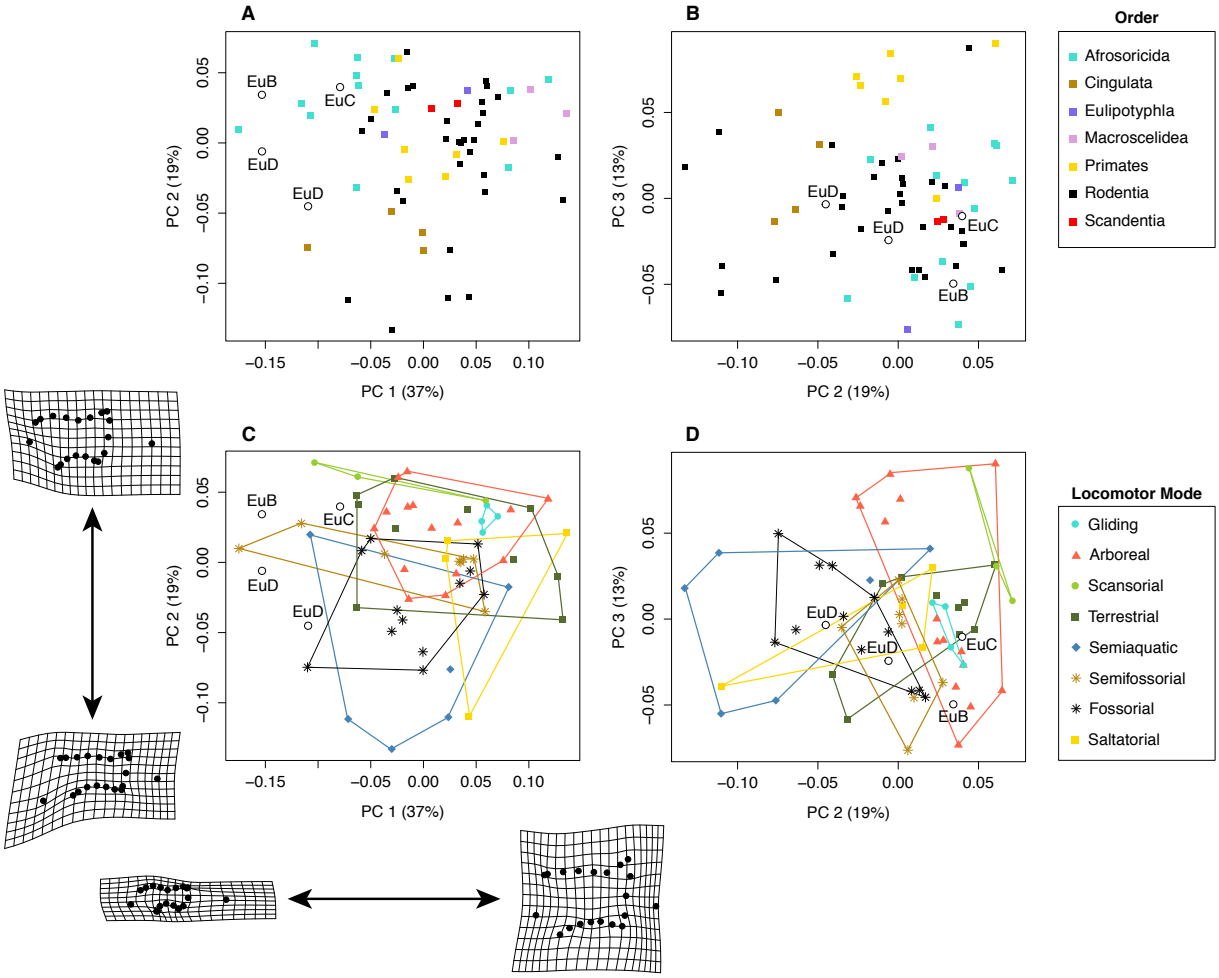

Figure 3.22. PC1 and PC2 results for reduced dataset with each locomotor group plotted separately (**A–H**) for clarity (data, legend, and fossil placement identical to Fig. 3.21C).

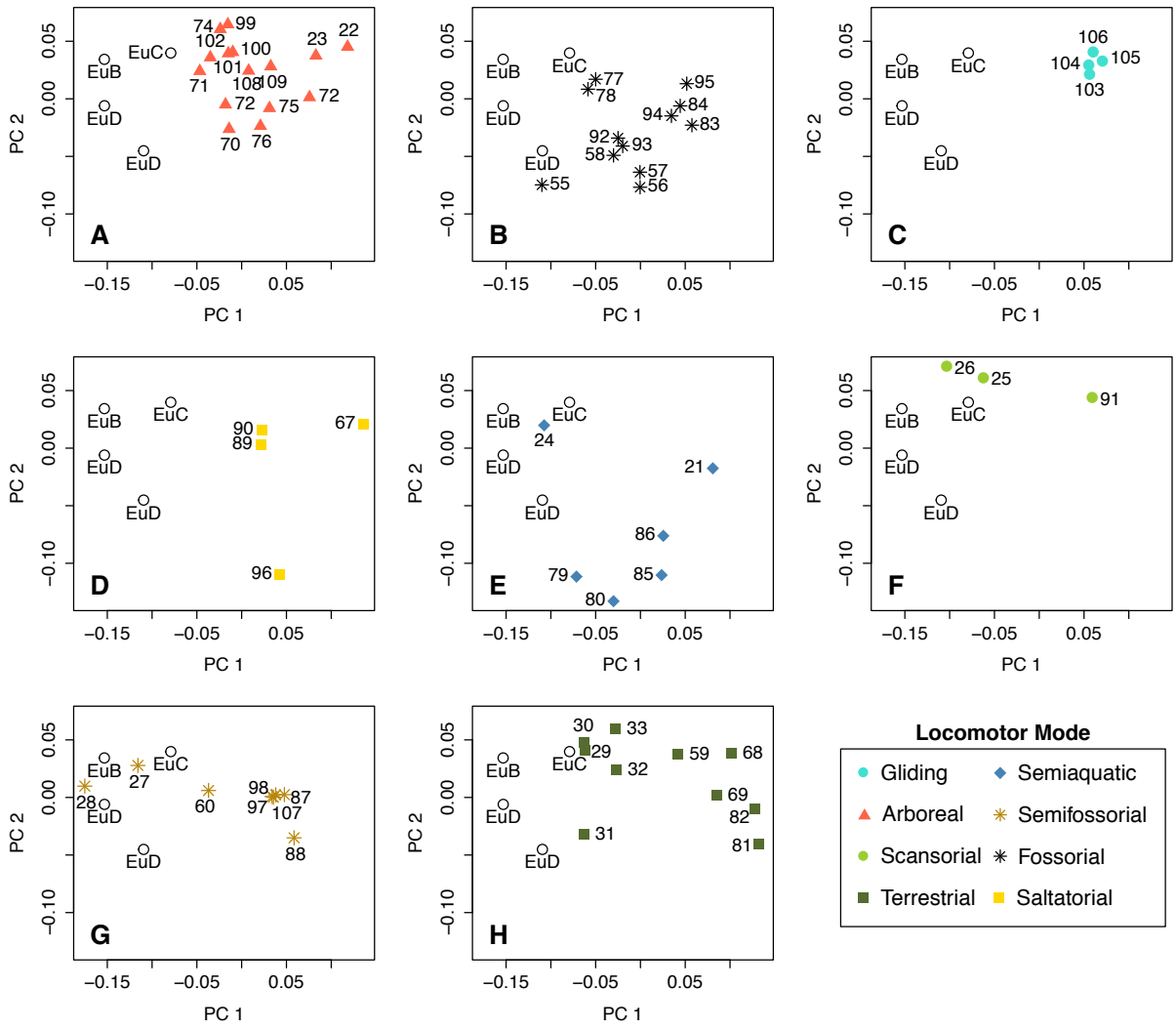

Figure 3.23. PC2 and PC3 results for reduced dataset with each locomotor group plotted separately (**A–H**) for clarity (data, legend, and fossil placement identical to Fig. 3.21D).

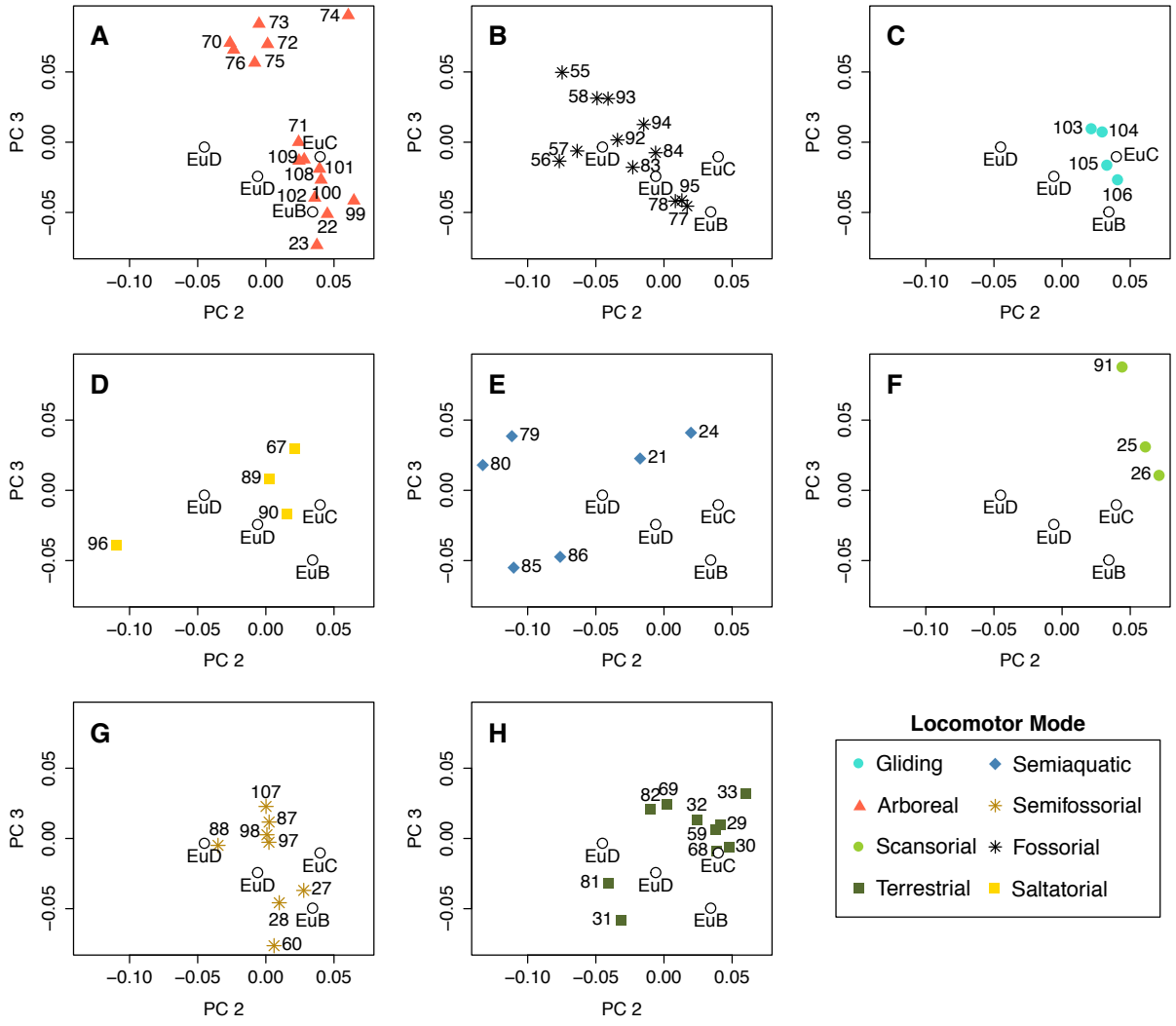

Figure 3.24. LDA results for modern reduced dataset according to locomotor group. (**A**) LD1 and LD2; (**B**) LD1 and LD3; and (**C**) LD2 and LD3.

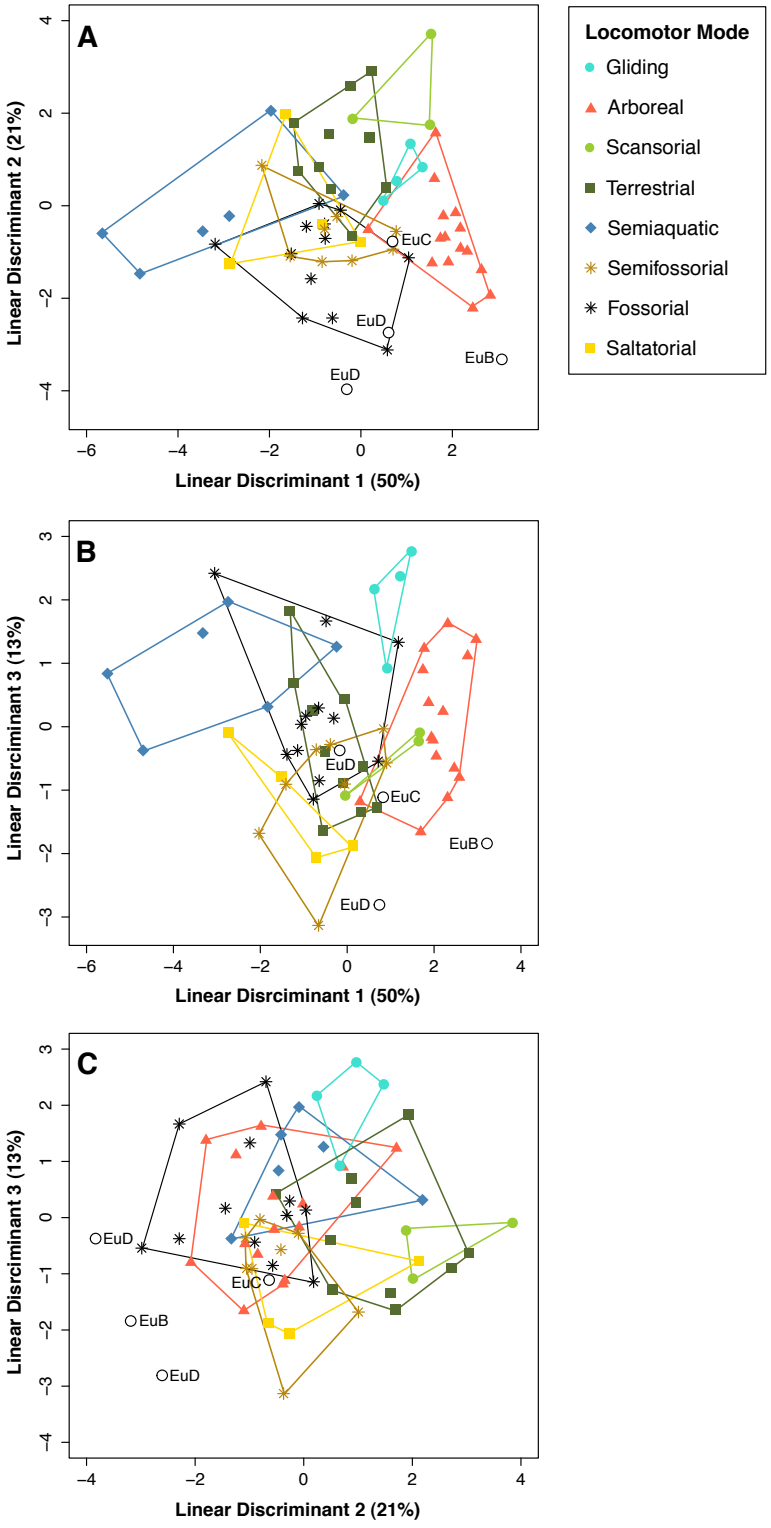

Tables

Table 3.1. Measurements taken on distal humeri in this study. Columns (from left to right) are: measurements (abbreviation and name); measurement description; taxon of study; and source reference for each measurement. We took the following measurements (Fig. 3.2) on all multituberculate and therian specimens, contingent upon specimen completeness (see Table 3.2). The anatomical view from which the measurement was taken is indicated in parentheses in the description, as it relates to either multituberculate (Mu) or therian (Th) humeri, see text for more details. Measurements are identical to those in the indicated sources, with the following exceptions: our measurement TDW is 'BW' of Szalay and Dagosto (1980) and measurement 5 of Argot (2001); NCW is measurement 6 of Argot (2001) and 'EEC' of Boyer et al. (2010); TLW is 'TLE' of Szalay and Dagosto (1980); measurements TL and CL are modified from Szalay and Dagosto (1980) and Boyer et al. (2010). Multituberculate measurements lacking references are based on the structurally (but not necessarily functional) analogous measurement for therian humeri (see Fig. 3.2).

Measurements		Description	Taxon	Source
TDW	Total Distal Width	Medial edge of specimen to lateral edge, measured at the maximum extensions of the entepicondyle and ectepicondyle; parallel to other distal width measures (anterior view in therians; ventral view in multituberculates)	Th, Mu	Deischl 1964; Szalay and Dagosto 1980; Argot 2001
AW	Articular Surface Width	Eu: Lateral edge of capitulum to medial edge of trochlea (anterior) Mu: Lateral edge of radial condyle to medial edge of ulnar condyle (ventral)	Th, Mu	Szalay and Dagosto 1980; Szalay and Sargis 2001;
TLW	Total Lateral Width	Eu: Medial edge of trochlea to lateral edge of ectepicondyle (anterior)	Th, Mu	Szalay and Dagosto 1980

		Mu: Medial edge of ulnar condyle to lateral edge of ectepicondyle (ventral)		
NCW	Entepicondylar Width	Eu: Medial edge of trochlear lip to medial edge of entepicondyle (anterior) Mu: From midpoint of groove between entepicondyle and ulnar condyle to medial edge of entepicondyle (ventral)	Th, Mu	Argot 2001; Boyer et al. 2010
TW	Trochlear Width	Medial edge of trochlea (trochlear lip) to lateral edge of trochlea (medial edge of intercondylar groove) (anterior)	Th	Szalay and Dagosto 1980; Boyer et al. 2010
CW	Capitulum Width	Lateral edge of capitulum to medial edge of intercondylar groove (anterior)	Th	Szalay and Dagosto 1980; Boyer et al. 2010
TH	Trochlear Height	Length from proximal margin to distal margin of trochlear lip (anterior)	Th	Szalay and Dagosto 1980; Boyer et al. 2010
CH	Capitulum Height	Length from proximal margin to distal margin of capitulum (anterior)	Th	
TL	Trochlear Length	Maximum length from anterior surface to posterior surface of trochlea, parallel to CL (distal)	Th	Szalay and Dagosto 1980; Boyer et al. 2010
CL	Capitulum Length	Length of capitulum articular surface, from anterior to posterior extent, parallel to TL (distal)	Th	Szalay and Dagosto 1980; Boyer et al. 2010
UCW	Ulnar Condyle Width	Medial edge of ulnar condyle to lateral edge of ulnar condyle (ventral)	Mu	
RCW	Radial Condyle Width	Medial edge of radial condyle to lateral edge of radial condyle (ventral)	Mu	
UCH	Ulnar Condyle Height	Length from proximal margin to distal margin of ulnar condyle (ventral)	Mu	
RCH	Radial Condyle Height	Length from proximal margin to distal margin of radial condyle (ventral)	Mu	
UCL	Ulnar Condyle Length	Maximum length from ventral surface to dorsal surface ulnar condyle, parallel to RCL (distal)	Mu	
RCL	Radial Condyle Length	Maximum length from ventral surface to dorsal surface radial condyle, parallel to UCL (distal)	Mu	

Table 3.2. Linear measurements of multituberculate distal humeri specimens. See Table 3.1 for measurement descriptions; all measurements on multituberculate humeri are taken in ventral view except for RCL and UCL, which are taken in distal view. All measurements are in millimeters. Abbreviations: Fm, Formation; HC, Hell Creek Formation; La, Lancian Biozone; Lan, Lancian Formation; Morph., Morphotype; Pu1, Puercan 1 Biozone; Pu3, Puercan 3 Biozone; Tu, Tullock Formation. Asterisks indicate minimum size values, where preserved morphology was measured but the full measurement was not possible, due to specimen breakage; "–" indicates specimen was too broken for measurement; "?" indicates more tentative assignment to morphotype, due to specimen breakage. Locality numbers follow the system of each institution; those beginning with "V" are UCMP localities; those beginning with "C" are UWBM localities (see Table S3.1 for additional locality details).

Specimen	Locality	Fm	Biozone	Morph.	TDW	AW	TLW	NCW	UCW	RCW	UCH	RCH	UCL	RCL
195999	V5620	Lan	La	MuA	3.695	2.060	2.550	1.045	0.950	1.115	1.365	1.195	1.625	1.525
195974	V65127	Tu	BCA	MuA	3.995	2.005	2.455	1.255	0.765	1.000	1.305	1.140	1.530	1.510
195982	V65127	Tu	BCA	MuA	–	2.040	2.210	–	0.865	1.170	1.405	1.055	1.445	–
122045	V70201	Tu	BCA	MuA	4.120	2.105	2.565	1.375	0.875	1.235	1.315	1.165	1.650	1.580
196956	V70201	Tu	BCA	MuA	–	1.960*	–	–	0.780	1.120*	1.225	1.005	1.275	–
196957	V70201	Tu	BCA	MuA	3.915	2.090	2.615	1.175	0.840	1.160	1.465	1.240	1.460	1.455
70976	C0338	Tu	BCA	MuA	–	1.850	2.420	–	0.855	1.070	1.345	1.150	1.440	1.400
70977	C0338	Tu	BCA	MuA	3.695	–	2.580	1.075	1.065	–	1.480	–	1.415	–
195998	V5620	Lan	La	?MuA	–	–	–	–	0.690	–	0.805	–	1.805	–
153016	V74111	Tu	Pu1	?MuA	–	2.165*	–	–	–	1.240	1.475*	1.240*	1.585	1.475*
195933	V99438	Tu	Pu3	MuB	–	–	–	1.240	1.080	–	1.465	–	1.670	–
174490	V73087	HC	La	MuC	–	3.555*	–	–	1.690	2.055	2.440	1.980	2.845	2.445
195997	V5620	Lan	La	MuC	–	2.525	3.150	–	0.985	1.360	1.925	1.600	2.145	2.000
174420	V70209	Tu	BCA	MuC	5.290	2.975	3.595	1.480	1.295	1.630	1.975	2.030*	2.130	1.975
153039	V84193	HC	Pu1	MuC	6.460	3.090	4.250	1.960	1.570	1.700	2.185	1.830	2.555	2.335
197687	V74111	Tu	Pu1	MuC	–	3.565*	–	–	1.480*	2.050*	2.240	1.885	2.330	–

195932	V99438	Tu	Pu3	MuC	5.350*	3.035	3.820	1.460*	1.505	1.640	2.180	1.765	2.515	2.295
195945	V74122	Tu	Pu3	MuC	5.590*	3.040	3.815	1.480	1.270	1.420	2.455	1.755	2.345	2.305
195990	V5620	Lan	La	MuD	7.310*	4.230*	5.470*	1.835*	–	2.160	–	2.135	–	2.350
174439	V70209	Tu	BCA	MuE	–	–	–	2.385	1.855	–	3.265	–	3.200	–
174442	V70209	Tu	BCA	MuE	–	–	–	–	1.965	–	2.730*	–	2.600*	2.680
195973	V65127	Tu	BCA	MuE	8.130	4.025	5.080	2.445	1.485	2.410	2.810	2.265	3.200	3.145
97031	C1845	Tu	BCA	MuE	8.420	4.400	5.230	2.595	2.000	2.565	2.695	2.485	3.355	3.335
174412	V84162	HC	Pu1	MuE	–	–	–	–	2.360	–	3.535	–	3.910	–
127384	V87001	HC	La	MuF	14.025	7.730	9.990	3.970	3.865	4.435	5.440	5.095	6.420	5.580
174400	V85092	HC	La	MuF	–	6.900	–	–	3.135	3.945	4.985	4.260	5.180	4.530
174232	V72207	HC	La	MuF	–	–	–	–	–	5.050	–	5.655	–	6.365
174225	V72207	HC	La	MuF	–	6.815*	–	3.255	3.435	4.215*	5.045	4.900	5.835	–
174218	V73097	HC	La	MuF	–	7.820*	–	–	2.450	4.325	5.605	5.145	6.420	–
101970	C1521	HC	La	MuF	13.705	6.945	9.105	3.995	2.985	3.915	5.030	3.900	5.030	4.405

Table 3.3. Linear measurements of therian distal humeri specimens. See Table 3.1 for measurement descriptions; all measurements on therian humeri are taken in anterior view except for CL and TL, which are taken in distal view. All measurements are in millimeters. Abbreviations: Fm, Formation; HC, Hell Creek Formation; La, Lancian Biozone; Morph., Morphotype; Pu1, Puercan 1 Biozone; Pu3, Puercan 3 Biozone; Tu, Tullock Formation. Asterisks indicate minimum size values, where preserved morphology was measured but the full measurement was not possible, due to specimen breakage; "–" indicates specimen was broken; "?" indicates more tentative assignment to morphotype; "‡" indicates specimen was used in 2D GM locomotor analyses. Locality numbers follow the system of each institution: those beginning with "V" are UCMP localities; those beginning with "C" are UWBM localities (see Table S3.1 for additional locality details). Five additional specimens from the BCA biozone (UCMP 151945, 151965, 151983, and 151984 from loc. V65127, and UCMP 174429 from loc. V70209) are tentatively attributed to EuD but are not listed below as they lack preservation sufficient for measurement, see text for more details.

Specimen	Locality	Fm	Biozone	Morph.	TDW	AW	TLW	NCW	TW	CW	TH	CH	TL	CL
127391	V88007	HC	La	ThA	4.900*	–	–	2.380	1.210	–	1.340	–	1.380	–
152394	V93169	HC	La	MeA	18.235*	–	–	–	–	–	–	–	–	–
153100	V99438	Tu	Pu3	EuA	6.400*	3.850	3.850	2.900*	1.330	2.406	1.630	1.579	1.756	1.920
97114‡	C1115	HC	La	EuB	8.53*	4.765	5.120	3.400*	1.705	2.895	1.960	1.945	2.355	2.335*
151991‡	V71203	HC	BCA	EuC	9.520	5.635	5.735	3.820	1.670	3.945	2.680	2.515	3.030	3.310
153023	V74111	Tu	Pu1	EuC	–	–	–	4.015	1.510*	–	2.500*	–	3.160	–
151985	V70201	Tu	BCA	EuD	7.810*	5.295	5.285	–	1.890	3.255	2.175	1.720	2.235	2.495
151944	V65127	Tu	BCA	EuD	8.845*	5.735	6.005	2.190*	2.185	3.655	1.940	2.320	2.230*	2.575*
151946	V65127	Tu	BCA	EuD	8.800*	5.270	6.060	–	1.970	3.255	1.665	2.080	2.185	2.510*
151964‡	V65127	Tu	BCA	EuD	9.225	5.340	5.700	3.550	1.750	3.585	1.645	2.005	2.225	2.380
153036‡	V65127	Tu	BCA	EuD	9.935	5.675	5.850	4.210	1.820	3.800	1.775	2.155	2.470	2.710
218901	V91065	Tu	Pu1	EuE	17.925*	10.685	10.850	7.175*	2.950	7.620	4.575	5.110	6.280	7.525

92928	C1163	Tu	Pu3	EuE	15.030*	9.550	9.700	–	2.640	6.960	4.330	4.580	5.120*	5.320
153089	V72129	Tu	Pu3	EuF	19.415*	17.280	17.395	–	5.480	11.820	6.945	7.280	8.735*	9.670
192678	V72124	Tu	Pu3	EuG	–	–	–	10.300	5.095	–	7.435	–	9.425*	–

Table 3.4. Modern mammalian specimens used in geometric morphometrics analyses. Species list and locomotor references are modified from Chen and Wilson 2015; see text for more details. All specimens are from the UWBM except for those with specimen numbers A2001 and S2008, which are taken from images of specimens in distal view in Argot (2001: fig. 8) and Salton and Sargis (2008: fig. 4.10), respectively. Code number assigned (and table sorted) as follows: clade, order, family, and locomotor mode. Locomotor mode abbreviations are as follows: A, arboreal; F, fossorial; G, gliding; S, saltatorial; Sa, semiaquatic; Sc, scansorial; Sf, semifossorial; T, terrestrial. Other abbreviations: F, female; LM, locomotor mode; M, male; Spec., specimen number; U, sex unknown.

Clade	Order	Code	LM	Genus	Species	Family	Spec.	Sex	Locomotor Reference
Metatheria									
	Dasyuromorphia								
		1	T	*Antechinus*	*swainsonii*	Dasyuridae	68900	M	Nowak 1999
		2	T	*Sarcophilus*	*harrisii*	Dasyuridae	20671	M	Van Valkenburgh 1987
	Didelphimorphia								
		3	A	*Caluromys*	*philander*	Didelphidae	A2001	U	Argot 2001; Nowak 1999
		4	A	*Caluromys*	*derbianus*	Didelphidae	32255	U	Argot 2001
		5	A	*Micoureus*	*demerarae*	Didelphidae	A2001	U	Argot 2001
		6	Sc	*Didelphis*	*virginiana*	Didelphidae	35525	F	Argot 2001
		7	Sc	*Didelphis*	*virginiana*	Didelphidae	74661	M	Argot 2001
		8	Sc	*Didelphis*	*marsupialis*	Didelphidae	A2001	U	Argot 2001; Nowak 1999
		9	Sc	*Marmosa*	*murina*	Didelphidae	A2001	U	Argot 2001; Nowak 1999
		10	T	*Metachirus*	*nudicaudatus*	Didelphidae	35438	F	Argot 2001; Delciellos and Vieira 2006
		11	T	*Monodelphis*	*brevicaudata*	Didelphidae	A2001	U	Argot 2001; Nowak 1999
	Diprotodontia								
		12	G	*Petaurus*	*breviceps*	Petauridae	34181	M	Smith 1973; Nowak 1999; Körtner and Geiser 2000
		13	G	*Petaurus*	*breviceps*	Petauridae	72928	U	Smith 1973; Nowak 1999; Körtner and Geiser 2000
		14	A	*Trichosurus*	*vulpecula*	Phalangeridae	68913	M	Nowak 1999
		15	S	*Potorous*	*tridactylus*	Potoroidae	41025	F	Bassarova et al. 2009
		16	S	*Potorous*	*tridactylus*	Potoroidae	34200	M	Bassarova et al. 2009
		17	S	*Aepyprymnus*	*rufescens*	Potoroidae	68898	F	Bassarova et al. 2009

		18	A	*Pseudocheirus*	*peregrinus*	Pseudocheiridae	68924	F	Bassarova et al. 2009
		19	A	*Pseudocheirus*	*peregrinus*	Pseudocheiridae	68908	M	Bassarova et al. 2009
	Peramelemorphia	20	T	*Perameles*	*nasuta*	Peramelidae	68919	F	Nowak 1999
Eutheria									
	Afrosoricida								
		21	Sa	*Potamogale*	*velox*	Potamogalidae	S2008	U	Nowak 1999; Salton and Sargis 2008
		22	A	*Dendrohyrax*	*arboreus*	Procaviidae	39039	F	Nowak 1999
		23	A	*Dendrohyrax*	*arboreus*	Procaviidae	39038	M	Nowak 1999
		24	Sa	*Limnogale*	*mergulus*	Tenrecidae	S2008	U	Nowak 1999; Salton and Sargis 2008
		25	Sc	*Echinops*	*telfairi*	Tenrecidae	34168	F	Endo et al. 2006; Salton and Sargis 2008
		26	Sc	*Echinops*	*telfairi*	Tenrecidae	S2008	U	Endo et al. 2006; Salton and Sargis 2008
		27	Sf	*Hemicentetes*	*semispinosus*	Tenrecidae	S2008	U	Nowak 1999; Salton and Sargis 2008
		28	Sf	*Oryzorictes*	*sp.*	Tenrecidae	S2008	U	Nowak 1999; Salton and Sargis 2008
		29	T	*Setifer*	*setosus*	Tenrecidae	S2008	U	Salton and Sargis 2008
		30	T	*Tenrec*	*ecaudatus*	Tenrecidae	S2008	U	Salton and Sargis 2008
		31	T	*Microgale*	*cowani*	Tenrecidae	S2008	U	Nowak 1999; Salton and Sargis 2008
		32	T	*Microgale*	*dobsoni*	Tenrecidae	S2008	U	Nowak 1999; Salton and Sargis 2008
		33	T	*Microgale*	*talazaci*	Tenrecidae	S2008	U	Nowak 1999; Salton and Sargis 2008
	Carnivora								
		34	T	*Vulpes*	*vulpes*	Canidae	39490	F	Lariviére and Pasitschniak-Arts 1996; Meachen-Samuels 2010
		35	T	*Vulpes*	*vulpes*	Canidae	39489	M	Lariviére and Pasitschniak-Arts 1996; Meachen-Samuels 2010
		36	Sc	*Urocyon*	*cinereoargenteus*	Felidae	77676	F	Van Valkenburgh 1987; Meachen-Samuels 2010
		37	Sc	*Urocyon*	*cinereoargenteus*	Felidae	35221	M	Van Valkenburgh 1987; Meachen-Samuels 2010
		38	Sc	*Suricata*	*suricatta*	Herpestidae	35470	F	van Staaden 1994; Iwaniuk et al. 1999
		39	Sc	*Suricata*	*suricatta*	Herpestidae	35469	M	van Staaden 1994; Iwaniuk et al. 1999
		40	Sf	*Mephitis*	*mephitis*	Mephitidae	35951	F	Wade-Smith and Verts 1982; Van Valkenburgh 1987; Samuels and Van Valkenburgh 2008
		41	Sf	*Mephitis*	*mephitis*	Mephitidae	39321	M	Wade-Smith and Verts 1982; Van Valkenburgh 1987; Samuels and Van Valkenburgh 2008
		42	Sa	*Lontra*	*canadensis*	Mustelidae	32226	F	Gingerich 2003
		43	Sa	*Lontra*	*canadensis*	Mustelidae	32230	M	Gingerich 2003
		44	Sa	*Mustela*	*vison*	Mustelidae	41780	F	Howell 1930; Lariviére 1999; Gingerich 2003
		45	Sa	*Mustela*	*vison*	Mustelidae	35223	M	Howell 1930; Lariviére 1999; Gingerich 2003
		46	Sc	*Gulo*	*gulo*	Mustelidae	14200	F	Van Valkenburgh 1987; Pasitschniak-Arts and Lariviére 1995
		47	Sc	*Gulo*	*gulo*	Mustelidae	34417	M	Van Valkenburgh 1987; Pasitschniak-Arts and Lariviére 1995
		48	Sf	*Spilogale*	*putorius*	Mustelidae	39331	F	Heinrich and Houde 2006
		49	Sf	*Spilogale*	*putorius*	Mustelidae	39155	M	Heinrich and Houde 2006

	50	T	*Mustela*	*erminea*	Mustelidae	39366	F	Nowak 1999
	51	T	*Mustela*	*erminea*	Mustelidae	72863	M	Nowak 1999
	52	T	*Mustela*	*putorius*	Mustelidae	32599	F	Nowak 1999
	53	T	*Mustela*	*putorius*	Mustelidae	58727	M	Nowak 1999
	54	A	*Paguma*	*larvata*	Viverridae	73281	U	Nowak 1999
Cingulata								
	55	F	*Cabassous*	*centralis*	Dasypodidae	34167	F	Nowak 1999
	56	F	*Dasypus*	*novemcinctus*	Dasypodidae	20735	F	Samuels and Van Valkenburgh 2008
	57	F	*Dasypus*	*novemcinctus*	Dasypodidae	22458	M	Samuels and Van Valkenburgh 2008
	58	F	*Euphractus*	*sexcinctus*	Dasypodidae	35468	M	Redford and Wetzel 1985; Nowak 1999
Eulipotyphla								
	59	T	*Echinosorex*	*gymnurus*	Erinaceidae	S2008	U	Nowak 1999; Salton and Sargis 2008
	60	Sf	*Solenodon*	*paradoxus*	Solenodontidae	S2008	U	Nowak 1999; Salton and Sargis 2008
Lagomorpha								
	61	S	*Brachylagus*	*idahoensis*	Leporidae	38628	F	Nowak 1999
	62	S	*Brachylagus*	*idahoensis*	Leporidae	38631	M	Nowak 1999
	63	S	*Lepus*	*americanus*	Leporidae	21111	F	Nowak 1999
	64	S	*Lepus*	*americanus*	Leporidae	33263	M	Nowak 1999
	65	Sf	*Ochotona*	*princeps*	Ochtonidae	18435	F	Nowak 1999
	66	Sf	*Ochotona*	*princeps*	Ochtonidae	60068	M	Nowak 1999
Macroscelidea								
	67	S	*Petrodromus*	*tetradactylus*	Macroscelididae	S2008	U	Salton and Sargis 2008
	68	T	*Elephantulus*	*rufescens*	Macroscelididae	35475	F	Nowak 1999
	69	T	*Elephantulus*	*rufescens*	Macroscelididae	34189	M	Nowak 1999
Primates								
	70	A	*Callithrix*	*pygmaea*	Cebidae	39003	F	Nowak 1999
	71	A	*Callithrix*	*pygmaea*	Cebidae	39005	M	Nowak 1999
	72	A	*Leontopithecus*	*rosalia*	Cebidae	75541	F	Nowak 1999
	73	A	*Saguinus*	*oedipus*	Cebidae	35406	F	Nyakatura et al. 2008
	74	A	*Saguinus*	*oedipus*	Cebidae	35405	M	Nyakatura et al. 2008
	75	A	*Saimiri*	*sciureus*	Cebidae	82302	F	Nowak 1999
	76	A	*Saimiri*	*sciureus*	Cebidae	39014	M	Nowak 1999
Rodentia								
	77	F	*Aplodontia*	*rufa*	Aplodontiidae	34071	F	Samuels and Van Valkenburgh 2008
	78	F	*Aplodontia*	*rufa*	Aplodontiidae	34058	M	Samuels and Van Valkenburgh 2008
	79	Sa	*Castor*	*canadensis*	Castoridae	34116	F	Nowak 1999
	80	Sa	*Castor*	*canadensis*	Castoridae	34588	M	Nowak 1999
	81	T	*Cavia*	*porcellus*	Caviidae	72830	F	Nowak 1999
	82	T	*Cavia*	*porcellus*	Caviidae	72831	M	Nowak 1999
	83	F	*Microtus*	*pennsylvanicus*	Cricetidae	76622	F	Nowak 1999

	84	F	*Microtus*	*pennsylvanicus*	Cricetidae	34326	M	Nowak 1999
	85	Sa	*Ondatra*	*zibethicus*	Cricetidae	34324	F	Howell 1930; Gingerich 2003
	86	Sa	*Ondatra*	*zibethicus*	Cricetidae	72879	M	Howell 1930; Gingerich 2003
	87	Sf	*Synaptomys*	*borealis*	Cricetidae	66559	F	Nowak 1999
	88	Sf	*Synaptomys*	*borealis*	Cricetidae	66561	M	Nowak 1999
	89	S	*Zapus*	*princeps*	Dipodidae	76721	F	Nowak 1999
	90	S	*Zapus*	*princeps*	Dipodidae	75136	M	Nowak 1999
	91	Sc	*Coendou*	*prehensilis*	Erethizontidae	34176	F	Nowak 1999
	92	F	*Thomomys*	*bottae*	Geomyidae	44624	F	Nowak 1999
	93	F	*Thomomys*	*bottae*	Geomyidae	38261	M	Nowak 1999
	94	F	*Chaetodipus*	*fallax*	Heteromyidae	47378	F	Lackey 1996
	95	F	*Chaetodipus*	*fallax*	Heteromyidae	47379	M	Lackey 1996
	96	S	*Dipodomys*	*deserti*	Heteromyidae	78740	F	Samuels and Van Valkenburgh 2008
	97	Sf	*Octodon*	*degus*	Octodontidae	48984	F	Nowak 1999
	98	Sf	*Octodon*	*degus*	Octodontidae	39501	M	Nowak 1999
	99	A	*Sciurus*	*aberti*	Sciuridae	35278	F	Nowak 1999
	100	A	*Sciurus*	*aberti*	Sciuridae	82349	M	Nowak 1999
	101	A	*Sciurus*	*carolinensis*	Sciuridae	20646	F	Nowak 1999
	102	A	*Sciurus*	*carolinensis*	Sciuridae	30010	M	Nowak 1999
	103	G	*Glaucomys*	*sabrinus*	Sciuridae	36334	F	Samuels and Van Valkenburgh 2008
	104	G	*Glaucomys*	*sabrinus*	Sciuridae	35129	M	Samuels and Van Valkenburgh 2008
	105	G	*Glaucomys*	*volans*	Sciuridae	43897	F	Nowak 1999
	106	G	*Glaucomys*	*volans*	Sciuridae	32254	M	Nowak 1999
	107	Sf	*Cynomys*	*ludovicianus*	Sciuridae	75774	M	Nowak 1999
Scandentia								
	108	Sc	*Tupaia*	*glis*	Tupaiidae	34227	F	Van Valkenburgh 1987
	109	Sc	*Tupaia*	*glis*	Tupaiidae	34225	M	Van Valkenburgh 1987

Table 3.5. Landmark number, location, type, and source reference for two-dimensional geometric morphometrics (2D GM) points on therian distal humeri. All points were digitized on distal images of specimens; see Fig. 3.3 for more details. Numbers in parentheses are the landmark number for the point within the referenced source. Abbreviations: LM, landmark; Type, landmark type according to Zelditch et al. 2004.

LM	Location	Type	Source Reference
1	Lateral point on the posterior trochlea	II	Steiner-Souza et al. 2010
2	Medial point on the posterior trochlea	II	Steiner-Souza et al. 2010
3	Medial point on the anterior trochlea	II	Steiner-Souza et al. 2010
4	Lateral point on the anterior capitulum	II	Steiner-Souza et al. 2010
5	Most lateral point on the ectepicondyle	III	Schutz and Guralnick 2007 (5); Steiner-Souza et al. 2010
6	Most medial point on the entepicondyle	III	Milne et al. 2009 (12); Steiner-Souza et al. 2010

SUPPLEMENTARY MATERIAL FOR

Humeri Morphotype Diversity and Locomotor Function in Latest Cretaceous and Early Paleogene Mammals from Eastern Montana

Table S3.1. Localities containing specimens used in this study. Locality numbers follow the system of each institution; those beginning with "V" are UCMP localities; those beginning with "C" are UWBM localities. All localities are in Montana except for V5620, which is in Wyoming. Abbreviations: Fm, formation; La, Lancian; n, number of specimens from the locality; Pu1, Puercan 1; Pu3, Puercan 3.

Loc. Number	Locality Name	County	Fm	Biozone	n
C0338	Bug Creek A	McCone	Hell Creek	mixed	2
C1115	Celeste's Magnificent Microsite	Garfield	Hell Creek	Lancian	1
C1163	MacDonald	Garfield	Tullock	Pu3	1
C1521	Wake Up	Garfield	Hell Creek	Lancian	1
C1845	Bug Creek	McCone	Hell Creek	mixed	1
V5620	Lull 2	Niobrara	Lance	Lancian	4
V65127	Bug Creek Anthills General	McCone	Hell Creek	mixed	11
V70201	Bug Creek Anthills C	McCone	Hell Creek	mixed	4
V70209	Bug Creek W	McCone	Hell Creek	mixed	4
V71203	Harbicht Hill 1	McCone	Hell Creek	mixed	1
V72129	Garbani 04-Nw-S Level 1	Garfield	Tullock	Pu3	1
V72207	Windy Hill	Garfield	Hell Creek	Lancian	2
V73087	Flat Creek 5	Garfield	Hell Creek	Lancian	1
V73097	Brownie Butte	Garfield	Hell Creek	Lancian	1
V74111	Worm Coulee 1	Garfield	Tullock	Pu1	3
V74122	Biscuit Springs	Garfield	Tullock	Pu3	1
V74124	Yellow Sand Hill 2	Garfield	Tullock	Pu3	1
V84162	Sand Cave	Garfield	Hell Creek	Pu1	1
V84193	Z-Line Quarry	McCone	Hell Creek	Pu1	1
V85092	Kmark II	McCone	Hell Creek	Lancian	1
V87001	O'Connor Site	Fallon	Hell Creek	Lancian	1
V88007	Spigot Bottle	Carter	Hell Creek	Lancian	1
V91065	Capping Channel	Garfield	Tullock	Pu1	1
V93169	Anne's Beast	Garfield	Hell Creek	Lancian	1
V99438	Garbani Sandy Channel	Garfield	Tullock	Pu3	3

Figure S3.1. Histograms illustrating the number of multituberculate (**A**) and therian (**B**) specimens in each biozone. Abbreviations: BCA, Bug Creek Anthills mixed-age assemblage; La, Lancian; Pu1, early Puercan; Pu3; middle-late Puercan. See text for morphotype details.

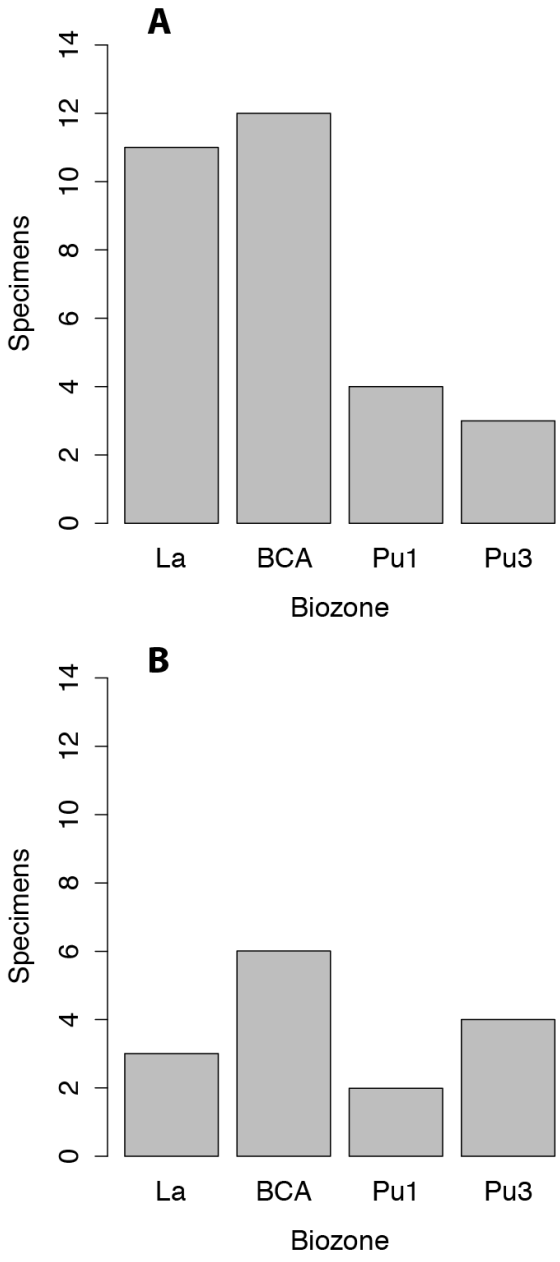

Table S3.2. Comparative multituberculate distal humeri used in this study. We follow the convention of Krause and Jenkins (1983) with regards to prefacing unassociated attributions with a query (e.g., for isolated material). Age data for Late Cretaceous and Paleogene North American taxa are given as NALMAs, respectively; ages of Asian taxa are given as geologic stages. Specimens from the Bug Creek Anthills localities (e.g., Deischl 1964; Krause and Jenkins 1983) are given a "Lancian–Pu1 mixed" age. All families are in the Infraorder Cimolodonta. See text for museum abbreviations.

Specimen Number	Taxon Name	Family	Age	Location	Reference
AMNH 77175	?*Mesodma primaeva*	Neoplagaiulacidae	Judithian	North America	Sahni 1972
AMNH 3011a	?*Meniscoessus conquistus*	Cimolomyidae	Lancian	North America	Cope 1884; Krause and Jenkins 1983
YPM 10612a	?*Meniscoessus robustus* (formerly *Dipriodon lunatus*)	Cimolomyidae	Lancian	North America	Marsh 1889; Krause and Jenkins 1983
MCZ 20786–20789	?*Mesodma* sp.	Neoplagaiulacidae	Lancian–Pu1 mixed	North America	Krause and Jenkins 1983
UMVP 1405	?*Mesodma formosa*	Neoplagaiulacidae	Lancian–Pu1 mixed	North America	Deischl 1964
UMVP 1403, 1406	?*Mesodma thompsoni*	Neoplagaiulacidae	Lancian–Pu1 mixed	North America	Deischl 1964
UMVP 1404	?*Cimexomys minor*	Neoplagaiulacidae	Lancian–Pu1 mixed	North America	Deischl 1964
UMVP 1407	?*Stygimys kuszmauli*	Eucosmodontidae	Lancian–Pu1 mixed	North America	Deischl 1964; Krause and Jenkins 1983
UA 11994	?*Stygimys kuszmauli*	Eucosmodontidae	Lancian–Pu1 mixed	North America	Krause and Jenkins 1983
MCZ 19529	?*Catopsalis*	Taeniolabididae	Lancian–Pu1 mixed	North America	Jenkins 1973
AMNH 3036	?*Taeniolabis taoensis*	Taeniolabididae	Puercan	North America	Sloan 1981
Cope 1884: Fig. 4b	*Taeniolabis taoensis* (formerly *Polymastodon taoensis*)	Taeniolabididae	Puercan	North America	Cope 1884
IVPP V8408, V9051	?*Lambdopsalis bulla*	Taeniolabididae	Late Paleocene	Asia	Kielan-Jaworowska and Qi 1990
USNM 9735	?*Ptilodus montanus*	Ptilodontidae	Torrejonian	North America	Krause and Jenkins 1983
USNM 6076	*Ptilodus montanus*	Ptilodontidae	Torrejonian	North America	Gidley 1909; Krause and Jenkins 1983
UA 9001	*Ptilodus kummae*	Ptilodontidae	Tiffanian	North America	Krause and Jenkins 1983
UA 11300	?*Ptilodus kummae*	Ptilodontidae	Tiffanian	North America	Krause and Jenkins 1983
UALVP 42816	*Microcosmodon conus*	Microcosmodontidae	Tiffanian	North America	Fox 2005
GISPS 8–2 PST	*Tugrigbaatar saichanensis*	Djadochtatheriidae	Campanian	Asia	Kielan-Jaworowska and Dashzeveg 1978
PSS-MAE 103	*Kryptobaatar dashzevegi*	Djadochtatheriidae	Campanian	Asia	Sereno 2006
PM 120/107	*Catopsbaatar catopsaloides*	Djadochtatheriidae	Campanian	Asia	Hurum and Kielan-Jaworowska 2008
URBAC 03-076	Multituberculata		Turonian	Asia	Chester et al. 2010
AMNH 118267	Multituberculata		Lancian–Pu1 mixed	North America	Kielan-Jaworowska and Gambaryan 1994

Table S3.3. Comparative therian fossils specimens used in this study. List of fossil specimens used for comparative study. We follow the convention of Krause and Jenkins with regards to prefacing unassociated attributions with a query (e.g., for isolated material). Age data for Late Cretaceous and Paleogene North and South American taxa are given as NALMAs and SALMAs, respectively; ages of European taxa are given as geologic stages. Specimens from the Bug Creek Anthills localities (e.g., Szalay and Dagosto 1980; Boyer et al. 2010) are given a "Lancian–Pu1 mixed" age. See text for museum abbreviations.

Specimen Number	Taxon Name	Higher Taxon	Family	Age	Location	References
Marsh 1889: Plate V, figs. 5-6	*Didelphodon vorax*	Didelphimorphia	Stagodontidae	Lancian	North America	Marsh 1889
MHNC 1249	*Mayulestes ferox*	Didelphimorphia	Mayulestidae	Tiupampan	South America	Muizon 1998
YPFB 6105, 6106, 6110, 6111	*Pucadelphys andinus*	Didelphimorphia	Didelphidae	Tiupampan	South America	Marshall et al. 1995
AMNH 118456	?*Procerberus formicarum*		Cimolestidae	Lancian–Pu1 mixed	North America	Boyer et al. 2010
UMVP 1837	?*Procerberus formicarum*		Cimolestidae	Lancian–Pu1 mixed	North America	Szalay and Dagosto 1980
UM 88105	?*Prodiacodon tauricinerei*	Leptictida	Leptictidae	Wasatchian	North America	Rose 1999
AMNH 16614	*Protoselene opisthacus*	archaic ungulate	Hyopsodontidae	Torrejonian	North America	Matthew 1937
NMMNH P-20949	*Tetraclaenodon puercensis*	archaic ungulate	Phenacodontidae	Torrejonian	North America	Kondrashov and Lucas 2012
AMNH 119994	?*Protungulatum donnae*	archaic ungulate	Arctocyonidae	Lancian–Pu1 mixed	North America	Boyer et al. 2010
UM 1836	?*Protungulatum donnae*	archaic ungulate	Arctocyonidae	Lancian–Pu1 mixed	North America	Szalay and Dagosto 1980
AMNH 16343	*Loxolophus hyattianus*	archaic ungulate	Artocyonidae	Puercan	North America	Matthew 1937
AMNH 16543	*Arctocyon corrugatus (*formerly *Claenodon corrugatus)*	archaic ungulate	Artocyonidae	Torrejonian	North America	Matthew 1937
AMNH 16591	*Chriacus sp.*	archaic ungulate	Artocyonidae	Torrejonian	North America	Matthew 1937
MNHN.F.CR17, MNHN.F.CR16	*Arctocyon primaevus*	archaic ungulate	Artocyonidae	Thanetian	Europe	Russell 1964; Argot 2013
USGS 2353	*Chriacus* sp.	archaic ungulate	Artocyonidae	Wasatchian	North America	Rose 1987; O'Leary and Rose 1995
AMNH 16500	*Ectoconus ditrigonus (*formerly *E. majusculus)*	archaic ungulate	Periptychidae	Puercan	North America	Matthew 1937

UNM-B029	*Mithrandir gillianus* (formerly *Gillisonchus gillianus)*	archaic ungulate	Periptychidae	Puercan	North America	Rigby 1981
AMNH 3636	?*Periptychus carinidens* (formerly *P. rhabdodon)*	archaic ungulate	Periptychidae	Torrejonian	North America	Matthew 1937
AMNH 17075	?*Periptychus carinidens* (formerly *P. rhabdodon)*	archaic ungulate	Periptychidae	Torrejonian	North America	Matthew 1937
USGS 2352	*Diacodexis metsiacus*	Artiodactyla	Diacodexeidae	Wasatchian	North America	Rose 1982
UALVP 49114	*Pronothodectes gaoi*	"Plesiadapiformes"	Plesiadapidae	Tiffanian	North America	Boyer et al. 2010
AMNH 17379	?*Nannodectes gidleyi (*formerly *Plesiadapis gidleyi)*	"Plesiadapiformes"	Plesiadapidae	Tiffanian	North America	Simpson 1935
UM 64588	*Plesiadapis rex*	"Plesiadapiformes"	Plesiadapidae	Tiffanian	North America	Boyer et al. 2010
MNHN BR 3L and B4L	*Plesiadapis tricuspidens*	"Plesiadapiformes"	Plesiadapidae	Thanetian	Europe	Szalay et al. 1975
UM 87990	*Plesiadapis cookei*	"Plesiadapiformes"	Plesiadapidae	Clarkforkian	North America	Bloch et al. 2007
UM 108210 and 82606	*Ignacius clarkforkensis*	"Plesiadapiformes"	Paramomyidae	Clarkforkian	North America	Bloch et al. 2007
UM 101963	*Carpolestes simpsoni*	"Plesiadapiformes"	Carpolestidae	Clarkforkian	North America	Bloch and Boyer 2002
AMNH 2549	*Pantolambda bathmodon*	Pantodonta		Torrejonian	North America	Matthew 1937
AMNH 16663	*Pantolambda bathmodon*	Pantodonta		Torrejonian	North America	Matthew 1937
AMNH 16410	*Onychodectes tisonensis*	Taeniodonta	Conoryctidae	Puercan	North America	Schoch 1986
TMM 41364-1	*Psittacotherium multifragum*	Taeniodonta	Stylinodontidae	Torrejonian	North America	Schoch 1986
FMNH P 26090	*Ectoganus gliriformis*	Taeniodonta	Stylinodontidae	Tiffanian-Clarkforkian	North America	Schoch 1986
FMNH P 26083	*Ectoganus lobdelli (*formerly *Lampadophorus expectatus)*	Taeniodonta	Stylinodontidae	Tiffanian-Clarkforkian	North America	Schoch 1986
YPM 27201	*Ectoganus* sp.	Taeniodonta	Stylinodontidae	Wasatchian	North America	Schoch 1986
YPM 11096	*Stylinodon mirus*	Taeniodonta	Stylinodontidae	Bridgerian	North America	Schoch 1986
AMNH 16610	Deltherium	Tillodontia	Deltatheriidae	Torrejonian	North America	Matthew 1937
PU 14389	Theria indet.			Fort Union Formation	North America	Jenkins 1973
LSUMG V-802	Theria indet.			Puercan	North America	Standhardt 1986

Table S3.4. Intraobserver error results. We performed five trials in which we plotted all six landmarks (LMs) on five specimens for each trial. Specimens were chosen to represent the overall variation in the study (i.e., at the maxima and minima of PC1 and PC2, see Fig. S3.11). We report the variances for each LM placement for each specimen across the five trials, as well as the mean variance across all LMs for a single specimen, and the mean variance across all specimens for a single LM. See Table S3.5 for F test comparison of differences in variance across all LMs. We report the genus and species, sex (in parentheses), and specimen number for each specimen used in this repeatability study. The specimen for *Caluromys philander* was taken from Argot (2001: fig. 8) and lacks sex information; see Methods. Specimen ID Numbers used in this study are the same throughout; see Table 4 for additional specimen information.

	Specimen Number	ID Number	LM1	LM2	LM3	LM4	LM5	LM6	Mean of Variances Across LMs
***Cavia porcellus* (F)**	UWBM 72830	80	5.453E-04	1.599E-04	1.096E-05	6.610E-05	1.795E-04	4.135E-05	1.672E-04
***Caluromys philander* (NA)**	Argot 2001: fig. 8	3	3.751E-05	4.613E-05	9.017E-05	2.406E-05	2.586E-05	6.837E-05	4.868E-05
***Dipodomys deserti* (F)**	UWBM 78740	95	7.200E-05	1.451E-05	3.171E-05	8.272E-05	1.913E-04	6.401E-06	6.643E-05
***Lepus americanus* (F)**	UWBM 21111	62	8.579E-06	4.393E-05	2.749E-04	1.938E-05	4.885E-05	5.885E-04	1.640E-04
***Mustela erminea* (M)**	UWBM 72863	51	9.250E-05	1.794E-04	3.547E-05	1.169E-05	7.590E-05	6.506E-05	7.668E-05
Mean of Variances Across Specimens			1.512E-04	8.878E-05	8.864E-05	4.079E-05	1.043E-04	1.539E-04	

Table S3.5. Results from F tests of variances pairwise across all landmarks. Specimens are those used in the repeatability study for measurement error (Table S3.4), variances were calculated across euclidean distances from the centroid for each landmark (LM), and across all five trials for a single specimen. P-values are reported for each pairwise F test, with significance as follows: * for $p < 0.05$; ** for $p < 0.01$.

		LM1	LM2	LM3	LM4	LM5	LM6
Cavia porcellus							
	LM1	–	0.262	**	0.065	0.307	*
	LM2	0.262	–	*	0.413	0.913	0.219
	LM3	**	*	–	0.110	*	0.227
	LM4	0.065	0.413	0.110	–	0.357	0.661
	LM5	0.307	0.913	*	0.357	–	0.184
	LM6	*	0.219	0.227	0.661	0.184	–
Caluromys philander							
	LM1	–	0.846	0.416	0.677	0.727	0.575
	LM2	0.846	–	0.532	0.544	0.589	0.712
	LM3	0.416	0.532	–	0.229	0.254	0.795
	LM4	0.677	0.544	0.229	–	0.946	0.336
	LM5	0.727	0.589	0.254	0.946	–	0.369
	LM6	0.575	0.712	0.795	0.336	0.369	–
Dipodomys deserti							
	LM1	–	0.150	0.447	0.896	0.367	*
	LM2	0.150	–	0.468	0.120	*	0.447
	LM3	0.447	0.468	–	0.376	0.110	0.150
	LM4	0.896	0.120	0.376	–	0.437	*
	LM5	0.367	*	0.110	0.437	–	**
	LM6	*	0.447	0.150	*	**	–
Lepus americanus							
	LM1	–	0.143	**	0.449	0.121	**
	LM2	0.143	–	0.103	0.447	0.921	*
	LM3	**	0.103	–	*	0.123	0.479
	LM4	0.449	0.447	*	–	0.392	**
	LM5	0.121	0.921	0.123	0.392	–	*
	LM6	**	*	0.479	**	*	–
Mustela erminea							
	LM1	–	0.537	0.376	0.070	0.853	0.741
	LM2	0.537	–	0.145	*	0.425	0.350
	LM3	0.376	0.145	–	0.308	0.479	0.571
	LM4	0.070	*	0.308	–	0.097	0.125
	LM5	0.853	0.425	0.479	0.097	–	0.885
	LM6	0.741	0.350	0.571	0.125	0.885	–

Table S3.6. Means, standard deviations, and percent preservation for multituberculate measurements by morphotype. We include all specimens except for the two specimens tentatively attributed to morphotype MuA (i.e., ?MuA), see text for more details. See Table 3.1 for measurement descriptions; see Table 3.2 for data (data excludes minimum values). NA indicates no specimens preserved the measurement (i.e., NA for means) or only one specimen preserved the measurement (i.e., NA for SD). Bold values indicate specimen percent preservation (i.e., the number of specimens that preserve that measurement divided by the total number of specimens in the morphotype) greater than or equal to 80%. We calculate the coefficient of variation (CV) for morphotypes containing more than two specimens. Abbreviations: CV, coefficient of variation; n, number of specimens; SD, standard deviation.

	TDW	AW	TLW	NCW	UCW	RCW	UCH	RCH	UCL	RCL
Full Dataset (n= 28)										
Mean	6.86	3.55	4.09	2.05	1.68	2.27	2.65	2.48	2.92	2.80
SD	3.86	1.95	2.33	1.02	0.90	1.32	1.46	1.55	1.64	1.44
% Preservation	39.29	57.14	57.14	53.57	**89.29**	71.43	**89.29**	78.57	**89.29**	67.86
MuA (n= 8)										
Mean	3.884	2.025	2.485	1.185	0.874	1.125	1.363	1.136	1.480	1.494
SD	0.187	0.093	0.140	0.135	0.096	0.083	0.085	0.081	0.121	0.069
% Preservation	62.50	75.00	**87.50**	62.50	**100.00**	75.00	**100.00**	**87.50**	**100.00**	62.50
CV	0.048	0.046	0.056	0.114	0.110	0.073	0.063	0.071	0.082	0.046
MuB (n= 1)										
Mean	NA	NA	NA	1.240	1.080	NA	1.465	NA	1.670	NA
SD	NA	NA	NA	NA	NA	NA	NA	NA	NA	NA
% Preservation	0.00	0.00	0.00	**100.00**	**100.00**	0.00	**100.00**	0.00	**100.00**	0.00
MuC (n= 7)										
Mean	5.875	2.933	3.726	1.640	1.386	1.634	2.200	1.803	2.409	2.226
SD	0.827	0.232	0.400	0.277	0.254	0.246	0.205	0.129	0.252	0.192
% Preservation	28.57	71.43	71.43	42.86	**85.71**	**85.71**	**100.00**	**85.71**	**100.00**	**85.71**
CV	0.141	0.079	0.107	0.169	0.183	0.151	0.093	0.072	0.105	0.086
MuD (n= 1)										
Mean	NA	NA	NA	NA	NA	2.160	NA	2.135	NA	2.350
SD	NA	NA	NA	NA	NA	NA	NA	NA	NA	NA
% Preservation	0.00	0.00	0.00	0.00	0.00	**100.00**	0.00	**100.00**	0.00	**100.00**
MuE (n= 5)										

Mean	8.275	4.213	5.155	2.475	1.933	2.488	3.076	2.375	3.416	3.053
SD	0.205	0.265	0.106	0.108	0.314	0.110	0.393	0.156	0.337	0.337
% Preservation	40.00	40.00	40.00	60.00	**100.00**	40.00	**80.00**	40.00	**80.00**	60.00
CV	0.025	0.063	0.021	0.044	0.162	0.044	0.128	0.066	0.099	0.110
MuF (n= 6)										
Mean	13.865	7.192	9.548	3.740	3.174	4.334	5.221	4.826	5.777	5.220
SD	0.226	0.467	0.626	0.420	0.526	0.461	0.282	0.639	0.660	0.928
% Preservation	33.33	50.00	33.33	50.00	**83.33**	**83.33**	**83.33**	**100.00**	**83.33**	66.67
CV	0.016	0.065	0.066	0.112	0.166	0.106	0.054	0.133	0.114	0.178

Table S3.7. Means, standard deviations, and percent preservation for therian measurements by morphotype. We include all specimens except for the specimen in morphotype MeA, which lacked any measureable features. See Table 3.1 for measurement descriptions; see Table 3.3 for data (data excludes minimum values). NA indicates no specimens preserved the measurement (i.e., NA for means) or only one specimen preserved the measurement (i.e., NA for SD). Bold values indicate specimen percent preservation (i.e., the number of specimens that preserve that measurement divided by the total number of specimens in the morphotype) greater than or equal to 80%. We calculate the coefficient of variation (CV) for morphotypes containing more than two specimens (i.e., only EuD). Abbreviations: CV, coefficient of variation; n, number of specimens; SD, standard deviation.

	TDW	AW	TLW	NCW	TW	CW	TH	CH	TL	CL
Full Dataset (n = 14)										
Mean	9.560	7.189	7.414	4.713	2.438	4.836	3.084	3.026	2.708	4.416
SD	0.357	3.926	3.888	2.812	1.351	2.838	2.084	1.824	1.360	2.836
% Preservation	21.43	78.57	78.57	42.86	**92.86**	78.57	**92.86**	78.57	71.43	57.14
EuA (n = 1)										
Mean	NA	3.850	3.850	NA	1.330	2.406	1.630	1.579	1.756	1.920
SD	NA	NA	NA	NA	NA	NA	NA	NA	NA	NA
% Preservation	0.00	**100.00**	**100.00**	0.00	**100.00**	**100.00**	**100.00**	**100.00**	**100.00**	**100.00**
EuB (n = 1)										
Mean	NA	4.765	5.120	NA	1.705	2.895	1.960	1.945	2.355	NA
SD	NA	NA	NA	NA	NA	NA	NA	NA	NA	NA
% Preservation	0.00	**100.00**	**100.00**	0.00	**100.00**	**100.00**	**100.00**	**100.00**	**100.00**	0.00
EuC (n = 2)										
Mean	9.520	5.635	5.735	3.918	1.670	3.945	2.680	2.515	3.095	3.310
SD	NA	NA	NA	0.138	NA	NA	NA	NA	0.092	NA
% Preservation	50.00	50.00	50.00	**100.00**	50.00	50.00	50.00	50.00	**100.00**	50.00
EuD (n = 5)										
Mean	9.580	5.463	5.780	3.880	1.923	3.510	1.840	2.056	2.279	2.528
SD	0.502	0.223	0.310	0.467	0.168	0.245	0.221	0.221	0.129	0.168
% Preservation	40.00	**100.00**	**100.00**	40.00	**100.00**	**100.00**	**100.00**	**100.00**	**80.00**	60.00
CV	0.052	0.041	0.054	0.120	0.087	0.070	0.120	0.108	0.057	0.066
EuE (n = 2)										
Mean	NA	10.118	10.275	NA	2.795	7.290	4.453	4.845	6.280	6.423

SD	NA	0.803	0.813	NA	0.219	0.467	0.173	0.375	NA	1.559
% Preservation	0.00	**100.00**	**100.00**	0.00	**100.00**	**100.00**	**100.00**	**100.00**	50.00	**100.00**
EuF (n = 1)										
Mean	NA	17.280	17.395	NA	5.480	11.820	6.945	7.280	NA	9.670
SD	NA	NA	NA	NA	NA	NA	NA	NA	NA	NA
% Preservation	0.00	**100.00**	**100.00**	0.00	**100.00**	**100.00**	**100.00**	**100.00**	0.00	**100.00**
EuG (n = 1)										
Mean	NA	NA	NA	10.300	5.095	NA	7.435	NA	NA	NA
SD	NA	NA	NA	NA	NA	NA	NA	NA	NA	NA
% Preservation	0.00	0.00	0.00	**100.00**	**100.00**	0.00	**100.00**	0.00	0.00	0.00
ThA (n = 1)										
Mean	NA	NA	NA	2.380	1.210	NA	1.340	NA	1.380	NA
SD	NA	NA	NA	NA	NA	NA	NA	NA	NA	NA
% Preservation	0.00	0.00	0.00	**100.00**	**100.00**	0.00	**100.00**	0.00	**100.00**	0.00

Table S3.8. The results of One-Way ANOVAs of difference for all multituberculate measurements across all morphotypes. Asterisks (****) indicate significant p-values (< 0.0001). Both biozone (b) and residuals (r) values are given for Sum of Squares, df, and Mean Squares. See Table 3.1 for measurement details; see Table 3.3 for data.

	TDW		AW		TLW		NCW		UCW		RCW		UCH		RCH		UCL		RCL	
	b	r	b	r	b	r	b	r	b	r	b	r	b	r	b	r	b	r	b	r
Sum of Squares	148.368	0.918	56.520	0.764	80.532	1.160	14.012	0.603	17.551	1.889	31.699	1.198	49.847	1.083	48.562	2.192	61.774	2.568	34.327	3.012
df	3	7	3	12	3	12	4	10	4	20	4	15	4	20	4	17	4	20	4	14
Mean Squares	49.456	0.131	18.840	0.064	26.844	0.097	3.503	0.060	4.388	0.094	7.925	0.080	12.462	0.054	12.141	0.129	15.444	0.128	8.582	0.215
F	377.07		295.97		277.59		58.10		46.45		99.19		230.16		94.17		120.27		39.89	
p-value	****		****		****		****		****		****		****		****		****		****	

Table S3.9. Probabilities from Tukey honest significant difference (HSD) post hoc test of multituberculate measurements by morphotype. All measurements had significant ANOVA results, and therefore all measurements were subjected to the Tukey HSD test and have results below. Significance indicated by the following: * for $p < 0.05$; ** for $p < 0.01$; *** for $p < 0.001$; **** for $p < 0.0001$. NA indicates the morphotype did not include that particular measurement and therefore could not be subjected to ANOVA or Tukey tests.

Measurement		MuA	MuB	MuC	MuD	MuE	MuF
TDW	**MuA**	–	NA	**	NA	****	****
	MuB	NA	–	NA	NA	NA	NA
	MuC	**	NA	–	NA	**	****
	MuD	NA	NA	NA	–	NA	NA
	MuE	****	NA	**	NA	–	****
	MuF	****	NA	****	NA	****	–
AW	**MuA**	–	NA	***	NA	****	****
	MuB	NA	–	NA	NA	NA	NA
	MuC	***	NA	–	NA	***	****
	MuD	NA	NA	NA	–	NA	NA
	MuE	****	NA	***	NA	–	****
	MuF	****	NA	****	NA	****	–
TLW	**MuA**	–	NA	***	NA	****	****
	MuB	NA	–	NA	NA	NA	NA
	MuC	***	NA	–	NA	***	****
	MuD	NA	NA	NA	–	NA	NA
	MuE	****	NA	***	NA	–	****
	MuF	****	NA	****	NA	****	–
NCW	**MuA**	–	1.000	0.158	NA	***	****
	MuB	1.000	–	0.635	NA	**	****
	MuC	0.158	0.635	–	NA	*	****
	MuD	NA	NA	NA	–	NA	NA
	MuE	***	**	*	NA	–	***
	MuF	****	****	****	NA	***	–
UCW	**MuA**	–	0.968	*	NA	***	****
	MuB	0.968	–	0.885	NA	0.123	****
	MuC	*	0.885	–	NA	0.056	****
	MuD	NA	NA	NA	–	NA	NA
	MuE	***	0.123	0.056	NA	–	****

	MuF	****	****	****	NA	****	–
RCW	**MuA**	–	NA	*	*	***	****
	MuB	NA	–	NA	NA	NA	NA
	MuC	*	NA	–	0.451	*	****
	MuD	*	NA	0.451	–	0.874	****
	MuE	***	NA	*	0.874	–	****
	MuF	****	NA	****	****	****	–
UCH	**MuA**	–	0.993	****	NA	****	****
	MuB	0.993	–	0.054	NA	****	****
	MuC	****	0.054	–	NA	***	****
	MuD	NA	NA	NA	–	NA	NA
	MuE	****	****	***	NA	–	****
	MuF	****	****	****	NA	****	–
RCH	**MuA**	–	NA	*	0.114	**	****
	MuB	NA	–	NA	NA	NA	NA
	MuC	*	NA	–	0.908	0.329	****
	MuD	0.114	NA	0.908	–	0.981	****
	MuE	**	NA	0.329	0.981	–	****
	MuF	****	NA	****	****	****	–
UCL	**MuA**	–	0.986	***	NA	****	****
	MuB	0.986	–	0.335	NA	**	****
	MuC	***	0.335	–	NA	**	****
	MuD	NA	NA	NA	–	NA	NA
	MuE	****	**	**	NA	–	****
	MuF	****	****	****	NA	****	–
RCL	**MuA**	–	NA	0.123	0.473	**	****
	MuB	NA	–	NA	NA	NA	NA
	MuC	0.123	NA	–	0.999	0.141	****
	MuD	0.473	NA	0.999	–	0.688	***
	MuE	**	NA	0.141	0.688	–	***
	MuF	****	NA	****	***	***	–

Figure S3.2. Boxplots for all multituberculate measurement with significant ANOVA results according to morphotype. Boxplots include minimum, quartiles, median, and maximum values. See Table 3.1 for measurements, Table 3.2 for data, and Tables S3.8 and S3.9 for ANOVA and Tukey HSD results, respectively. Specimens tentatively attributed to morphotype MuA (i.e., ?MuA), were not included in ANOVA and Tukey tests.

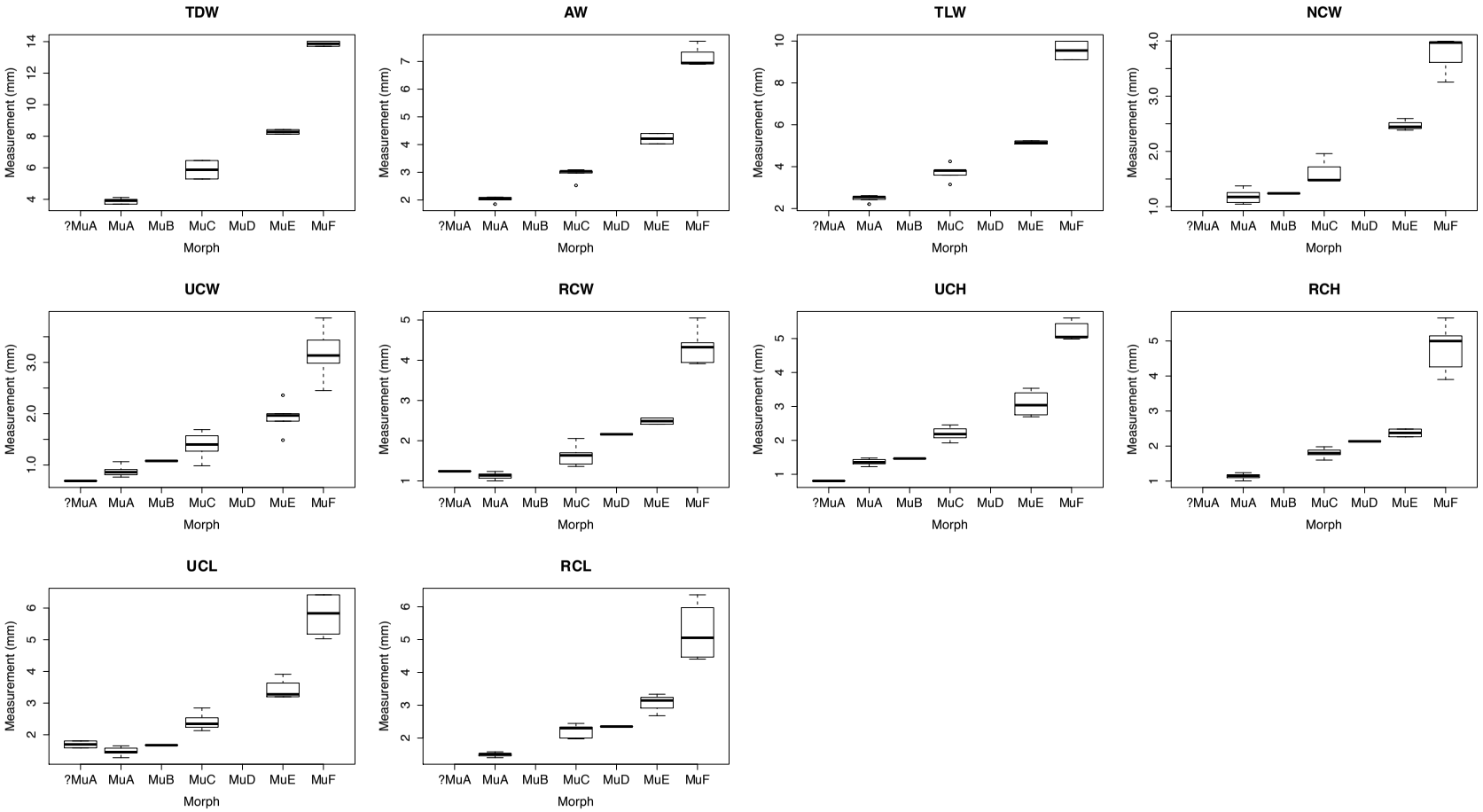

Figure S3.3. Variances for all multituberculate measurement with significant ANOVA results according to morphotype. See Figure S3.2 for means, maxima, minima, and quartiles. See Table 3.1 for measurements, Table 3.2 for data, and Tables S3.8 and S3.9 for ANOVA and Tukey HSD results, respectively.

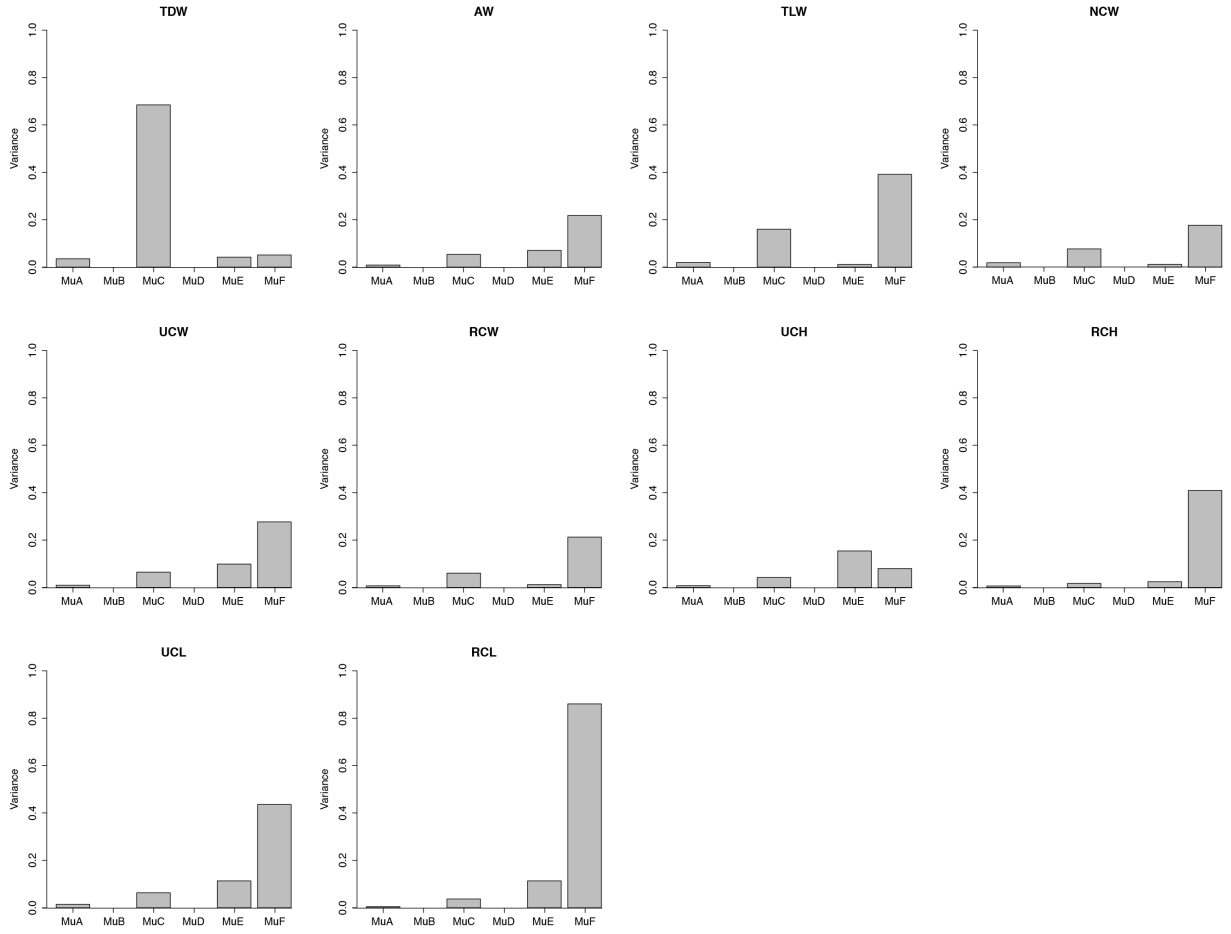

Figure S3.4. Principal Components 1 and 2 on the full set of variables (i.e., measurements; excluding TDW, AW, and TLW; n = 10 specimens). All measurements are standardized to (i.e., "relative to") RCW. The first and second principal components explain 60% and 20% of the variation, respectively. See Table S3.10 for all principal component loadings and variances. Plotted multituberculate morphotypes include: MuA (blue), MuC (red), MuE (orange), and MuF (green). See Table 3.1 for measurements, and Table 3.2 for data.

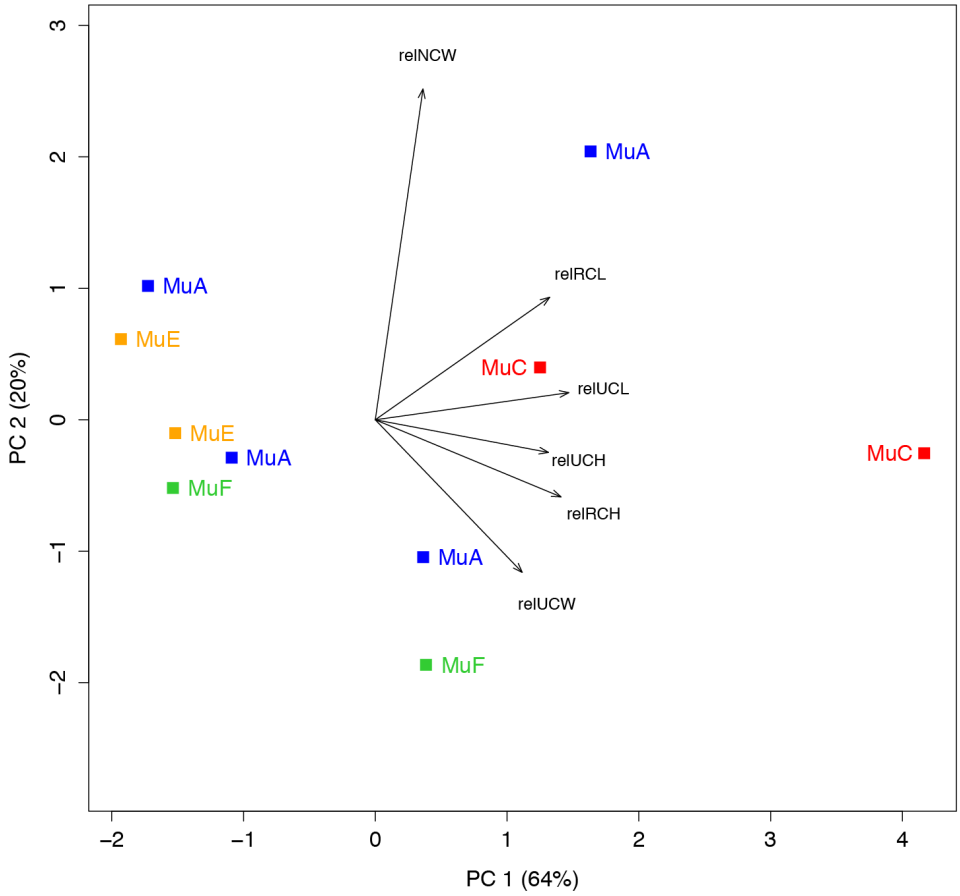

Table S3.10. Measurement loading and variance results of Principal Components Analysis on linear measurements of multituberculate specimens from our assemblage (n = 10). Measurements include NCW, RCH, RCL, UCH, UCL, and UCW, all standardized to RCW (Table 3.1; Fig. S3.4). Loadings in bold represent dominant loadings for each principal component (i.e., values greater than (1/(number of columns)^2).

	PC1	PC2	PC3	PC4	PC5	PC6
Loadings						
relUCL	**0.490**	0.069	0.120	0.354	-0.130	**0.774**
relRCH	**0.470**	-0.196	-0.096	-0.236	**0.822**	-0.019
relRCL	**0.441**	0.311	-0.206	**0.597**	-0.044	**-0.556**
relUCH	**0.438**	-0.083	**-0.537**	**-0.527**	**-0.485**	-0.027
relNCW	0.121	**0.839**	0.329	**-0.413**	0.050	-0.004
relUCW	0.372	-0.387	**0.733**	-0.122	-0.261	-0.303
Variance						
Percent Variance	0.637	0.199	0.085	0.048	0.022	0.009
Cumulative Variance	0.637	0.836	0.921	0.969	0.991	1.000

Figure S3.5. Principal Components 1 and 2 on measurements NCW, RCH, UCH, and UCW, and standardized to (i.e., "relative to") RCW. The first and second principal components explain 61% and 23% of the variation, respectively. See Table S3.11 for all principal component loadings and variances. Plotted multituberculate morphotypes include: MuA (blue), MuC (red), MuE (orange), and MuF (green). This dataset is similar to that of Fig. S3.6 but excludes measurement RCL and includes one additional specimen (n = 11). See Table 3.1 for measurements, and Table 3.2 for data.

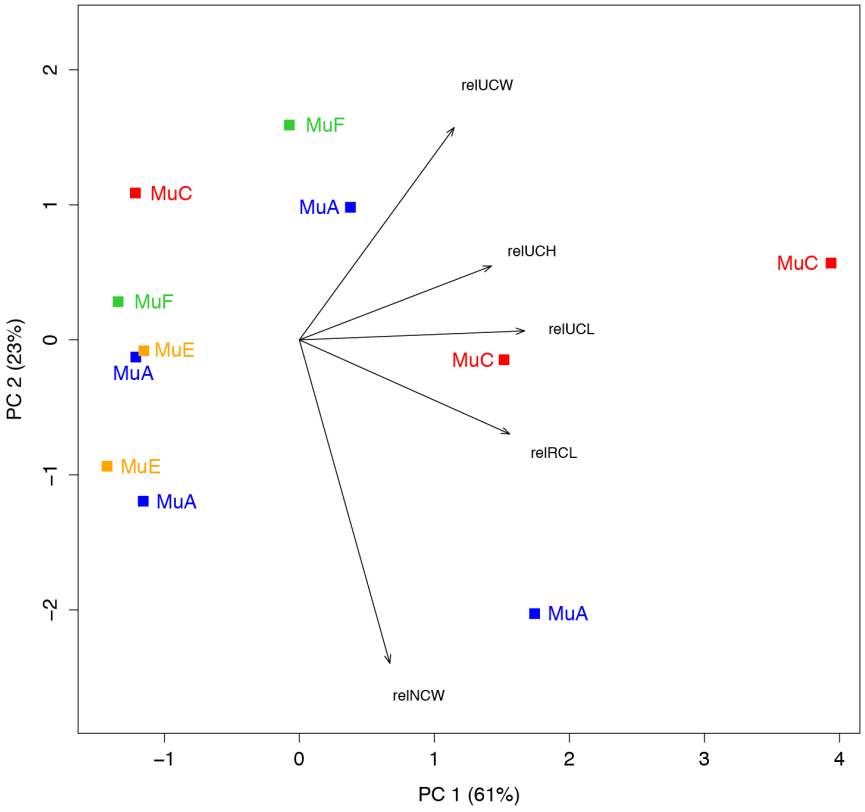

Table S3.11. Measurement loading and variance results of Principal Components Analysis on linear measurements of multituberculate specimens from our assemblage (n = 11). Measurements include NCW, RCL, UCH, UCL, and UCW, all standardized to RCW (Table 3.1; Fig. S3.5). Loadings in bold represent dominant loadings for each principal component.

	PC1	PC2	PC3	PC4	PC5
Loadings					
relUCL	**0.556**	0.022	0.092	-0.309	**-0.766**
relRCL	**0.519**	-0.232	-0.201	**-0.557**	**0.571**
relUCH	**0.474**	0.183	**-0.602**	**0.615**	0.030
relNCW	0.223	**-0.798**	0.366	0.423	0.012
relUCW	0.382	**0.524**	**0.674**	0.196	0.294
Variance					
Percent Variance	0.608	0.231	0.099	0.052	0.010
Cumulative Variance	0.608	0.839	0.938	0.990	1.000

Figure S3.6. Principal Components 1 and 2 on measurements NCW, RCH, UCH, and UCW, and standardized to ("relative to") RCW, see Table 3.1 for measurements. The first and second principal components explain 44% and 24% of the variation, respectively. See Table S3.12 for all principal component loadings and variances. Plotted multituberculate morphotypes include: MuA (blue), MuC (red), MuE (orange), and MuF (green; Table 3.2); published specimens include: ?*Cimexomys minor*, UMVP 1404 (Deischl 1964); *Microcosmodon conus*, UALVP 42816 (Fox 2005); *Mesodma formosa*, UMVP 1405 (Deischl 1964); *M. thompsoni* (A), UMVP 1406 (Deischl 1964); *M. thompsoni* (B), UMVP 1403 (Deischl 1964); Multituberculata, AMNH 118267 (Kielan-Jaworowska and Gambaryan 1994); *Stygimys kuszmauli* (C), UA 11994 (Krause and Jenkins 1983); and *S. kuszmauli* (D), UMVP 1407 (Deischl 1964; Krause and Jenkins 1983); see Table S3.2 for additional details on published material.

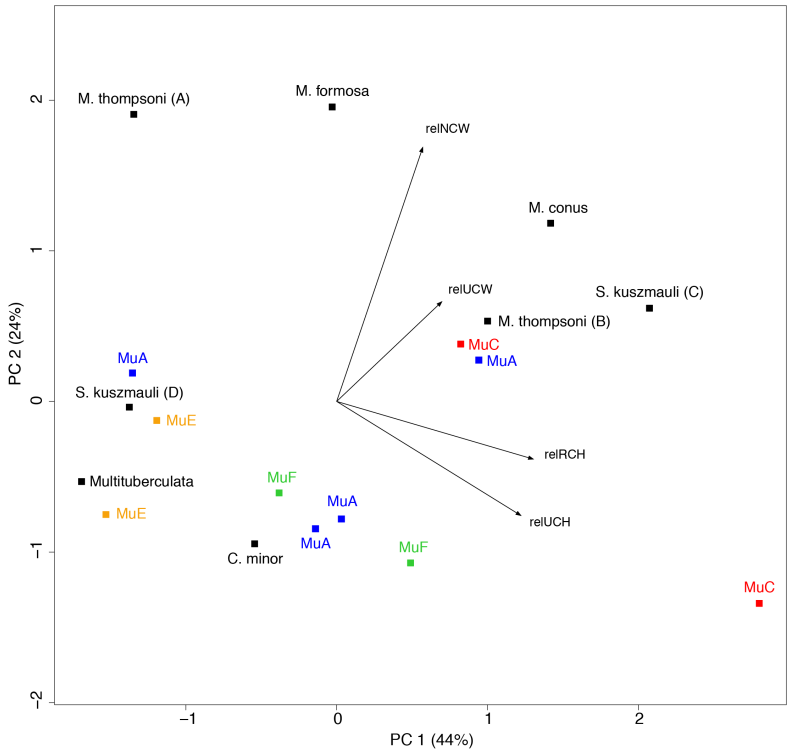

Table S3.12. Measurement loading and variance results of Principal Components Analysis on linear measurements of multituberculate specimens. Measurements include NCW, RCH, UCH, and UCW, all standardized to RCW (Table 3.1; Fig. S3.6). Specimens include nine specimens from our assemblage and seven specimens from the published literature (see Fig. S3.6 for more details). Loadings in bold represent dominant loadings for each principal component.

	PC1	PC2	PC3	PC4
Loadings				
relRCH	**0.652**	-0.191	-0.100	**-0.727**
relUCH	**0.610**	-0.379	-0.182	**0.672**
relNCW	0.285	**0.843**	-0.446	0.095
relUCW	0.348	0.331	**0.871**	0.106
Variance				
Percent Variance	0.435	0.238	0.224	0.103
Cumulative Variance	0.435	0.673	0.897	1.000

Table S3.13. The results of One-Way ANOVAs of difference for all therians measurements across all morphotypes. Significance indicated by the following: * for $p < 0.05$; ** for $p < 0.01$; *** for $p < 0.001$; **** for $p < 0.0001$. Both biozone (b) and residuals (r) values are given for Sum of Squares, df, and Mean Squares. See Table 3.1 for measurement details; see Table 3.3 for data.

	TDW		AW		TLW		NCW		UCW		RCW		UCH		RCH		UCL		RCL	
	b	r	b	r	b	r	b	r	b	r	b	r	b	r	b	r	b	r	b	r
Sum of Squares	0.002	0.252	153.315	0.844	150.124	1.047	39.311	0.237	21.757	0.161	80.078	0.459	51.904	0.225	32.942	0.336	16.590	0.059	53.800	2.487
df	1	1	5	5	5	5	3	2	7	5	5	5	7	5	5	5	5	4	4	3
Mean Squares	0.002	0.252	30.663	0.169	30.025	0.209	13.104	0.118	3.108	0.032	16.016	0.092	7.415	0.045	6.588	0.067	3.318	0.015	13.450	0.829
F	0.010		181.730		143.440		110.667		96.810		174.614		164.692		98.036		226.415		16.223	
p-value	0.938		****		****		**		****		****		****		****		****		*	

Table S3.14. Probabilities from Tukey honest significant difference (HSD) post hoc test of therian measurements by morphotype. Measurements subjected to the Tukey HSD test are those with significant ANOVA results (i.e., all measurements except TDW); see Table 3.1 for measurements and Table 3.3 for data. Significance indicated by the following: * for $p < 0.05$; ** for $p < 0.01$; *** for $p < 0.001$; **** for $p < 0.0001$. NA indicates the morphotype did not include that particular measurement and therefore could not be subjected to ANOVA or Tukey tests.

		EuA	EuB	EuC	EuD	EuE	EuF	EuG	ThA
AW	**EuA**	–	0.643	0.155	0.094	***	****	NA	NA
	EuB	0.643	–	0.681	0.655	***	****	NA	NA
	EuC	0.155	0.681	–	0.998	**	****	NA	NA
	EuD	0.094	0.655	0.998	–	***	****	NA	NA
	EuE	***	***	**	***	–	***	NA	NA
	EuF	****	****	****	****	***	–	NA	NA
	EuG	NA	NA	NA	NA	NA	NA	–	NA
	ThA	NA	NA	NA	NA	NA	NA	NA	–
TLW	**EuA**	–	0.463	0.182	0.073	***	****	NA	NA
	EuB	0.463	–	0.916	0.769	**	****	NA	NA
	EuC	0.182	0.916	–	1.000	**	***	NA	NA
	EuD	0.073	0.769	1.000	–	***	****	NA	NA
	EuE	***	**	**	***	–	***	NA	NA
	EuF	****	****	***	****	***	–	NA	NA
	EuG	NA	NA	NA	NA	NA	NA	–	NA
	ThA	NA	NA	NA	NA	NA	NA	NA	–
NCW	**EuA**	–	NA	NA	NA	NA	NA	NA	NA
	EuB	NA	–	NA	NA	NA	NA	NA	NA
	EuC	NA	NA	–	0.999	NA	NA	*	0.162
	EuD	NA	NA	0.999	–	NA	NA	*	0.169
	EuE	NA	NA	NA	NA	–	NA	NA	NA
	EuF	NA	NA	NA	NA	NA	–	NA	NA
	EuG	NA	NA	*	*	NA	NA	–	**
	ThA	NA	NA	0.162	0.169	NA	NA	**	–
TW	**EuA**	–	0.794	0.852	0.219	*	***	***	0.999
	EuB	0.794	–	1.000	0.929	*	***	***	0.574
	EuC	0.852	1.000	–	0.872	*	***	***	0.638
	EuD	0.219	0.929	0.872	–	*	***	***	0.126

	EuE	*	*	*	*	–	***	**	**
	EuF	***	***	***	***	***	–	0.776	***
	EuG	***	***	***	***	**	0.776	–	***
	ThA	0.999	0.574	0.638	0.123	**	***	***	–
CW	**EuA**	–	0.847	0.093	0.121	***	****	NA	NA
	EuB	0.847	–	0.289	0.511	***	****	NA	NA
	EuC	0.093	0.289	–	0.771	**	***	NA	NA
	EuD	0.121	0.511	0.771	–	***	****	NA	NA
	EuE	***	***	**	***	–	***	NA	NA
	EuF	****	****	***	****	***	–	NA	NA
	EuG	NA	NA	NA	NA	NA	NA	–	NA
	ThA	NA	NA	NA	NA	NA	NA	NA	–
TH	**EuA**	–	0.932	0.139	0.972	**	***	***	0.962
	EuB	0.932	–	0.391	0.999	**	***	***	0.524
	EuC	0.139	0.391	–	0.125	*	***	***	0.059
	EuD	0.972	0.999	0.125	–	***	****	****	0.487
	EuE	**	**	*	***	–	**	***	***
	EuF	***	***	***	****	**	–	0.724	***
	EuG	***	***	***	****	***	0.724	–	****
	ThA	0.962	0.524	0.059	0.487	***	***	****	–
CH	**EuA**	–	0.901	0.261	0.592	**	***	NA	NA
	EuB	0.901	–	0.653	0.998	**	***	NA	NA
	EuC	0.261	0.653	–	0.623	**	***	NA	NA
	EuD	0.592	0.998	0.623	–	***	***	NA	NA
	EuE	**	**	**	***	–	**	NA	NA
	EuF	***	***	***	***	**	–	NA	NA
	EuG	NA	NA	NA	NA	NA	NA	–	NA
	ThA	NA	NA	NA	NA	NA	NA	NA	–
TL	**EuA**	–	0.128	**	0.096	***	NA	NA	0.393
	EuB	0.128	–	*	0.989	***	NA	NA	*
	EuC	**	*	–	**	***	NA	NA	**
	EuD	0.096	0.989	**	–	***	NA	NA	*
	EuE	***	***	***	***	–	NA	NA	***
	EuF	NA	NA	NA	NA	NA	–	NA	NA
	EuG	NA	NA	NA	NA	NA	NA	–	NA
	ThA	0.393	*	**	*	***	NA	NA	–
CL	**EuA**	–	NA	0.810	0.970	0.101	*	NA	NA
	EuB	NA	–	NA	NA	NA	NA	NA	NA
	EuC	0.810	NA	–	0.932	0.235	0.060	NA	NA
	EuD	0.970	NA	0.932	–	0.069	*	NA	NA
	EuE	0.101	NA	0.235	0.069	–	0.215	NA	NA
	EuF	*	NA	0.060	*	0.215	–	NA	NA
	EuG	NA	NA	NA	NA	NA	NA	–	NA
	ThA	NA	NA	NA	NA	NA	NA	NA	–

Figure S3.7. Boxplots for all therian measurement with significant ANOVA results according to morphotype (i.e., all measurement except TDW). Boxplots include minimum, quartiles, median, and maximum values. See Table 3.1 for measurements, Table 3.3 for data, and Tables S3.13 and S3.14 for ANOVA and Tukey HSD results, respectively. The specimen attributed to morphotype MeA was not included in ANOVA and Tukey tests because it lacked any morphologies preserving our measurements.

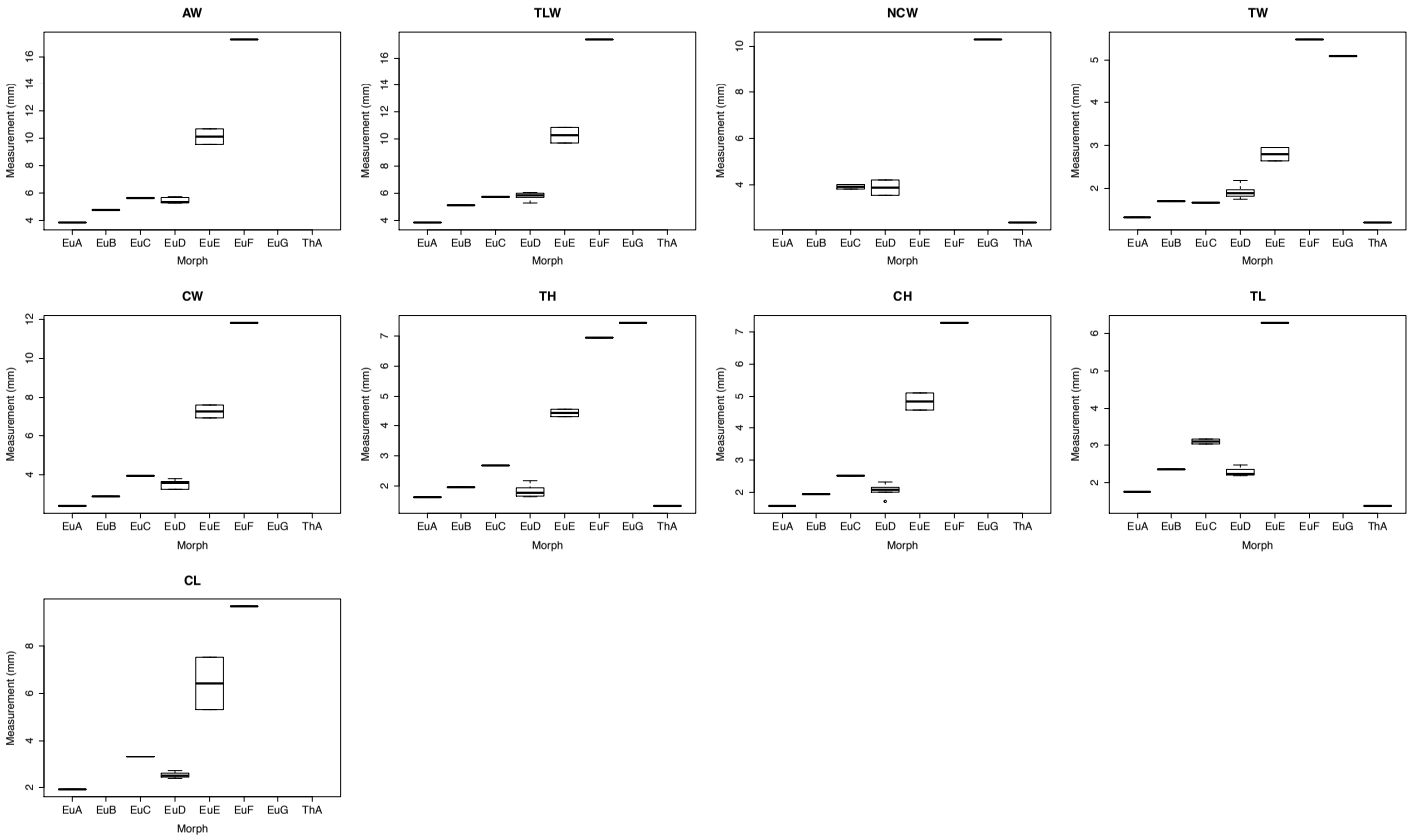

Figure S3.8. Variances for therian measurements with significant ANOVA results according to morphotype (i.e., all measurements except TDW) and preserving at least two specimens (i.e., only EuC, EuD, and EuE; see Table S3.7). See Figure S3.7 for means, maxima, minima, and quartiles. See Table 3.1 for measurements, Table 3.3 for data, and Tables S3.13 and S3.14 for ANOVA and Tukey HSD results, respectively.

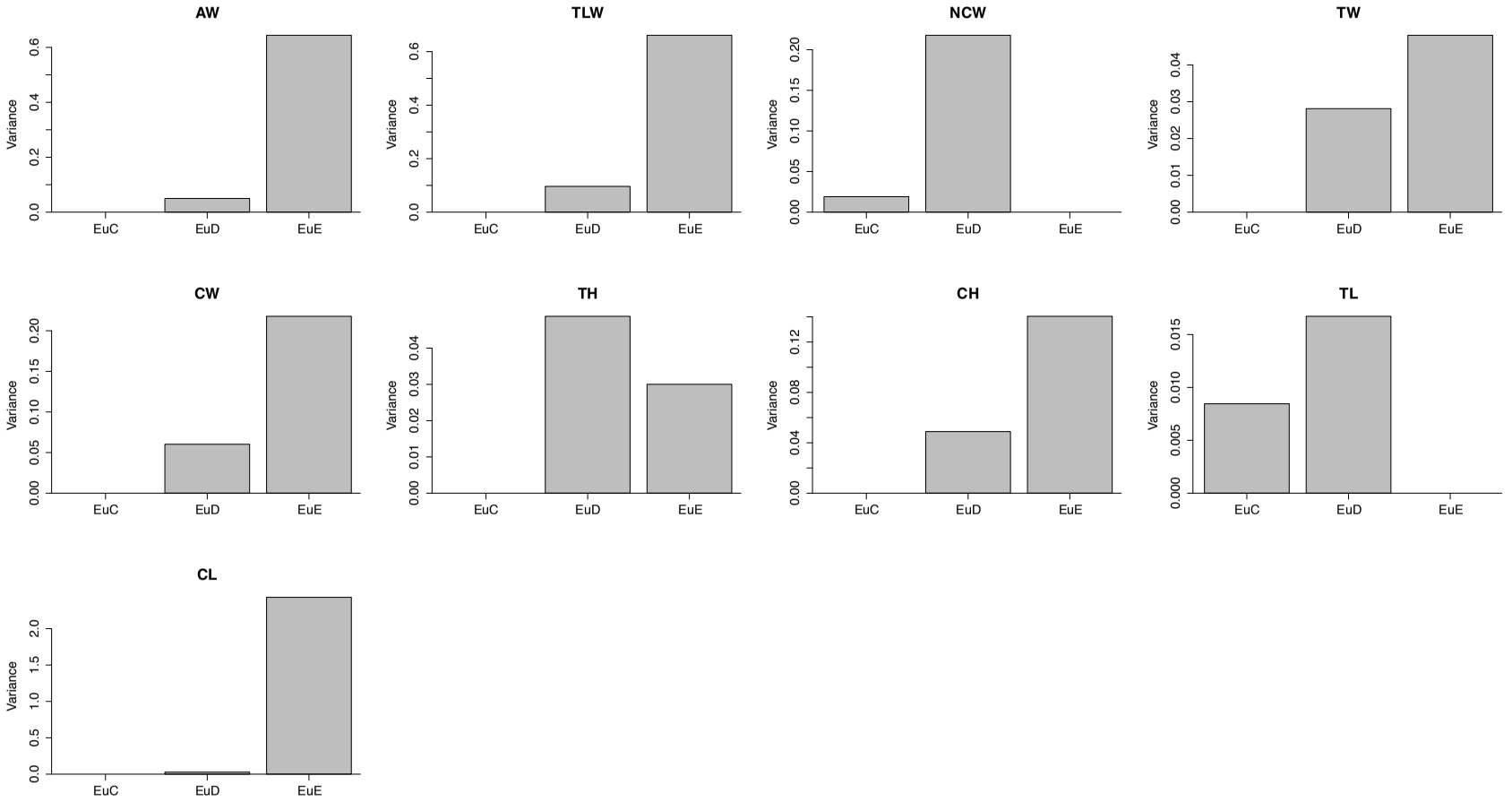

Table S3.15. Means and standard deviations for multituberculate measurements for entire dataset and by biozone. For measurement descriptions see Table 3.1; for data see Table 3.2. NA indicates no specimens preserved the measurement (i.e., NA for mean) or only one specimen preserved the measurement (i.e., NA for SD). Bold values indicate specimen percent preservation (i.e., the number of specimens that preserve that measurement divided by the total number of specimens) greater than or equal to 80%. Abbreviations: BCA, Bug Creek Anthills specimens of mixed age (see text for details); n, number of specimens; Pu1, early Puercan 1 biozone; Pu3, late Puercan biozone; SD, standard deviation.

	TDW	AW	TLW	NCW	UCW	RCW	UCH	RCH	UCL	RCL
Full Dataset (n = 30)										
Mean	6.859	3.551	4.089	2.049	1.639	2.219	2.576	2.482	2.826	2.801
SD	3.864	1.954	2.334	1.022	0.903	1.302	1.472	1.555	1.607	1.440
% Preservation	36.67	53.33	53.33	50.00	**86.67**	70.00	**86.67**	73.33	**90.00**	63.33
Lancian (n = 11)										
Mean	10.475	5.232	6.199	3.066	2.243	3.151	3.627	3.587	4.145	3.650
SD	5.874	2.709	3.891	1.390	1.194	1.474	1.950	1.687	2.018	1.806
% Preservation	27.27	45.45	36.36	36.36	**81.82**	**81.82**	**81.82**	**90.91**	**81.82**	72.73
BCA (n = 12)										
Mean	5.366	2.686	3.194	1.723	1.220	1.530	1.844	1.438	2.009	2.135
SD	2.054	1.006	1.177	0.637	0.485	0.621	0.732	0.586	0.828	0.800
% Preservation	58.33	66.67	75.00	66.67	**100.00**	66.67	**91.67**	66.67	**91.67**	66.67
Pu1 (n = 4)										
Mean	6.460	3.090	4.250	1.960	1.965	1.470	2.653	1.858	2.595	2.335
SD	NA	NA	NA	NA	0.559	0.325	0.764	0.039	0.970	NA
% Preservation	25.00	25.00	25.00	25.00	50.00	50.00	75.00	50.00	**100.00**	25.00
Pu3 (n = 3)										
Mean	NA	3.038	3.818	1.360	1.285	1.530	2.033	1.760	2.177	2.300
SD	NA	0.004	0.004	0.170	0.213	0.156	0.511	0.007	0.447	0.007
% Preservation	0.00	66.67	66.67	66.67	**100.00**	66.67	**100.00**	66.67	**100.00**	66.67

Table S3.16. Means and standard deviations for therian measurements by biozone. We include all specimens except for the specimen in morphotype MeA, which lacked any measureable features. For measurement descriptions see Table 3.1; for data see Table 3.3 (data excludes minimum values). NA indicates no specimens preserved the measurement (i.e., NA for means) or only one specimen preserved the measurement (i.e., NA for SD). Bold values indicate specimen percent preservation (i.e., the number of specimens that preserve that measurement divided by the total number of specimens) greater than or equal to 80%. Abbreviations: BCA, Bug Creek Anthills specimens of mixed age (see text for details); n, number of specimens; Pu1, early Puercan 1 biozone; Pu3, late Puercan biozone; SD, standard deviation.

	TDW	AW	TLW	NCW	TW	CW	TH	CH	TL	CL
Full Dataset (n = 14)										
Mean	9.560	7.189	7.414	4.713	2.438	4.836	3.084	3.026	2.708	4.416
SD	0.357	3.926	3.888	2.812	1.351	2.838	2.084	1.824	1.360	2.836
% Preservation	21.43	78.57	78.57	42.86	**92.86**	78.57	92.86	78.57	71.43	57.14
Lancian (n = 2)										
Mean	NA	4.765	5.120	2.380	1.458	2.895	1.650	1.945	1.868	NA
SD	NA	NA	NA	NA	0.350	NA	0.438	NA	0.689	NA
% Preservation	0.00	50.00	50.00	50.00	**100.00**	50.00	**100.00**	50.00	**100.00**	0.00
BCA (n = 6)										
Mean	9.560	5.492	5.773	3.860	1.881	3.583	1.980	2.133	2.429	2.724
SD	0.357	0.212	0.278	0.332	0.182	0.282	0.396	0.272	0.354	0.414
% Preservation	50.00	**100.00**	**100.00**	50.00	**100.00**	**100.00**	**100.00**	**100.00**	**83.33**	66.67
Pu1 (n = 2)										
Mean	NA	10.685	10.850	4.015	2.950	7.620	4.575	5.110	4.720	7.525
SD	NA	NA	NA	NA	NA	NA	NA	NA	2.206	NA
% Preservation	0.00	50.00	50.00	50.00	50.00	50.00	50.00	50.00	**100.00**	50.00
Pu3 (n = 4)										
Mean	NA	10.227	10.315	10.300	3.636	7.062	5.085	4.480	1.756	5.637
SD	NA	6.741	6.793	NA	1.987	4.708	2.676	2.852	NA	3.885
% Preservation	0.00	75.00	75.00	25.00	**100.00**	75.00	**100.00**	75.00	25.00	75.00

Table S3.17. The results of One-Way ANOVAs of difference for all multituberculate measurements across all biozones. Asterisk indicates significant p-values (< 0.05). Both biozone (b) and residuals (r) values are given for Sum of Squares, df, and Mean Squares. See Table 3.1 for measurement details; see Table 3.2 for data and Table S3.18 for Tukey HSD results.

	TDW		AW		TLW		NCW		UCW		RCW		UCH		RCH		UCL		RCL	
	b	r	b	r	b	r	b	r	b	r	b	r	b	r	b	r	b	r	b	r
Sum of Squares	54.980	94.306	20.851	36.433	25.180	56.513	5.946	8.669	5.972	14.405	13.689	20.215	16.729	37.464	22.739	28.015	24.477	42.655	10.034	27.305
df	2	8	3	12	3	12	3	11	3	22	3	17	3	22	3	18	3	23	3	15
Mean Squares	27.490	11.788	6.950	3.036	8.393	4.709	1.982	0.788	1.991	0.655	4.563	1.189	5.576	1.703	7.580	1.556	8.159	1.855	3.345	1.820
F	2.332		2.289		1.782		2.515		3.040		3.837		3.275		4.870		4.399		1.837	
p-value	0.159		0.130		0.130		0.112		0.050		*		*		*		*		0.184	

Table S3.18. Probabilities from Tukey honest significant difference (HSD) post hoc test of multituberculate measurements by biozones. Measurements subjected to the Tukey HSD test are those with significant ANOVA results: radial condyle width (RCW), ulnar condyle height (UCH), radial condyle height (RCH), and ulnar condyle length (UCL). Significance indicated by the following: * for $p < 0.05$; ** for $p < 0.01$.

Measurement		Lancian	BCA	Pu1	Pu3
RCW	**Lancian**	–	*	0.237	0.264
	BCA	*	–	1.000	1.000
	Pu1	0.237	1.000	–	1.000
	Pu3	0.264	1.000	1.000	–
UCH	**Lancian**	–	*	0.682	0.286
	BCA	*	–	0.777	0.996
	Pu1	0.682	0.777	–	0.936
	Pu3	0.286	0.996	0.936	–
RCH	**Lancian**	–	**	0.310	0.267
	BCA	**	–	0.973	0.988
	Pu1	0.310	0.973	–	1.000
	Pu3	0.267	0.988	1.000	–
UCL	**Lancian**	–	*	0.258	0.162
	BCA	*	–	0.881	0.998
	Pu1	0.258	0.881	–	0.977
	Pu3	0.162	0.998	0.977	–

Figure S3.9. Boxplots (above) and variances (below) for each multituberculate measurement with significant ANOVA results according to biozone. Boxplots include minimum, quartiles, median, and maximum values. See Table 3.1 for measurements, Table 3.2 for data, Table S3.6 for means, and Tables S3.17 and S3.18 for ANOVA and Tukey HSD results, respectively. Asterisks indicate pairs of significantly different values in Tukey tests (i.e., Lancian specimens are significantly larger than BCA specimens for all measurements).

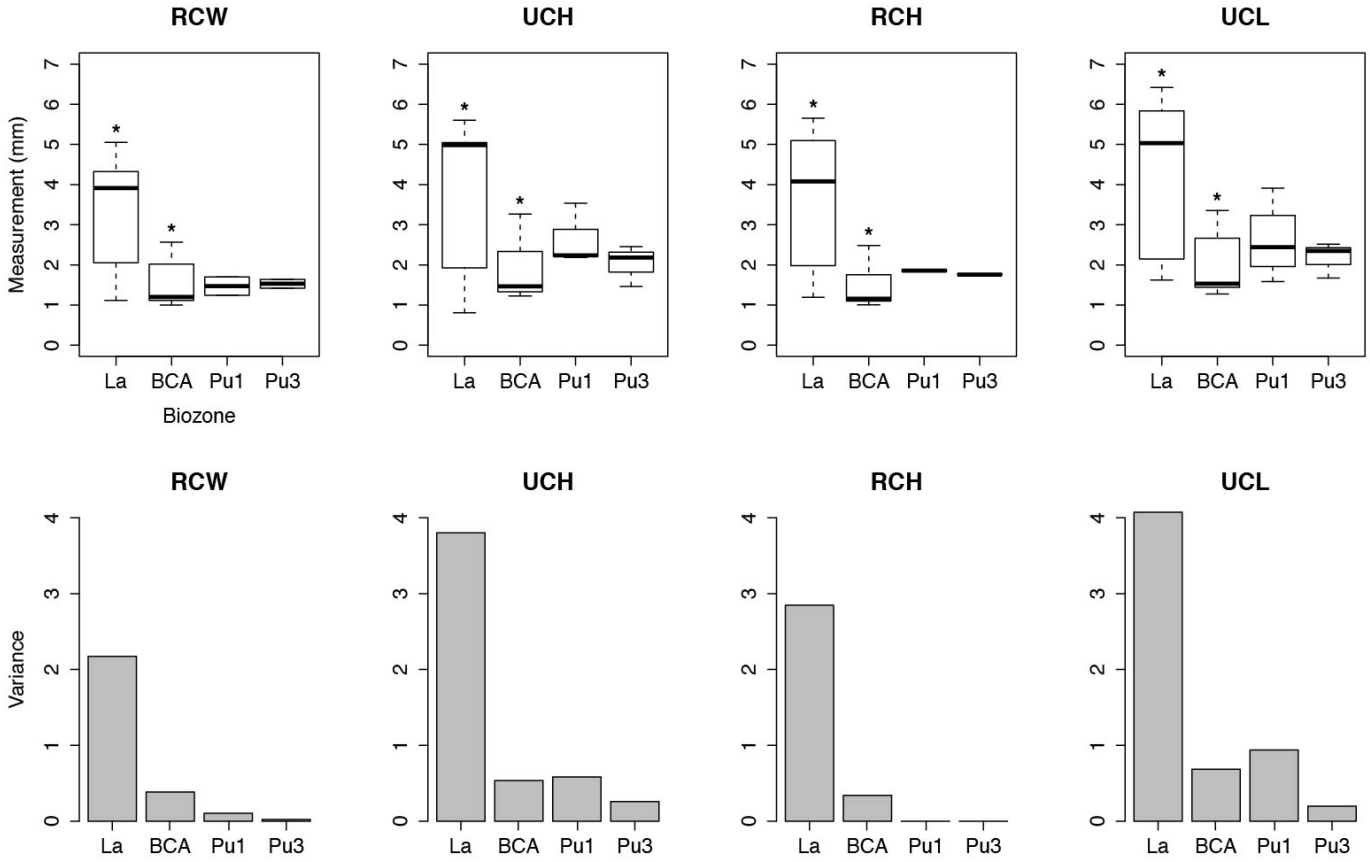

Table S3.19. The results of One-Way ANOVAs of difference for all therians measurements across all biozones (for all measurements with specimens in at least three biozones, i.e., excluding TDW). Significance is as follows: * for $p < 0.05$; ** for $p < 0.01$. Both biozone (b) and residuals (r) values are given for Sum of Squares, df, and Mean Squares. See Table 3.1 for measurement details and Table 3.3 for data.

	AW		TLW		NCW		TW		CW		TH		CH		TL		CL	
	b	r	b	r	b	r	b	r	b	r	b	r	b	r	b	r	b	r
Sum of Squares	63.066	91.093	58.483	92.688	39.327	0.220	9.791	12.127	35.811	44.726	29.665	22.464	16.641	16.637	10.805	5.844	25.591	30.696
df	3	7	3	7	3	2	3	9	3	7	3	9	3	7	3	6	2	5
Mean Squares	21.022	13.013	19.494	13.241	13.109	0.110	3.264	1.347	11.937	6.389	9.888	2.496	5.547	2.377	3.602	0.974	12.795	6.139
F	1.615		1.472		119.066		2.422		1.868		3.962		2.334		3.698		2.084	
p-value	0.270		0.302		**		0.133		0.223		*		0.160		0.081		0.220	

Table S3.20. Probabilities from Tukey honest significant difference (HSD) post hoc test of therian measurements by biozones. Measurements subjected to the Tukey HSD test are those with significant ANOVA results, only entepicondyle condyle width (NCW) and trochlea height (TH). Significance is as follows: * for $p < 0.05$; ** for $p < 0.01$.

Measurement		Lancian	BCA	Pu1	Pu3
NCW	**Lancian**	–	0.147	0.176	**
	BCA	0.147	–	0.973	**
	Pu1	0.176	0.973	–	*
	Pu3	**	**	*	–
TH	**Lancian**	–	0.994	0.470	0.125
	BCA	0.994	–	0.465	0.056
	Pu1	0.470	0.465	–	0.991
	Pu3	0.125	0.056	0.991	–

Figure S3.10. Boxplot (left) and variance (right) for eutherian NCW measurement, which had significant ANOVA results according to biozone. Boxplot includes minimum, quartiles, median, and maximum values; variance shown for biozones with n > 1. See Table 3.1 for measurements, Table 3.3 for data, Table S3.7 for means, and Tables S3.19 and S3.20 for ANOVA and Tukey HSD results, respectively. Asterisks indicate pairs of significantly different values in Tukey tests (i.e., Pu3 specimens are significantly larger than Lancian and BCA specimens).

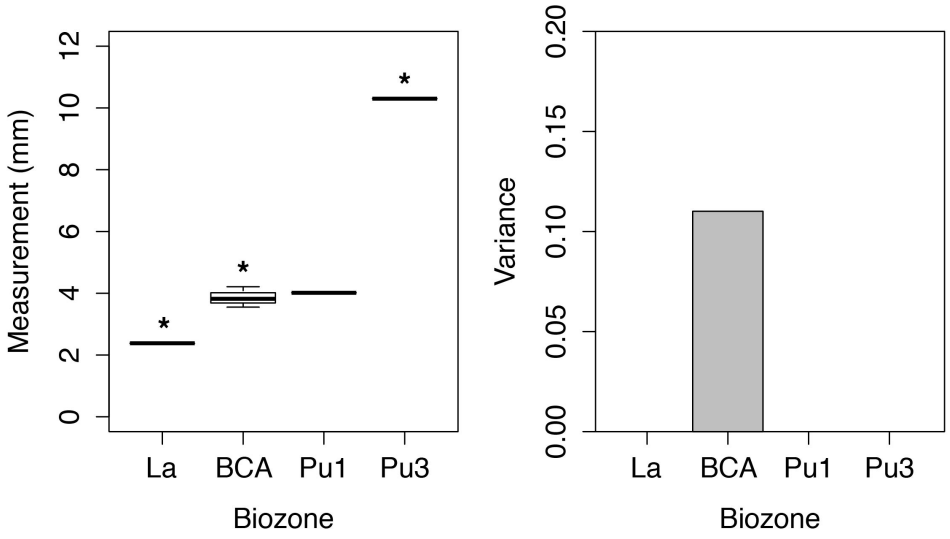

Table S3.21. Eigenvalues, proportion of variance, and cumulative variance explained from PCAs. We conducted PCAs on two separate datasets: one "full dataset" that included all modern taxa (Table 3.4), and one "reduced dataset" of eutherians that excluded carnivorans and lagomorphs (see text for more details). Of the 40 total principal components in each PCA, we report only PCs that explained at least 1% of the variance.

	Eigenvalues	Proportion of Variance	Cumulative Variance
Full Dataset			
PC1	0.0067938	46%	46%
PC2	0.0018609	13%	59%
PC3	0.0016220	11%	70%
PC4	0.0011623	8%	78%
PC5	0.0007075	5%	83%
PC6	0.0004502	3%	86%
PC7	0.0003615	2%	88%
PC8	0.0003264	2%	91%
PC9	0.0003162	2%	93%
PC10	0.0002115	1%	94%
PC11	0.0001540	1%	95%
Reduced Dataset			
PC1	0.0042641	37%	37%
PC2	0.0021872	19%	56%
PC3	0.0015529	13%	69%
PC4	0.0007259	6%	75%
PC5	0.0007226	6%	82%
PC6	0.0004394	4%	85%
PC7	0.0003591	3%	89%
PC8	0.0003120	3%	91%
PC9	0.0002451	2%	93%
PC10	0.0001782	2%	95%
PC11	0.0001404	1%	96%

Figure S3.11. Principal Component Analysis (PCA) of all modern taxa with specimens labeled. PC1 and PC2 explain 46% and 13% of the total variance, respectively (Table S3.21). Partial warp shapes indicate the minimum and maximum of PC1. Black circles are metatherians, gray circles are eutherians. See Table 3.4 for specimen information. We note the orientation of the maximum and minimum of PC1 is reversed here compared to Figs. 3.3, 3.20–21); this is a function of the arbitrary assignment of maximum and minimum in PC space, and it does not affect the shape interpretation.

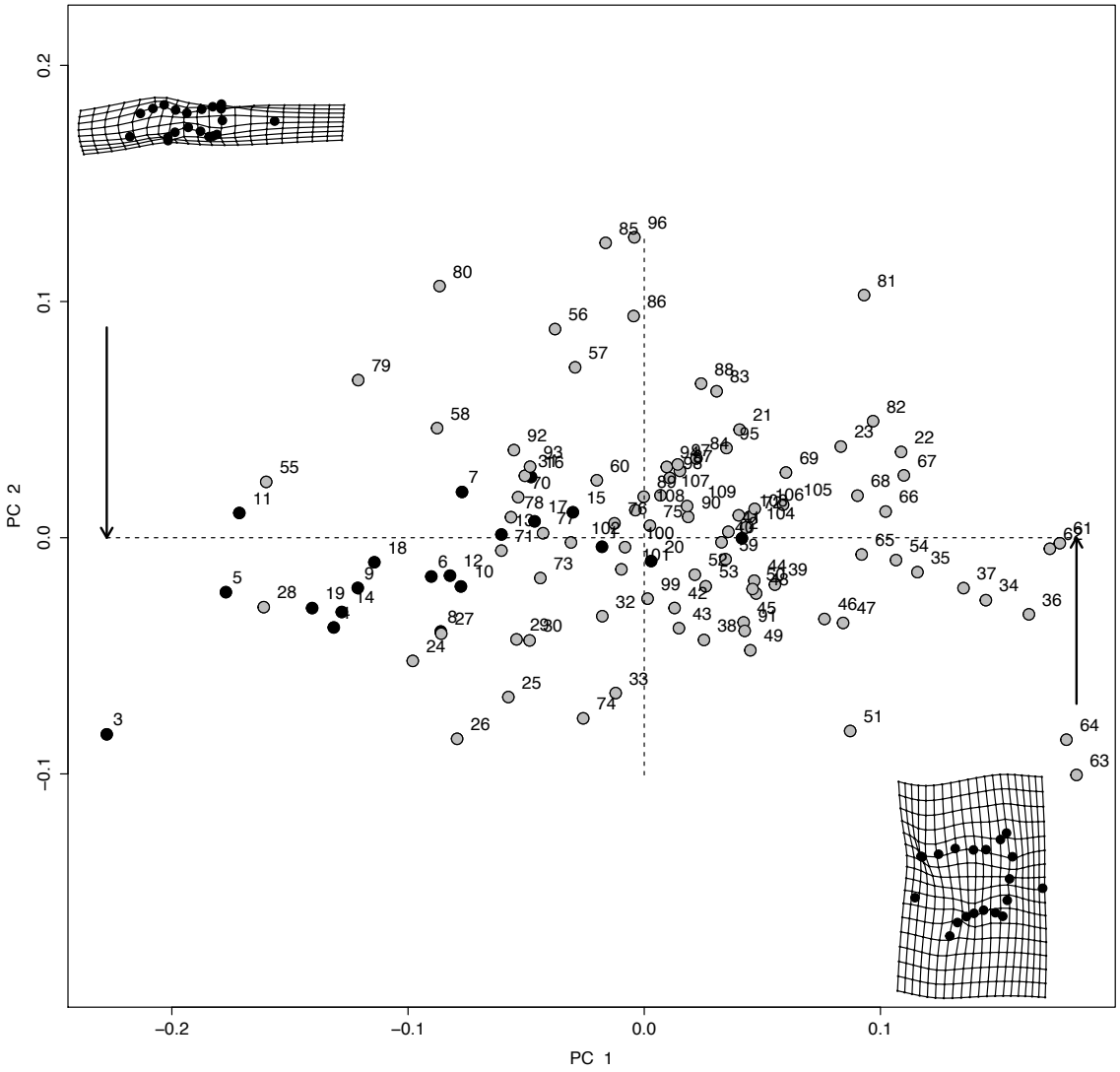

Figure S3.12. Principal Component Analysis (PCA) of all modern taxa with specimens labeled. PC2 and PC3 explain 13% and 11% of the total variance, respectively (Table S3.21). Partial warp shapes indicate the minimum and maximum of PC2. Black circles are metatherians, gray circles are eutherians. See Table 3.4 for specimen information.

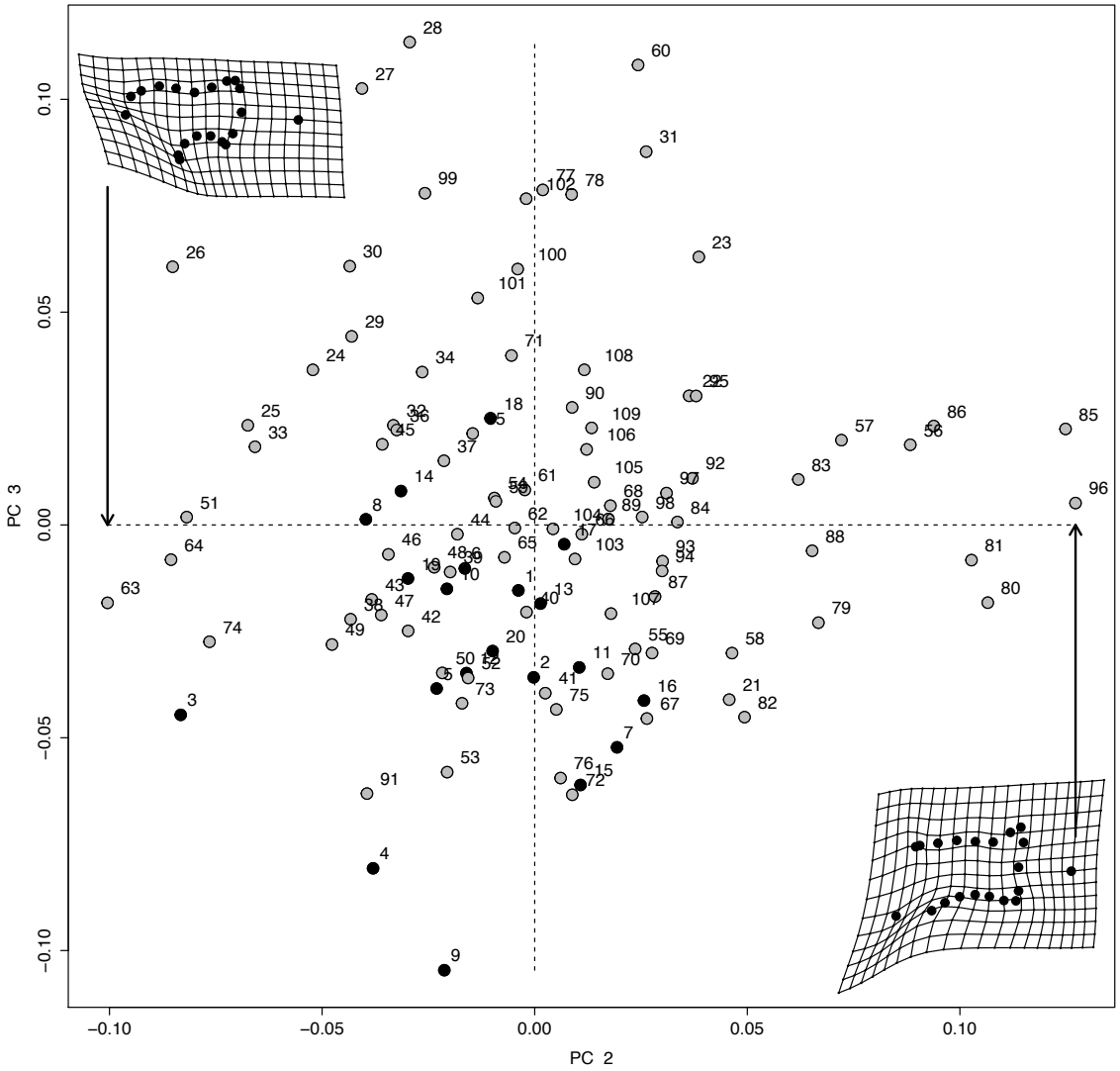

Table S3.22. LDA results for the reduced dataset of extant mammals with known locomotion. LDA analyses used all significant principal components (i.e., those which represented at least 1% of the variation).

	Locomotor Group Means							
	A	**F**	**G**	**S**	**Sa**	**Sc**	**Sf**	**T**
PC1	0.01276	-0.00884	0.06054	0.05556	-0.01318	-0.03556	-0.01427	0.02452
PC2	0.02255	-0.02874	0.03102	-0.01765	-0.07145	0.05872	0.00177	0.01686
PC3	0.01071	-0.00397	-0.00655	-0.00441	0.00296	0.04311	-0.01621	0.00011
PC4	-0.00049	-0.01497	0.00582	0.00888	0.01229	0.00693	0.00257	0.02051
PC5	0.00474	-0.00238	-0.03417	0.00849	-0.00719	-0.00493	0.00250	0.00677
PC6	0.01928	-0.00531	0.00733	-0.02232	-0.00779	-0.01032	-0.00525	-0.01245
PC7	-0.00652	-0.00415	0.01422	-0.00893	0.01796	0.02135	-0.01010	0.01034
PC8	-0.00155	0.00139	0.01861	0.00473	0.00458	-0.00357	0.00581	-0.00768
PC9	0.00265	0.00418	0.00749	-0.00980	0.00657	-0.01905	-0.00713	0.00275
PC10	0.00117	-0.00358	-0.00796	0.00495	0.00051	-0.00717	0.00358	-0.00140
PC11	0.00427	0.00338	0.00415	0.00051	-0.00679	0.00198	-0.00687	-0.00108

	Coefficients of Linear Discriminants					
	LD1	**LD2**	**LD3**	**LD4**	**LD5**	**LD6**
PC1	2.94717	2.27578	2.17796	9.41316	-6.31096	-4.86250
PC2	26.91399	13.17848	-4.77661	4.56211	2.92216	0.42556
PC3	7.31164	6.68984	1.18431	-11.66506	2.81487	-1.24342
PC4	-5.70621	22.80368	-3.22197	4.88143	-18.81627	11.10793
PC5	2.06893	-3.58513	-21.96368	-10.27321	-13.82449	-4.63802
PC6	48.82373	-21.34994	19.54012	-11.13995	-10.35859	23.00979
PC7	-20.15756	43.27913	29.14487	-15.39684	0.14397	3.82854
PC8	-6.88752	-9.20087	17.93410	29.18532	19.67257	17.61627
PC9	-3.79714	-16.85835	37.88225	-4.34904	-33.12376	-12.11852
PC10	-4.01667	-13.76100	-24.49836	5.73548	-20.80180	21.90751
PC11	44.60443	-8.70142	17.22111	-4.55220	6.04990	-51.18676
Proportions of Trace	**50.42%**	**21.25%**	**13.29%**	**5.64%**	**4.95%**	**3.18%**

Table S3.23. LDA predictions for locomotor mode for modern specimens in this study. LDA correctly predicts locomotor mode of modern specimens with an accuracy of 74.19%. Published locomotor mode (LM) is indicated, as well as predicted locomotor mode; asterisks indicate specimens whose locomotor mode was incorrectly predicted. See Table 4 for additional specimen information.

Specimen	*Genus*	*species*	Family	Order	Code	LM	LM Prediction
S2008	*Potamogale*	*velox*	Potamogalidae	Afrosoricida	21	Sa	T*
39039	*Dendrohyrax*	*arboreus*	Procaviidae	Afrosoricida	22	A	A
39038	*Dendrohyrax*	*arboreus*	Procaviidae	Afrosoricida	23	A	Sf*
S2008	*Limnogale*	*mergulus*	Tenrecidae	Afrosoricida	24	Sa	F*
34168	*Echinops*	*telfairi*	Tenrecidae	Afrosoricida	25	Sc	Sc
S2008	*Echinops*	*telfairi*	Tenrecidae	Afrosoricida	26	Sc	T*
S2008	*Hemicentetes*	*semispinosus*	Tenrecidae	Afrosoricida	27	Sf	T*
S2008	*Oryzorictes*	*sp.*	Tenrecidae	Afrosoricida	28	Sf	Sf
S2008	*Setifer*	*setosus*	Tenrecidae	Afrosoricida	29	T	T
S2008	*Tenrec*	*ecaudatus*	Tenrecidae	Afrosoricida	30	T	T
S2008	*Microgale*	*cowani*	Tenrecidae	Afrosoricida	31	T	T
S2008	*Microgale*	*dobsoni*	Tenrecidae	Afrosoricida	32	T	T
S2008	*Microgale*	*talazaci*	Tenrecidae	Afrosoricida	33	T	Sc*
34167	*Cabassous*	*centralis*	Dasypodidae	Cingulata	55	F	Sa*
20735	*Dasypus*	*novemcinctus*	Dasypodidae	Cingulata	56	F	F
22458	*Dasypus*	*novemcinctus*	Dasypodidae	Cingulata	57	F	F
35468	*Euphractus*	*sexcinctus*	Dasypodidae	Cingulata	58	F	F
S2008	*Echinosorex*	*gymnurus*	Erinaceidae	Erinaceomorpha	59	T	T
S2008	*Solenodon*	*paradoxus*	Solenodontidae	Soricomorpha	60	Sf	Sf
S2008	*Petrodromus*	*tetradactylus*	Macroscelididae	Macroscelidea	67	S	T*
35475	*Elephantulus*	*rufescens*	Macroscelididae	Macroscelidea	68	T	T
34189	*Elephantulus*	*rufescens*	Macroscelididae	Macroscelidea	69	T	T
39003	*Callithrix*	*pygmaea*	Cebidae	Primates	70	A	A
39005	*Callithrix*	*pygmaea*	Cebidae	Primates	71	A	A
75541	*Leontopithecus*	*chrysomela*	Cebidae	Primates	72	A	A
35406	*Saguinus*	*oedipus*	Cebidae	Primates	73	A	A
35405	*Saguinus*	*oedipus*	Cebidae	Primates	74	A	A
82302	*Saimiri*	*sciureus*	Cebidae	Primates	75	A	A
39014	*Saimiri*	*sciureus*	Cebidae	Primates	76	A	A
34071	*Aplodontia*	*rufa*	Aplodontiidae	Rodentia	77	F	Sf*
34058	*Aplodontia*	*rufa*	Aplodontiidae	Rodentia	78	F	Sf*
34116	*Castor*	*canadensis*	Castoridae	Rodentia	79	Sa	Sa

34588	*Castor*	*canadensis*	Castoridae	Rodentia	80	Sa	Sa
72830	*Cavia*	*porcellus*	Caviidae	Rodentia	81	T	T
72831	*Cavia*	*porcellus*	Caviidae	Rodentia	82	T	T
76622	*Microtus*	*pennsylvanicus*	Cricetidae	Rodentia	83	F	F
34326	*Microtus*	*pennsylvanicus*	Cricetidae	Rodentia	84	F	F
34324	*Ondatra*	*zibethicus*	Cricetidae	Rodentia	85	Sa	Sa
72879	*Ondatra*	*zibethicus*	Cricetidae	Rodentia	86	Sa	Sa
66559	*Synaptomys*	*borealis*	Cricetidae	Rodentia	87	Sf	F*
66561	*Synaptomys*	*borealis*	Cricetidae	Rodentia	88	Sf	Sf
76721	*Zapus*	*princeps*	Dipodidae	Rodentia	89	S	Sf*
75136	*Zapus*	*princeps*	Dipodidae	Rodentia	90	S	S
34176	*Coendou*	*prehensilis*	Erethizontidae	Rodentia	91	Sc	Sc
44624	*Thomomys*	*bottae*	Geomyidae	Rodentia	92	F	F
38261	*Thomomys*	*bottae*	Geomyidae	Rodentia	93	F	F
47378	*Chaetodipus*	*fallax*	Heteromyidae	Rodentia	94	F	S*
47379	*Chaetodipus*	*fallax*	Heteromyidae	Rodentia	95	F	A*
78740	*Dipodomys*	*deserti*	Heteromyidae	Rodentia	96	S	F*
48984	*Octodon*	*degus*	Octodontidae	Rodentia	97	Sf	A*
39501	*Octodon*	*degus*	Octodontidae	Rodentia	98	Sf	Sf
35278	*Sciurus*	*aberti*	Sciuridae	Rodentia	99	A	A
82349	*Sciurus*	*aberti*	Sciuridae	Rodentia	100	A	A
20646	*Sciurus*	*carolinensis*	Sciuridae	Rodentia	101	A	A
30010	*Sciurus*	*carolinensis*	Sciuridae	Rodentia	102	A	A
36334	*Glaucomys*	*sabrinus*	Sciuridae	Rodentia	103	G	G
35129	*Glaucomys*	*sabrinus*	Sciuridae	Rodentia	104	G	G
43897	*Glaucomys*	*volans*	Sciuridae	Rodentia	105	G	G
32254	*Glaucomys*	*volans*	Sciuridae	Rodentia	106	G	G
75774	*Cynomys*	*ludovicianus*	Sciuridae	Rodentia	107	Sf	Sf
34227	*Tupaia*	*glis*	Tupaiidae	Scandentia	108	A	A
34225	*Tupaia*	*glis*	Tupaiidae	Scandentia	109	A	A

Table S3.24. LDA results and predicted locomotor mode for fossil specimens in this study. Prediction probabilities that are in bold are the top ranked locomotor mode (i.e., rank of 1); all ranks are shown for predictions probabilities, but percentages are shown only for > 0.00%. Abbreviations: Spec. Number, specimen number; Loc. locality; M. morphotype; Bioz., biozone.

Spec. Number	Loc.	M.	Bioz.	Prediction Probabilities								Rank							
				A	F	G	S	Sa	Sc	Sf	T	1	2	3	4	5	6	7	8
97114	C1115	EuB	La	**99.39%**	0.17%					0.44%		A	Sf	F	T	Sc	S	G	Sa
151991	V71203	EuC	BCA	27.10%	9.44%	0.02%	0.17%		0.16%	**61.01%**	2.10%	Sf	A	F	T	S	Sc	G	Sa
151964	V65127	EuD	BCA	0.82%	**93.29%**		0.04%			5.85%		F	Sf	A	S	Sa	T	G	Sc
153036	V65127	EuD	BCA	25.36%	23.94%		0.07%			**50.54%**	0.09%	Sf	F	A	T	S	Sc	Sa	G

Supplemental References Cited

Argot, C. 2001. Functional-adaptive anatomy of the forelimb in the Didelphidae, and the paleobiology of the Paleocene marsupials *Mayulestes ferox* and *Pucadelphys andinus*. Journal of Morphology 247: 51–79.

Argot, C. 2013. Postcranial analysis of a Carnivoran-like archaic ungulate: the case of *Arctocyon primaevus* (Arctocyonidae, Mammalia) from the Late Paleocene of France. Journal of Mammalian Evolution 20: 83–114.

Bloch, J.I. and D.M. Boyer. 2002. Grasping primate origins. Science 298: 1606–1610.

Bloch, J.I., M.T. Silcox, D.M. Boyer, and E.J. Sargis. 2007. New Paleocene skeletons and the relationship of plesiadapiforms to crown-clade primates. Proceedings of the National Academy of Sciences 104: 1159–1164.

Boyer, D.M., G.V.R. Prasad, D.W. Krause, M. Godinot, A. Goswami, O. Verma, and J.J. Flynn. 2010. New postcrania of *Deccanolestes* from the Late Cretaceous of India and their bearing on the evolutionary and biogeographic history of euarchontan mammals. Naturwissenschaften 97: 365–77.

Chester, S.G.B., E.J. Sargis, F.S. Szalay, J.D. Archibald, and A.O. Averianov. 2010. Mammalian distal humeri from the Late Cretaceous of Uzbekistan. Acta Palaeontologica Polonica 55: 199–211.

Cope, E.D. 1884. The Tertiary Marsupialia. American Naturalist 18: 686–97.

Deischl, D.G. 1964. The postcranial anatomy of Cretaceous multituberculate mammals, unpublished M.Sc. thesis, University of Minnesota, Minneapolis.

Fox, R.C. 2005. Microcosmodontid multituberculates (Allotheria, Mammalia) from the Paleocene and Late Cretaceous of western Canada. Palaeontographica Canadiana 23: 1–109.

Gidley, J.W. 1909. Notes on the fossil mammalian genus *Ptilodus*, with descriptions of new species. Proceedings of the United States National Museum 36: 611–627.

Hurum, J.H. and Z. Kielan-Jaworowska. 2008. Postcranial skeleton of a Cretaceous multituberculate mammal *Catopsbaatar*. Acta Palaeontologica Polonica 53: 545–566.

Jenkins, F.A., Jr. 1973. The functional anatomy and evolution of the mammalian humero-ulnar articulation. American Journal of Anatomy 137: 281–98.

Krause, D.W. and F.A. Jenkins, Jr. 1983. The postcranial skeleton of North American multituberculates. Bulletin of the Museum of Comparative Zoology 150: 199–246.

Kielan-Jaworowska, Z. and D. Dashzeveg. 1978. New Late Cretaceous mammal locality in Mongolia and a description of a new multituberculate. Acta Paleontologica Polonica 23: 115–130.

Kielan-Jaworowska, Z. and P.P. Gambaryan. 1994. Postcranial anatomy and habits of Asian multituberculate mammals. Fossils and Strata 36: 1–92.

Kielan-Jaworowska, Z. and T. Qi. 1990. Fossorial adaptations of a taeniolabidoid multituberculate mammal from the Eocene of China. Vertebrata PalAsiatica 28: 81–94.

Kondrashov, P.E. and S.G. Lucas. 2012. Nearly complete skeleton of *Tetraclaenodon* (Mammalia, Phenacodontidae) from the Early Paleocene of New Mexico: morpho-functional analysis. Journal of Paleontology 86: 25–43.

Marsh, O.C. 1889. Discovery of Cretaceous Mammalia. American Journal of Science 38: 81–92.

Marshall, L.G., C. de Muizon, and D. Sigogneau-Russell. 1995. *Pucadelphys andinus* (Marsupialia, Mammalia) from the Early Paleocene of Bolivia. Mémoires du Muséum National D'Histoire Naturelle 165: 91–164.

Matthew, W.D. 1937. Paleocene faunas of the San Juan Basin, New Mexico. Transactions of the American Philosophical Society 30: 1–523.

Muizon, C. 1998. *Mayulestes ferox*, a bohyaenoid (Metatheria, Mammalia) from the early Palaeocene of Bolivia. Phylogenetic and palaeobiologic implications. Geodiversitas 20: 19–142.

O'Leary, M.A., J.I. Bloch, J.J. Flynn, T.J. Gaudin, A. Giallombardo, N.P. Giannini, S.L. Goldberg, B.P. Kraatz, Z.-X. Luo, J. Meng, X. Ni, M.J. Novacek, F.A. Perini, Z.S. Randall, G.W. Rougier, E.J. Sargis, M.T. Silcox, N.B. Simmons, M. Spaulding, P.M. Velazco, M. Weksler, J.R. Wible, and A.L. Cirranello. 2013. The placental mammal ancestor and the post-K-Pg radiation of placentals. Science 339: 662–67.

Rigby, J.K. Jr., 1981. A skeleton of *Gillisonchus gillianus* (Mammalia; Condylarthra) from the Early Paleocene (Puercan) Ojo Alamo Sandstone, San Juan Basin, New Mexico, with comments on the local stratigraphy of Betonnie Tsosie Wash, in: S.G. Lucas, J.K. Rigby Jr., and B.S. Kues (Eds.), Advances in San Juan Basin Paleontology. University of New Mexico Press, Albuquerque, pp. 89–126.

Rose, K.D. 1982. Skeleton of *Diacodexis*, oldest known artiodactyl. Science 216: 621–623.

Rose, K.D. 1987. Climbing adaptations in the early Eocene mammal *Chriacus* and the origin of Artiodactyla. Science 236: 314–316.

Rose, K. 1999. Postcranial skeleton of Eocene Leptictidae (Mammalia), and its implications for behavior and relationships. Journal of Vertebrate Paleontology 19: 355–72.

Russell, D.E. 1964. Les mammifères paléocènes d'Europe. Mémoires du Muséum National D'Histoire Naturelle, Série C. Sciences de la Terre 13: 1–324.

Sahni, A. 1972. The vertebrate fauna of the Judith River Formation, Montana. Bulletin of the American Museum of Natural History 147: 323–412.

Schoch, R.M. 1986. Systematics, functional morphology and macroevolution of the extinct mammalian order Taeniodonta. Peabody Museum of Natural History, Yale University Bulletin 42: 1–307.

Sereno, P.C. 2006. Shoulder girdle and forelimb in multituberculates: evolution of parasagittal forelimb posture in mammals, in: Carrano, M.T., T.J. Gaudin, R.W. Blob, and J.R. Wible (Eds.), Amniote Paleobiology: Perspectives on the Evolution of Mammals, Birds, and Reptiles, University of Chicago Press, Chicago, pp. 315–366.

Simpson, G.G. 1935. The Tiffany Fauna, Upper Paleocene II.–structure and relationships of *Plesiadapis*. American Museum Novitates 816: 1–30.

Sloan, R.E. 1981. Systematics of Paleocene multituberculates from the San Juan Basin, New Mexico, in: Lucas, S.G., J.K. Rigby Jr., and B.S. Kues. (Eds.), Advances in San Juan Basin Paleontology. University of New Mexico Press, Albuquerque, pp. 127–160.

Standhardt, B.R. 1986. Vertebrate paleontology of the Cretaceous/Tertiary transition of Big Bend National Park, Texas, Ph.D. dissertation. Louisiana State University and Agricultural and Mechanical College, Baton Rouge.

Szalay, F.S. and M. Dagosto. 1980. Locomotor adaptations as reflected on the humerus of Paleogene primates. Folia Primatologica 34: 1–45.

Szalay, F.S., I. Tattersall, and R.L. Decker. 1975. Phylogenetic relationships of Plesiadapis-postcranial evidence. Contributions to Primatology 5: 136–166.

CHAPTER 4:

LOCOMOTOR FUNCTION IN MAMMAL ASTRAGALI FROM THE CRETACEOUS-PALEOGENE BOUNDARY IN EASTERN MONTANA

Abstract

The astragalus is directly involved in movement at the ankle; its morphology reflects compromises between differential load bearing, stability, and mobility, which make it an excellent element for studies of function, locomotion, and substrate/habitat preference. This link between astragalus morphology, locomotor ecology, and substrate preference has been shown in a wide range of extant mammals. Here we use this functional morphology relationship to investigate mammalian locomotor ecology (e.g., climbing, digging, swimming) and substrate preference (e.g., arboreal, fossorial, aquatic) for mammals at the Cretaceous-Paleogene (K-Pg) boundary. In this study, we provide the first three-dimensional geometric morphometric (3D GM) analysis of mammal astragali from the well-studied and well-sampled K-Pg study area of eastern Montana. To quantitatively assess morphology and predict locomotion for these fossils, we assembled a large, phylogenetically broad, comparative dataset of extant mammals of known locomotion. We micro-CT scanned all material and used 3D GM methods to quantify shape and morphofunctional relationships among locomotor groups. Then, we applied this framework to 24 fossil specimens to assess morphology and to predict locomotion for fossil mammals in our study area. Fossil material analyzed includes early Paleogene from the Puercan North American Land Mammal "age" as well as material from the stratigraphically mixed Bug Creek Anthills. Specifically, we include Pu1 and Pu3 postcrania that have previously been attributed to the archaic ungulate *Protungulatum* and leptictid *Procerberus*, one Pu3 astragalus that has been attributed to the plesiadapiform *Purgatorius*,

and one Pu3 astragalus that we attribute to a large archaic ungulate (possibly *Baioconodon* or *Bubagonia*).

Results show astragalus morphology in extant placental and marsupial mammals is significantly influenced by both phylogeny and locomotor mode. Phylogenetically, fossil astragali are most similar to the astragali of eutherian extant taxa, which quantitatively supports their taxonomic attribution to Eutheria. Ecologically, we find saltatorial, semifossorial, and to a lesser extent fossorial taxa consistently group together at one extreme of the morphofunctional continuum; arboreal, and to a lesser extent scansorial, taxa group together at the other extreme; semiaquatic and terrestrial taxa are often intermediate. Locomotor predictions from results of combined quantitative and qualitative analyses suggest: *Protungulatum* was terrestrial and potential semifossorial; *Procerberus* was likely more scansorial and had an ankle that was even more flexible than that of *Protungulatum*; *Purgatorius* appears to be the most arboreal of all fossil taxa; and the large archaic ungulate was terrestrial and scansorial. Despite small sample sizes and fragmentary material, this study demonstrates the potential for quantitative inference of locomotor mode for K-Pg fossil taxa, and complements the small but growing body of literature exploring postcranial patterns from this critical period in earth history.

1. Introduction

Intensive research on mammalian extinction and recovery across the Cretaceous-Paleogene (K-Pg) boundary has inferred patterns of taxonomic diversity, morphological disparity, body-size changes, and dietary shifts from the dental fossil record (e.g., Alroy 1999; Smith et al. 2010; Wilson 2004, 2013, 2014; Wilson et al. 2012; O'Leary et al. 2013; Raia et al. 2013); however, study of the postcranial fossil record has been hindered by a lack of articulated or associated skeletons and by high rates of breakage among functionally informative elements (e.g., limb bones; Deischl 1964; Krause and Jenkins 1983; Borths and Hunter 2008; DeBey and Wilson 2014). Despite the difficulties in the study of rare and fragmentary mammal postcrania, they are presently the only direct means to test hypotheses of K-Pg mass extinction and subsequent recovery (e.g., Sheltering Hypothesis; Robertson et al. 2004) related to mammalian locomotor ecology (e.g., climbing, digging, swimming) and substrate preference (e.g., arboreal, fossorial, aquatic).

Among mammalian skeletal elements, the astragalus is compact and durable, easily identified, and has lower rates of breakage than other postcranial elements and even other tarsals (e.g., calcanea; Szalay and Decker 1974). Consequently, sample sizes of relatively complete astragali, while lower than dental sample sizes (e.g., Archibald 1982; Lofgren 1995; Wilson 2014), are often higher than those for other postcranial elements in K-Pg vertebrate microfossil assemblages (DeBey and Wilson 2014). Moreover, because the astragalus is directly involved in movement at the ankle (e.g., foot dorsiflexion, and ankle mediolateral rotation; e.g., Szalay and Decker 1974; Szalay 1994; Carrano 1997; Salton and Szalay 2004; Polly 2008), its morphology reflects compromises between differential load

bearing, stability, and mobility, which make it an excellent element for studies of function (e.g., habitual movement), locomotion (e.g., climbing), and substrate/habitat preference (e.g., arboreality; Szalay and Decker 1974). This link between astragalus morphology and locomotor ecology and substrate preference has been shown in a wide range of extant mammals using functional morphology and traditional morphometrics as well as two-dimensional geometric morphometrics (e.g., DeGusta and Vrba 2003; Salton and Szalay 2004; Polly 2008; Davis and McHorse 2013; Chen and Wilson 2015). Increasingly, three-dimensional geometric morphometrics (3D GM) is being used to compare shapes of tarsals because it enables analysis of the entire surface of the element and greater precision in capturing the shape of the functionally significant, curved surfaces in these elements (e.g., Polly 2008; Polly and MacLeod 2008; Boyer and Seiffert 2013; Fabre et al. 2014).

Previous research on astragali from this geologic interval included the qualitative and quantitative descriptive and functional morphology work on therian astragali from the Cretaceous (e.g., Godinot and Prasad 1994; Prasad and Godinot 1994; Szalay and Sargis 2006; Fabre et al. 2014) and Paleocene (e.g., Szalay and Decker 1974; Szalay 1977, 1994; Szalay and Sargis 2001; Chester et al. 2015). Previous research on K-Pg astragali from our study area specifically included qualitative and quantitative (i.e., traditional morphometrics, 2D and 3D GM) analyses that were largely limited to material from the Bug Creek Anthills (e.g., Sloan and Van Valen 1965; Szalay and Decker 1974; Szalay 1977; but see Chester et al. 2015), which is a time-averaged assemblage of latest Cretaceous and earliest Paleogene material (Lofgren 1995; Clemens 2002); consequently, it is suboptimal for analyses of faunal change through time. Additionally, some studies use K-Pg fossil astragali from our study area (i.e., from the Bug Creek Anthills) as comparative material in

the study of other fossils (e.g., Szalay et al. 1975; Rigby 1981; Godinot and Prasad 1994; Horovitz 2000; Boyer et al. 2010; Fabre et al. 2014; Chester et al. 2015); however, a comprehensive, 3D GM quantitative analysis of the locomotor capabilities of these specimens themselves has yet to be conducted.

Here, we provide the first 3D GM analysis of mammal astragali from the well-studied and well-sampled K-Pg study area of eastern Montana. First, to quantitatively assess morphology and predict locomotion for these fossils, we assembled a large, phylogenetically broad, comparative dataset of extant mammals of known locomotion. We micro-CT scanned all material and used 3D GM methods to quantify shape and morphofunctional relationships among locomotor groups. Then, we applied this framework to 24 fossil specimens to assess morphology and to predict locomotion for fossil mammals in our study area. We discuss the ecomorphological implications of these results in the context of other postcranial research on K-Pg mammals. This study complements the small but growing body of literature exploring postcranial patterns from this critical period in earth history (Borths and Hunter 2008; DeBey and Wilson 2014; Chester et al. 2015).

Institutional Abbreviations—**UCMP**, University of California Museum of Paleontology, Berkeley, California, U.S.A.; **USNM**, United States National Museum, Washington, D.C., U.S.A.; **UWBM**, University of Washington Burke Museum, Seattle, Washington, U.S.A.

2. Materials

2.1. Study Area and Specimens

Fossil specimens used in this study are from Paleogene-age deposits in eastern Montana. All specimens are from deposits in the uppermost Hell Creek and Tullock formations, from fossil localities in Garfield and McCone counties (Fig. S4.1; Table S4.1). Our eastern Montana study area is tied into a high-resolution chronostratigraphic framework that spans ~3.2 Ma across the K-Pg boundary (Archibald 1982; Swisher et al. 1993; Lofgren 1995; Clemens 2002; Renne et al. 2013; Wilson 2005, 2014; LeCain et al. 2014; Moore et al. 2014; Sprain et al. 2015). In the Western Interior of North America, the K-Pg boundary is approximately coincident with the boundary between the Lancian and Puercan North American Land Mammal "ages" (NALMAs; Cifelli et al. 2004; Lofgren et al. 2004; Sprain et al. 2015; but see Fox 1989 and Kelly 2014). Most fossil localities in the Hell Creek Formation are Lancian in age (ca. 68–66.04 Ma; Swisher et al. 1993; Renne et al. 2011, 2013; Sprain et al. 2015; Wilson 2014). However, in eastern Garfield County and Western McCone County, some localities in the uppermost Hell Creek Formation are earliest Paleogene (Puercan) in age (Lofgren 1995; Sprain et al. 2015); we include three specimens from three of these localities in McCone County (UCMP localities [locs.] V87038, V87098, and V87101). Specimens from the lowermost Tullock Formation are early Puercan (Pu1 interval zone, ca. 66.04–65.97 Ma), whereas those from the middle part of the Tullock Formation are late Puercan (Pu3 interval zone, ca. 65.74–65.12 Ma; Swisher et al. 1993; Renne et al. 2011, 2013; Wilson 2014; Sprain et al. 2015). Local faunas in our study area referable to the Pu2 interval zone (65.97–65.74 Ma; Sprain et al. 2015) have yet to be found

or described (e.g., Clemens 2015). Our study also includes astragali specimens from the temporally mixed Bug Creek Anthills assemblages, which are composed of both Lancian and earliest Puercan specimens (Lancian-Pu1 mixed; Lofgren 1995; Clemens 2002).

Our fossil sample includes 24 complete astragali from 15 localities. Of these astragali, four specimens were from two Pu1 localities, six specimens were from four Pu3 localities, and an additional 14 specimens were from nine localities in the temporally mixed Bug Creek Anthills assemblages (Lancian–Pu1 mixed age; Tables 1, S1; Fig. S4.1).

2.2. Taxonomic Scope

The Puercan and Lancian-Puercan mixed-age assemblages from our study areas consist of isolated teeth, fragmentary jaws, and isolated postcrania of multituberculates, metatherians, and eutherians (e.g., Archibald 1982; Clemens 2002; Wilson 2014). We chose to focus on the astragali of eutherians because (1) the morphology of multituberculate astragali are highly divergent (e.g., Granger and Simpson 1929; Deischl 1964; Jenkins and Krause 1983; Krause and Jenkins 1983; Szalay 1994; Kielan-Jaworowska and Gambaryan 1994); (2) locomotor inference is more reliable for fossil taxa that have extant relatives of known locomotor mode (i.e., metatherians and eutherians); and (3) metatherian astragali are absent from our sample of astragali.

2.3. Specimen Morphotypes

We subdivided our sample of K-Pg fossil astragali into four morphotypes (A, B, C, and D) on the basis of shape and size. Eleven specimens were placed in morphotype A, 11 in morphotype B, and one each in morphotypes C and D (Table 4.1). We compared

morphotypes to previously published astragali from our study area (e.g., Szalay and Decker 1974; Szalay 1977, 1994; Fabre et al. 2014; Chester et al. 2015) and from younger deposits (e.g., Matthew 1937; Rose 1987; Argot 2013).

Specimens in morphotype A are identical to those previously attributed to the archaic ungulate *Protungulatum* (Szalay and Decker 1974; Szalay 1977, 1994; Prasad and Godinot 1994; Szalay and Sargis 2001; Fabre et al. 2014; Chester et al. 2015). Specimens in morphotype B are identical to those previously attributed to the cimolestid *Procerberus* (Szalay and Decker 1974; Szalay 1977, 1994; Prasad and Godinot 1994; Szalay and Sargis 2001; Fabre et al. 2014; Chester et al. 2015). The lone specimen in morphotype C was previously attributed to the "plesiadapiform" primate *Purgatorius* (Chester et al. 2015).

The specimen in morphotype D, the largest specimen in our study, has not been previously attributed to taxon. We attribute this morphotype to an archaic ungulate on the basis of the following features: a shallow trochlea, broad and robust astragalar head, mediolaterally wide navicular facet that is dorsoventrally taller medially, presence of an astragalar foramen, and anteroposteriorly short, mediolaterally thick neck (e.g., Matthew 1937; Szalay and Decker 1974; Szalay 1977, 1994; Rigby 1981; Rose 1987; Argot 2013; Fabre et al. 2014; Chester et al. 2015). Specifically, this specimen specifically most closely resembles the astragali that have been attributed to *Protungulatum* (e.g., Szalay and Decker 1974; Szalay 1977, 1994), *Arctocyon primaevus* (Russell 1964; Argot 2013), and *Mithrandir gillianus* (formerly *Gillisonchus gillianus*; Rigby 1981); rather than the gracile astragali attributed to *Chriacus* (Szalay and Lucas 1996), *Apheliscus*, and *Haplomylus* (Penkrot et al. 2008), or the more robust astragali that have been attributed to *Ectoconus*, *Loxolophus*, and *Periptychus* (Matthew 1937). However, morphotype D differs from those taxa in

anteroposterior length (i.e., it is half the size of *Arctocyon* and 2.5x–3x the size of ?*Protungulatum* morphotype A), and in morphology (it is shorter dorsoventrally, the articulation for the medial malleolus is more shallowly sloping, the astragalar foramen is shifted more ventrally, and the neck is longer than in all of the above taxa). The presence of this large morphotype in Pu3 deposits suggests potential taxonomic affinity for one the largest archaic ungulates in the area, *Baioconodon* or *Bubagonia* (Clemens 2002; Wilson 2014). Lacking comparative astragali material from even larger Pu3 taxa in our study area, e.g., triisodontid *Eoconodon*, taeniodont *Wortmania*, and an unnamed pantodont (Clemens 2002; Wilson 2014), we are unable to compare this to our material; however, our specimen has a much longer astragalar neck than younger pantodont *Pantolambda bathmodon* (Matthew 1937), and differs greatly from younger taeniodonts *Onychodectes*, *Psittacotherium*, and *Stylinodon* in head, neck, and sustentacular facet morphology (Matthew 1937; Schoch 1986). As this specimen clearly resembles archaic ungulate taxa, we attribute it to taxon, although we note this specimen is fragmentary (missing the distal astragalofibular facet, most of the ectal facet, and the superomedial margin of the ectal facet), and therefore taxonomic affinity should be considered a hypothesis.

Because all comparative material for morphotypes A–D were found as isolated elements, we follow Krause and Jenkins (1983) and DeBey and Wilson (2014) in using a query ('?') to indicate the relative uncertainty of these (and others') taxonomic attributions. We direct the reader to the discussion of isolated element attributions to taxon for K-Pg mammals in DeBey and Wilson (in prep).

2.4. Comparative Extant Mammal Specimens

To infer locomotor preference among our fossil therian specimens, we compared our material to astragali of extant taxa of known locomotor mode. Our sample of small mammals is a subset of the sample in Chen and Wilson (2015), which broadly sampled taxonomic and locomotor mode diversity. We broadened our taxonomic sampling by adding select small-bodied carnivorans, cingulatans, lagomorphs, an afrosoricid, and a scandentian (Table 4.2). We included one specimen of each taxon. Our sample of extant eutherian and metatherian astragali numbers 51 total individuals, from 48 genera in 13 mammalian orders (Tables 2; Fig. 4.2). We categorized all species as arboreal, gliding, fossorial, semifossorial, scansorial, semiaquatic, or terrestrial according to the definitions in Chen and Wilson (2015; Table 4.3; Fig. 4.2). These locomotor mode designations were taken from the literature (e.g., Nowak 1999) and were based on observations in the wild.

3. Methods

We quantify and compare shape among our fossil astragali via three-dimensional geometric morphometrics (3D GM). This analysis allows (1) a quantitative comparison of shape across fossil and extant specimens that is independent of size, and (2) a more comprehensive investigation and visualization of the particular areas of the astragalus that are driving the variation in the sample (Zelditch et al. 2004). Because some of our fossil specimens are abraded or fractured in some areas, we opted to not conduct analyses that utilize a surface grid or "eigensurface" (e.g., Polly and MacLeod 2008, Boyer et al. 2014). Instead we analyzed morphology by placing points on a 3D mesh (e.g., Gladman et al. 2013; Fabre et al. 2014).

3.1. Micro-CT Scanning and Post-Processing

Astragali specimens were scanned in three dimensions using a high-resolution microCT scanner (Skyscan 1174, Bruker MicroCT, Kontich, Belgium; 2013). Resolution of the astragali scans was according to the size of the bone. The smallest specimens, e.g., the shrew mole *Neurotrichus gibbsii*, were scanned at 9.6 um; larger-bodied species, such as the carnivoran *Vulpes vulpes* and the rodent *Castor canadensis*, were scanned at a lower resolution of 60.37 um. Fine detail, including bone texture, was visible at these resolutions (Table S4.2).

CT scans were reconstructed using NRecon version 1.6.9.18 (Bruker MicroCT; 2014). We adjusted reconstruction parameters (e.g., ring artifacts reduction, beam hardening) to produce scans that were as clear and clean as possible. We consistently

applied minimal smoothing (i.e., averaging) so as not to lose data. Reconstructed scans were output as jpeg files (with a few exceptions output as tiff files; full reconstruction details are available in Table S4.2).

Reconstructed scans were transformed into 3D models with Mimics software (Mimics Research 17.0; Materialise NV, Leuven, Belgium; 2014). We first created a "mask" on the reconstruction, with upper and lower thresholds set to capture the bone morphology and eliminate noise or "scatter" introduced during scanning and reconstruction (see full model details in Table S4.3). We created 3D models from these masks, and output models as "Stereo lithography files" (.stl) meshes (Table S4.3).

All model meshes were cleaned using Geomagic Studio 2014.1.0 (3D Systems, SC, USA; 2014) to reduce file size and eliminate any remaining noise. Cleaning of scans is standard practice in 3D geometric morphometrics to e.g., reduce spike artifacts and fill small holes that are by-products of scanning, reconstruction, or modeling parameters (i.e., Gladman et al. 2013). Because our study is focused on the exterior surface of the astragalus, we also eliminated internal bone structure (e.g., internal vertices, which increase file size). Also in Geomagic, right astragali were reflected to appear as lefts. We decimated (i.e., downsampled) especially large files (e.g., 1,000,000+ polygons) to 50–75% of the original number of triangles; these reductions greatly reduced file size but did not significantly reduce shape resolution (Table S4.3). Cleaned .stl files were exported as "Standard Polygonal Mesh" files (.ply). Finally, we added one astragalus of the extant scandentian *Ptilocercus lowii* (Table 4.2) and one fossil astragalus (UCMP 159709 from loc. V99438; Table 4.1) from the MorphoSource website (http://morphosource.org; see Tables S4–S5 for specimen, scanning, and funding details) to our sample.

3.2. Morphological Variation Using 3D Geometric Morphometrics

Our landmarks and semilandmarks (LMs and SLMS, respectively) predominantly characterize the shape of articular surfaces, and as such are homologous and morphologically and functionally informative (Bookstein 1991; Zelditch et al. 2004). We selected 13 landmarks (Fig. 4.3) to plot on each specimen, based on Fabre et al. (2014) with minor adjustments (Table 4.4). We also used semilandmarks (SLMs) to more comprehensively characterize shape of curves (Zelditch et al. 2004; Gunz and Mitteroecker 2013; Wilson 2013). We designated three curves (i.e., 23 SLMs) for plotting on each specimen; all curves are anchored at the endpoints by LMs (Fig. 4.3; Table 4.4; Fabre et al. 2014).

Points and curves were digitized on .ply files using the software Idav Landmark 3.0 (version 3.0.0.6; Wiley et al. 2005). Points (LMs) were placed on specimens using the 'single point' function; curves were designated with the curve function. Curves are designated in Landmark using three points (two LMs to anchor the endpoints of the curve, and a middle point that functions as a SLM). We resampled each curve for a specific number of points that are equally distributed by length between the midpoint SLM and endpoint LM (Fig. 4.4; Table 4.4). Because all curves are designated using only three points, we traced simple curves (i.e., trochlea curvature), rather than complex curves (i.e., outlines of articular surfaces). Resultant curves lay flat against the surface of the specimen. All points were plotted by one of us (L.B.D.) over a period of two weeks, eliminating inter-observer bias and minimizing intra-observer error variability over time.

We performed Procrustes generalized least squares (GLS) superimposition (Rohlf and Slice 1990; Zelditch et al. 2004) to remove the effects of translation, rotation, and scale

on landmark and curve configurations so that only shape differences remained (Kendall 1977; Zelditch et al. 2004). For curves specifically, we designated every other point as either a "helper" or a "slider." Helper points anchor the curve, and sliders are allowed to slide within a pair of helper points, which minimizes Procrustes difference among points along the curve (Gunz and Mitteroecker 2013; Wilson 2013; Fabre et al. 2014). Then one computes a Procrustes superimposition from these slid coordinates. Subsequently all SLMs were allowed to slide with respect to the average Procrustes shape (Gunz and Mitteroecker 2013). After superimposition, we deleted all helper points from subsequent analyses, and designated curve SLMs (i.e., points within a curve) as separate from LMs (i.e., stand alone points, and curve endpoints).

Following Procrustes superimposition, resultant shape data from all LMs and SLMs was subjected to principal components analysis (PCA) to examine the variation in shape. In each case we conducted PCAs on extant taxa only, and projected fossils into this morphospace following methodology of DeBey and Wilson (in prep). First we calculated a mean shape for all specimens, and subtracted this from the Procrustes superimposed dataset to produce Procrustes residuals (Polly and MacLeod 2008; Wilson 2013). Second, we conducted PCAs on the covariance matrix of the residuals of the extant specimens only, and used singular value decomposition to calculate the eigenvectors for the extant dataset (Polly and MacLeod 2008). Third, we determined PCA scores for fossil specimens by calculating the dot product of the eigenvectors and the Procrustes residuals of the fossil specimens.

We conducted a Procrustes non-parametric multivariate analysis of variance (Procrustes PERMANOVA) on Procrustes distances of the 3D LM and SLM coordinates to

quantify the relative amount of shape variation attributable to locomotor mode and/or taxonomic order (as a proxy for phylogeny; Goodall 1991). Specifically we tested three hypotheses: whether astragali shapes were significantly different with respect to 1) locomotor modes, 2) taxonomic order, or 3) locomotor mode and order as covariables.

We used linear discriminant analysis (LDA) to maximize differences among a priori groups and predict locomotor groups based on astragalus shape (Mitteroecker and Bookstein 2011). This ordination method uses the principal components and an external variable (i.e., locomotor function) to train the LDA function, and then generates an assessment of how often the function can correctly predict the known locomotor function of each extant mammal in our dataset. We also used LDA to rank predicted locomotor modes for our K-Pg fossil specimens.

All analyses were conducted within RStudio version 0.98.1062 (RStudio 2012) in R version 3.1.2 (R Core Team 2014). Procrustes superimpositions, designation of particular points (i.e., helpers, sliders, LMs, and SLMs), all PCA and PERMANOVA analyses were performed using the 'geomorph' package (Adams and Otarola-Castillo 2013). LDA analyses were performed using the 'lda' function from the 'MASS' package (Venables and Ripley 2002).

4. Results

4.1. Full Dataset

We chose to evaluate the astragalus morphospace defined by PCs 1–3; together, these PCs represent 49.1% of the total variance and each represents >10% of the variance (Fig. 4.5; Table 4.5). Extant mammals plot in the morphospace largely according to phylogeny (Fig. 4.5), rather than by locomotor group (Fig. 4.6). Eutherians cluster more closely in the morphospace, and occupy less of PC2, than do metatherians (Fig. 4.5). Within the eutherian morphospace, cingulatans are located at maxima of PCs 1–3, and carnivorans, scandentian *Ptilocercus*, and primates at the minima of PC1, PC2, and PC3, respectively (Fig. 4.5). Within the metatherian morphospace, diprotodonts are located at the minimum of PC1 and maximum of PC2, didelphimorphs at the minimum of PC2 and maximum of PC3, and the peramelemorph *Perameles* at the minimum of PC3 (Fig. 4.5). All of our fossils are located within or nearest to the eutherian morphospace for PCs 1–3, and within the metatherian morphospace for PCs 2–3 (Fig. 4.5). Specifically, fossil specimens are located nearest to rodent, carnivoran, and eulipotyphlan taxa, and select lagomorphs (*Ochotona*), scandentians (*Tupaia*), macroscelideans (*Elephantulus*), and primates; fossil specimens are consistently far from cingulatans (Fig. 4.5).

We visualized shape deformation for PCs 1–3 using three-dimensional warps of PC scores from minima to maxima. PC1 represents 23% of the total variance (Table 4.5) and change along this axis corresponds to differences in overall mediolateral width and dorsoventral height, and the shape and size of the head, ectal facet, and groove for the flexor fibularis tendon. In this morphospace, specimens with high scores on PC1 have a

mediolaterally wide astragalar body, wide groove for the flexor fibularis tendon, mediolaterally narrow astragalar head, mediolaterally wide ectal facet, and are dorsoventrally short. These specimens include all metatherians in our sample as well as cingulatan eutherians (Fig. 4.5). In contrast, specimens with low scores on PC1 are mediolaterally narrower and dorsoventrally taller, and have a wider astragalar head. These include carnivorans *Mustela vison* and *M. erminea* and *Gulo gulo*, and the scandentian *Ptilocercus* (Fig. 4.5). Among eutherians, carnivorans, scandentians, primates, lagomorphs, and eulipotyphlans are generally located lower on PC1, whereas cingulatans and rodents are located higher on PC1 (Fig. 4.5).

Despite the clear phylogenetic signal, PC1 discriminates among some locomotor groups for both eutherians and metatherians. Among metatherians, arboreal and scansorial specimens (high on PC1) are separate from saltatorial specimens (lower on PC1; Fig. 4.6). This pattern is consistent with the observation that the astragali of saltatorial metatherians are dorsoventrally taller and mediolaterally narrower (with locomotion more restricted parasagittally), than are those of arboreal and scansorial metatherians (Szalay 1994). Among eutherians, arboreal and terrestrial taxa (low on PC1) are generally separate from fossorial taxa (higher on PC1; Fig. 4.6), a pattern that is consistent with the observation that astragali of fossorial taxa are more robust and have a larger groove for the flexor fibularis tendon (involved in plantarflexion) relative to the more gracile astragali of arboreal taxa (e.g., Szalay 1994; Salton and Szalay 2004; Polly 2008). Fossil specimens plot near the origin of PC1, and this axis discriminates well between morphotypes A and B (Figs. 5–6). Specimens in morphotype A (?*Protungulatum*) are among the most robust of our fossil specimens (i.e., mediolaterally wide and proximodistally short) and therefore have

the highest PC1 scores (Figs. 5–6). In contrast, specimens in morphotype B (?*Procerberus*) are more gracile (i.e., mediolaterally narrow and proximodistally long) and have the lowest PC1 scores of our fossil specimens (Figs. 5–6). The specimens in morphotypes C (?*Purgatorius*) and D (?archaic ungulate) are located within the PC1 morphospace of morphotype B (Figs. 5–6). Morphotype C is dorsoventrally tall and has a mediolaterally narrower trochlea, and is lower on PC1, than is morphotype A (Figs. 5–6). The body of the specimen in morphotype D (?archaic ungulate) is broken laterally and the specimen appears mediolaterally narrower than it naturally is; we find that the placement of this specimen along PC1 (i.e., nearer to morphotype B than ?*Protungulatum* morphotype A, and mediolaterally narrower than extant mammals) is potentially a function of specimen breakage (Figs. 5–6).

PC2 represents 14% of the total variance (Table 4.5) and change along this axis corresponds to differences in proximodistal length, location of the astragalar head relative to the body, and shape of the trochlea and ectal and medial astragalotibial facets. Specimens with high scores on PC2 are proximodistally shorter, have an astragalar head that is more offset the body medially (i.e., more perpendicular to the body), and have an especially wide lateral trochlear ridge distally. These specimens include the metatherians *Potorous* and *Aepyprymnus*, as well as all cingulatans, the rodents *Coendou* and *Sciurus aberti*, and the afrosoricid *Echinops* among eutherians (Fig. 4.5). Specimens with low scores on PC2 are proximodistally longer, have a dorsoventrally shorter medial astragalotibial facet (i.e., LM 12 shifted dorsally), and have an ectal facet that has a ventrally shifted medial edge (i.e., LM 1 shifted ventrally). These specimens include *Trichosurus* and both

didelphimorph metatherians, and the scandentian *Ptilocercus* and both saltatorial lagomorphs (*Lepus* and *Brachylagus*).

The PC2 axis discriminates among metatherian locomotor groups well, but there does not appear to be a locomotor pattern among eutherians. Among metatherians, PC2 separates saltatorial (high scores on PC2) from arboreal, gliding, and scansorial taxa (low scores on PC2; Fig. 4.6). The saltatorial and terrestrial metatherians generally have astragali with e.g., a dorsoventrally taller head, whereas arboreal and scansorial metatherians, which are habitual inverters, have a medially extensive and transversely oriented head and astragalonavicular facet (Szalay and Decker 1974; Szalay 1994; Salton and Szalay 2004). As with PC1, fossil specimens are generally located near the middle of the PC2 axis (Figs. 5–6). Specimens in morphotype B (high scores on PC2) have astragalar heads that are more perpendicular to the astragalus body and a relatively longer lateral trochlear ridge than all other morphotypes; PC2 discriminates morphotype B from all other morphotypes fairly well (Figs. 5–6). PC2 does not discriminate among morphotypes A, C, and D; they share features characteristic of extant specimens at the minimum of PC2: medial and lateral trochlear ridges that are approximately equal in length, a head that is somewhat offset the astragalus body, and a ventrally shifted LM 1 (Figs. 5–6).

PC3 represents 11% of the total variance (Table 4.5) and change along this axis corresponds to differences in trochlea mediolateral width and proximodistal length and mediolateral head width. Specimens with high scores on PC3 generally have a wider distance between trochlear ridges (specifically, between the points of maximum curvature on the trochlear ridges), a trochlear surface that is less distally extensive, and a head that is mediolaterally wide. Among eutherians, these specimens include all cingulatans and the

rodents *Castor*, *Dipodomys*, *Aplodontia*, and all cricetids; among metatherians, only the didelphid *Caluromys* is near the maximum of PC3 (Fig. 4.5). In contrast, specimens with low scores on PC3 have a mediolaterally narrower distance between trochlear ridges, a longer trochlea distally, and a mediolaterally narrow head. These specimens are mostly metatherians (e.g., *Perameles*, *Potorous*, and *Trichosurus*); eutherians with low scores on PC3 include primates, the scandentian *Ptilocercus*, and the afrosoricid *Echinops* (Fig. 4.5). Metatherians that located low on PC3 have a mediolaterally narrow trochlear surface; however, LM placement along the maxima of trochlear curvature is synonymous with trochlear width in eutherians but may not be in metatherians that have a wide, flat dorsal articulation (e.g., Szalay 1994; Argot 2002).

As with PC2, locomotor patterns on PC3 may differ between metatherians and eutherians; however, not all locomotor categories are common to both metatherians and eutherians and thus we are unable to explicitly test this hypothesis. For example, among eutherians PC3 discriminates fossorial and semifossorial taxa (high on PC3) from arboreal, gliding, and terrestrial taxa (low on PC3; Fig. 4.6), but we lack fossorial and semifossorial metatherians for comparison. All fossil specimens are located approximately in the middle of PC3 (Figs. 5–6). PC3 does not discriminate between morphotypes A and B (?*Protungulatum* and ?*Procerberus*, respectively), as each occupy approximately the same region on PC3 (Figs. 5–6); specimens in morphotypes C and D also occur within this region of PC3. We note that morphotype D (?archaic ungulate) has a larger PC3 score than morphotype C (?*Purgatorius*; Figs. 5–6), suggestive of a narrower trochlea in the former than the latter, but we suggest this is a function of specimen breakage in morphotype D (Fig. 4.1)

On the basis of these results, we pruned metatherians and cingulatans from our dataset for a few reasons. First, there is substantial separation between metatherians and eutherians in this morphospace, and we detect a difference in locomotor patterns between these two groups. Second, metatherians define the maxima and minima of PC2, and their extreme morphological difference may obscure patterns present among eutherians. Third, morphotype assignment suggests that all fossil specimens are eutherian, which is supported by the pattern of fossil placement in the morphospace; as such, functional morphology patterns across metatherian specimens are unlikely to be analogous for these fossil specimens (or extant eutherians; e.g., Jenkins and McClearn 1984; Szalay 1994; Chen and Wilson 2015). Finally, because our dataset samples more eutherians than metatherians, we can ameliorate any effects of sampling biases by removing metatherians. Although cingulatans are eutherians, we removed them for reasons similar to those for the metatherians. First, despite phylogenetic distance, the pattern of placement for cingulatans is closer to that of metatherians; and like metatherians, cingulatans consistently fall far from our fossil specimens. Second, they have an astragalar morphology that is sufficiently unique to define the maxima among eutherians for all three PCs; as such, they could obscure more nuanced locomotor patterns that are present across the rest of the eutherian sample. We therefore conducted subsequent analyses on pruned datasets that included what were deemed the most appropriate analog taxa for comparison with our K-Pg fossil specimens.

4.2. Reduced Dataset (metatherians and cingulatans removed)

We removed metatherians and cingulatans from the dataset and conducted a new Procrustes superimposition and PCA on this reduced dataset (PC1–3 explains 41.6% of the total variance; Table 4.5). The locomotor signal within this eutherian dataset, especially on PC2, is improved relative to the full dataset. Within this morphospace, we see clear discrimination among fossil morphotypes, particularly for morphotypes A, B, and C.

For this reduced dataset, PC1 represents 17% of the total variance (Table 4.5) and change along this axis corresponds to differences in specimen proximodistal length and mediolateral width, depth of the trochlear groove, and, to a lesser extent, the groove for the flexor fibularis tendon and the shape of the ectal facet. Specimens with high scores on PC1 are more robust (i.e., proximodistally short and mediolaterally wide), with a proximodistally short and dorsoventrally deep trochlear groove, and a wider ectal facet. These include nearly all rodents (i.e., *Sciurus aberti*, *Coendou*, *Cynomys*, *Ondatra*, *Dipodomys*) followed by macroscelidean *Elephantulus* and afrosoricid *Echinops* (Fig. 4.7). In contrast, specimens with low scores on PC1 are proximodistally long (especially at the astragalar neck and head), have a trochlea that is mediolaterally narrow, proximodistally long, and dorsoventrally shallow, a narrower ectal facet, and have a ventrally shifted groove for the flexor fibularis tendon. These specimens include the scandentian *Ptilocercus* and all mustelid carnivorans (*Mustela vison*, *M. erminea*, *M. putorius*; Fig. 4.7). As with the full dataset, the pattern of distribution in this morphospace reflects phylogeny more than locomotor mode (Figs. 7–8). Our fossil specimens plot near the origin of PC1; morphotypes C (?*Purgatorius*) and D (?archaic ungulate), each with a narrower ectal facet and ventrally shifted groove for the flexor fibularis tendon, have lower scores on PC1 than do most specimens in morphotypes A (?*Protungulatum*) and B (?*Procerberus*; Figs. 7–8).

PC2 represents 13% of the total variance (Table 4.5) and change along this axis corresponds to differences in the location of the astragalar head relative to the body, and to a lesser extent, the shape of the distal trochlear surface and the dorsoventral height of the medial astragalotibial facet. Specimens with high scores on PC2 (e.g., all lagomorphs and some rodents; Fig. 4.7) have a head that is more in line with the astragalar body and a deeper excavation on the distal surface of the trochlea (i.e., LM 8 is shifted proximally). In contrast, specimens with low scores on PC2 (e.g., Sciurus spp., the afrosoricid *Echinops*, the macroscelidean *Elephantulus*; Fig. 4.7) have a head that is more perpendicular to the body (shifted medially relative to the body), and some specimens have a medial astragalotibial facet that is dorsoventrally tall (e.g., *Sciurus* spp.; Fig. 4.7).

Some discrimination among locomotor groups is detectable along PC2: saltatorial and fossorial taxa have high scores; arboreal, gliding, and scansorial taxa have low scores; whereas semifossorial and terrestrial specimens are intermediate and overlapping (terrestrial taxa have slightly lower PC2 scores than semifossorial taxa do; Fig. 4.8). This discrimination is consistent with functional inferences of the distal trochlear surface (i.e., at LM8); that is, the presence of an excavation/hollowing on the distal trochlear surface (high scores on PC2; Fig. 4.8) is correlated with tibial contact and high loads in locomotor modes (saltatorial, fossorial, semifossorial) that require extreme dorsiflexion (e.g., leaping, galloping, or stabilizing during forelimb digging; Godinot and Dagosto 1983; Hildebrand 1985; Dagosto 1988; Rose 1999; Salton and Szalay 2004). In contrast, arboreal and scansorial, which have low scores on PC2, lack this hollowing on the distal trochlear surface (Salton and Szalay 2004; Fig. 4.8). On PC2, semiaquatic carnivorans and rodents plot in different parts of the morphospace: semiaquatic carnivorans are located nearest terrestrial,

scansorial, arboreal, and semifossorial carnivorans, whereas semiaquatic rodents are located nearest saltatorial and fossorial rodents (Figs. 7–8), which suggests a phylogenetic signal on this axis. On PC2, fossil specimens are located at the middle and towards the maximum (Figs. 7–8). Among our fossil specimens, those in morphotype A (?*Protungulatum*) have an astragalar head that is the most in line with the astragalar body; as a result, these specimens have the highest scores on PC2 (Figs. 7–8), despite lacking any hollowing at the distal trochlear surface (LM8). Specimens in morphotypes B (?*Procerberus*) and C (?*Purgatorius*) have a head that is more perpendicular (medially offset) to the astragalar body; as a result, they are located lower on PC2 (Figs. 7–8). Morphotype B is nearest to semifossorial rodents and carnivorans, and semiaquatic, scansorial, and terrestrial carnivorans on PC2; morphotype C is nearest to arboreal primates and carnivorans, and scansorial, terrestrial, and semiaquatic carnivorans on PC2 (Figs. 7–8). The specimen in morphotype D (?archaic ungulate) has a head that is oriented similarly to that of morphotype A, and is therefore located fairly high on PC2; this specimen is nearest to the fossorial rodent *Aplodontia*, the fossorial eulipotyphlan *Scalopus*, and the semifossorial rodent *Synaptomys* on this PC2 axis (Figs. 7–8).

PC3 represents 12% of the total variance (Table 4.5) and change along this axis describes dorsoventral head height, and to a lesser extent the relative sizes of medial and lateral trochlear ridges. Specimens with high scores on PC3 have a dorsoventrally tall head and a lateral trochlear ridge that is longer than the medial, and are generally proximodistally long and mediolaterally narrow; specimens with low PC3 scores have the reverse morphology. Lagomorphs, both species of *Glaucomys*, and most primates have the highest PC3 scores, whereas the scandentian *Tupaia*, and the carnivorans *Lontra* and *Gulo*

have the lowest PC3 scores (Fig. 4.7); the rodents *Castor* and *Ondatra*, and eulipotyphlans *Scalopus* and *Scapanus* are also have low scores on PC3, but none have medial trochlear ridges that are proximodistally longer than the lateral (Fig. 4.7).

PC3 discriminates well among locomotor and morphotype groups. On this axis, gliding, saltatorial, and arboreal taxa (high scores on PC3) are separate from fossorial and semiaquatic taxa (low scores on PC3); semifossorial, scansorial, and terrestrial taxa are intermediate and overlapping the above groups (Fig. 4.8). The longer lateral trochlear ridge (i.e., high scores on PC3) corresponds to a larger articulation with the fibular malleolus, and restricted mobility in the parasagittal plane for saltatorial specimens or a lateral brace during climbing for arboreal and gliding specimens (Salton and Szalay 2004). That specimens with high scores on PC3 are generally proximodistally longer also implies increased propulsive abilities for saltatorial locomotion (e.g., Salton and Szalay 2004). In this morphospace, all fossil specimens are located relatively low on PC3 (Figs. 7–8). Specimens within morphotype A (?*Protungulatum*) have medial and lateral ridges that are approximately equal in length, and are generally located lower on PC3; a number of morphotype A specimens fall beyond the minimum of PC3 for extant taxa (Figs. 7–8). Specimens within morphotype B (?*Procerberus*) have longer lateral trochlear ridges and are therefore located the highest on PC3 of the fossils in our sample, nearest to fossorial, semifossorial, terrestrial, and scansorial taxa, and nearer to arboreal taxa than the other fossil morphotypes (Fig. 4.8). Morphotype C (?*Purgatorius*) is proximodistally short and robust relative to other fossil specimens and has trochlear ridges that are approximately equal in length; it is located at the absolute minimum of PC3, nearest to specimens of morphotype A and extant scansorial *Tupaia* and semiaquatic *Lontra*, and far from arboreal

specimens (Figs. 7–8). On PC3, morphotype D (?archaic ungulate) is generally located between morphotypes A and B, nearest to the fossorial eulipotyphlan *Scalopus* and semiaquatic *Lontra* (Figs. 7–8); the broken lateral ridge of this specimen artificially reduces the lateral ridge length relative to the medial, and therefore this specimen may fall higher on PC3 were it not for its fragmentary state (Fig. 4.1).

4.3. Further Reduced Dataset

We pruned the dataset a final time to 1) refine our sample towards the most appropriate analogs for our specimens, and 2) ameliorate sampling biases across taxa. First, we removed gliding eutherians (i.e., flying squirrels), which consistently plotted far from our fossil taxa and therefore likely less relevant to locomotor inference in the fossil taxa. Second, if a single specimen was the sole representative for a taxonomic order, we removed it (i.e., afrosoricid *Echinops* and macroscelidean *Elephantulus*; Table 4.2) because we could not rule out whether its location in the morphospace primarily reflected locomotor mode or phylogeny. For example, scansorial afrosoricid *Echinops* had the lowest score on PC2, whereas other scansorial taxa do not plot so extreme on this axis; without other afrosoricid taxa, we are unable to determine whether this is primarily a functional or phylogenetic trend. As with the previous dataset reduction, we conducted a new Procrustes superimposition and principal components analysis on this final, most reduced dataset (Figs. 9–10; Table 4.5); all subsequent analyses are conducted on this dataset.

In this morphospace, PC1 represents 19% of the total variance (Table 4.5) and change along this axis describes the shape of the astragalus body and the position of the astragalar head. Specimens with high PC1 scores have a mediolaterally wide astragalar

body (specifically with a wide trochlea and laterally extensive ectal facet), and a mediolaterally deeper trochlear groove. These specimens include e.g., the rodents *Castor*, *Ondatra*, *Sciurus*, and *Coendou* (Fig. 4.9). In contrast, specimens with low PC1 scores are proximodistally long, with a mediolaterally narrow astragalar body, mediolaterally flat trochlea, and medially-shifted astragalar head (more perpendicular to the astragalus body); these specimens include the scandentian *Ptilocercus*, the carnivorans *Mustela vison*, *M. erminea*, and *Gulo*, and the lagomorph *Lepus* (Fig. 4.9).

The distribution of extant taxa along PC1 strongly reflects phylogeny rather than locomotor mode (Figs. 4.9–10); the exception to this pattern are the scandentians, which differ from one another in locomotor mode and are segregated in the morphospace (Fig. 4.9). PC1 discriminates moderately well among some fossil morphotypes. Morphotypes C and D have lower scores on PC1 than morphotypes A and B do. That morphotype D (?archaic ungulate) is located nearer to morphotype C (?*Purgatorius*) on this PC than to the mean of morphotype A (?*Protungulatum*) is most likely due to breakage in this specimen, specifically at the ectal facet and the lateral trochlear ridge.

PC2 represents 17% of the total variance (Table 4.5) and change along this axis describes the relative position of the astragalar head, the size, shape, and position of the ectal facet, and the size and shape of the fibular facet and lateral trochlear ridge. Specimens with high PC2 scores have an astragalar head that is displaced medially relative to the body (i.e., the sustentacular facet is more perpendicular to the body), a large and mediolaterally wide ectal facet that is proximally shifted relative to the trochlea, a trochlea that is characterized at the proximal end by a lateral ridge that is less ventrally extensive, and a fibular facet that has a larger articular surface distally; these specimens include the

scandentian *Tupaia*, the rodent *Coendou*, and the carnivoran *Lontra* (Fig. 4.9). In contrast, specimens with low PC2 scores have an ectal facet that is mediolaterally narrow and proximodistally long, a mediolaterally narrow trochlea, and an astragalus head and body that are in line with one another; these specimens include the lagomorphs *Brachylagus*, *Lepus*, and *Ochotona* (Fig. 4.9).

Locomotor groups are spread along PC2, from saltatorial and semifossorial taxa (low PC2 scores), to fossorial, arboreal terrestrial, and semiaquatic taxa (near the PC2 origin), and scansorial taxa (high PC2 scores; Fig. 4.10). This locomotor gradient indicates that scansorial taxa (i.e., high PC2 scores) have an astragalus with wider trochlea, larger fibular facet, larger and mediolaterally more extensive ectal facet, and astragalar head that is more perpendicular to the body, all suggestive of greater rotational abilities (e.g., inversion and eversion) and stability during climbing (Salton and Szalay 2004; Chester et al. 2015). Among fossils, PC2 only discriminates morphotype C (?*Purgatorius*) from all other morphotypes. Morphotype C is located high on PC2, beyond even extant taxa (i.e., the scansorial rodent *Coendou* and the scandentian *Tupaia*; Figs. 9–10). The morphology of this specimen is consistent with that of scansorial specimens high on PC2, e.g., a larger ectal facet than in morphotypes A, B, and D, an astragalar head that is more perpendicular to the body, and a lateral ridge of the trochlea that is less ventrally extensive.

PC3 describes 11% of the total variance (Table 4.5) and change along this axis describes the shapes of the medial and lateral trochlear ridges. Specimens with high scores on PC3 have proximodistally long and dorsoventrally short trochlear ridges and associated facets on either side of the trochlea (i.e., medial astragalotibial facet medially, and fibular facet laterally); these specimens include the carnivorans *Paguma* and *Mustela vison*, the

rodent *Coendou*, and the primate *Saguinus* (Fig. 4.9). In contrast, specimens with low scores on PC3 generally have the reverse condition, with proximodistally short and dorsoventrally tall medial and/or lateral trochlear ridges. At the minimum of PC3, the scandentians *Tupaia* and *Ptilocercus* have tightly curved lateral trochlear ridges, eulipotyphlans *Scapanus*, *Scalopus*, and *Urotrichus* have tightly curved medial trochlear ridges and taller lateral ridges, and rodents *Aplodontia* and *Octodon* have tightly curved medial and lateral trochlear ridges (Fig. 4.9).

PC3 discriminates between terrestrial (higher on PC3) and saltatorial (lower on PC3) taxa (Fig. 4.10). This distribution of locomotor modes is largely consistent with functional implications of the astragalotibial and fibular facets (and the corresponding tibia and fibula malleoli, respectively); taller facets restrict movement of the foot to the parasagittal plane, and therefore saltatorial taxa are expected to be lower on PC3 (Szalay 1977; Salton and Szalay 2004). More generally, arboreal, terrestrial, and semiaquatic taxa are located higher on PC3, whereas fossorial and semifossorial taxa (and scansorial *Tupaia*) are located lower on PC3 (Fig. 4.10). The placement of fossorial taxa (e.g., eulipotyphlans) low on PC3, with their dorsoventrally deep lateral trochlear ridge (i.e., fibular malleolus) and relatively shallow medial trochlear ridge (i.e., tibial malleolus), is consistent with the lateral stabilization required for eversion and flexion during digging (Salton and Szalay 2004). PC3 discriminates fairly well between morphotypes A and B, with specimens in morphotype B generally located higher, and specimens in morphotype A located lower on PC3 (Figs. 9–10); however, both morphotypes A and B have moderately curved medial and lateral trochlear ridges and generally are located near the origin of PC3. Morphotypes C and D are both located near the origin of PC3 and generally at between specimens in

morphotypes A and B; morphotype C is slightly more negative than morphotype D (Figs. 9–10).

Procrustes PERMANOVA results suggest astragali shape in our final sample of extant mammals is significantly different across both locomotor mode ($r^2 = 0.26$, $P < 0.05$; Table 4.6) and taxonomic order ($r^2 = 0.43$, $P < 0.05$; Table 4.6), but taxonomy explains more of the variance in the dataset than does locomotor mode alone. Astragali shape is significantly different in the model containing both locomotor mode and order; within this model order explains more of the variance than does locomotor mode ($r^2 = 0.33$ and $r^2 = 0.26$, respectively; Table 4.6).

We conducted a linear discriminant function analysis (LDA) on this most reduced dataset to 1) remove some effects of phylogeny, 2) examine more explicitly the variance with respect to locomotor function in our dataset, and 3) predict locomotor mode for our fossil specimens. Because the first three principal components in this final dataset only represented 47% of the total variance and there are 17 PCs that each represent >1% of the variance, we conducted an LDA on all 17 principal components of this most reduced dataset. This LDA model predicts locomotor function with 95% accuracy (Table 4.7); the only two specimens misclassified were the saltatorial rodent *Dipodomys*, which was misclassified as fossorial, and the semifossorial *Ochotona*, which was misclassified as saltatorial. We reduced the LDA space to the first three axes (LDs 1–3, explaining 58%, 19%, and 14% of the between-group variance in the data, respectively) for visualization and interpretation. This LDA model discriminates among arboreal, scansorial, fossorial, and terrestrial locomotor modes well; semifossorial, saltatorial, and semiaquatic taxa show some overlap (Fig. 4.11). In this LDA morphospace, morphotype A (?*Protungulatum*) plots

high and morphotype B (?*Procerberus*) plots low for LDs 1–2, morphotype C plots highest on LD3, and morphotype D plots centrally in all plots (Fig. 4.11). LDA predictions generated for each fossil suggest 82% of specimens in morphotype A are fossorial, all other specimens are predicted to be semifossorial (UCMP 152018 and 197518, from locs. in the BCA and Pu3 biozones, respectively; Table 4.8); this is consistent with the placement of morphotype A in the LDA morphospace (Fig. 4.11A,B). Most specimens in morphotype B (82%) are predicted to be semifossorial, but two specimens are predicted to be arboreal (UCMP 151955 and 192514, from BCA and Pu3 biozones, respectively; Table 4.8). Morphotype C is predicted to be semifossorial (98.03% prediction probability), followed by terrestrial (1.38%; Table 4.8). Morphotype D is predicted to be semifossorial (97.5% prediction probability), followed by fossorial (2.06%; Table 4.8).

5. Discussion

5.1. Astragalus shape reflects phylogeny and locomotor mode

Across all three partitions of the data from extant mammals, results indicate morphology of the astragalus is influenced by phylogeny. In our most inclusive dataset, metatherians and eutherians clustered separately from one another in the morphospace, with only the widest eutherian astragali (i.e., armadillos) plotting near metatherians; the gross similarity of metatherian and cingulatan astragali has been previously recognized, if only qualitatively (Szalay 1977). In this morphospace, our fossils (all eutherian) clustered most closely with mediolaterally narrower eutherian astragali, consistently far from both metatherians and cingulatans. The removal of metatherians and cingulatans from the dataset improved discrimination among locomotor modes somewhat, as did a subsequent reduction to ameliorate sampling biases. Nevertheless, PC1 exhibited a strong phylogenetic signal across all dataset partitions; PERMANOVA results also indicated a strong and significant effect of phylogeny on astragalus shape. This phylogenetic signal is not surprising given that other studies, including those with even narrower phylogenetic sampling, have detected a similar phylogenetic influence on astragali shape (e.g., Szalay 1977; Fabre et al. 2014; Chester et al. 2015). More narrowly, within an order (i.e., carnivorans or rodents) we detect a locomotor signal that is consistent with that of other phylogenetically restrictive datasets (e.g., carnivorans; Polly 2008). Thus, analysis of fossil elements within a phylogenetically broad sample of extant mammals may prove useful in attributing fossils to taxonomic groups (i.e., morphotype A and B are eutherians).

Despite phylogenetic effects, we also find a significant locomotor signal in our sample of extant mammals. This pattern is most evident along PC2; it holds across metatherians (Fig. 4.6), and within both eutherian datasets (Figs. 8, 10). Our results show that saltatorial, semifossorial, and to a lesser extent fossorial taxa consistently group together at one extreme of the morphofunctional continuum; arboreal, and to a lesser extent scansorial, taxa group together at the other extreme; semiaquatic and terrestrial taxa are often intermediate. Although we ultimately excluded gliding taxa from our most restrictive dataset partition, earlier analyses indicated gliding taxa most consistently grouped with arboreal and near scansorial taxa in the morphospace. Both eutherian datasets exhibit the same morphological signal with respect to the relative position of the astragalus head and body: saltatorial, semifossorial, and fossorial taxa have an astragalar head that is more in line with the astragalar body, whereas arboreal and scansorial taxa have a head that is more medially offset, or perpendicular to, the body. This locomotor gradient correlated with functionally important morphological differences in the degree of hollowing on the distal trochlear surface (reduced dataset partition) and the size and shape of the fibular facet and lateral trochlear ridge (narrowest dataset partition), both critical for joint stability and range of locomotion (e.g., Szalay 1977; Salton and Szalay 2004; Polly 2008; Chester et al. 2015). The separation of arboreal and scansorial locomotor modes from fossorial and semifossorial locomotor modes is similar to in other analyses of the astragalus (e.g., Polly 2008; Fabre et al. 2015) as well as more comprehensive studies of the appendicular skeleton (e.g., Chen and Wilson 2015).

Within locomotor groups, we find differences in relative ecospace occupation. For example, fossorial and terrestrial taxa appear to occupy relatively narrow areas of the

morphospace, which in particular might reflect poor phylogenetic sampling within these locomotor groups (i.e., the fossorial group is made up of only rodents, eulipotyphlans, and cingulatans, whereas the only terrestrial taxa in our final, most reduced dataset are carnivorans). In contrast, semifossorial taxa, and to a lesser extent scansorial taxa, occupy wider regions of the morphospaces. The large polygons enclosing the semifossorial and scansorial morphospaces indicate wide variance on more than one axis (i.e., in addition to the more phylogenetically informed PC1). This may be a function of greater sampling of semifossorial taxa; however, we had an even higher sampling of arboreal species and this locomotor mode occupies less of the morphospace than semifossorial species do. Both semifossorial and scansorial locomotor modes are 'intermediate' locomotor modes, between fossorial and terrestrial, and terrestrial and arboreal, respectively. Thus, we expect semifossorial species, which perform locomotor functions that overlap with both terrestrial (e.g., running, walking) and fossorial (e.g., digging) species to occupy both terrestrial and fossorial areas of the morphospace, and to potentially have a wider occupation than either terrestrial or fossorial species alone (e.g., Chen and Wilson 2015), which we detect in our eutherian PCA morphospaces. Similarly, we expect scansorial species to overlap with both terrestrial and arboreal areas of the morphospace, and to possibly have a wider occupation than either terrestrial or arboreal species alone (e.g., Chen and Wilson 2015), which we also detect in our eutherian PCA morphospaces.

5.2. Locomotor Inferences for Fossil Astragali

Morphotype A (?*Protungulatum*) plotted near scansorial, semiaquatic, semifossorial, and fossorial taxa in the morphospace from the narrowest dataset partition; LDA results predicted this morphotype was predominantly fossorial. PCA and LDA affinities for this morphotype are consistent with hypotheses that ?*Protungulatum* tarsals are more indicative of terrestrial than arboreal locomotion (e.g., Szalay and Decker 1974). Qualitatively, several morphological features of ?*Protungulatum* astragali imply a more terrestrial mode of locomotion: (1) a head shape that has a shorter medial edge (in distal view) compared to that of early primates; e.g., Szalay and Decker 1974); (2) the presence and position of the astragalar canal, which restricts the range of plantarflexion (Szalay and Decker 1974); and (3) an astragalofibular facet that indicates the fibula was weight bearing, as in other terrestrial taxa (Szalay and Decker 1974; Szalay 1984; Kondrashov and Lucas 2012). In addition to these terrestrial characteristics, ?*Protungulatum* astragali have a few morphological features that imply an increased range of motion beyond obligate terrestrial taxa, including a rounded sustentacular facet and a mobile distal tarsus (i.e., large and rounded head and navicular facet; Rose 1987; Szalay and Sargis 2006). Our quantitative predictions of a fossorial and/or semifossorial locomotor mode are consistent with studies that suggest this taxon had terrestrial locomotion with considerable foot mobility (e.g., Szalay and Decker 1974; Szalay 1984; Szalay and Sargis 2006). These results are also consistent with qualitative and quantitative analyses on ?*Protungulatum* humeri, which concluded entepicondyle morphology is indicative of strong medial flexors muscles, conceivably used for grasping or digging (Szalay and Dagosto 1980; DeBey and Wilson in prep).

Morphotype B (?*Procerberus*) plotted near arboreal, scansorial, semifossorial, fossorial, and terrestrial taxa in the morphospace from the narrowest dataset partition; LDA results predict these specimens to be predominantly semifossorial. Compared to ?*Protungulatum*, ?*Procerberus* astragali have (1) more extreme plantarflexion capabilities, based on the larger arc of the medial trochlear tibial and the absence of the astragalar foramen; (2) increased lateral stability, based on the more vertical fibular facet; and (3) a highly mobile foot at the transverse tarsal joint, based on the extensive navicular facet (e.g., Szalay and Decker 1974; Szalay 1977). These features suggest ?*Procerberus* was likely more scansorial than ?*Protungulatum* (e.g., Szalay and Decker 1974; Szalay 1977). These predictions are consistent with some of our PCA and LDA results, although our results additionally suggest semifossorial locomotion. Functionally ?*Procerberus* astragali have been compared to those of squirrels (e.g., Szalay 1977), which are scansorial animals that also exhibit digging behaviors. Unfortunately, the astragalus and the rest of the hind limb might not exhibit morphological indications of semifossorial behavior in mammals that dig using their forearms (Nowak 1999); instead, the astragalus might better reflect substrate use (i.e., terrestrial or arboreal surfaces; Chen and Wilson 2015) in these mammals. Our analysis of humeri of an earliest Paleocene (Pu1) leptictid (possibly ?*Procerberus*) from our study area showed that this taxon had a mobile elbow joint, capable of frequent supination and/or powerful grasping of the hand, and likely was fossorial or semifossorial (DeBey and Wilson in prep). If this humerus morphotype is from the same taxon as astragalus morphotype B (?*Procerberus*), it would further inform locomotor behavior in this taxon, rather than conflict with the astragali results presented here.

Morphotype C (?*Purgatorius*) had a position in the PCA morphospaces was highly labile. It was nearest scansorial and semifossorial taxa in the narrowest dataset partition; LDA results strongly predict this morphotype is semifossorial. These semifossorial affinities are surprising given previous conclusions for arboreality in this specimen and other plesiadapiform astragali (e.g., Szalay and Decker 1974; Chester et al. 2015). Qualitatively, morphotype C has a number of characters that are correlated with arboreal locomotion, including: (1) an enlarged, medial extension of the navicular facet on the head, a dorsoventrally tall medial portion of the head, and a large, saddle-shaped ectal facet, all of which facilitate foot eversion and inversion (e.g., Szalay and Decker 1974; Szalay 1994; Chester et al. 2015); (2) a very large trochlea (mediolaterally and proximodistally) and a distal trochlear surface that extends on to the neck, which both suggest increased degrees of dorsiflexion beyond that of ?*Protungulatum* and ?*Procerberus* (e.g., Szalay and Decker 1974; Chester et al. 2015); (3) a large groove for the flexor fibularis tendon, which facilitates plantarflexion and enables pedal grasping (Bloch et al. 2007; Chester et al. 2015; and (4) a reduced fibular facet that results in a less restrictive ankle joint (e.g., Szalay and Decker 1974; Szalay 1994; Chester et al. 2015). As stated above, our LDA function conceivably over-represented the occurrence of semifossoriality among our fossil specimens, and the placement of this morphotype in the PCA morphospaces nearer to scansorial and arboreal taxa compared to the other morphotypes, is potentially suggestive of more arboreality in morphotype C. Phylogenetically, we expected this ?plesiadapiform primate astragalus to plot nearer to extant primates than it does; however, in a traditional morphometrics analysis of plesiadapiform and euprimates, this specimen plotted closer to other plesiadapiform taxa than to extinct and extant euprimates (Chester et al. 2015). It is

possible therefore that our sample of only extant astragali lacks phylogenetically similar taxa and appropriate analogs for the locomotor type in morphotype C; analyses of Cretaceous eutherian astragali (e.g., *Deccanolestes*) that superficially resemble those of primates came to similar conclusions (Fabre et al. 2014). Despite difficulties in quantitative analyses of arboreality for this morphotype, qualitative evidence in support of arboreality/scansoriality for this taxon comes from elsewhere in the postcranial skeleton. Specifically, humeri and femora material attributed to this taxon exhibit arboreal capabilities, with increased femur flexibility (e.g., greater lateral rotation, small greater trochanter), and powerful thigh extension (e.g., distal position of third trochanter; DeBey and Wilson 2014), and strong grasping muscles of the humerus (e.g., medially extensive entepicondyle), and increased forearm rotation (e.g., spherical capitulum; DeBey and Wilson in prep). We conclude that the qualitative and quantitative evidence for locomotor capabilities in the astragalus of ?*Purgatorius* imply arboreality beyond what is exhibited by our other astragalus morphotypes.

Morphotype D, which we attribute to a Pu3 large-bodied ?archaic ungulate of Pu3 age, plotted nearest to scansorial, semiaquatic, semifossorial, and fossorial taxa in the narrowest dataset partition; LDA results strongly predict that morphotype D was semifossorial. This morphotype is the largest and is qualitatively quite different from all other fossil specimens; however, it does not show as much quantitative morphological difference as we would expect, and we suggest this is due breakage on the lateral side of the specimen. Qualitatively, this morphotype most closely resembles morphotype A and the Late Paleocene arboreal/scansorial *Arctocyon* (Argot 2013). Morphotype D differs from archaic ungulate *Arctocyon* in the following ways: (1) it is dorsoventrally shorter for both

the trochlea and the astragalar head, and has (2) a longer neck, (3) a longer sustentacular facet with more space distally between the sustentacular and navicular facets, (4) a less concave groove for the flexor fibularis, (5) a less concave trochlea, and (6) an even more reduced medial articulation for the tibial malleolus than *Arctocyon* (Argot 2013). These differences may imply reduced power during dorsiflexion (e.g., less robust groove for flexor fibularis tendon), but otherwise a scansorial locomotor inference for *Arctocyon* appears appropriate for morphotype D (Rose 1987; Argot 2013). Unfortunately, the fibular and ectal facets, informative of upper and lower ankle joint mobility, respectively, are both broken in this specimen. Although isolated and therefore unassociated with this astragalus, humeri from our study area that we attributed to large archaic ungulates (DeBey and Wilson in prep) are inferred to be arboreal or scansorial, on the basis of qualitative comparisons with *Arctocyon primaevus* (Argot 2013). Moreover, other elements in the *Arctocyon* postcranial skeleton are not specialized for digging (Argot 2013), in contrast with skeletal material from the Paleocene taeniodont *Stylinodon* (e.g. Schoch 1986; Matthew 1937). On the basis of qualitative comparison with other material and our quantitative analyses, we tentatively conclude that this specimen had a generalized locomotor mode, capable of scansorial activities.

In light of our results, we make some recommendations for future quantitative morphofunctional analyses of K-Pg mammalian tarsals. First, the composition and structure of an extant dataset is of utmost importance for quantitative comparison of fossil elements using either linear measurements and indices (e.g., Chen and Wilson 2015; Chester et al. 2015), or 2D and 3D GM studies (e.g., Polly 2008; Boyer et al. 2010; Boyer and Seiffert 2013). Due to unevenness in taxonomic and locomotor group sampling, we were

unable to compare fossorial and semifossorial morphofunctional patterns between metatherian and eutherians because we were lacking any metatherians in these locomotor groups. Similarly, we ultimately removed all gliding taxa from our analyses because both species were rodents (and in the same genus), and we were unable to determine whether placement in the morphospace was predominantly due to phylogeny or locomotor mode. We acknowledge the relative oversampling of semifossorial taxa in our narrowest dataset partition may be driving the semifossorial LDA predictions for fossil astragali. We suggest future studies specifically balance locomotor sampling more evenly across taxonomic groups where possible, especially when attempting to infer locomotion across a diverse sample of extant taxa.

Second, although our objective was to broadly sample astragali and avoid a priori assumptions about shape and associated locomotor function, we suggest more focused sampling of astragali may yield better functional inferences. Our extant sample captured significant morphological variation (e.g., including extreme saltatorial lagomorphs *Brachylagus* and *Lepus*); however, generally all fossil specimens consistently plotted centrally in the principal components morphospaces (i.e., nearer to the morphologically more conservative lagomorph *Ochotona*), which is suggestive of a more generalized astragalar morphology among fossils than among our extant sample. A more conservative morphological sample that is tailored towards relevant morphologies present among fossil specimens (e.g., Chen and Wilson 2015), or particular locomotor modes (e.g., Chester et al. 2015), could yield more conclusive morphofunctional patterns and better discrimination among locomotor groups, although this hypothesis should be tested broadly.

Finally, we suggest 3D GM studies using landmarks placed on the mammalian astragalus are difficult given the complexity of the element. Using SLMs in addition to LMs in these 3D GM studies can improve characterization of the margins of articular surfaces (e.g., medial and lateral trochlear ridge curvature). However, the functional significance of the astragali effectively lies in the shapes of its articular surfaces, and functionally significant aspects of articular surface shape (e.g., curvature) are difficult to capture with LMs or SLMs and may be better-captured using 3D GM mesh or surface analyses (e.g., Polly 2008; Boyer and Seiffert 2013; Boyer et al. 2015). In particular, the shape of the neck, head, and navicular and ectal facets are difficult to capture using LMs or SLMs, which is unfortunate given both the phylogenetic and functional significance of these areas (e.g., Szalay and Decker 1974; Chester et al. 2015). Although they suffer from their own challenges, more automated 3D shape analyses are becoming increasingly widespread, and geometric morphometrics analyses of complex tarsal shapes stand to benefit greatly from their development (e.g., Polly 2008; Boyer et al. 2011, 2015; Boyer and Seiffert 2013).

6. Conclusion

Results of our 3D GM analyses on astragali suggest morphology is suggestive of both phylogeny and locomotor mode, a finding consistent with other studies (e.g., Fabre et al. 2014). Despite the complication of phylogenetic effects, our results indicate early Paleogene astragali are suggestive of predominantly semifossorial, scansorial, and arboreal locomotion. We find specimens attributable to ?*Protungulatum* to be suggestive of semifossoriality, and specimens attributable to ?*Procerberus* to be slightly more scansorial but with similar semifossorial affinities. We find a medium-sized archaic ungulate from Pu3 deposits is quantitatively suggestive of semifossorial locomotion but has qualitative morphologies suggestive of scansorial capabilities. We do not detect a strong quantitative signal for arboreality in a specimen attributable to Pu3 plesiadapiform ?*Purgatorius*, although this specimen exhibits qualitative features associated with arboreal locomotion. Future studies should broaden phylogenetic sampling (i.e., more mammalian orders) and also increase sampling within taxonomic and locomotor groups to further explore the morphofunctional trends of this complex tarsal element.

7. Acknowledgements

We thank the many individuals whose fieldwork, curation, and research efforts have made this work possible, in particular W. A. Clemens, D. Lofgren, and the many UCMP field crews and volunteers, who collected, sorted, identified, and curated these fossil specimens, and P. Holroyd (UCMP), and J. Bradley, R. Eng, and C. Sidor (UWBM) for access to collections. We are grateful to N. Kunwar for CT scanning of UCMP and UWBM specimens, to N. Gilroy, L. Heilicher, A. Kriedberg, N. Kunwar, and A. Szember for processing of CT scans. We are thankful to D. Boyer, S. Chester, and all the individuals who made their CT scans available through MorphoSource (morphosource.org). We thank S. Chester, W. A. Clemens, E. Nesbitt, C. Sidor, C. Strömberg and the members of the Wilson Lab for valuable suggestions, discussion, and comments on drafts of this manuscript. We thank S. Smith for support with analyses. Funding for this project was provided to LBD by the National Science Foundation Gradate Research Fellowship, the Charlotte Cornell Crary Distinguished Teaching Fellowship, the Henry and Frances Decker Fellowship, the Evolving Earth Foundation, the Doris O. and Samuel P. Welles Fund, the Montana Bureau of Land Management, and the University of Washington Graduate and Professional Student Senate and Department of Biology. Funding for this project was provided to GPW by the University of Washington Department of Biology.

References Cited

Adams, D.C. and E. Otarola-Castillo. 2013. Geomorph: an R package for the collection and analysis of geometric morphometric shape data. Methods in Ecology and Evolution 4: 393–399.

Alroy, J. 1999. The fossil record of North American mammals: evidence for a Paleocene evolutionary radiation. Systematic Biology 48: 107–118.

Archibald, J.D. 1982. A study of Mammalia and geology across the Cretaceous-Tertiary boundary in Garfield County, Montana. University of California Publications in Geological Sciences 122: 1–286.

Argot, C. 2001. Functional-adaptive anatomy of the forelimb in the Didelphidae, and the paleobiology of the Paleocene marsupials *Mayulestes ferox* and *Pucadelphys andinus*. Journal of Morphology 247: 51–79.

Argot, C. 2002. Functional-Adaptive Analysis of the Hindlimb Anatomy of Extant Marsupials and the Paleobiology of the Paleocene Marsupials *Mayulestes ferox* and *Pucadelphys andinus*. Journal of Morphology 253: 76–108.

Argot, C. 2013. Postcranial analysis of a Carnivoran-like archaic ungulate: the case of *Arctocyon primaevus* (Arctocyonidae, Mammalia) from the Late Paleocene of France. Journal of Mammalian Evolution 20: 83–114.

Bassarova, M., C.M. Janis, and M. Archer. 2009. The calcaneum—on the heels of marsupial locomotion. Journal of Mammalian Evolution 16:1–23.

Bloch, J.I., M.T. Silcox, D.M. Boyer, and E.J. Sargis. 2007. New Paleocene skeletons and the relationship of plesiadapiforms to crown-clade primates. Proceedings of the National Academy of Sciences 104: 1159–1164.

Bookstein, F.L. 1991. Morphometric Tools for Landmark Data: Geometry and Biology. Cambridge University Press, Cambridge.

Borths, M. and J. Hunter. 2008. Gimme shelter? Locomotor trends and mammalian survivorship at the K-Pg boundary. Journal of Vertebrate Paleontology 28: 3A.

Boyer, D.M. and E.R. Seiffert. 2013. Patterns of astragalar fibular facet orientation in extant and fossil primates and their evolutionary implications. American Journal of Physical Anthropology 151: 420–47.

Boyer, D.M., E.R. Seiffert, E.L. Simons. 2010. Astragalar morphology of *Afradapis*, a large adapiform primate from the earliest late Eocene of Egypt. American Journal of Physical Anthropology 143: 383–402.

Boyer, D.M., Y. Lipman, E.S. Clair, J. Puente, B.A. Patelb, T. Funkhouser, J. Jernvall, I. Daubechies. 2011. Algorithms to automatically quantify the geometric similarity of anatomical surfaces. Proceedings of the National Academy of Sciences 108: 18221–18226.

Boyer, D.M., J. Puente, J.T. Gladman, C. Glynn, S. Mukherjee, G.S. Yapuncich, and I. Daubechies. 2015. A new fully automated approach for aligning and comparing shapes. Anatomical Record 298: 249–276.

Carrano, M.T. 1997. Morphological indicators of foot posture in mammals: a statistical and biomechanical analysis. Zoological Journal of the Linnean Society 121: 77–104.

Chen, M. and G.P. Wilson. 2015. A multivariate approach to infer locomotor modes in Mesozoic mammals. Paleobiology 41: 280–312.

Chester, S.G.B., J.I. Bloch, D.M. Boyer, and W.A. Clemens. 2015. Oldest known euarchontan tarsals and affinities of Paleocene *Purgatorius* to primates. Proceedings of the National Academy of Sciences 112: 1487–1492.

Cifelli , R.L., J.J. Eberle, D.L. Lofgren, J.A. Lillegraven, and W.A. Clemens. 2004. Mammalian biochronology of the latest Cretaceous, in: M.O. Woodburne (Ed.), Late Cretaceous and

Cenozoic mammals of North America: biostratigraphy and geochronology. Columbia University Press, New York, pp. 21-42.

Clemens, W.A. 2002. Evolution of the mammalian fauna across the Cretaceous-Tertiary boundary in northeastern Montana and other areas of the Western Interior, in: J.H. Hartman, K.R. Johnson, and D.J. Nichols (Eds.), The Hell Creek Formation and the Cretaceous-Tertiary Boundary in the Northern Great Plains: An Integrated Continental Record of the End of the Cretaceous. Geological Society of America Special Paper 361, Boulder, pp. 217–245.

Clemens, W.A. 2015. *Prodiacodon crustulum* (Leptictidae, Mammalia) from the Tullock Member of the Fort Union Formation, Garfield and McCone counties, Montana, USA. PaleoBios 32: 1–17.

Dagosto, M. 1988. Implications of postcranial evidence for the origin of euprimates. Journal of Human Evolution 17: 35–56.

Davis, E.B. and B.K. McHorse. 2013. A method for improved identification of postcrania from mammalian fossil assemblages: multivariate discriminant function analysis of camelid astragali. Paleontologica Electronica 16: 1–15.

DeBey, L.B. and G.P. Wilson. 2014. Mammalian femora across the Cretaceous-Paleogene boundary in eastern Montana. Cretaceous Research 51: 361–85.

Deischl, D.G. 1964. The postcranial anatomy of Cretaceous multituberculate mammals, unpublished M.Sc. thesis, University of Minnesota, Minneapolis.

DeGusta, D. and E. Vrba. 2003. A method for inferring paleohabitats from the functional morphology of bovid astragali. Journal of Archaeological Science 30: 1009–1022.

Endo, H., T. Yonezawa, F. Rakotondraparany, M. Sasaki, and M. Hasegawa. 2006. The adaptational strategies of the hindlimb muscles in the Tenrecidae species including the aquatic web-footed tenrec (*Limnogale mergulus*). Annals of Anatomy 188: 383–390.

Fabre, A.-C., R. Cornette, A. Perrard, D.M. Boyer, G.V.R. Prasad, J.J. Hooker, and A. Goswami. 2014. A three-dimensional morphometric analysis of the locomotory ecology of *Deccanolestes*, a

eutherian mammal from the Late Cretaceous of India. Journal of Vertebrate Paleontology 34: 146–156.

Fox, R.C. 1989. The Wounded Knee local fauna and mammalian evolution near the Cretaceous-Tertiary boundary, Saskatchewan, Canada. Palaeontographica, Abteilung A 208: 11–59.

Gingerich, P.D. 2003. Land-to-sea transition in early whales: evolution of Eocene Archaeoceti (Cetacea) in relation to skeletal proportions and locomotion of living semiaquatic mammals. Paleobiology 29: 429–454.

Gladman, J.T., D.M. Boyer, E.L. Simons, and E.R. Seiffert. 2013. A calcaneus attributable to the primitive late Eocene anthropoid *Proteopithecus sylviae*: Phenetic affinities and phylogenetic implications. American Journal of Physical Anthropology 151: 372–397.

Godinot, M. and M. Dagosto. 1983. The astragalus of *Necrolemur* (Primates, Microchoerinae). Journal of Paleontology 57: 1321–1324.

Godinot, M. and G.V.R. Prasad. 1994. Discovery of Cretaceous arboreal eutherians. Naturwissenschaften 81: 79–81.

Goodall, C.R. 1991. Procrustes methods in the statistical analysis of shape. Journal of the Royal Statistical Society B 53: 285–339.

Granger, W. and G.G. Simpson. 1929. A revision of the Tertiary Multituberculata. Bulletin of the American Museum of Natural History 56: 601–676.

Gunz, P. and P. Mitteroecker. 2013. Semilandmarks: a method for quantifying curves and surfaces. Hystrix, the Italian Journal of Mammalogy 24: 103–109.

Heinrich, R. and P. Houde. 2006. Postcranial anatomy of *Viverravus* (Mammalia, Carnivora) and implications for substrate use in basal Carnivora. Journal of Vertebrate Paleontology 26: 422–435

Hildebrand, M. 1985. Digging in quadrupeds, in: M. Hildebrand, D.M. Bramble, K.F. Liem, and D.B. Wake (Eds.), Functional Vertebrate Morphology. Harvard University Press, Cambridge, pp. 89–109.

Hildebrand, M. and G. Goslow. 1998. Analysis of Vertebrate Structure. Wiley, New York.

Horovitz, I. 2000. The tarsus of *Ukhaatherium nessovi* (Eutheria, Mammalia) from the Late Cretaceous of Mongolia: An appraisal of the evolution of the ankle in basal therians. Journal of Vertebrate Paleontology 20: 547–560.

Horovitz, I. 2003. Postcranial skeleton of *Ukhaatherium nessovi* (Eutheria, Mammalia) from the Late Cretaceous of Mongolia. Journal of Vertebrate Paleontology 23: 857–68.

Howell, A.B. 1930. Aquatic Mammals. Charles C. Thomas, Springfield, Illinois.

Iwaniuk, A.N., S.M. Pellis, and I.Q. Whishaw. 1999. The relationship between forelimb morphology and behavior in North American carnivores (Carnivora). Canadian Journal of Zoology 77: 1064–1074.

Jenkins, F.A., Jr. and D. McClearn. 1984. Mechanisms of hind foot reversal in climbing mammals. Journal of Morphology 182: 197–219.

Jenkins, F.A. and D.W. Krause. 1983. Adaptations for climbing in North American multituberculates (Mammalia). Science 220: 712–715.

Kelly, T.S. 2014. Preliminary report on the mammals from Lane's Little Jaw Site Quarry: a Latest Cretaceous (earliest Puercan?) Local Fauna, Hell Creek Formation, southeastern Montana. Paludicola 10: 50–91.

Kielan-Jaworowska, Z. and P.P. Gambaryan. 1994. Postcranial anatomy and habits of Asian multituberculate mammals. Fossils and Strata 36: 1–92.

Kendall, D.G. 1977. The diffusion of shape. Advances in Applied Probability 9: 428–430.

Kondrashov, P.E. and S.G. Lucas. 2012. Nearly complete skeleton of *Tetraclaenodon* (Mammalia, Phenacodontidae) from the Early Paleocene of New Mexico: morpho-functional analysis. Journal of Paleontology 86: 25–43.

Körtner, G. and F. Geiser. 2000. Torpor and activity patterns in free-ranging sugar gliders *Petaurus breviceps* (Marsupialia). Oecologia 123: 350–357.

Krause, D.W. and F.A. Jenkins, Jr. 1983. The postcranial skeleton of North American multituberculates. Bulletin of the Museum of Comparative Zoology 150: 199–246.

Lackey, J.A. 1996. *Chaetodipus fallax*. Mammalian Species 517: 1–6.

Lariviére, S. 1999. *Mustela vison*. Mammalian Species 608: 1–9.

Lariviére, S. and M. Pasitschniak-Arts. 1996. *Vulpes vulpes*. Mammalian Species 537: 1–11.

LeCain, R., W.C. Clyde, G.P. Wilson, and J. Riedel. 2014. Magnetostratigraphy of the Hell Creek and lower Fort Union Formations in northeastern Montana, in: G.P. Wilson, W.A. Clemens, J.R. Horner, and J.H. Hartman (Eds.), Through the End of the Cretaceous in the Type Locality of the Hell Creek Formation in Montana and Adjacent Areas. Geological Society of America Special Paper 503, Boulder. pp. 137–147.

Lofgren, D.L. 1995. The Bug Creek Problem and the Cretaceous-Tertiary transition at McGuire Creek, Montana. University of California Publications in Geological Sciences 140: 1–185.

Lofgren, D.L., J.A. Lillegraven, W.A. Clemens, P.D. Gingerich, and T.E. Williamson. 2004. Paleocene biochronology: The Puercan through Clarkforkian land mammal ages, in: M.O. Woodburne (Ed.), Late Cretaceous and Cenozoic Mammals of North America: Biostratigraphy and Geochronology. Columbia University Press, New York, pp. 43–105.

Matthew, W.D. 1937. Paleocene faunas of the San Juan Basin, New Mexico. Transactions of the American Philosophical Society 30: 1–523.

Meachen-Samuels, J. 2010. Comparative scaling of humeral cross-sections of felids and canids using radiographic images. Journal of Mammalian Evolution 17: 193–209.

Mitteroecker, P. and F. Bookstein. 2011. Linear discrimination, ordination, and the visualization of selection gradients in modern morphometrics. Evolutionary Biology 38: 100–114.

Moore, J.R., G.P. Wilson, M. Sharma, H.R. Hallock, D.R. Braman, and P. Renne. 2014. Assessing the relationships of the Hell Creek–Fort Union contact, Cretaceous-Paleogene boundary, and Chicxulub impact ejecta horizon at the Hell Creek Formation lectostratotype, Montana, USA, in: G.P. Wilson, W.A. Clemens, J.R. Horner, and J.H. Hartman (Eds.), Through the End of the Cretaceous in the Type Locality of the Hell Creek Formation in Montana and Adjacent Areas. Geological Society of America Special Paper 503, Boulder, pp. 123–136.

Nowak, R.M. 1999. Walker's Mammals of the World. Johns Hopkins University Press, Baltimore.

Nyakatura, J.A., M.S. Fischer, and M. Schmidt. 2008. Gait parameter adjustments of cotton-top tamarins (*Saguinus oedipus*, Callitrichidae) to locomotion on inclined arboreal substrates. American Journal of Physical Anthropology 135: 13–26.

O'Leary, M.A., J.I. Bloch, J.J. Flynn, T.J. Gaudin, A. Giallombardo, N.P. Giannini, S.L. Goldberg, B.P. Kraatz, Z.-X. Luo, J. Meng, X. Ni, M.J. Novacek, F.A. Perini, Z.S. Randall, G.W. Rougier, E.J. Sargis, M.T. Silcox, N.B. Simmons, M. Spaulding, P.M. Velazco, M. Weksler, J.R. Wible, and A.L. Cirranello. 2013. The placental mammal ancestor and the post-K-Pg radiation of placentals. Science 339: 662–67.

Pasitschniak-Arts, M. and S. Lariviére. 1995. *Gulo gulo*. Mammalian Species 499: 1–10.

Penkrot, T.A., S.P. Zack, K.D. Rose, and J.I. Bloch. 2008. Postcranial morphology of *Apheliscus* and *Haplomylus* (Condylarthra, Apheliscidae): evidence for a Paleocene Holarctic origin of Macroscelidea, in: E.J. Sargis and M. Dagosto (Eds.), Mammalian evolutionary morphology: a tribute to Frederick S. Szalay. Springer, Dordrecht, pp. 73-106.

Polly, P.D. 2007. Limbs in mammalian evolution, in: B.K. Hall (Ed.) Fins into Limbs: Evolution, Development, and Transformation. University of Chicago Press, Chicago, pp. 1–24.

Polly, P.D. 2008. Adaptive zones and the pinniped ankle: a 3D quantitative analysis of carnivoran tarsal evolution, in: E. Sargis and M. Dagosto (Eds.), Mammalian Evolutionary Morphology: a Tribute to Frederick S. Szalay. Springer, Dordrecht, pp. 167–196.

Polly, P.D. and N. MacLeod. 2008. Locomotion in fossil Carnivora: an application of eigensurface analysis for morphometric comparison of 3D surfaces. Palaeontologia Electronica 11: 1–13.

Prasad, G.V.R. and M. Godinot. 1994. Eutherian tarsal bones from the Late Cretaceous of India. Journal of Paleontology 68: 892–902.

R Core Team. 2014. R: A language and environment for statistical computing (Version 3.1.2). R Foundation for Statistical Computing, Vienna, Austria. URL http://www.R-project.org/.

RStudio. 2012. RStudio: Integrated development environment for R (Version 0.98.1062). Boston, MA. URL http://www.rstudio.com/.

Raia, P., F. Carotenuto, F. Passaro, P. Piras, D. Fulgione, L. Werdelin, J. Saarinen, and M. Fortelius. 2012. Rapid action in the Palaeogene, the relationship between phenotypic and taxonomic diversification in Coenozoic mammals. Proceedings of the Royal Society B: Biological Sciences 280: 20122244.

Redford, K.H. and R.M. Wetzel. 1985. *Euphractus sexcinctus*. Mammalian Species 252: 1–4.

Renne, P.R., G. Balco, K.R. Ludwig, R. Mundil, and K. Min. 2011. Response to the comment by W.H. Schwartz et al. on "Joint determination of 40K decay constants and 40Ar*/40K for the Fish Canyon sanidine standard, and improved accuracy for the 40Ar/39Ar geochronology" by P.R. Renne et al. (2010). Geochimica et Cosmochimica Acta 75: 5097–5100.

Renne, P.R., A.L. Deino, F.J. Hilgen, K.F. Kuiper, D.F. Mark, W.S. Mitchell III, L.E. Morgan, R. Mundil, and J. Smit. 2013. Time scales of critical events around the Cretaceous-Paleogene boundary. Science 339: 684–687.

Rigby Jr., J.K. 1981. A skeleton of *Gillisonchus gillianus* (Mammalia; Condylarthra) from the Early Paleocene (Puercan) Ojo Alamo Sandstone, San Juan Basin, New Mexico, with comments on the

local stratigraphy of Betonnie Tsosie Wash, in: S.G. Lucas, J.K. Rigby Jr., and B.S. Kues (Eds.), Advances in San Juan Basin Paleontology. University of New Mexico Press, Albuquerque, pp. 89–126.

Robertson, D.S., M.C. McKenna, O.B. Toon, S. Hope, and J.A. Lillegraven 2004. Survival in the first hours of the Cenozoic. Geological Society of America Bulletin 116: 760–768.

Rohlf, F.J. and D. Slice. 1990. Extensions of the Procrustes method for the optimal superimposition of landmarks. Systematic Zoology 39: 40–59.

Rose, K.D. 1987. Climbing adaptations in the early Eocene mammal *Chriacus* and the origin of Artiodactyla. Science 236: 314–316.

Rose, K. 1999. Postcranial skeleton of Eocene Leptictidae (Mammalia), and its implications for behavior and relationships. Journal of Vertebrate Paleontology 19: 355–72.

Russell, D.E. 1964. Les mammifères paléocènes d'Europe. Mémoires du Muséum National D'Histoire Naturelle, Série C. Sciences de la Terre 13: 1–324.

Salton, J.A., and E.J. Sargis. 2008. Evolutionary morphology of the Tenrecoidea (Mammalia) forelimb skeleton, in: E.J. Sargis and M. Dagosto (Eds.), Mammalian Evolutionary Morphology: a Tribute to Frederick S. Szalay. Springer, Dordrecht, pp. 51–71.

Salton, J.A. and F.S. Szalay. 2004. The tarsal complex of Afro-Malagasy Tenrecoidea: a search for phylogenetically meaningful characters. Journal of Mammalian Evolution 11: 73–104.

Samuels, J.X., J.A. Meachen, and S.A. Sakai. 2013. Postcranial morphology and the locomotor habits of living and extinct carnivorans. Journal of Morphology 274: 121–146.

Samuels, J.X. and B. Van Valkenburgh. 2008. Skeletal indicators of locomotor adaptations in living and extinct rodents. Journal of Morphology 269: 1387–1411.

Schoch, R.M. 1986. Systematics, functional morphology and macroevolution of the extinct mammalian order Taeniodonta. Peabody Museum of Natural History, Yale University Bulletin 42: 1–307.

Sloan, R.E. and L. Van Valen. 1965. Cretaceous mammals from Montana. Science 148: 220–227.

Smith, M.J. 1973. *Petaurus breviceps*. Mammalian Species 30:1–5.

Smith, F.A., A.G. Boyer, J.H. Brown, D.P. Costa, T. Dayan, S.K.M. Ernest, A.R. Evans, M. Fortelius, J.L. Gittleman, M.J. Hamilton, L.E. Harding, K. Lintulaakso, S.K. Lyons, C. McCain, J.G. Okie, J.J. Saarinen, R.M. Sibly, P.R. Stephens, J. Theodor, and M.D. Uhen. 2010. The evolution of maximum body size of terrestrial mammals. Science 330: 1216–1219.

Sprain, C.J., P.R. Renne, G.P. Wilson, and W.A. Clemens. 2015. High-resolution chronostratigraphy of the terrestrial Cretaceous-Paleogene transition and recovery interval in the Hell Creek region, Montana. Geological Society of America Bulletin. 127: 393–409.

Swisher, C.C., III, L. Dingus, and R.F. Butler. 1993. 40Ar/39Ar dating and magnetostratigraphic correlation of the terrestrial Cretaceous-Paleogene boundary and Puercan mammal age, Hell Creek–Tullock formations, eastern Montana. Canadian Journal of Earth Sciences 30: 1981–1996.

Szalay, F.S. 1977. Phylogenetic relationships and a classification of the eutherian Mammalia. NATO Advances Study Institute Series. Series A, Life Sciences 14: 315–374.

Szalay, F.S. 1984. Arboreality: is it homologous in metatherian and eutherian mammals?, in M.K. Hecht, B. Wallace, and G.T. Prance (Eds.), Evolutionary Biology Vol. 18. Plenum Press, New York, pp. 215–258.

Szalay, F.S. 1994. Evolutionary History of the Marsupials and an Analysis of Osteological Characters. Cambridge University Press, New York.

Szalay, F.S. and M. Dagosto. 1980. Locomotor adaptations as reflected on the humerus of Paleogene primates. Folia Primatologica 34: 1–45.

Szalay, F.S. and R.L. Decker. 1974. Origins, evolution, and function of the tarsus in Late Cretaceous Eutheria and Paleocene primates, in: F. A. Jenkins Jr. (Ed.), Primate Locomotion. Academic Press, Inc., New York, pp. 223–259.

Szalay, F.S. and S.G. Lucas. 1996. The postcranial morphology of Paleocene *Chriacus* and *Mixodectes* and the phylogenetic relationships of archontan mammals. New Mexico Museum of Natural History and Science Bulletin 7: 1–47.

Szalay, F.S. and E.J. Sargis, 2001. Model-based analysis of postcranial osteology of marsupials from the Palaeocene of Itaborai (Brazil) and the phylogenetics and biogeography of Metatheria. Geodiversitas 23: 139–302.

Szalay, F.S. and E.J. Sargis. 2006. Cretaceous therian tarsals and the metatherian-eutherian dichotomy. Journal of Mammalian Evolution 13: 171–210.

Szalay, F.S., I. Tattersall, and R.L. Decker. 1975. Phylogenetic relationships of Plesiadapis-postcranial evidence. Contributions to Primatology 5: 136–166.

van Staaden, M.J. 1994. *Suricata suricatta*. Mammalian Species 483:1–8.

Van Valkenburgh, B. 1987. Skeletal indicators of locomotor behavior in living and extinct carnivores. Journal of Vertebrate Paleontology 7: 162–82.

Venables, W.N. and B.D. Ripley. 2002. Modern Applied Statistics with S. Fourth Edition. Springer, New York.

Wade-Smith, J. and B.J. Verts. 1982. *Mephitis mephitis*. Mammalian Species 173:1–7.

Wiley, D.F., N. Amenta, D.A. Alcantara, D. Ghosh, Y.J. Kil, E. Delson, W. Harcourt-Smith, F.J. Rohlf, K. St. John, B. Hamann, R. Motani, S. Frost, A.L. Rosenberger, L. Tallman, T. Disotell, R. O'Neill. 2005. Evolutionary morphing. Visualization, VIS 05, IEEE, pp. 431–438.

Wilson, G.P. 2004. A quantitative assessment of evolutionary and ecological change in mammalian faunas leading up to and across the Cretaceous-Tertiary boundary in northeastern Montana. Unpublished Ph.D. dissertation, University of California Berkeley, Berkeley.

Wilson, G.P. 2005. Mammalian faunal dynamics during the last 1.8 million years of the Cretaceous in Garfield County, Montana. Journal of Mammalian Evolution 12: 53–75.

Wilson, G.P. 2013. Mammals across the K/Pg boundary in northeastern Montana, U.S.A.: dental morphology and body-size patterns reveal extinction selectivity and immigrant fueled ecospace filling. Paleobiology 39: 429–469.

Wilson, G.P. 2014. Mammalian extinction, survival, and recovery dynamics across the Cretaceous-Paleogene boundary in northeastern Montana, in: G.P. Wilson, W.A. Clemens, J.R. Horner, and J.H. Hartman (Eds.), Through the End of the Cretaceous in the Type Locality of the Hell Creek Formation in Montana and Adjacent Areas. Geological Society of America Special Paper 503, Boulder, pp. 365–392.

Wilson, G.P., A.R. Evans, I.J. Corfe, P.D. Smits, M. Fortelius, and J. Jernvall. 2012. Adaptive radiation of multituberculate mammals before the extinction of dinosaurs. Nature 483: 457–460.

Zelditch, M.L., D.L. Swiderski, H.D. Sheets, and W.L. Fink. 2004. Geometric Morphometrics for Biologists: a Primer. Elsevier Academic Press, Amsterdam.

Figures

Figure 4.1. Cretaceous and Paleogene fossil astragali in our study. Figured are morphotypes A (?*Protungulatum*), B (?*Procerberus*), C (?*Purgatorius*), and D (?archaic ungulate). Images show astragali in plantar, dorsal, and distal views (left to right). See Table 4.1 for additional fossil specimen information. Scale bars equal to 1 mm.

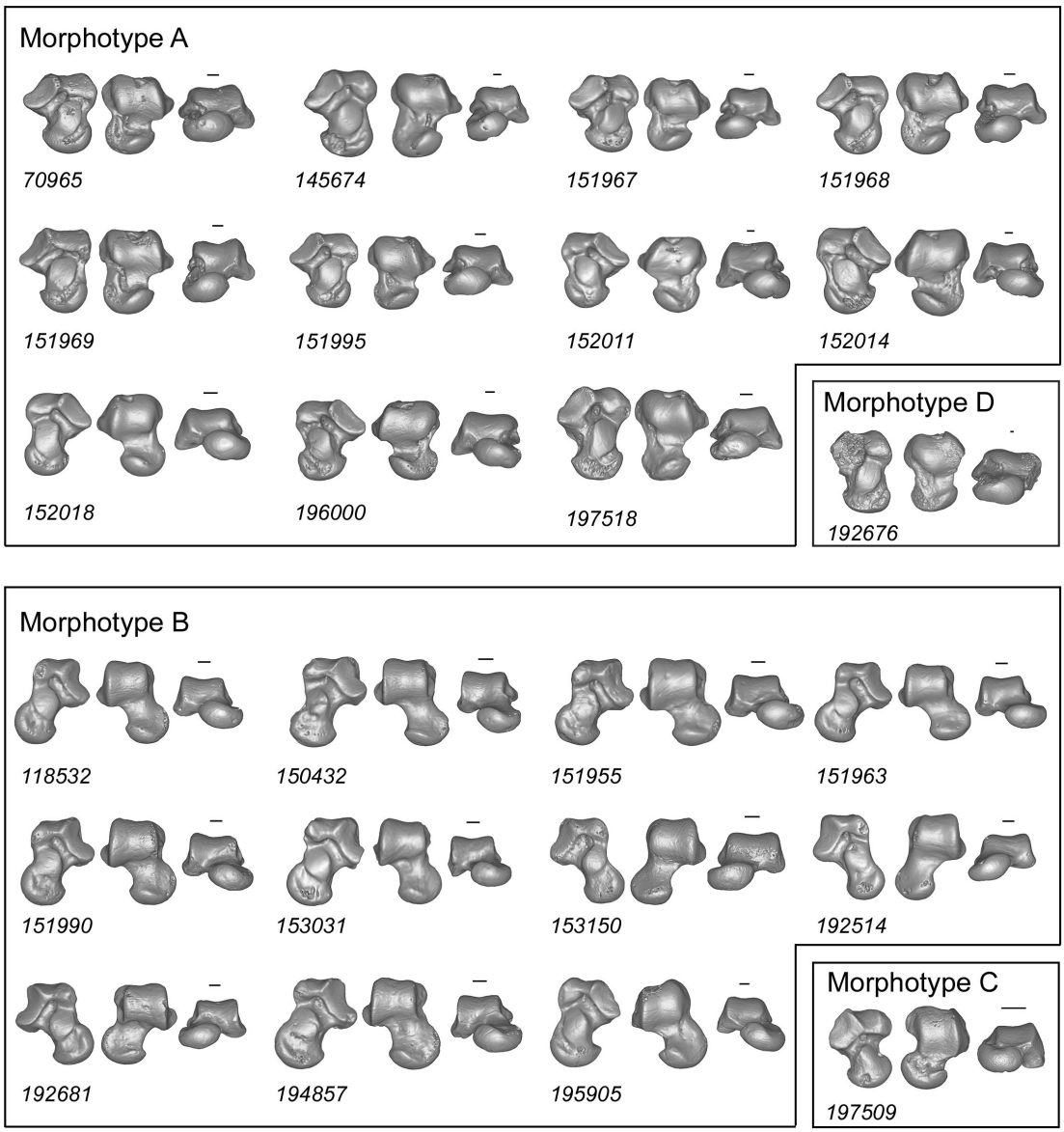

Figure 4.2. Taxonomic sampling of extant taxa in each locomotor mode in our dataset. See Table 4.2 for more details.

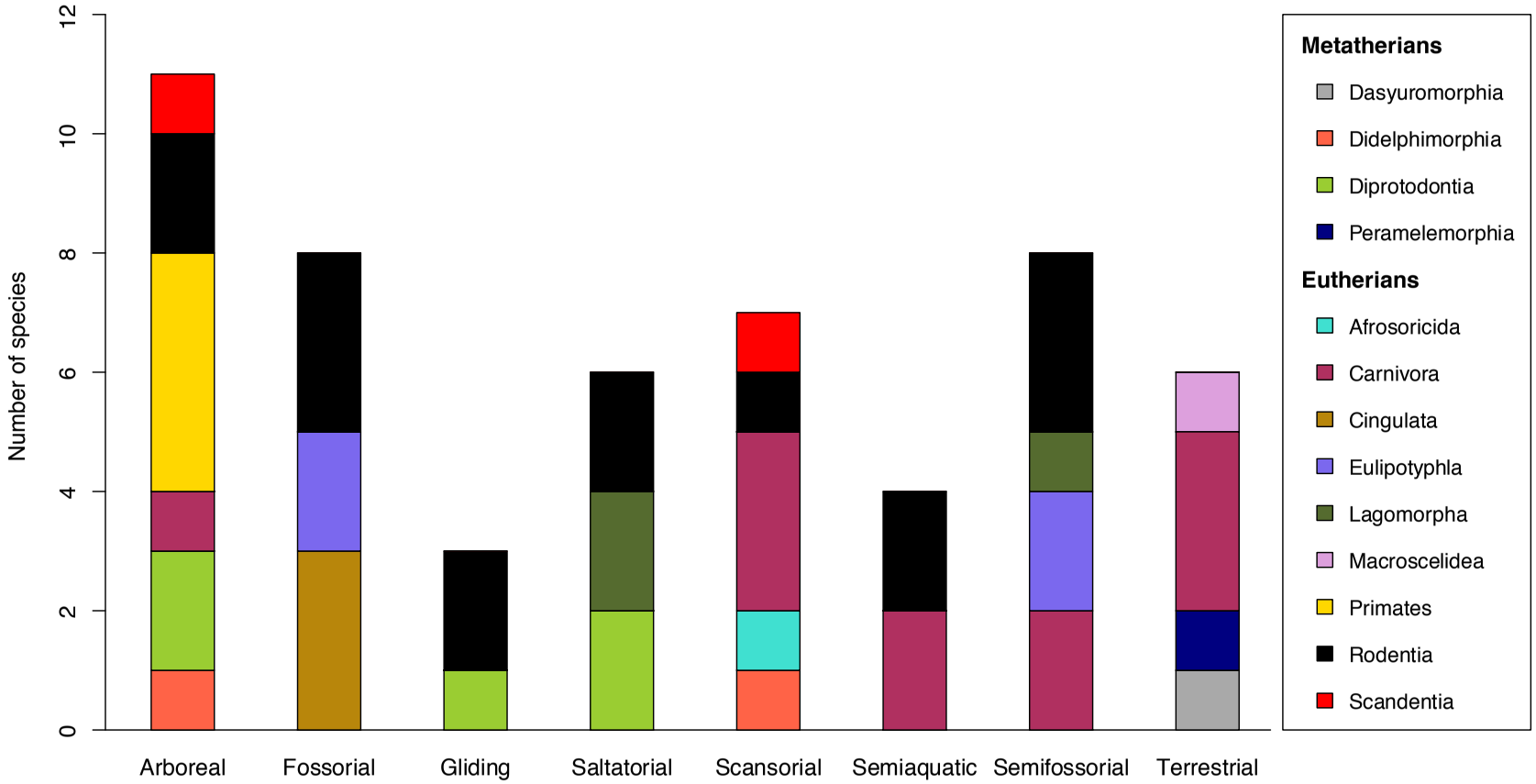

Figure 4.3. Select modern astragali included in our study. Images show left eutherian humerus (top) with facet and surfaces labeled, and select metatherian and eutherian astragali (bottom) in plantar, dorsal, and distal views (left to right) with the locomotor mode for each species. See Table 4.2 for specimen numbers of figured specimens and additional taxonomic information. Figure modified after Fabre et al. (2014). Scale bars equal to 1 mm.

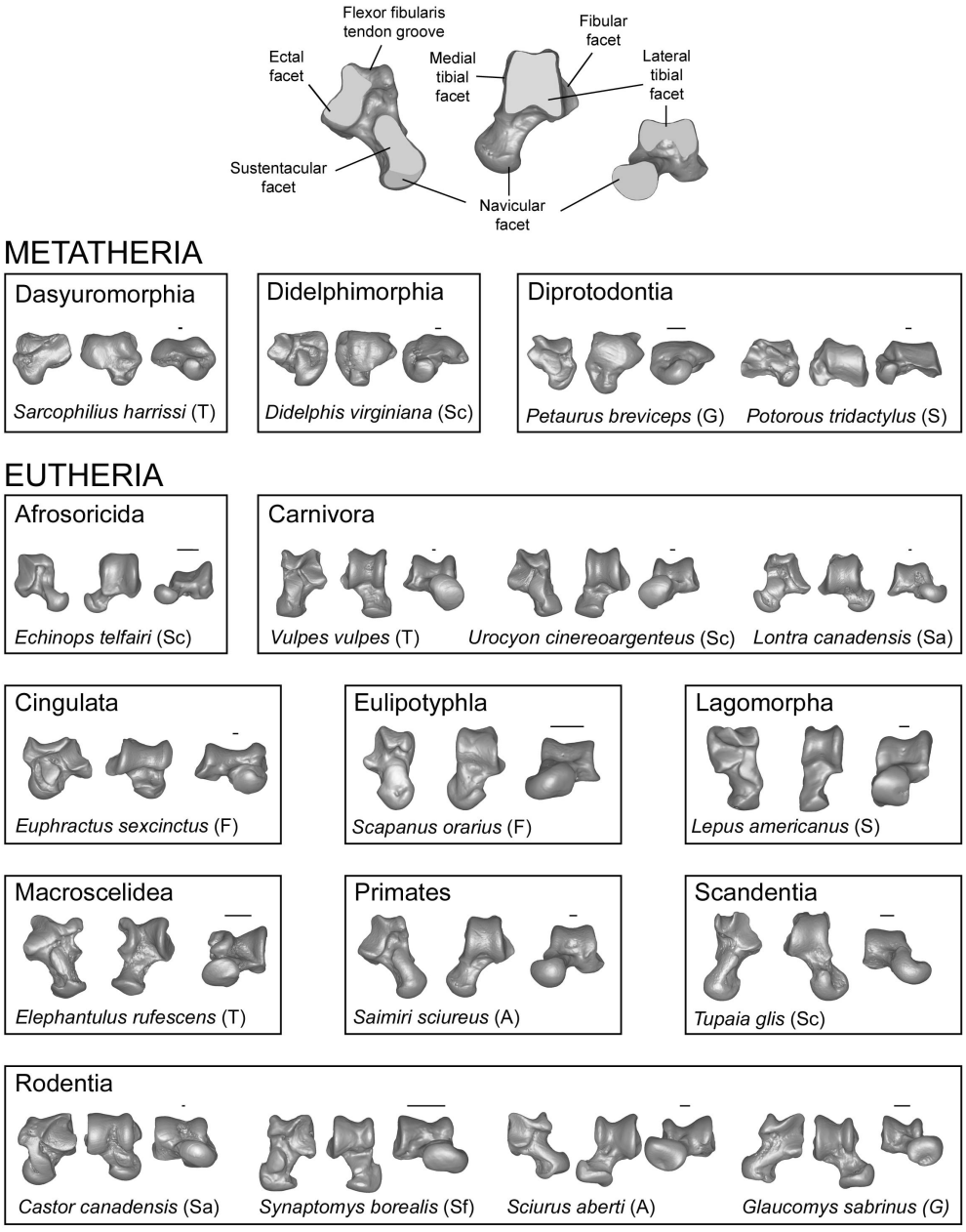

Figure 4.4. Landmarks (LMs) and semilandmarks (SLMs) used in this study. Left astragalus is figured in lateral (**A**), plantar (**B**), medial (**C**), dorsal (**D**), distal (**E**), and proximal (**F**) views. Black circles are LMs; gray circles are SLMs (shown are both helper and slider points). SLMs are placed along curves, with middle points designated with LMs (i.e., LMs 16, 18, and 21). See Table 4.4 for LM and SLM descriptions, and text for more on designation of SLMs slider and helper points.

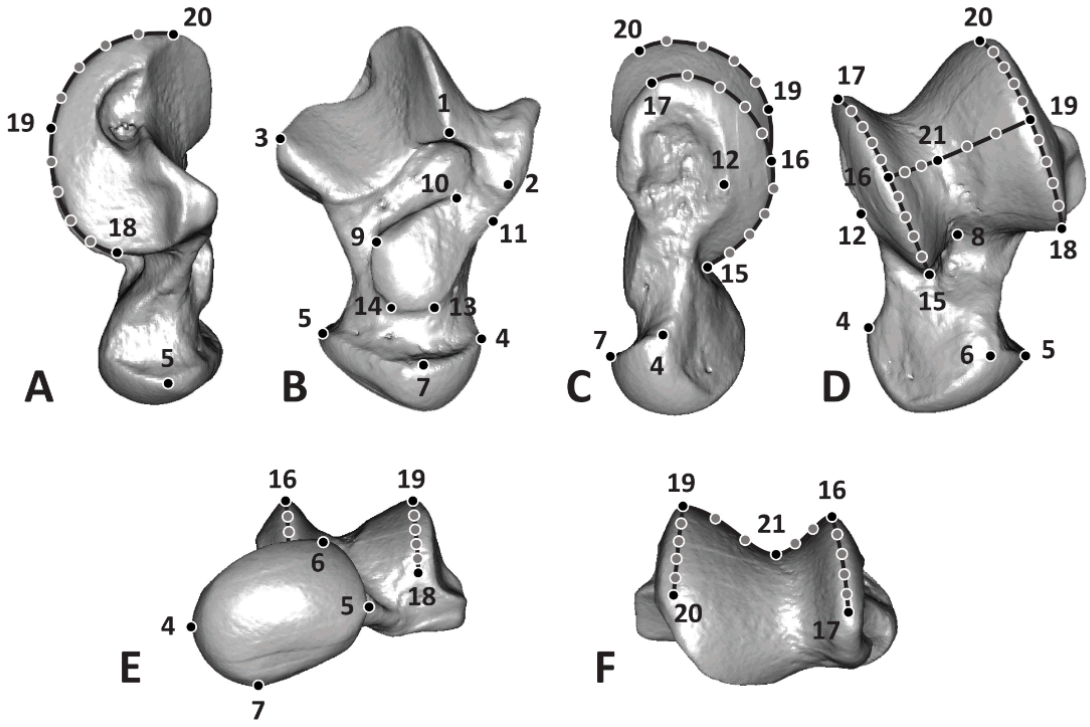

Figure 4.5. Results of the principal components analysis performed on the 3D GM data for all astragali in our dataset. Fossil astragali are projected into the morphospace defined by extant taxa. **A**, PCs 1 and 2; **B**, PCs 1 and 3; **C**, PCs 2 and 3. Extant metatherians are indicated by closed circles and gray lines; extant eutherians with closed squares and black lines; fossil specimens with open circles and dotted lines. For extant mammal orders and fossil ages, see legend.

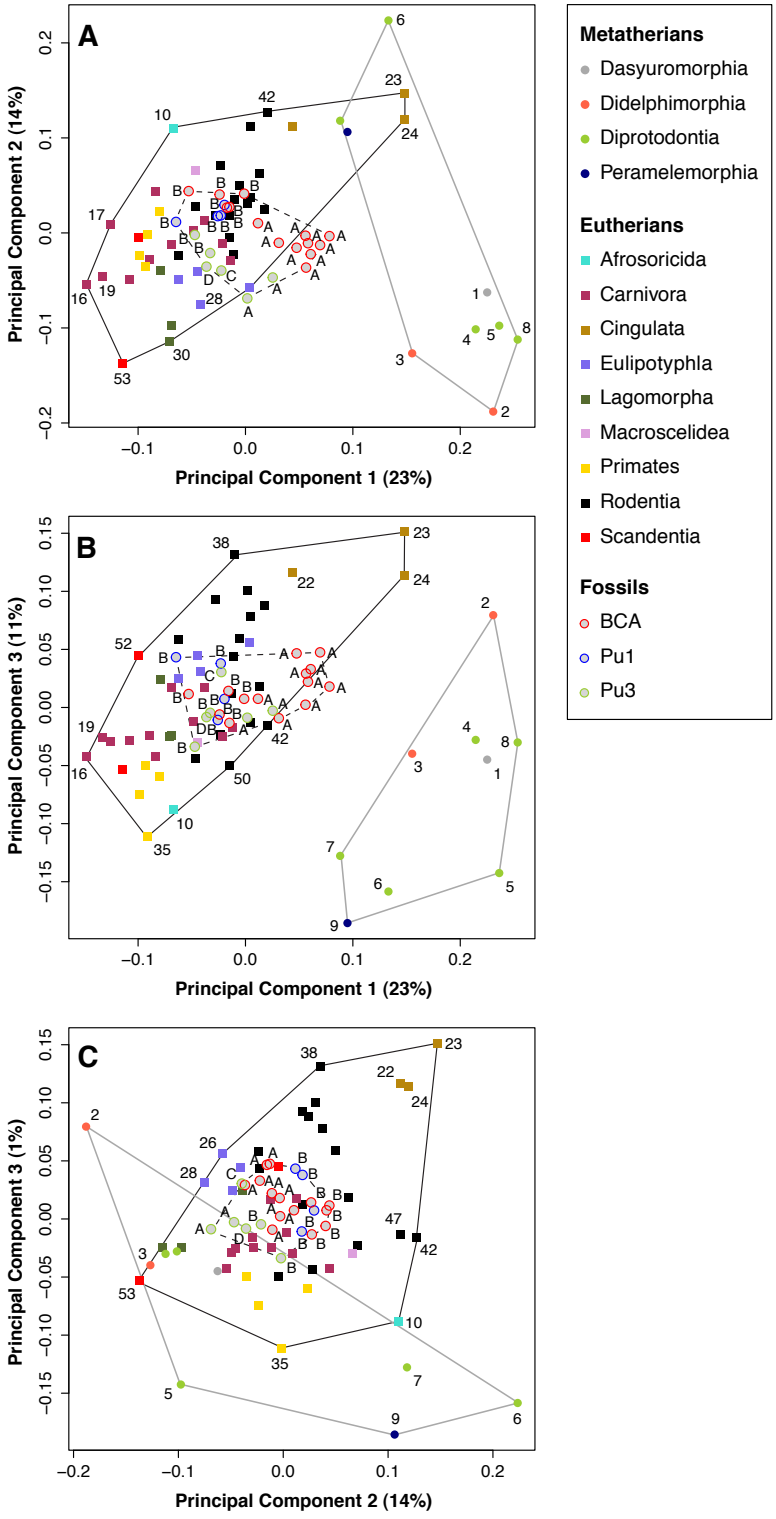

Figure 4.6. Results of principal component analysis performed on the 3D GM data with our full dataset of extant mammals, plotted according to locomotor group. **A**, PCs 1 and 2; **B**, PCs 1 and 3; **C**, PCs 2 and 3. Fossil specimens were projected into the morphospace defined by extant mammals (see text for details). Only color-coding and legend here differ from Fig. 4.5, otherwise all data is identical.

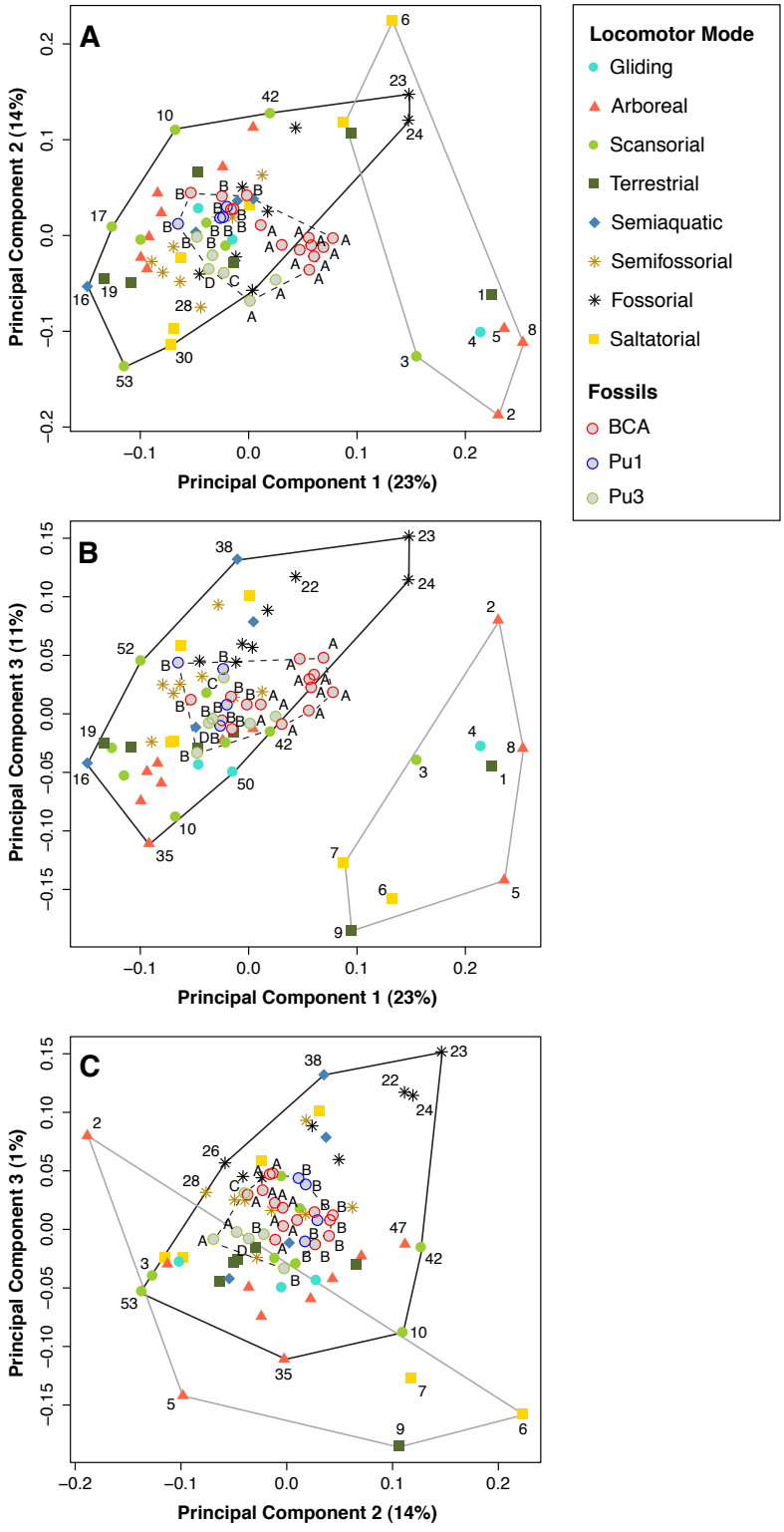

Figure 4.7. Results of the principal components analysis performed on the 3D GM data for astragali in our eutherian reduced dataset. **A**, PCs 1 and 2; **B**, PCs 1 and 3; **C**, PCs 2 and 3. Fossil astragali are projected into the morphospace defined by extant taxa. Dotted lines enclose our fossil specimens within this morphospace.

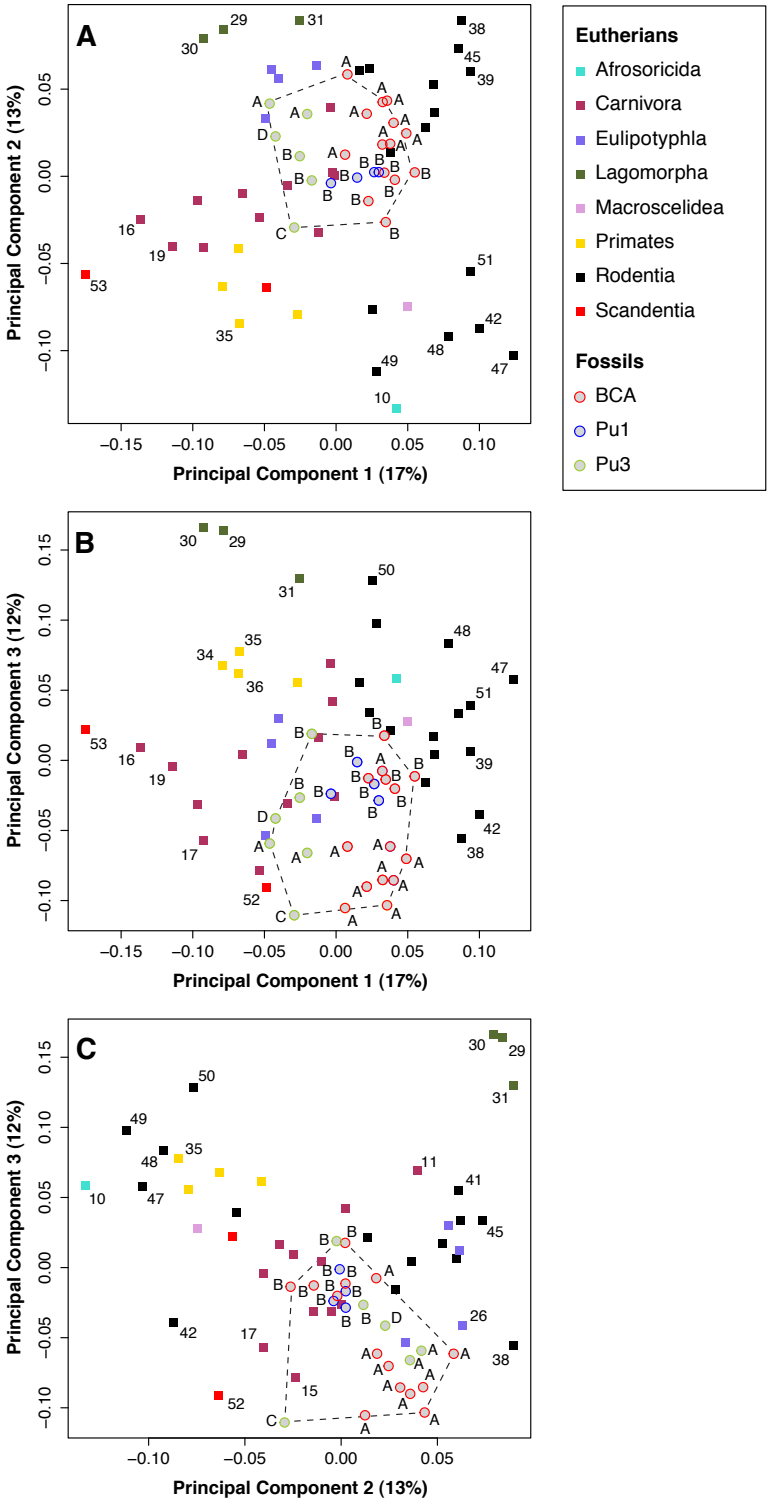

Figure 4.8. Results of the principal components analysis performed on the 3D GM data for astragali in our eutherian reduced dataset. **A**, PCs 1 and 2; **B**, PCs 1 and 3; **C**, PCs 2 and 3. Fossil astragali are projected into the morphospace defined by extant taxa. Data is identical to that of Fig. 4.7, with points here color-coded by locomotor group. Colored lines enclose locomotor groups containing three or more specimens; dotted black lines enclose fossil specimens within this morphospace.

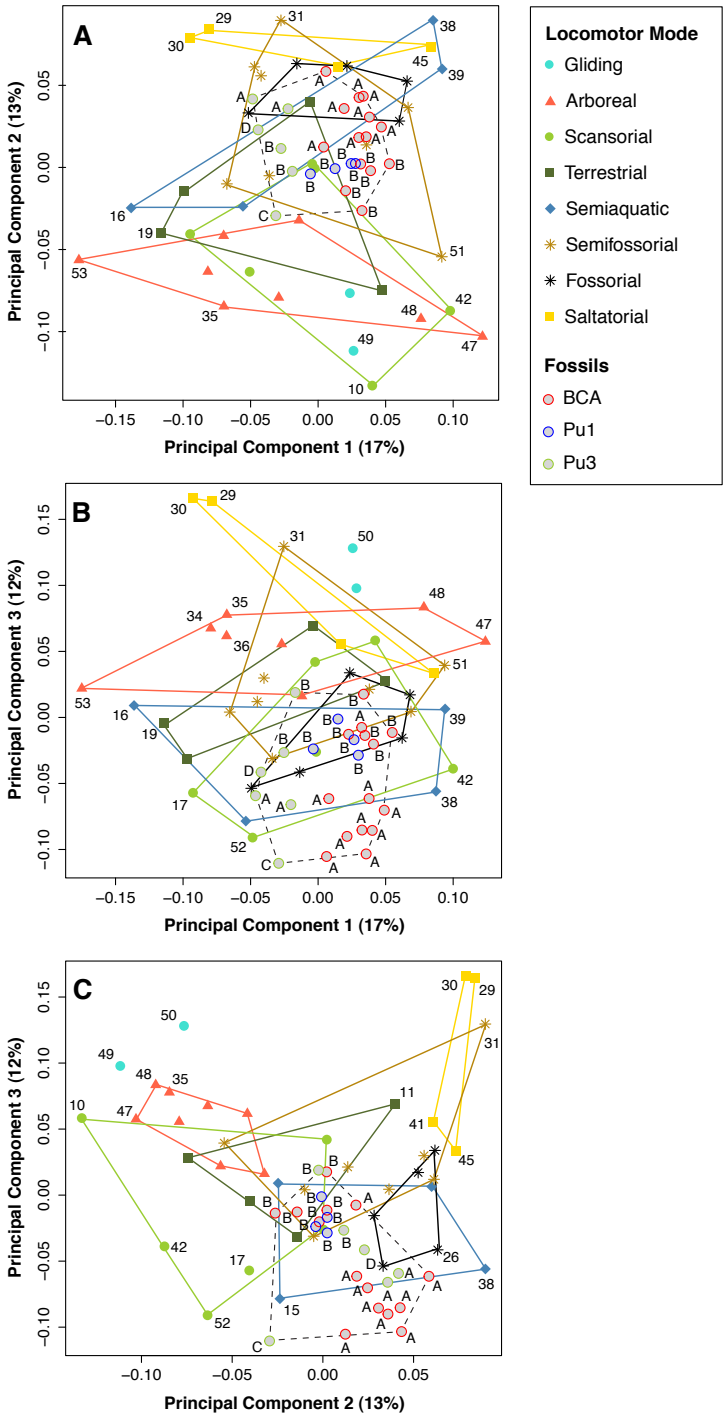

Figure 4.9. Results of the principal components analysis performed on the 3D GM data for astragali in our further reduced eutherian dataset. **A**, PCs 1 and 2; **B**, PCs 1 and 3; **C**, PCs 2 and 3. Fossil astragali are projected into the morphospace defined by extant taxa. Dotted lines enclose fossils.

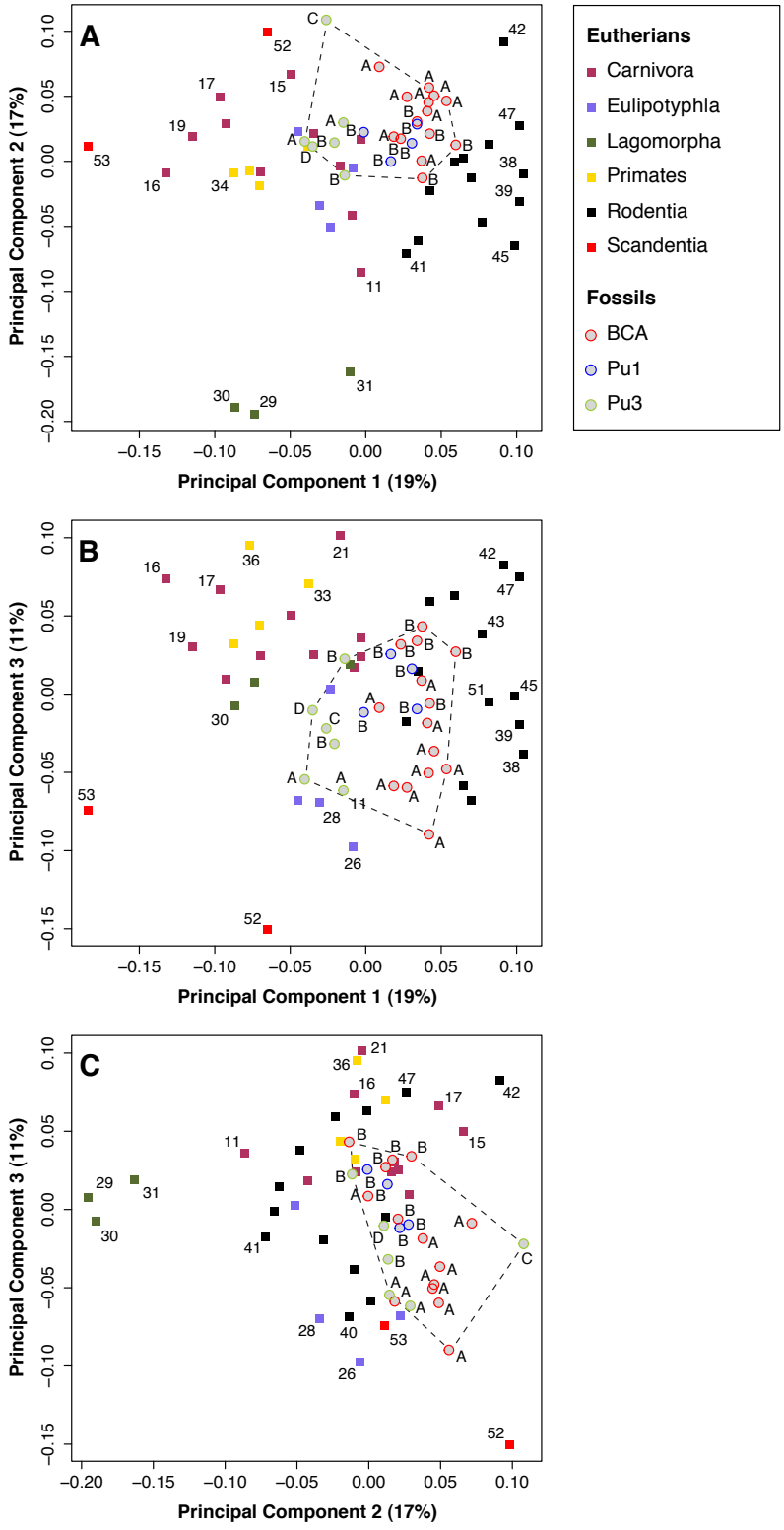

Figure 4.10. Results of the principal components analysis performed on the 3D GM data for astragali in our further eutherian reduced dataset. **A**, PCs 1 and 2; **B**, PCs 1 and 3; **C**, PCs 2 and 3. Fossil astragali are projected into the morphospace defined by extant taxa. Data is identical to that of Fig. 4.9, with points here color-coded by locomotor group. Colored lines enclose locomotor groups containing three or more specimens; dotted black lines enclose fossil specimens within this morphospace.

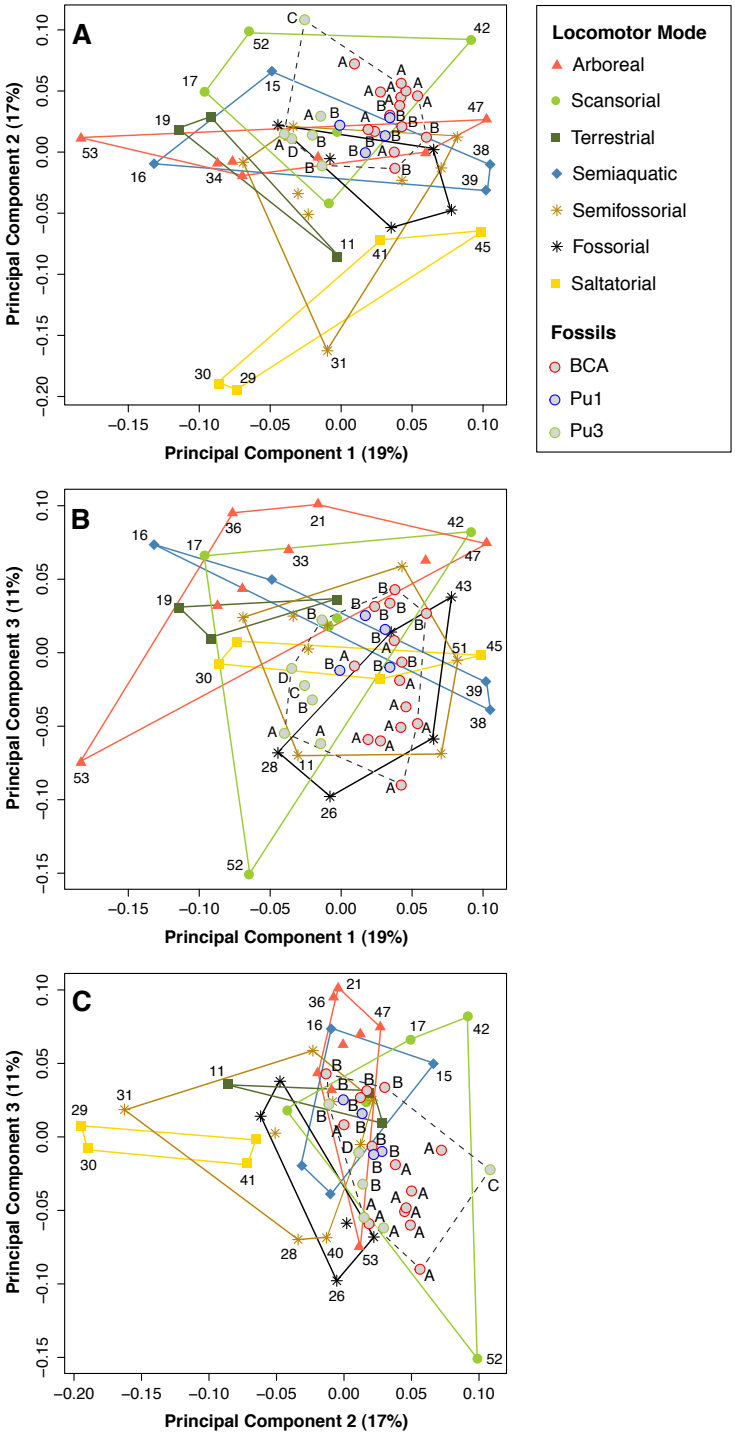

Figure 4.11. Results of the linear discriminant function analysis performed on PCA results for astragali in our narrowest eutherian dataset (see PCA results in Figs. 9–10). **A**, LDs 1 and 2; **B**, LDs 1 and 3; **C**, LDs 2 and 3. Colored lines enclose locomotor groups; dotted black lines enclose specimens within fossil morphotypes A and B. See Table 4.2 for extant specimens.

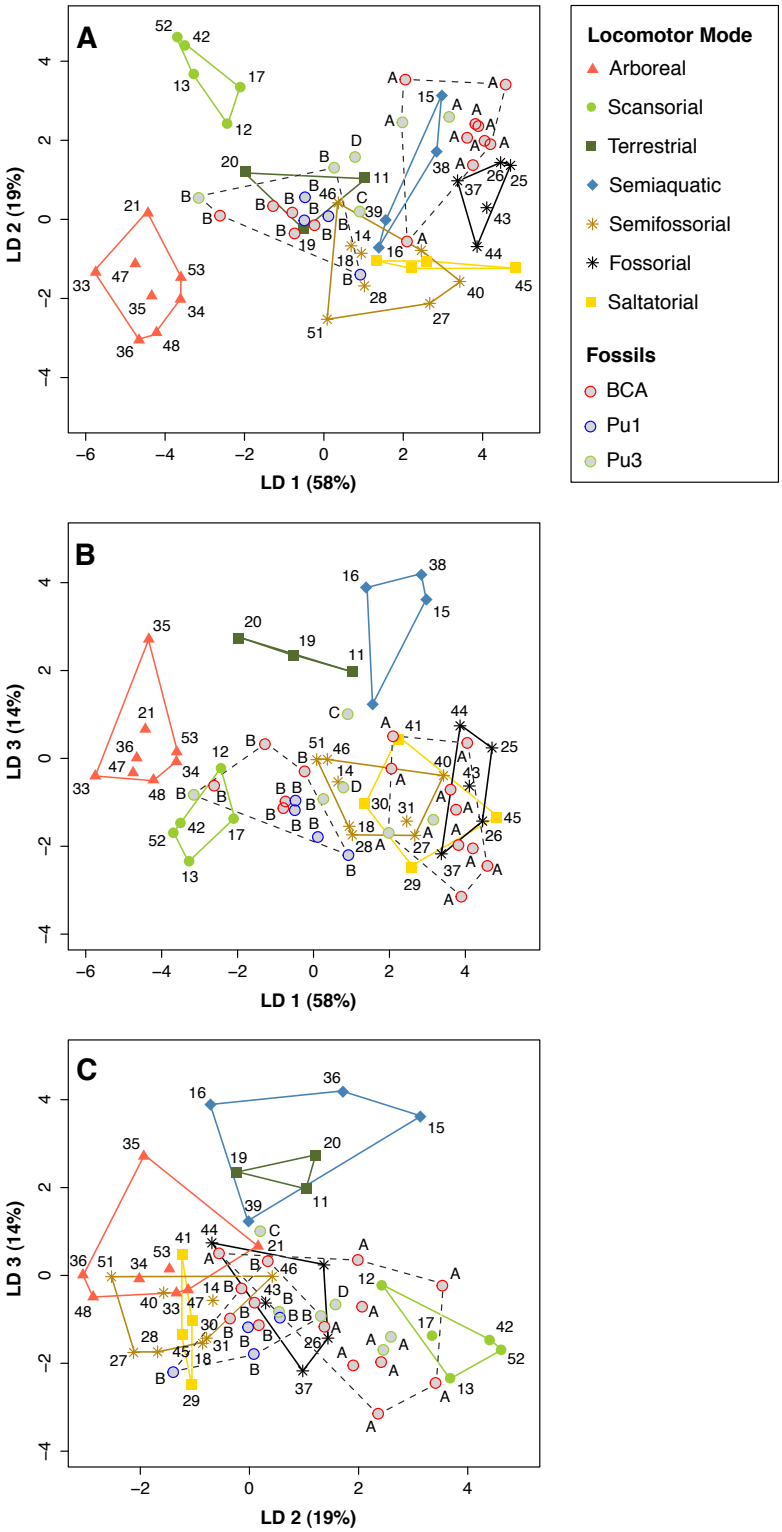

Tables

Table 4.1. Fossil therian astragali specimens used in this study. Abbreviations: Pu1, Puercan 1 Biozone; Pu3, Puercan 3 Biozone. Locality numbers follow the system of each institution: those beginning with "V" are UCMP localities; those beginning with "C" are UWBM localities (see Table S4.1 for additional locality details). See text for morphotype description

Specimen	Locality Number	Biozone	Right/Left	Morphotype
70965	C0338	BCA	L	A
118532	V70201	BCA	R	B
151955	V65127	BCA	R	B
151963	V65127	BCA	R	B
151967	V65127	BCA	L	A
151968	V65127	BCA	L	A
151969	V65127	BCA	L	A
151990	V71203	BCA	R	B
151995	V87098	BCA	L	A
152011	V84043	BCA	R	A
152014	V87101	BCA	R	A
152018	V87038	BCA	R	A
153150	V70201	BCA	L	B
196000	V82014	BCA	R	A
150432	V74110	Pu1	R	B
153031	V74111	Pu1	R	B
192681	V74111	Pu1	L	B
194857	V74111	Pu1	R	B
145674	V73080	Pu3	L	A
192514	V74122	Pu3	L	B
192676	V74125	Pu3	L	D
195905	V73080	Pu3	R	B
197509	V99438	Pu3	L	C
197518	V99438	Pu3	L	A

Table 4.2. Modern mammalian specimens used in geometric morphometrics analyses. Species list and locomotor references are modified from Chen and Wilson 2015; see text for more details. Code number was assigned (and the table sorted) as follows: clade, order, family, and locomotor mode. Locomotor mode abbreviations are as follows: A, arboreal; F, fossorial; G, gliding; S, saltatorial; Sa, semiaquatic; Sc, scansorial; Sf, semifossorial; T, terrestrial (see Table 4.3). Other abbreviations: F, female; L, left astragalus; LM, locomotor mode; M, male; R, right astragalus; Spec., specimen number; U, sex unknown. Single asterisk indicates specimens images present in Fig. 4.3. All specimens are from the UWBM, except 488072 (double asterisk indicates it is a USNM specimen; see Table S4.3 for details).

Clade	Order	Code	LM	Genus	Species	Family	Spec.	L/R	Sex	Locomotor Reference
Metatheria										
	Dasyuromorphia									
		1	T	*Sarcophilus*	*harrisii*	Dasyuridae	20671*	R	M	Van Valkenburgh 1987
	Didelphimorphia									
		2	A	*Caluromys*	*derbianus*	Didelphidae	32255	R	U	Argot 2001
		3	Sc	*Didelphis*	*virginiana*	Didelphidae	77674*	L	M	Argot 2001
	Diprotodontia									
		4	G	*Petaurus*	*breviceps*	Petauridae	72928*	L	U	Smith 1973; Nowak 1999; Körtner and Geiser 2000
		5	A	*Trichosurus*	*vulpecula*	Phalangeridae	68913	R	M	Nowak 1999
		6	S	*Potorous*	*tridactylus*	Potoroidae	34200*	L	M	Bassarova et al. 2009
		7	S	*Aepyprymnus*	*rufescens*	Potoroidae	68898	R	F	Bassarova et al. 2009
		8	A	*Pseudocheirus*	*peregrinus*	Pseudocheiridae	68924	L	F	Bassarova et al. 2009
	Perameleomorphia	9	T	*Perameles*	*nasuta*	Peramelidae	68919	R	F	Nowak 1999
Eutheria										
	Afrosoricida									
		10	Sc	*Echinops*	*telfairi*	Tenrecidae	34168*	L	F	Endo et al. 2006; Salton and Sargis 2008

Carnivora									
	11	T	*Vulpes*	*vulpes*	Canidae	39490*	R	F	Lariviére and Pasitschniak-Arts 1996; Meachen-Samuels 2010
	12	Sc	*Urocyon*	*cinereoargenteus*	Felidae	35221*	L	M	Van Valkenburgh 1987; Meachen-Samuels 2010
	13	Sc	*Suricata*	*suricatta*	Herpestidae	35470	L	F	van Staaden 1994; Iwaniuk et al. 1999
	14	Sf	*Mephitis*	*mephitis*	Mephitidae	35951	L	F	Wade-Smith and Verts 1982; Van Valkenburgh 1987; Samuels and Van Valkenburgh 2008
	15	Sa	*Lontra*	*canadensis*	Mustelidae	32230*	R	M	Gingerich 2003
	16	Sa	*Mustela*	*vison*	Mustelidae	35223	L	M	Howell 1930; Lariviére 1999; Gingerich 2003
	17	Sc	*Gulo*	*gulo*	Mustelidae	34936	L	F	Van Valkenburgh 1987; Pasitschniak-Arts and Lariviére 1995
	18	Sf	*Spilogale*	*putorius*	Mustelidae	38625	L	M	Heinrich and Houde 2006
	19	T	*Mustela*	*erminea*	Mustelidae	39366	L	F	Nowak 1999
	20	T	*Mustela*	*putorius*	Mustelidae	58727	R	M	Nowak 1999
	21	A	*Paguma*	*larvata*	Viverridae	73281	L	U	Nowak 1999
Cingulata									
	22	F	*Cabassous*	*centralis*	Dasypodidae	34167	L	F	Nowak 1999
	23	F	*Dasypus*	*novemcinctus*	Dasypodidae	22458	L	M	Samuels and Van Valkenburgh 2008
	24	F	*Euphractus*	*sexcinctus*	Dasypodidae	35468*	R	M	Redford and Wetzel 1985; Nowak 1999
Eulipotyphla									
	25	F	*Scalopus*	*aquaticus*	Talpidae	38637	L	F	Nowak 1999
	26	F	*Scapanus*	*orarius*	Talpidae	34236*	L	F	Hildebrand 1985; Nowak 1999
	27	Sf	*Neurotrichus*	*gibbsii*	Talpidae	60340	L	M	Nowak 1999
	28	Sf	*Urotrichus*	*talpoides*	Talpidae	35360	R	M	Nowak 1999
Lagomorpha									
	29	S	*Brachylagus*	*idahoensis*	Leporidae	38628	L	F	Nowak 1999
	30	S	*Lepus*	*americanus*	Leporidae	33263*	L	M	Nowak 1999
	31	Sf	*Ochotona*	*princeps*	Ochtonidae	60062	R	M	Nowak 1999
Macroscelidea									
	32	T	*Elephantulus*	*rufescens*	Macroscelididae	35475*	L	F	Nowak 1999
Primates									
	33	A	*Callithrix*	*pygmaea*	Cebidae	39005	L	M	Nowak 1999
	34	A	*Leontopithecus*	*rosalia*	Cebidae	75541	L	F	Nowak 1999
	35	A	*Saguinus*	*oedipus*	Cebidae	75539	R	F	Nyakatura et al. 2008
	36	A	*Saimiri*	*sciureus*	Cebidae	39014*	L	M	Nowak 1999

Rodentia									
	37	F	*Aplodontia*	*rufa*	Aplodontiidae	34058	L	M	Samuels and Van Valkenburgh 2008
	38	Sa	*Castor*	*canadensis*	Castoridae	81972*	R	M	Nowak 1999
	39	Sa	*Ondatra*	*zibethicus*	Cricetidae	72879	L	M	Howell 1930; Gingerich, 2003
	40	Sf	*Synaptomys*	*borealis*	Cricetidae	66559*	R	F	Nowak 1999
	41	S	*Zapus*	*princeps*	Dipodidae	76721	L	F	Nowak 1999
	42	Sc	*Coendou*	*prehensilis*	Erethizontidae	34176	L	F	Nowak 1999
	43	F	*Thomomys*	*bottae*	Geomyidae	44623	L	M	Nowak 1999
	44	F	*Chaetodipus*	*fallax*	Heteromyidae	47379	L	M	Lackey 1996
	45	S	*Dipodomys*	*deserti*	Heteromyidae	78740	L	F	Samuels and Van Valkenburgh 2008
	46	Sf	*Octodon*	*degus*	Octodontidae	48984	L	F	Nowak 1999
	47	A	*Sciurus*	*aberti*	Sciuridae	35278	L	F	Nowak 1999
	48	A	*Sciurus*	*carolinensis*	Sciuridae	20646*	L	F	Nowak 1999
	49	G	*Glaucomys*	*sabrinus*	Sciuridae	35129*	R	M	Samuels and Van Valkenburgh 2008
	50	G	*Glaucomys*	*volans*	Sciuridae	43897	L	F	Nowak 1999
	51	Sf	*Cynomys*	*ludovicianus*	Sciuridae	75774	L	M	Nowak 1999
Scandentia									
	52	Sc	*Tupaia*	*glis*	Tupaiidae	34225*	L	M	Van Valkenburgh 1987
	53	A	*Ptilocercus*	*lowii*	Tupaiidae	488072**	R	F	Nowak 1999

Table 4.3. Definitions of locomotor modes used in this study. Locomotor modes are those in Chen and Wilson (2015: table 2), which are modified from Hildebrand and Goslow (1998), Polly (2007), Samuels and Van Valkenburgh (2008), and Samuels et al. (2013).

Locomotor Mode	Descriptive Definition
Arboreal	Spend most of the time in trees foraging, traveling, resting, but occasionally travel on the ground
Gliding	Bridge gaps between trees by gliding usually with patagium
Fossorial	Efficiently dig burrows for shelter or foraging underground exclusively
Saltatorial	Capable of jumping using both hind limbs simultaneously for high-speed transportation over long distance
Scansorial	Capable of climbing for escape, eating, or leisure, and probably spend a considerable time both in the trees and on the ground
Semiaquatic	Capable of swimming for dispersal, escape, or foraging as well as on the ground
Semifossorial	Regularly dig for food or to build burrows for shelter, but do not exclusively live underground
Terrestrial	Spend most of time on the ground, but able to swim, climb, and burrow occasionally, but not specialized for those

Table 4.4. Definition of the landmarks (LMs) used for 3D geometric morphometric analyses in this study. Descriptions with superscripts indicate corresponding LM number in Fabre et al. (2014). Curves are traced between LMs 14 and 16 (midpoint at LM15; eight SLMs), LMs 17 and 19 (midpoint at LM18; eight SLMs), and LMs 15 and 18 (midpoint at LM20; four SLMs). See Fig. 4.2 for LM and SLM placement.

LM	Definition
1	Most distomedial point of the ectal facet[3]
2	Tip of the protuberance distomedial of the flexor fibularis tendon groove[7]
3	Most proximolateral point of the ectal facet
4	Most proximomedial point of the navicular facet[14]
5	Most proximolateral point of the navicular facet[16]
6	Point of maximum convexity of the dorsal side of the navicular facet between LMs 4 and 6
7	Point of maximum convexity of the plantar side of the navicular facet between LMs 4 and 6
8	Point of maximum of concavity between LMs 15 and 18[19]
9	Most proximolateral point of the sustentacular facet[10]
10	Most proximal point of the sustentacular facet[11]
11	Most proximomedial point of the sustentacular facet[12]
12	Most lateral point of the ectal facet
13	Most distomedial point of the sustentacular facet[13]
14	Most distolateral point of the sustentacular facet[17]
15	Most distomedial point of the medial ridge of the lateral tibial facet[18]
16	Point of maximum of convexity of the medial ridge of the lateral tibial facet[24]
17	Most proximomedial point of the medial ridge of the lateral tibial facet[23]
18	Most distolateral point of the lateral ridge of the lateral tibial facet[20]
19	Point of maximum convexity of the lateral ridge of the lateral tibial facet[21]
20	Most proximolateral point of the lateral ridge of the lateral tibial facet[22]
21	Point of maximum concavity on the tibial trochlea, between points 16 and 19

Table 4.5. PCA results for full and reduced datasets. We report eigenvalues, standard deviations (sd), proportion of variance, and cumulative proportion of variance for principal components describing >1% of the variance (i.e., PCs 1–17 for all datasets; see text for dataset details).

	Full Dataset				Reduced Dataset 1				Reduced Dataset 2			
	Eigenvalues	sd	Proportion of Variance	Cumulative Proportion	Eigenvalues	sd	Proportion of Variance	Cumulative Proportion	Eigenvalues	sd	Proportion of Variance	Cumulative Proportion
PC1	0.010790	0.103873	23.3%	23.3%	0.005285	0.072698	16.8%	16.8%	0.005686	0.075407	19.0%	19.0%
PC2	0.006628	0.081413	14.3%	37.7%	0.004133	0.064287	13.1%	29.9%	0.004097	0.064011	13.7%	32.7%
PC3	0.005283	0.072683	11.4%	49.1%	0.003688	0.060727	11.7%	41.6%	0.003319	0.057612	11.1%	43.8%
PC4	0.003180	0.056392	6.9%	56.0%	0.003574	0.059783	11.3%	52.9%	0.002951	0.054327	9.9%	53.6%
PC5	0.003093	0.055617	6.7%	62.7%	0.002493	0.049934	7.9%	60.8%	0.002441	0.049408	8.2%	61.8%
PC6	0.002376	0.048745	5.1%	67.8%	0.001698	0.041202	5.4%	66.2%	0.001511	0.038875	5.1%	66.8%
PC7	0.001718	0.041451	3.7%	71.5%	0.001368	0.036980	4.3%	70.5%	0.001372	0.037036	4.6%	71.4%
PC8	0.001594	0.039923	3.4%	75.0%	0.001063	0.032607	3.4%	73.9%	0.001060	0.032559	3.5%	75.0%
PC9	0.001312	0.036224	2.8%	77.8%	0.000947	0.030770	3.0%	76.9%	0.000977	0.031264	3.3%	78.2%
PC10	0.001074	0.032779	2.3%	80.2%	0.000799	0.028269	2.5%	79.4%	0.000834	0.028886	2.8%	81.0%
PC11	0.000916	0.030266	2.0%	82.1%	0.000756	0.027487	2.4%	81.8%	0.000722	0.026866	2.4%	83.4%
PC12	0.000887	0.029788	1.9%	84.1%	0.000702	0.026498	2.2%	84.0%	0.000676	0.026002	2.3%	85.7%
PC13	0.000756	0.027491	1.6%	85.7%	0.000654	0.025580	2.1%	86.1%	0.000577	0.024013	1.9%	87.6%
PC14	0.000643	0.025348	1.4%	87.1%	0.000561	0.023684	1.8%	87.9%	0.000521	0.022824	1.7%	89.4%
PC15	0.000611	0.024719	1.3%	88.4%	0.000528	0.022978	1.7%	89.6%	0.000421	0.020523	1.4%	90.8%
PC16	0.000563	0.023729	1.2%	89.6%	0.000443	0.021039	1.4%	91.0%	0.000377	0.019422	1.3%	92.0%
PC17	0.000503	0.022437	1.1%	90.7%	0.000390	0.019739	1.2%	92.2%	0.000325	0.018018	1.1%	93.1%

Table 4.6. PERMANOVA results for the final dataset of extant mammals with known locomotion. Abbreviations: df, degrees of freedom; LM, locomotor mode; order, taxonomic order (see Table 4.2 for more details); MS, mean square; SS, sum of squares Procrustes distances.

Model	df	SS	MS	R^2	F ratio	p-value
LM	6	0.2768	0.0461	0.2569	1.7282	0.01
Residuals	30	0.8007	0.0267			
Total	36	1.0775	0.0299			
Order	5	0.4626	0.0925	0.4294	4.6655	0.01
Residuals	31	0.6148	0.0198			
Total	36	1.0775	0.0299			
LM	6	0.2768	0.0461	0.2569	2.5988	0.01
Order	5	0.3570	0.0714	0.3313	4.0222	0.01
Residuals	25	0.4437	0.0177			
Total	36	1.0775	0.0299			

Table 4.7. LDA results for the reduced dataset of extant mammals with known locomotion. LDA predicts locomotor mode with 94.6% accuracy.

	Locomotor Group Means						
	A	**F**	**S**	**Sa**	**Sc**	**Sf**	**T**
PC1	-0.03850	0.02516	-0.00833	0.00659	-0.01623	0.00365	-0.06970
PC2	0.00109	-0.01809	-0.13038	0.00384	0.04288	-0.03234	-0.01294
PC3	0.05055	-0.03455	-0.00491	0.01622	0.00777	-0.00183	0.02513
PC4	-0.06916	0.01130	-0.02904	0.05113	-0.02321	-0.00392	0.01620
PC5	0.03777	-0.02384	-0.02496	-0.00583	-0.05329	0.01147	0.01821
PC6	-0.00370	-0.00436	-0.01754	-0.01089	0.02079	-0.00946	0.02845
PC7	-0.01569	-0.00494	-0.01110	-0.04235	-0.01225	0.00716	-0.04594
PC8	-0.00781	-0.00059	-0.00957	0.02215	-0.00308	-0.03107	0.00741
PC9	-0.01395	0.02223	-0.00819	-0.03373	-0.00587	-0.00596	-0.00960
PC10	-0.00264	0.00832	0.00794	0.00699	-0.01220	0.00717	0.02274
PC11	0.00454	0.00966	0.01416	-0.00705	0.03319	-0.00013	0.00782
PC12	0.00379	-0.00939	0.02427	0.01142	0.02852	0.00205	0.01311
PC13	-0.01573	-0.01142	-0.01764	-0.01910	-0.00423	-0.00659	0.00251
PC14	0.00934	-0.00585	0.00045	-0.00978	0.01521	-0.00306	-0.00652
PC15	0.02236	0.02589	0.02620	0.02992	0.00809	0.00920	0.01592
PC16	0.00390	0.00294	-0.00072	0.01051	0.00470	0.00034	-0.02554

	Coefficients of Linear Discriminants					
	LD1	**LD2**	**LD3**	**LD4**	**LD5**	**LD6**
PC1	11.82925	1.21752	-2.99376	-2.36823	4.48418	1.06926
PC2	-20.63290	13.77119	4.89107	-12.11906	2.45564	-0.06455
PC3	-23.44444	-5.31201	6.75512	1.76039	0.39474	1.60831
PC4	31.51521	11.44829	11.58620	-4.19972	-2.08478	6.05001
PC5	-15.32317	-22.39385	9.56967	-6.11236	-3.21064	-0.01710
PC6	-14.16597	13.98441	1.64955	-1.60982	-9.74979	-3.08519
PC7	6.49998	-8.05299	-22.28423	-7.14465	1.95183	4.18764
PC8	0.75421	16.54206	22.09079	6.56247	6.37646	-11.81480
PC9	18.39635	3.38053	-18.76133	-8.42783	-5.54156	-18.95694
PC10	23.31864	-8.05418	9.77874	0.29679	-11.06938	-2.29870
PC11	-15.90402	24.54093	-18.54666	9.28009	-3.49888	-6.97108
PC12	-17.13884	19.93198	-2.54286	23.79004	-2.67776	13.98658
PC13	-2.88043	10.25722	-4.62890	-6.65991	-17.25054	3.59402
PC14	-45.44276	7.23859	-15.92631	4.87169	4.64534	-1.64383
PC15	17.94439	-10.10781	20.08573	11.41518	17.48053	-22.42043
PC16	-1.81689	3.21419	-7.80148	-5.32436	40.41169	7.88319
Proportions of Trace	**58.00%**	**19.18%**	**13.66%**	**4.10%**	**3.62%**	**1.44%**

Table 4.8. Predicted locomotor mode for fossil specimens in this study. LDA prediction probabilities in bold are the top ranked locomotor mode (i.e., rank of 1); – indicates a prediction probability of < 0.00%.

Specimen Number	Locality	Morph	Biozone	Prediction Probabilities							Rank						
				A	F	S	Sa	Sc	Sf	T	1	2	3	4	5	6	7
70965	C0338	A	BCA	–	**99.75%**	–	–	–	0.25%	–	F	Sf	S	Sa	T	Sc	A
151955	V65127	B	BCA	**96.12%**	–	–	–	2.00%	1.87%	0.02%	A	Sc	Sf	T	Sa	F	S
151963	V65127	B	BCA	0.01%	0.01%	0.01%	0.01%	–	**99.92%**	0.04%	Sf	T	A	Sa	Sc	S	F
151967	V65127	A	BCA	–	**95.68%**	–	–	–	4.31%	–	F	Sf	Sa	T	S	Sc	A
151968	V65127	A	BCA	–	**99.61%**	–	–	–	0.39%	–	F	Sf	S	T	Sa	Sc	A
151969	V65127	A	BCA	–	**99.56%**	–	–	–	0.44%	–	F	Sf	S	Sa	T	Sc	A
118532	V70201	B	BCA	0.02%	–	–	–	0.03%	**99.94%**	0.01%	Sf	Sc	A	T	F	S	Sa
153150	V70201	B	BCA	1.40%	–	–	0.01%	0.30%	**49.38%**	48.90%	Sf	T	A	Sc	Sa	S	F
151990	V71203	B	BCA	0.04%	–	–	–	–	**99.95%**	–	Sf	A	Sc	T	F	Sa	S
196000	V82014	A	BCA	–	**99.98%**	–	–	–	0.02%	–	F	Sf	S	Sa	Sc	T	A
152011	V84043	A	BCA	–	**85.76%**	–	0.65%	0.05%	12.96%	0.58%	F	Sf	Sa	T	Sc	S	A
152018	V87038	A	BCA	–	2.44%	0.01%	0.03%	–	**97.42%**	0.11%	Sf	F	T	Sa	S	A	Sc
151995	V87084	A	BCA	–	**89.15%**	–	–	–	10.85%	–	F	Sf	Sa	S	T	Sc	A
152014	V87101	A	BCA	–	**97.97%**	–	0.01%	–	2.00%	0.02%	F	Sf	T	Sa	S	Sc	A
150432	V74110	B	Pu1	0.01%	0.01%	–	–	0.17%	**99.67%**	0.13%	Sf	Sc	T	F	A	S	Sa
153031	V74111	B	Pu1	0.05%	0.04%	–	–	0.01%	**99.90%**	0.01%	Sf	A	F	Sc	T	S	Sa
192681	V74111	B	Pu1	–	0.03%	–	–	–	**99.97%**	–	Sf	F	Sc	S	A	T	Sa
194857	V74111	B	Pu1	–	0.12%	–	–	–	**99.88%**	–	Sf	F	S	A	Sa	T	Sc
145674	V73080	A	Pu3	–	**96.77%**	–	–	–	3.23%	–	F	Sf	T	S	Sa	Sc	A
195905	V73080	B	Pu3	–	0.20%	–	–	0.10%	**99.61%**	0.08%	Sf	F	Sc	T	Sa	S	A
192514	V74122	B	Pu3	**70.42%**	–	–	–	29.25%	0.17%	0.16%	A	Sc	Sf	T	S	Sa	F
192676	V74125	D	Pu3	–	2.06%	0.01%	0.06%	0.06%	**97.53%**	0.28%	Sf	F	T	Sc	Sa	S	A
197509	V99438	C	Pu3	–	0.40%	–	0.19%	–	**98.03%**	1.38%	Sf	T	F	Sa	S	A	Sc
197518	V99438	A	Pu3	–	41.75%	0.01%	–	0.01%	**58.19%**	0.05%	Sf	F	T	Sc	S	Sa	A

SUPPLEMENTARY MATERIAL FOR

Locomotor Function in Mammal Astragali from the Cretaceous-Paleogene Boundary in Eastern Montana

Table S4.1. Localities containing specimens used in this study. Locality numbers follow the system of each institution; those beginning with "V" are UCMP localities; those beginning with "C" are UWBM localities. All localities are in Montana. Abbreviations: BCA, Bug Creek Anthills, mixed age (see text for details); Fm, formation; n, number of specimens from the locality; Pu1, Puercan 1; Pu3, Puercan 3.

Loc. Number	Locality Name	County	Fm	Biozone	n
C0338	Bug Creek A	McCone	Hell Creek	BCA	1
V65127	Bug Creek Anthills General	McCone	Hell Creek	BCA	5
V70201	Bug Creek Anthills C	McCone	Hell Creek	BCA	2
V71203	Harbicht Hill 1	McCone	Hell Creek	BCA	1
V73080	Garbani 13-NW Harley's High	Garfield	Tullock	Pu3	2
V74110	Hell's Hollow-Channel	Garfield	Tullock	Pu1	1
V74111	Worm Coulee 1	Garfield	Tullock	Pu1	3
V74122	Biscuit Springs	Garfield	Tullock	Pu3	1
V74125	Yellow Sand Hill 3	Garfield	Tullock	Pu3	1
V82014	Big Bugger Extension	McCone	Hell Creek	BCA	1
V84043	Laurie's Painted Rock	McCone	Hell Creek	BCA	1
V87038	Up Up-the-Creek 3	McCone	Hell Creek	BCA	1
V87098	Little Roundtop	McCone	Hell Creek	BCA	1
V87101	Second Level	McCone	Hell Creek	BCA	1
V99438	Garbani Sandy Channel	Garfield	Tullock	Pu3	2

Figure S4.1. Map of localities in northeastern Montana producing astragali specimens used in this study. Localities span the early and middle Puercan biozones (Pu1 and Pu3, in blue stars and green triangles, respectively), as well as the time-averaged and stratigraphically mixed localities representative of the Bug Creek Anthills fauna (red squares). All localities are located within Garfield and McCone counties. Locality names and details are given in Table 4.1. Map is modified from Wilson et al. (2014).

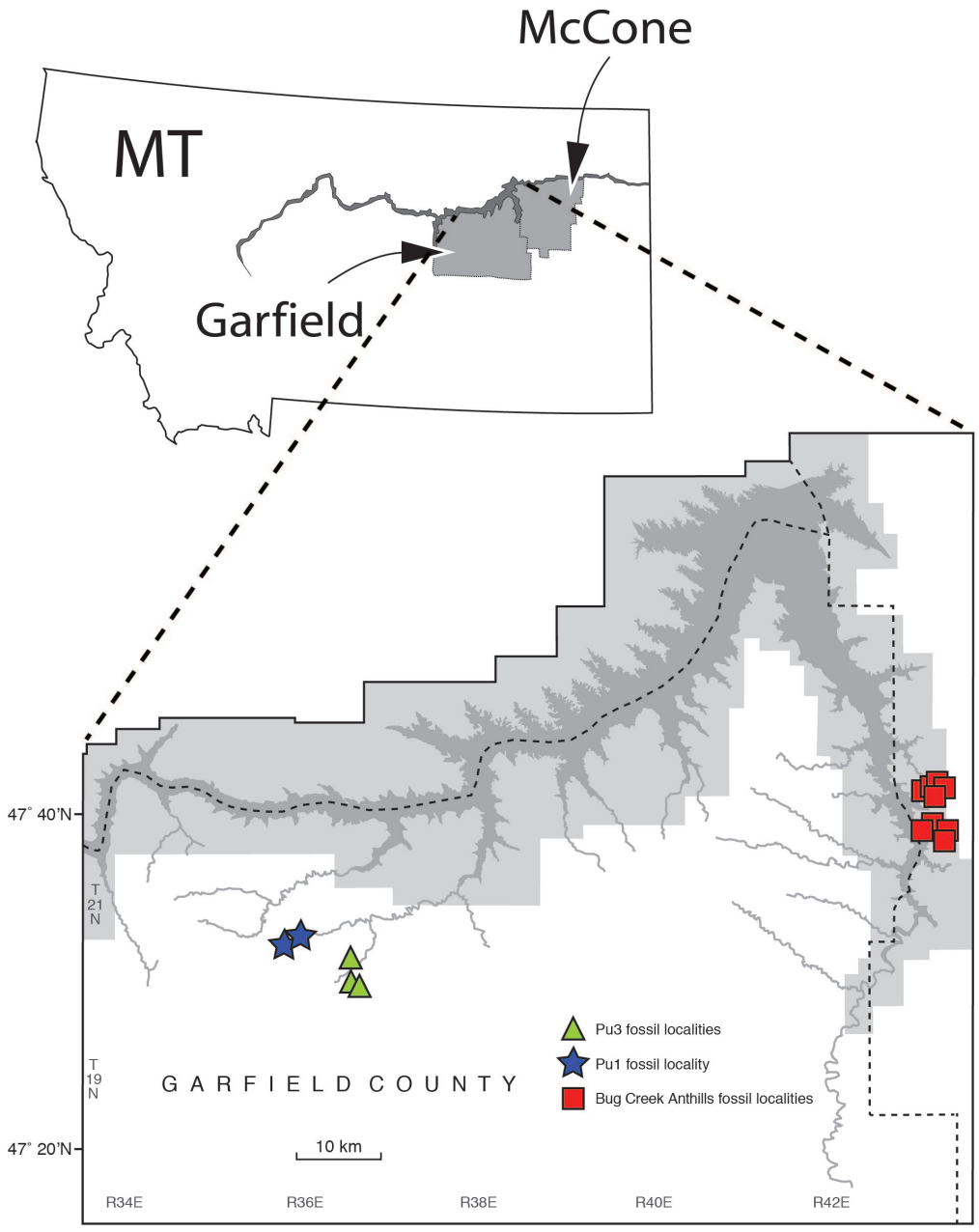

Table S4.2. Scanning calibrations (filter, cam pixels, exposure times, and scan time) and reconstruction parameters (beam hardening, ring artifact reduction, post alignment, smoothing, and dynamic range) used for modern mammalian and fossil specimens used in this study. All specimens were mounted in Styrofoam, and scanned with a rotational degree of 0.3 degrees, at 50 Kv and 800 μA, and with random movement selected. All specimens were scanned using a frame averaging of 8 (8 images averaged into one), except UWBM 77674 (*Didephis virginiana*), which was scanned with a frame averaging of 6. Abbreviations are as follows: Sm., smoothing; PA, post alignment; RR, ring artifacts reduction; BH, beam hardening; Exp. time, exposure time (milliseconds).

				Scanning Parameters					Reconstruction Parameters					
													Dynamic range	
Code	Specimen number	Genus	Species	Filter (mm)	Cam pixels	Pixel size	Exp. Time (ms)	Scan time (min)	BH	RR	PA	Sm.	Low	High
1	20671	*Sarcophilus*	*harrisii*	0.25 Al	large	40.47	1000	111	32	0	0.5	1	0.0107	0.110
2	32255	*Caluromys*	*derbianus*	none	small	17.21	1600	174	28	15	-1	1	0.0473	0.306
3	77674	*Didelphis*	*virginiana*	0.25 Al	large	36.16	1000	88	23	0	0.5	1	0.0131	0.0854
4	72928	*Petaurus*	*breviceps*	0.25 Al	small	14.29	4500	440	34	0	-1	1	0.0121	0.119
5	68913	*Trichosurus*	*vulpecula*	0.25 Al	large	34.42	1000	110	35	0	0	1	0.0056	0.117
6	34200	*Potorous*	*tridactylus*	0.25 Al	large	40.47	1000	111	30	0	-1	1	0.0112	0.118
7	68898	*Aepyprymnus*	*rufescens*	0.25 Al	large	34.42	1000	110	31	0	-1	1	0.008	0.114
8	68924	*Pseudocheirus*	*peregrinus*	0.25 Al	large	46.26	1000	111	26	0	-76.5	1	0.0175	0.0964
9	68919	*Perameles*	*nasuta*	0.25 Al	large	46.63	1000	171	20	0	-0.5	1	0.0144	0.113
10	34168	*Echinops*	*telfairi*	none	small	14.54	1600	172	35	0	0.5	2	0.0193	0.338
11	39490	*Vulpes*	*vulpes*	0.25 Al	large	53.22	1000	112	22	0	0	1	0.0123	0.0924
12	35221	*Urocyon*	*cinereoargenteus*	0.25 Al	large	46.63	1000	111	30	3	-1.5	1	0.0086	0.0987
13	35470	*Suricata*	*suricatta*	0.25 Al	large	46.63	1000	111	21	5	0.5	1	0.0172	0.121
14	35951	*Mephitis*	*mephitis*	0.25 Al	large	59.14	1000	113	20	0	58	1	0.005	0.0875
15	32230	*Lontra*	*canadensis*	0.25 Al	large	46.26	1000	111	26	10	-77	1	0.0129	0.0827

16	35223	*Mustela*	*vison*	0.25 Al	small	24.07	4500	448	21	0	2.5	1	0.0143	0.0977
17	34936	*Gulo*	*gulo*	0.25 Al	large	59.14	1000	113	25	5	-58	1	0.0101	0.0956
18	38625	*Spilogale*	*putorius*	0.25 Al	large	46.63	1000	171	20	0	-0.5	1	0.0144	0.113
19	39366	*Mustela*	*erminea*	none	small	17.21	1600	173	22	5	-1	1	0.0496	0.269
20	58727	*Mustela*	*putorius*	0.25 Al	small	24.07	4500	448	21	10	3.5	1	0.017	0.113
21	73281	*Paguma*	*larvata*	0.25 Al	small	23.13	4500	447	23	0	-155.5	1	0.0143	0.102
22	34167	*Cabassous*	*centralis*	0.25 Al	large	34.42	1000	110	35	0	-0.5	1	0.00598	0.107
23	22458	*Dasypus*	*novemcinctus*	0.25 Al	large	46.26	1000	111	21	10	-73.5	1	0.0208	0.101
24	35468	*Euphractus*	*sexcinctus*	0.25 Al	large	34.42	1000	110	30	0	-1.5	2	0	0.101
25	38637	*Scalopus*	*aquaticus*	none	small	12.09	1600	171	28	5	-4	1	0.0616	0.324
26	34236	*Scapanus*	*orarius*	none	small	12.09	1600	172	26	5	-4	1	0.0783	0.334
27	60340	*Neurotrichus*	*gibbsii*	none	small	9.89	1600	171	25	0	0.5	1	0.0766	0.338
28	35360	*Urotrichus*	*talpoides*	none	small	9.89	1600	171	25	0	0.5	1	0.0766	0.338
29	38628	*Brachylagus*	*idahoensis*	0.25 Al	small	17.21	4000	396	20	0	-0.5	2	0.0196	0.125
30	33263	*Lepus*	*americanus*	0.25 Al	large	60.37	1000	173	20	0	0	1	0.0128	0.0876
31	60062	*Ochotona*	*princeps*	none	small	9.89	1600	171	20	0	-1.5	1	0.0346	0.279
32	35475	*Elephantulus*	*rufescens*	none	small	12.09	1600	48	25	5	-1	1	0.0719	0.302
33	39005	*Callithrix*	*pygmaea*	none	small	14.54	1600	173	23	5	0.5	1	0.0606	0.280
34	75541	*Leontopithecus*	*rosalia*	0.25 Al	large	60.37	1000	173	20	0	0	1	0.0128	0.0876
35	75539	*Saguinus*	*oedipus*	0.25 Al	small	23.31	4000	400	20	5	-0.5	2	0.0152	0.110
36	39014	*Saimiri*	*sciureus*	0.25 Al	large	36.16	1000	111	20	0	0.5	1	0.0125	0.102
37	34058	*Aplodontia*	*rufa*	0.25 Al	small	26.32	4500	450	23	0	130.5	1	0.00483	0.123
38	81972	*Castor*	*canadensis*	0.25 Al	large	60.37	1000	112	30	0	-0.5	1	0.0075	0.104
39	72879	*Ondatra*	*zibethicus*	0.25 Al	large	29.07	1000	110	30	0	1	2	0.0061	0.13
40	66559	*Synaptomys*	*borealis*	none	small	9.89	1600	171	23	15	2	1	0.0760	0.327
41	76721	*Zapus*	*princeps*	none	small	12.09	1600	172	26	5	-4.5	1	0.0514	0.298
42	34176	*Coendou*	*prehensilis*	0.25 Al	large	46.63	1000	111	31	0	0.5	1	0.0071	0.095
43	44623	*Thomomys*	*bottae*	none	small	14.54	1600	172	26	5	-3	1	0.0487	0.31134
44	47379	*Chaetodipus*	*fallax*	none	small	14.54	1600	172	35	5	1	1	0.0367	0.319
45	78740	*Dipodomys*	*deserti*	none	small	17.21	1600	174	25	5	-1.5	1	0.0612	0.267

46	48984	*Octodon*	*degus*	0.25 Al	small	12.09	4000	392	20	5	-1	2	0.0238	0.126
47	35278	*Sciurus*	*aberti*	0.25 Al	small	17.21	4000	396	20	10	-1	2	0.0262	0.124
48	20646	*Sciurus*	*carolinensis*	0.25 Al	small	23.31	4000	400	23	0	1	1	0.0236	0.114
49	35129	*Glaucomys*	*sabrinus*	none	small	14.54	1600	172	26	5	-3	1	0.0487	0.311
50	43897	*Glaucomys*	*volans*	none	small	12.09	1600	171	21	10	-4	1	0.0537	0.261
51	75774	*Cynomys*	*ludovicianus*	0.25 Al	large	34.42	1000	110	30	0	-0.5	2	0.00808	0.113
52	34225	*Tupaia*	*glis*	0.25 Al	small	20.23	4000	418	30	5	0	2	0.00882	0.116
NA	151990	Fossil	NA	1 Al	large	33.38	2180	217	20	7	1	1	0.00503	0.163
NA	196000	Fossil	NA	1 Al	small	19.91	8600	827	34	0	-1	1	0.0199	0.168
NA	152011	Fossil	NA	1 Al	large	59.14	8600	225	33	15	-1.5	1	0.0246	0.15
NA	70965	Fossil	NA	1 Al	small	19.91	8600	827	34	0	-1.5	1	0.023	0.169
NA	151968	Fossil	NA	1 Al	small	23.13	8600	832	34	0	0	1	0.0091	0.123
NA	151969	Fossil	NA	1 Al	small	23.13	8600	832	34	0	0	1	0.0091	0.123
NA	151955	Fossil	NA	1 Al	small	19.9	8600	826	33	5	-0.5	1	0.0179	0.156
NA	151967	Fossil	NA	1 Al	small	29.57	8600	842	34	0	-1.5	1	0.0198	0.147
NA	151963	Fossil	NA	1 Al	small	23.13	8600	833	34	0	-2	1	0.0168	0.144
NA	118532	Fossil	NA	1 Al	small	19.91	8600	827	34	0	-2.5	1	0.0188	0.155
NA	153150	Fossil	NA	1 Al	small	16.69	8600	818	25	0	-2.5	1	0.00569	0.167
NA	150432	Fossil	NA	1 Al	small	16.69	8600	823	34	0	-5.5	1	0.0257	0.189
NA	153031	Fossil	NA	1 Al	small	29.57	8600	842	34	0	-1.5	1	0.0198	0.147
NA	192681	Fossil	NA	1 Al	small	16.69	8600	823	34	0	-0.5	1	0.0241	0.153
NA	194857	Fossil	NA	1 Al	small	16.69	8600	823	34	0	-5.5	1	0.0257	0.189
NA	152018	Fossil	NA	1 Al	small	19.9	8600	826	33	5	-0.5	1	0.0179	0.156
NA	151995	Fossil	NA	1 Al	small	19.91	8600	827	34	0	-1	1	0.0199	0.168
NA	152014	Fossil	NA	1 Al	large	33.38	2180	219	34	0	-1.5	1	0.0175	0.179
NA	195905	Fossil	NA	1 Al	small	19.91	8600	827	34	0	-1.5	1	0.023	0.169
NA	145674	Fossil	NA	1 Al	large	59.14	8600	225	33	15	-1.5	1	0.0246	0.15
NA	192514	Fossil	NA	1 Al	small	19.91	8600	827	34	0	-2.5	1	0.0188	0.155
NA	192676	Fossil	NA	1 Al	large	59.14	2180	225	34	5	0	1	0.0278	0.139
NA	197518	Fossil	NA	1 Al	small	16.69	8600	823	34	0	-0.5	1	0.0241	0.153

Table S4.3. Mimics (mimics threshold) and Geomagic (polygon number) parameters used for modern mammalian and fossil specimens used in this study. Asterisks indicate specimens in *Didelphis*, *Mustela vison*, and *Saimiri* that were reconstructed in NRecon as tiff files (rather than jpegs), and therefore have different threshold values in Mimics.

				Mimics Threshold		Polygon Number	
Code	Specimen Number	Genus	Species	Lower Value	Upper Value	Pre-cleaning	Post-cleaning
1	20671	*Sarcophilus*	*harrisii*	55	255	430,020	129,156
2	32255	*Caluromys*	*derbianus*	56	255	235,536	114,776
3	77674	*Didelphis*	*virginiana*	20430*	65535*	146,348	85,532
4	72928	*Petaurus*	*breviceps*	105	255	982,802	355,664
5	68913	*Trichosurus*	*vulpecula*	75	255	265,356	97,292
6	34200	*Potorous*	*tridactylus*	80	255	91,700	47,390
7	68898	*Aepyprymnus*	*rufescens*	75	255	259,356	124,100
8	68924	*Pseudocheirus*	*peregrinus*	101	255	399,310	162,354
9	68919	*Perameles*	*nasuta*	107	249	28,556	25,032
10	34168	*Echinops*	*telfairi*	94	242	41,152	29,862
11	39490	*Vulpes*	*vulpes*	71	255	237,292	106,996
12	35221	*Urocyon*	*cinereoargenteus*	49	255	174,172	116,306
13	35470	*Suricata*	*suricatta*	87	255	59,280	32,088
14	35951	*Mephitis*	*mephitis*	56	255	953,916	252,596
15	32230	*Lontra*	*canadensis*	113	255	4,893,710	445,709
16	35223	*Mustela*	*vison*	13932*	65535*	167,708	82,472
17	34936	*Gulo*	*gulo*	77	255	6,342,688	306,074
18	38625	*Spilogale*	*putorius*	62	255	33,272	21,740
19	39366	*Mustela*	*erminea*	59	255	110,060	51,498
20	58727	*Mustela*	*putorius*	62	255	278,668	111,430

21	73281	*Paguma*	*larvata*	103	255	8,391,643	433,904
22	34167	*Cabassous*	*centralis*	45	255	467,612	110,532
23	22458	*Dasypus*	*novemcinctus*	65	255	1,948,218	853,254
24	35468	*Euphractus*	*sexcinctus*	87	255	274,132	141,782
25	38637	*Scalopus*	*aquaticus*	73	255	151,444	71,184
26	34236	*Scapanus*	*orarius*	61	255	96,048	49,976
27	60340	*Neurotrichus*	*gibbsii*	59	255	80,456	40,890
28	35360	*Urotrichus*	*talpoides*	86	255	66,748	39,654
29	38628	*Brachylagus*	*idahoensis*	82	255	353,976	127,490
30	33263	*Lepus*	*americanus*	65	254	28,340	24,966
31	60062	*Ochotona*	*princeps*	66	255	305,824	131,088
32	35475	*Elephantulus*	*rufescens*	66	255	116,308	65,264
33	39005	*Callithrix*	*pygmaea*	53	255	210,060	87,506
34	75541	*Leontopithecus*	*rosalia*	68	255	28,844	15,994
35	75539	*Saguinus*	*oedipus*	84	255	373,688	113,516
36	39014	*Saimiri*	*sciureus*	13880*	65535*	192,868	85,566
37	34058	*Aplodontia*	*rufa*	97	255	7,743,086	186,852
38	81972	*Castor*	*canadensis*	82	255	504,692	188,888
39	72879	*Ondatra*	*zibethicus*	70	255	117,100	101,936
40	66559	*Synaptomys*	*borealis*	59	255	69,828	45,888
41	76721	*Zapus*	*princeps*	71	255	94,232	48,862
42	34176	*Coendou*	*prehensilis*	97	255	174,900	119,414
43	44623	*Thomomys*	*bottae*	54	255	141,340	81,254
44	47379	*Chaetodipus*	*fallax*	98	255	32,472	22,230
45	78740	*Dipodomys*	*deserti*	55	255	98,864	60,768
46	48984	*Octodon*	*degus*	83	255	217,696	130,874
47	35278	*Sciurus*	*aberti*	70	255	395,644	184,840
48	20646	*Sciurus*	*carolinensis*	72	255	178,888	101,342
49	35129	*Glaucomys*	*sabrinus*	75	255	152,780	73,384

50	43897	*Glaucomys*	*volans*	53	255	163,880	72,716
51	75774	*Cynomys*	*ludovicianus*	99	255	78,292	56,600
52	34225	*Tupaia*	*glis*	107	255	92,152	58,634
NA	151990	Fossil	NA	NA	255	340,084	127,648
NA	196000	Fossil	NA	87	255	4,574,466	1,079,674
NA	152011	Fossil	NA	72	255	599,130	201,180
NA	70965	Fossil	NA	80	255	3,644,577	355,607
NA	151968	Fossil	NA	83	255	2,106,512	587,124
NA	151969	Fossil	NA	68	255	283,348	105,648
NA	151955	Fossil	NA	107	255	1,420,352	507,228
NA	151967	Fossil	NA	67	255	1,449,096	360,126
NA	151963	Fossil	NA	96	255	1,130,190	316,762
NA	118532	Fossil	NA	81	255	1,827,028	526,266
NA	153150	Fossil	NA	85	255	910,400	295,178
NA	150432	Fossil	NA	80	255	1,945,792	582,344
NA	153031	Fossil	NA	73	255	555,378	216,160
NA	192681	Fossil	NA	67	255	2,856,250	855,936
NA	194857	Fossil	NA	91	255	1,945,938	582,712
NA	152018	Fossil	NA	107	255	2,094,278	544,811
NA	151995	Fossil	NA	107	255	3,785,150	922,558
NA	152014	Fossil	NA	82	255	2,085,896	545,316
NA	195905	Fossil	NA	72	255	4,042,642	875,350
NA	145674	Fossil	NA	40	255	274,419	143,808
NA	192514	Fossil	NA	91	255	2,296,228	705,472
NA	192676	Fossil	NA	NA	255	6,811,492	71,124
NA	197518	Fossil	NA	62	255	3,216,988	415,468

Table S4.4. Astragali specimens downloaded from MorphoSource used in this study. We report specimen number, MorphoSource Media Number, specimen sex, file size, and resolution as they appear in MorphoSource; the fossil specimen (i.e., *Purgatorius* sp.) lacks sex data ("NA"). All downloaded files were 3D Meshes (Polygon File Format, .ply) lacking any calibrations, and all reported 'NA' for frame averaging and 'air' for the wedge (i.e., the physical mount during scanning).

Genus	species	Specimen Number	Sex	Modern or Fossil	MorphoSource Media Number	File Size (Mb)	Resolution (mm)		
							X	Y	Z
Purgatorius	sp.	UCMP-197509	NA	Fossil	M5011	6.76	0.010	0.010	0.010
Ptilocercus	towii	USNM-488072	F	Modern	M4641	NA	0.0205	0.0205	0.0205

Table S4.5. Copyright information, grant support, and technician information for MorphoSource media (i.e., specimens; Table S4.3) used in this study. All specimens are copyrighted, and have the following copyright permission: "Permission to use media on MorphoSource granted by copyright holder" and the following copyright license: "Attribution-NonCommercial CC BY-NC-reuse but noncommercial." USNM specimen copyright is held by Doug Boyer; UCMP specimen copyright is held by UCMP. Institutional and facility abbreviations: **SBU**, Stony Brook University; **UCMP** University of California Museum of Paleontology, Berkeley, California, U.S.A; **USNM**, United States National Museum, Washington, D.C., U.S.A. Other abbreviations: DB, Doug Boyer; Inst., Institution; KS, Ksenia Sokolova; NSF, National Science Foundation; Tech., Technician. See MorphoSource website for additional scan details (http://morphosource.org/).

Media Number	Inst.	Grant support	Media Citation Instructions	Facility	Tech.
M5011	UCMP	NSF SBE-1028505 (to E.J. Sargis and S.G.B.Chester), the Leakey Foundation (S.G.B. Chester), and a Brooklyn College Tow Faculty Travel Fellowship (S.G.B. Chester), NSF SBR-9616194 (to G.F. Gunnell, P.D. Gingerich, and J.I. Bloch), Yale Institute for Biospheric Studies (to J.I. Bloch), NSF BCS 1317525 (to E. Seiffert and D.M. Boyer); NSF EAR 9505847 (to W.A. Clemens)	Doug M. Boyer provided access to these data originally appearing in Chester et al. (2015), the collection of which was funded by various sponsors (see Grant support on Morphosource page). The files were downloaded from www.MorphoSource.org, Duke University	Yale Core Center for Musculoskeletal Disorder	DB, KS
M4641	USNM	NSF BCS 1317525	Doug Boyer provided access to these data originally appearing in Boyer and Seiffert (2013)NSF BCS 1317525. The files were downloaded from www.MorphoSource.org, Duke University.	SBU Center for Biotechnology	DB, KS

Supplemental References Cited

Wilson, G.P., D.G. DeMar Jr., and G. Carter. 2014. Extinction and survival of salamander and salamander-like amphibians across the Cretaceous-Paleogene boundary in northeastern Montana, in: G.P. Wilson, W.A. Clemens, J.R. Horner, and J.H. Hartman (Eds.), Through the End of the Cretaceous in the Type Locality of the Hell Creek Formation in Montana and Adjacent Areas. Geological Society of America Special Paper 503, Boulder, pp. 271–297.

CHAPTER 5:

CONCLUDING REMARKS

This study represents the first quantitative analysis of postcranial ecomorphology for multiple elements from mammals across three successive K-Pg faunas, and a critical step towards understanding the role of locomotor ecology in mass extinction and recovery dynamics. Despite the novelty and strengths of this study, we first acknowledge there are weaknesses associated with using isolated elements for postcranial locomotor interpretations. Ecomorphological studies of whole skeletons have shown robust and successful locomotor function discrimination among phylogenetically diverse samples of mammals (e.g., Chen and Wilson 2015), and study of the entire skeleton may increase the likelihood of capturing first principle biomechanical relationships that are informative of locomotor mode. Analyses of whole skeletons can be particularly informative in cases where functional signals differ across elements (e.g., Chen and Wilson 2015; Fabre et al. 2015), and study of whole skeletons may help to overcome complications introduced by increasing within-group functional diversity (e.g., functionally diverse forms accomplishing fossorial locomotion; Chen and Wilson 2015; Fabre et al. 2015). Regardless of the apparent strengths of studying whole skeletons, most material in the fossil record is found as isolated elements, a fact which is especially true for K-Pg mammals (e.g., Deischl 1964; Sloan and Van Valen 1965; Szalay and Decker 1974; Clemens 2002; DeBey and Wilson 2014). Development of robust methods to analyze isolated elements is critical to quantitative analyses of postcranial material and subsequent inferences of locomotor ecology. Below we interpret the results of this dissertation for locomotor diversity and body size in the context of proposed K-Pg extinction and recovery dynamics.

1. LOCOMOTOR AND BODY SIZE PATTERNS ACROSS THE K-PG BOUNDARY

1.1. *"Ecologically marginalized" Mesozoic mammals on a dinosaur-dominated landscape*

The ecological dominance of dinosaurs on Mesozoic landscapes and the comparative ecological marginalization of contemporaneous mammals used to be widely held among paleontologists. Mesozoic mammals were hypothesized to be small-bodied locomotor generalists with nocturnal habits and insectivorous diets (e.g., Lillegraven et al. 1987; Rose 2006), restricted to these ecological niches by selection pressures imposed by dinosaurs (e.g. Van Valen and Sloan 1977; Lillegraven et al. 1987; Stucky 1990). With the recent discovery of ecologically diverse Mesozoic mammals (e.g., Luo et al. 2003; Luo and Wible 2005; Meng et al. 2006; Luo 2007) our understanding of ecomorphological diversification among early mammalian lineages has begun to change (e.g., Luo 2007; Chen and Wilson 2015). Recent analyses show the number of occupied ecomorphological lineages present among Mesozoic mammals includes semiaquatic, terrestrial, scansorial, arboreal, fossorial, semifossorial, and gliding forms (Luo 2007; Chen and Wilson 2015), suggesting Mesozoic mammals were not restricted to roles as locomotor generalists. These studies focused on Jurassic and Early Cretaceous material (see references in Luo 2007 and Chen and Wilson 2015), but we would expect younger, latest Cretaceous deposits to include similarly or even more diverse locomotor forms.

Unexpectedly, our results do not suggest a latest Cretaceous assemblage that was ecologically diverse with respect to locomotor function. Although samples sizes are

admittedly low for this interval zone, our analyses point to the presence of many multituberculates with arboreal locomotion and saltatorial capabilities (i.e., humeri and femora; DeBey and Wilson 2014), one humerus from an arboreal eutherian, and one humerus from a metatherian that is potentially semiaquatic (i.e., *Didelphodon vorax*; Szalay 1994; Longrich 2005; Borths and Hunter 2008; but see Fox and Naylor 2006). In total, we find evidence of arboreal and semifossorial locomotion, and tentative evidence of saltatorial and semiaquatic locomotion. Critically, none of these taxa have the more extreme postcranial morphologies seen among other Mesozoic mammals (i.e., fossorial *Fruitafossor*, semiaquatic *Castorocauda*; Luo and Wible 2005; Ji et al. 2006; Luo 2007), and we lack evidence for terrestrial, scansorial, fossorial, and gliding forms. We acknowledge that using the single metatherian and single eutherian humerus morphotypes to represent the full locomotor diversity of metatherians and eutherians in our study area (11 and 8 known Lancian species, respectively; Wilson 2014) is problematic; however, until more Lancian postcrania are discovered and analyzed, we interpret the pattern for available fossils. As such, if we take the locomotor signal present among our small sample sizes as indicative of the broader Lancian community, we would conclude that the Lancian fauna was composed of mammals with fewer locomotor modes than in older Mesozoic faunas.

We suggest taxonomic composition is a significant factor in this potential decrease in locomotor mode diversity from the Jurassic and Early Cretaceous to the latest Cretaceous. The postcrania of these ecomorphologically diverse (i.e., Jurassic and Early Cretaceous) and comparatively conservative (i.e., latest Cretaceous) faunas represent significantly different taxa. In contrast to the therian (eutherian and metatherian) and allotherian (multituberculate) assemblages of the Lancian faunas in our study area, the

ecomorphologically diverse Jurassic and Early Cretaceous faunas are predominantly composed of non-therian and non-allotherian taxa (e.g., Luo 2007; Chen and Wilson 2015; but see Ji et al. 2002 and Luo et al. 2003). These non-therians include the Middle and Late Jurassic docodontans *Castorocauda* and *Haldanodon*, respectively (Ji et al. 2006; Chen and Wilson 2015), Middle Jurassic ?eutriconodontan *Volaticotherium* (Meng et al. 2006), Late Jurassic *Fruitafossor* (Luo and Wible 2005; Chen and Wilson 2015), Early Cretaceous eutriconodontans *Gobiconodon*, *Jeholodens*, *Liaoconodon*, *Repenomamus*, and *Yanoconodon* (Ji et al. 1999; Hu et al. 2005; Hu 2006; Chen and Wilson 2015), and Early Cretaceous symmetrodontans *Akidolestes*, *Maotherium*, and *Zhangheotherium* (Hu et al. 1997, 1998; Ji et al. 2009; Chen and Luo 2013; Chen and Wilson 2015). This pattern of difference among therians, and non-therians with respect to locomotor function is mirrored in the dental literature, such that declines in abundances of triconodonts, symmetrodonts, docodonts, and eupantotherians during the mid-Cretaceous reduced dental and diet diversity among Late Cretaceous mammals (Grossnickle and Polly 2013). Additionally, latest Cretaceous multituberculates had a greater dental morphological diversity than contemporaneous eutherians (e.g., Wilson et al. 2012; Wilson 2013), which is also detected here for multituberculate postcrania. Thus, for both dental and postcranial data, non-therians and therians generally exhibit different patterns of diversification in Mesozoic assemblages.

We note three additional factors that may or may not explain the differences in locomotor diversity. First, the preservation of many Jurassic and early Cretaceous mammals (i.e., whole elements and nearly complete skeletons) differs greatly from the isolated and fragmentary elements studied here. The preserved elements I chose to focus on (humeri, femora, astragali) are suggestive of diverse locomotor function in these older

Mesozoic fossils, but preservation may be an explanation for these differences as locomotor signals can differ across elements in a single skeleton (e.g., Chen and Wilson 2015; Fabre et al. 2015). This is a weakness of all analyses on isolated elements that cannot be avoided. Second, differences in specimen location (e.g., Asia versus North America) are unlikely to be driving patterns of locomotor difference because ecologically diverse Mesozoic mammals have been found in North American rocks (i.e., *Fruitafossor* was found in Colorado; Luo and Wible 2005). Finally, this study encompasses three separate faunas from a relatively short period of geologic time and one location. Although this case study is informative of a geographically- and temporally-constrained pattern, it cannot be expected to detect levels of locomotor diversity that could be found in studies that are broader geographically and/or temporally.

1.2. *Evidence of behavioral mode selectivity at the K-Pg mass extinction?*

Some locomotor behaviors have been hypothesized to mitigate extinction risk, particularly "sleep-and-hide" behaviors that buffer animals from changing environmental conditions (Liow et al. 2009). Robertson et al. (2004) extrapolated this trend to hypothesize that behaviors that protected animals from a global heat pulse of infrared radiation from ejecta reentering the atmosphere (e.g., aquatic swimming or underground burrowing) would be selected for during the K-Pg mass extinction. The "Sheltering Hypothesis" (Robertson et al. 2004) therefore predicts a relative increase in fossorial, semifossorial, and/or semiaquatic adaptations among early Paleocene mammals (i.e., Pu1). None of our qualitative (i.e., femora) or quantitative (i.e., humeri and astragali) analyses identified semiaquatic adaptations among our Pu1 taxa; further, we did not find evidence of

semiaquatic behavior among the other biozones either (except for Lancian humerus attributed to *Didelphodon vorax*, proposed to be semiaquatic based on other postcranial elements; Szalay 1994; Longrich 2005; Borths and Hunter 2008). We do, however, find quantitative support for semifossorial locomotion among the Pu1 eutherian postcrania in our study. Specifically, we find evidence of semifossorial locomotion among ?*Protungulatum* humeri and astragali, and among Pu1 ?*Procerberus* humeri. Some morphologies present in these postcrania are also suggestive of possibly more generalized terrestrial or scansorial locomotion (?*Protungulatum* and ?*Procerberus*, respectively). In contrast, among younger Pu3 faunas, we detect strong qualitative evidence for arboreal and scansorial locomotion among specimens attributed ?*Purgatorius* and to a large archaic ungulate, respectively. Quantitatively these specimens also showed support for semifossorial locomotion although this may be a bias inherent in the analysis of the comparative sample. We note that according to the dental record, *Procerberus* sp. is present in both Pu1 and Pu3 biozones (e.g., Clemens 2002; Wilson 2014), but our Pu3 sample excludes any ?*Procerberus* postcrania; *Protungulatum* is restricted to the Pu1, which is supported by our postcranial sample (e.g., Clemens 2002; Wilson 2014). We note the increased semifossoriality (n = 2 morphotypes) in the Pu1 compared to the Pu3, but we urge cautious interpretation of these results as the morphotype richness and sample sizes are small for both eutherian Pu1 and Pu3 postcrania.

1.3. *Body size selectivity at the K-Pg mass extinction*

Body size and certain locomotor modes are highly correlated (e.g., Jenkins and Parrington 1976; Nowak 1999), such that any locomotor-mode selectivity across the K-Pg

boundary might also produce a pattern of body size selectivity (and vice versa). Small body size negatively correlates with extinction risk (e.g., Harries and Knorr 2009), and faunas immediately following mass extinctions, "survival faunas," may exhibit the "Lilliput Effect" of reduced mean body size for diverse taxa (e.g., vertebrates, invertebrates, plants; Twitchett 2007; Keller and Abramovich 2009; Huttenlocker 2014). Advantages for mammals of small body sizes include easy camouflage from predators, low energy expenditures required during escape, a wide variety of available microhabitats, and potentially high reproductive rates (e.g., Bourlière 1975; Lillegraven et al. 1987); all would be beneficial following the extreme ecological perturbation of a mass extinction event. Following the K-Pg mass extinction, general ecological disruption and decrease in primary productivity (e.g., Wilf et al. 2006) could similarly have selected for smaller body sizes among Puercan mammals. Results from femora and humeri from our study area show an increase in body size in the earliest Paleocene (Pu1) that is inconsistent with this Lilliput Effect. However, immigration coincident with the K-Pg boundary brought an influx of new taxa into the Pu1 fauna. The Pu1 size increase appears to be driven by these "immigrant" taxa, which were significantly larger than Pu1 "resident" taxa. As, Pu1 residents were also significantly smaller than Lancian taxa, this is consistent with the Lilliput Effect. We note Pu1 sample sizes are the smallest for all element types, so these results should be taken cautiously; however, dental data similarly indicates a strong pattern of body size reduction across the K-Pg boundary (e.g., Wilson 2013). Despite the fact that Lilliput Effects are also seen for some non-mammalian K-Pg taxa (e.g., Keller 1988; Hansen et al. 1993; Aberhan et al. 2007), others do not show a decrease in body size (e.g., bivalves, bryozoans; Jablonski

and Raup 1995; Lockwood 2005; Sogot et al. 2014), and hint at more complex mechanisms of end-Cretaceous extinction and Early Paleocene recovery (e.g., Jablonski 1996).

1.4. *Faunal recovery and early Paleocene mammals: Decoupled locomotor-mode expansion and body-size increases?*

The younger Pu3 assemblage is typical of a more "recovered" fauna, and in this biozone we find both significant increases in body size and evidence for diversification of locomotor modes. Although difficult to compare to one another, results from the Pu3 indicate a large increase in body size (~2 orders of magnitude) and a potentially more modest expansion of locomotor modes (increase in scansorial and arboreal morphologies among eutherians, and appearance of fossorial multituberculates), and thus suggest a potential decoupling of changes in body size and locomotor mode diversity. Specifically, this research tentatively suggests that increases in body size may occur at a more rapid pace than ecomorphological diversification with respect to locomotor mode. Further study of locomotor mode diversification following the K-Pg in our study area should therefore extend into successively younger deposits (i.e., later Paleocene Torrejonian 1 biozone; Clemens 2002; Clemens and Wilson 2009). Postcrania from younger deposits in the Western Interior (i.e., Pu3, Torrejonian 1, and younger faunas; e.g., Matthew 1937) should also be examined quantitatively with respect to locomotor mode diversification to test the hypothesis of decoupled body size increases and locomotor mode diversification following the K-Pg mass extinction.

1.5. *Vegetational Structure*

The habitat structure of eastern Montana changed dramatically from the latest Cretaceous to the early Paleogene (e.g., Fastovsky 1987; Johnson 2002; Nichols and Johnson 2008), which may dictate some of the postcrania diversity patterns detected in this study. Rock strata indicate fine-grained sediments in the Hell Creek Formation are representative of a broad, alluvial plain with moderately sized meandering rivers (Fastovsky 1987). In contrast, the overlying Tullock Formation contains strata characteristic of more standing water and large ponds, with larger and more laterally continuous coals, and much larger stream channels than in the Hell Creek Formation (Fastovsky 1987). These results suggest a more open paleoenvironment during the latest Cretaceous, and a more heavily forested and closed habitat in the Paleocene (Johnson 2002; Nichols and Johnson 2008). Paleobotanical data, specifically macrofloral and palynological, corroborate this interpretation and suggest an angiosperm-dominated Late Cretaceous landscape, extensive megafloral extinction at the K-Pg boundary, and Paleocene floras dominated by mire (swamp and bog) taxa consistent with closed habitats and higher water tables (Johnson 2002). Our therian humeri results are consistent with the hypothesis of fewer arboreal mammals on more sparsely forested Cretaceous landscapes, and increased arboreality among eutherians in the more densely forested Paleocene. Lacking abundant hiding areas during the Cretaceous, we might also expect to find more semifossorial or fossorial mammals; we indeed find evidence of semifossorial habit in one Lancian eutherian humerus. That all Lancian multituberculates are suggestive of arboreality, with saltatorial capabilities may suggest differences in latest Cretaceous habitat occupation among therians and non-therians (allotherians), although sample sizes must increase greatly to test this hypothesis. Finally, we detect expansion in both the arboreal, fossorial,

and terrestrial locomotor modes in the Pu3, which may suggest increased niche partitioning among mammals on the post-non-avian dinosaur terrestrial landscape. Again, this hypothesis should be tested quantitatively as more material becomes available.

2. CONCLUSION

In conclusion, this dissertation represents an important and novel contribution to the study of ecomorphological patterns at the K-Pg mass extinction. Admittedly small sample sizes are suboptimal for statistically significant conclusions, and fragmentary and isolated material make taxonomic comparisons challenging. Despite these difficulties, the results of this study reinforce the value of postcranial data. Future work on postcrania will hopefully continue to enrich our understanding of this dynamic time in mammalian history.

References Cited

Aberhan, M., S. Weidemeyer, W. Kiessling, R.A. Scasso, and F.A. Medina. 2007. Faunal evidence for reduced productivity and uncoordinated recovery in Southern Hemisphere Cretaceous–Paleogene boundary sections. Geology 35: 227–230.

Borths, M. and J. Hunter. 2008. Gimme shelter? Locomotor trends and mammalian survivorship at the K-Pg Boundary. Journal of Vertebrate Paleontology 28: 3A.

Bourlière, F. 1975. Mammals, small and large: the ecological implications of size, in: F.B. Golley, K. Petrusewicz and L. Ryszkowski (Eds.), Small Mammals: Their Productivity and Population Dynamics. Cambridge University Press, Cambridge.

Chen, M. and Z.-X. Luo. 2013. Postcranial skeleton of the Cretaceous mammal *Akidolestes cifellii* and its locomotor adaptations. Journal of Mammalian Evolution 20: 159–189.

Chen, M. and G.P. Wilson. 2015. A multivariate approach to infer locomotor modes in Mesozoic mammals. Paleobiology 41: 280–312.

Clemens, W.A. 2002. Evolution of the mammalian fauna across the Cretaceous-Tertiary boundary in northeastern Montana and other areas of the Western Interior, in: J.H. Hartman, K.R. Johnson, and D.J. Nichols (Eds.), The Hell Creek Formation and the Cretaceous-Tertiary Boundary in the Northern Great Plains: An Integrated Continental Record of the End of the Cretaceous. Geological Society of America Special Paper 361, Boulder, pp. 217–245.

Clemens, W.A. and G.P. Wilson. 2009. Early Torrejonian mammalian local faunas from Northeastern Montana, U.S.A., in: L.B. Albright III (Ed.), Papers on Geology,

Vertebrate Paleontology, and Biostratigraphy in Honor of Michael O. Woodburne. Museum of Northern Arizona Bulletin, Flagstaff, Arizona, 1–48.

DeBey, L.B. and G.P. Wilson. 2014. Mammalian femora across the Cretaceous-Paleogene boundary in eastern Montana. Cretaceous Research 51: 361–85.

Deischl, D.G. 1964. The Postcranial Anatomy of Cretaceous Multituberculate Mammals, unpublished M.Sc. thesis, University of Minnesota, Minneapolis, 85 pp.

Fabre, A.-C., M.J. Salesa, R. Cornette, M. Antón, J. Morales, and S. Peigné. 2015. Quantitative inferences on the locomotor behaviour of extinct species applied to *Simocyon batalleri* (Ailuridae, Late Miocene, Spain). The Science of Nature 102: 30.

Fastovsky, D.E. 1987. Paleoenvironments of vertebrate-bearing strata during the Cretaceous-Paleogene transition, eastern Montana and western North Dakota. PALAIOS 2: 282–295.

Fox, R. C. and B. G. Naylor. 2006. Stagodontid marsupials from the Late Cretaceous of Canada and their systematic and functional implications. Acta Palaeontologica Polonica 51: 13–36.

Grossnickle, D.M. and P.D. Polly 2013. Mammal disparity decreases during the Cretaceous angiosperm radiation. Proceedings of the Royal Society B 280: 20132110

Hansen, T.A., B.R. Farrell, and B. Upshaw. 1993. The first 2 million years after the Cretaceous–Tertiary boundary in east Texas: rate and paleoecology. Paleobiology 19: 251–265.

Harries, P.J. and P.O. Knorr. 2009. What does the 'Lilliput Effect' mean? Palaeogeography, Palaeoclimatology, Palaeoecology 284: 4–10.

Hu, Y.-M. 2006. Postcranial morphology of *Repenomamus* (Eutriconodonta, Mammalia): implications for the higher-level phylogeny of mammals. Ph.D. dissertation. City University of New York, New York.

Hu, Y.-M., Y.-Q. Wang, Z.-X. Luo, and C.-K. Li. 1997. A new symmetrodont mammal from China and its implications for mammalian evolution. Nature 390: 137–142.

Hu, Y.-M., Y.-Q. Wang, C.-K. Li, and Z.-X. Luo. 1998. Morphology of dentition and forelimb of *Zhangheotherium*. Vertebrata PalAsiatica 36: 102–125.

Hu, Y.-M., J. Meng, Y.-Q. Wang, and C.-K. Li. 2005. Large Mesozoic mammals fed on young dinosaurs. Nature 433: 149–152.

Huttenlocker, A. 2014. Body size reductions in nonmammalian eutheriodont therapsids (Synapsida) during the end-Permian mass extinction. PLoS ONE 9(2): e87553. doi:10.1371/journal.pone.0087553.

Jablonski, D. 1996. Body size and macroevolution, in: D. Jablonski, D.H. Erwin, and J.H. Lipps (Eds.), Evolutionary Paleobiology. Chicago. University Press, Chicago, pp. 256–289.

Jablonski, D. and D.M. Raup. 1995. Selectivity of end-Cretaceous marine bivalve extinctions. Science 268: 389–391

Jenkins, F. A.,and F. Parrington. 1976. Postcranial skeletons of Triassic mammals *Eozostrodon*, *Megazostrodon* and *Erythrotherium*. Philosophical Transactions of the Royal Society of London B 273: 387–431.

Ji, Q., Z.-X. Luo, and S.-A. Ji. 1999. A Chinese triconodont mammal and mosaic evolution of the mammalian skeleton. Nature 398: 326–330.

Ji, Q., Z.-X. Luo, C.-Z. Yuan, J.R. Wible, J.-P. Zhang, and J.A. Georgi. 2002. The earliest known eutherian mammal. Nature 416: 816–822.

Ji, Q., Z.-X. Luo, C.–X. Yuan, and A.R. Tabrum. 2006. A swimming mammaliaform from the Middle Jurassic and ecomorphological diversification of early mammals. Science 311: 1123–1127.

Ji Q., Z.-X. Luo, Z.-L. Zhang, C.-X. Yuan, and L. Xu. 2009. Evolutionary development of the middle ear in Mesozoic therian mammals. Science 326: 278–231.

Johnson, K.R. 2002. Megaflora of the Hell Creek and lower Fort Union Formations in the western Dakotas: Vegetational response to climate change, the Cretaceous-Tertiary boundary event, and rapid marine transgression, in: J.H. Hartman, K.R. Johnson, and D.J. Nichols (Eds.), The Hell Creek Formation and the Cretaceous-Tertiary Boundary in the Northern Great Plains: An Integrated Continental Record of the End of the Cretaceous. Geological Society of America Special Paper 361, Boulder, pp. 329–391.

Keller, G. 1988. Extinction, survivorship and evolution of planktic foraminifera across the Cretaceous/Tertiary boundary at El Kef, Tunisia. Marine Micropaleontology 13: 239–263.

Keller, G. and S. Abramovich. 2009. Lilliput effect in late Maastrichtian planktic foraminifera: Response to environmental stress. Palaeogeography, Palaeoclimatology, Palaeoecology 284: 47–62.

Lillegraven, J.A., S.D. Thompson, B.K. McNab, and J.L. Patton.1987. The origin of eutherian mammals. Biological Journal of the Linnean Society 32: 281–336.

Liow, L.H., M. Fortelius, K. Lintulaakso, H. Mannila, and N.C. Stenseth. 2009. Lower extinction risk in sleep-or-hide mammals. American Naturalist 173: 264–272.

Lockwood, R. 2005. Body size, extinction events, and the early Cenozoic record of veneroid bivalves; a new role for recoveries? Paleobiology 31: 578–590.

Longrich, N. 2005. Aquatic specialization in marsupials from the Late Cretaceous of North America. Cranbrook Institiute of Science Miscellaneous Publications (Evolution of Aquatic Tetrapods Convention Abstracts) V 1: 53.

Luo, Z.-X. 2007. Transformation and diversification in early mammal evolution. Nature 450: 1011–1019.

Luo, Z.-X., Q. Ji., J.R. Wible, and C.-X. Yuan. 2003. An Early Cretaceous tribosphenic mammal and metatherian evolution. Science 302: 1934–1940.

Luo, Z.-X. and J.R. Wible 2005. A Late Jurassic digging mammal and Early mammalian diversification. Science 308: 103–107.

Matthew, W.D. 1937. Paleocene faunas of the San Juan Basin, New Mexico. Transactions of the American Philosophical Society 30: 1–523.

Meng, J., Y.-M. Hu, Y.-Q. Wang, X.-L. Wang, and C.-K. Li. 2006. A Mesozoic gliding mammal from northeastern China. Nature 444: 889–893.

Nichols, D.J. and K.R. Johnson. 2008. Plants and the K–T Boundary. Cambridge University Press, Cambridge.

Nowak, R.M. 1999. Walker's Mammals of the World. Johns Hopkins University Press, Baltimore.

Rose. K.D. 2006. The postcranial skeleton of early Oligocene *Leptictis* (Mammalia: Leptictida), with a preliminary comparison to *Leptictidium* from the middle Eocene of Messel. Palaeontographica Abteilung A 278: 37-56.

Robertson, D.S., M.C. McKenna, O.B. Toon, S. Hope, and J.A. Lillegraven. 2004. Survival in the first hours of the Cenozoic. Geological Society of America Bulletin 116: 760–768.

Sogot C.E., E.M. Harper, and P.D. Taylor. 2014. The Lilliput Effect in colonial organisms: cheilostome bryozoans at the Cretaceous–Paleogene mass extinction. PLoS ONE 9: e87048.

Sloan, R.E. and L. Van Valen. 1965. Cretaceous mammals from Montana. Science 148: 220–227.

Stucky, R.K. 1990. Evolution of land mammal diversity in North America during the Cenozoic. Current Mammalogy 2: 375–432.

Szalay, F.S. 1994. Evolutionary History of the Marsupials and an Analysis of Osteological Characters. Cambridge University Press, New York.

Szalay, F.S. and and R.L. Decker. 1974. Origins, evolution, and function of the tarsus in Late Cretaceous Eutheria and Paleocene primates, in: F.A. Jenkins Jr. (Ed.), Primate Locomotion. Academic Press, Inc., New York, pp. 223–259.

Twitchett, R.J. 2007. The Lilliput effect in the aftermath of the end-Permian extinction event. Palaeogeography, Palaeoclimatology, Palaeoecology 252: 132–144.

Van Valen, L. and R.E. Sloan. 1977. Ecology and the extinction of dinosaurs. Evolutionary Theory 2: 37–64.

Wilf, P., K.R. Johnson, and B.T. Huber. 2003. Correlated terrestrial and marine evidence for global climate changes before mass extinction at the Cretaceous–Paleogene boundary. Proceedings of the National Academy of Sciences: 599–604.

Wilson, G.P. 2013. Mammals across the K/Pg boundary in northeastern Montana, U.S.A.: Dental morphology and body-size patterns reveal extinction selectivity and immigrant-fueled ecospace filling. Paleobiology 39: 429–469.

Wilson, G.P. 2014. Mammalian extinction, survival, and recovery dynamics across the Cretaceous-Paleogene boundary in northeastern Montana, in: G.P. Wilson, W.A. Clemens, J.R. Horner, and J.H. Hartman (Eds.), Through the End of the Cretaceous in the Type Locality of the Hell Creek Formation in Montana and Adjacent Areas. Geological Society of America Special Paper 503, Boulder, pp. 365–392.

Wilson, G.P., A.R. Evans, I.J. Corfe, P.D. Smits, M. Fortelius, and J. Jernvall. 2012. Adaptive radiation of multituberculate mammals before the extinction of dinosaurs. Nature 483: 457–460.